Journal of Engineering

ISSN 1726-4073

A Scientific Refereed Journal Published by College of Engineering University of Baghdad

May

2014

Number 5

Volume 20

مجلة الهندسة

ISSN 1726-4073

مجلة علمية محكمة تصدرها
كلية الهندسة ـ جامعة بغداد

أيار
2014

العدد 5

المجلد 20

قائمة المحتويات

القسم العربي:

العنوان	الصفحة
اثر تكنولوجيا النظم ألمنشئية في النتاج المعماري المعاصر	**1 – 24**

م.د.صفاء الدين حسين علي

Fabricating a new Rheometer for Concrete

Prof. Dr. Rafa Hashem Shaker
College of Engineering
University of Baghdad
rafiishaker@yahoo.co.in

Prof. Dr. Nada Mahdi Fawzi
College of Engineering
University of Baghdad
naljalawi@yahoo.com

Lect. Dr. Laith Al-Jabri
College of Engineering
University of Baghdad
laithjabri@yahoo.com

ABSTRACT

A new concrete rheometer is introduced including its innovation, actual design, working rules, calibration, and reliability. A modified design of Tattersall two-point device is created. Some of components are purchased from local and foreign markets, while other components and the manufacturing process are locally fabricated. The matching viscosity method of determining the mixer viscometer constants is demonstrated and followed to relate torque and rotational speed to yield stress and viscosity (Bingham parameters). The calibration procedures and its calculation are explained. Water is used as a Newtonian fluid, while; cement paste (cement + water) with w/c ratio equal to (0.442) is used as a non-Newtonian fluid. The cement paste is tested in "Petroleum Research and Development Center" by "OFITE Model 800 Viscometer". In order to verify the reliability of the new rheometer, an Artificial Neural Network (ANN) model with a well selected bank of data is constructed; and (16) Mixes of Self Compacting Concrete (SCC) are constructed, mixed and tested by the new Rheometer. The results from model (predicted) and those from the experimental work (measured) were found to have very good degrees of correlation and matching, which indicates that the new rheometer can be reliable.

Key Words: rheology, rheometer, SCC, yield stress, viscosity, ANN.

تصنيع جهاز قياس الانسيابية (الريوميتر) للخرسانة

أ.د.رافع هاشم شاكر
جامعة بغداد – كلية الهندسة

أ.د. ندى مهدي فوزي
جامعة بغداد – كلية الهندسة

م.د. ليث الجابري
الجامعة المستنصرية – كلية الهندسة

الخلاصة

تضمن البحث عرض علمي لعملية تطوير وتصنيع جهاز جديد لقياس الانسيابية (Rheometer) خاص بالخرسانة الطرية بما في ذلك الابتكار والتجديد في التصاميم السابقة للجهاز وبيان مباديء التشغيل والاسس النظرية والعملية للمعايرة والموثوقية. تم إعتماد تصميم محدث ومطور لجهاز (Tattersall two-point device). تم شراء بعض من الاجزاء الخاصة بالجهاز من الاسواق المحلية والاجنبية ، في حين تم تصنيع الاجزاء الاخرى وأجراء عملية الربط والتصنيع الكاملة محليا. تم توضيح واعتماد نظرية (مماثلة اللزوجة) المستندة الى ايجاد الثوابت التي تربط مابين قيم العزم والسرعة الدورانية وبين قيم إجهاد الخضوع واللزوجة. تم توضيح عملية المعايرة والنتائج الخاصة بها. تم استخدام الماء كسائل نيوتيبني ، في حين تم استخدام عجينة (الاسمنت - الماء) وبنسبة (0.442) (ماء/اسمنت) كسائل لا نيوتيبني. تم فحص عجينة (الاسمنت – الماء) في مركز البحوث والتطوير النفطي ، حيث تم الفحص بجهاز "OFITE Model 800 Viscometer". لغرض التحقق من موثوقية عمل الجهاز الجديد تم تصميم وتنفيذ موديل من نوع الشبكات العصبية الصناعية ، كما تم تصميم وخلط وفحص (16) خلطة من الخرسانة ذاتية الرص بواسطة جهاز الانسابيبة الجديد. تم مقارنة النتائج المستحصلة من الموديل مع تلك المستحصلة من الجزء العملي وكانت النتائج ذات درجات ارتباط وتطابق عالية مما يؤشر امكانية الاعتماد على عمل الجهاز.

الكلمات الرئيسية: الانسيابيه ,الريوميتر ،الخرسانه ذاتية الراس،أجهاد الخضوع،الزوجه،برنامج احصائي.

1. INTRODUCTION

Rheology is the science of the deformation and flow of matter, and the emphasis on flow means that it is concerned with the relationships between stress, strain, rate of strain, and time. Fluid rheology is well established, widely used science that is directly applicable to workability of fresh concrete. The characterization of rheology of fresh concrete is complicated by the fact that concrete is a complex material with time-dependent properties and includes wide range of particle sizes. In measuring rheological parameters of concrete, it is essential to know the flow properties over a wide range of shear stresses and shear strain rates. Various constitutive equations have been developed, the listing of such equations are given by **Whorlow, 1992. Ferraris, 1999. and Hackley, and Ferraris, 2001.** However, the most commonly used equation that is applied to fresh concrete is the Bingham Equation, where flow is described by the Eq. (1).

$$\tau = \tau_o + \mu\dot{\gamma} \qquad \text{Eq. (1)}$$

where :

τ = shear stress;

μ = plastic viscosity;

τ_o = yield stress; and

$\dot{\gamma}$ = shear strain or shear rate = dv / dy

2.RHEOLOGY OF SCC

SCC is a highly flowable concrete that is able to flow into places without vibration. Because SCC is essentially defined in terms of its workability, the characterization and control of rheology is crucial for the successful production of SCC. In terms of rheology, SCC exhibits a yield stress near zero and a moderate plastic viscosity. **Ferraris at al., 2000. and Koehler and Fowler, 2007.** stated that if the rheological properties that characterize SCC are examined, the yield stress must be zero or very low and the viscosity must be controlled. Empirical tests simulate a field condition and measure a quantity, such as a distance or time that is related to an aspect of workability. Empirical tests measure values that are related to fundamental rheological properties only indirectly, **Koehler and Fowler, 2007**. In empirical tests, the geometry of the concrete and the stresses acting on it at any given time are changing and not fully known, making it difficult to isolate the effects of fundamental flow properties. Therefore, rheological parameters can be preferable to empirical parameters, provided they can be measured in a practical manner and related to field placement requirements. **Fig.1** shows how two concretes could have one identical parameter and a very different second parameter. Therefore, it is important to use a test that will describe the concrete flow, by measuring (at least) both factors, **Ferraris, 1999.**

3.RHEOMETRIC APPARATUS

In order to determine real values of stress and rate (at the same point) an absolute instrument is needed, where the determination is made on the basis of a known mathematical description of flow occurring in the instrument and on the basis of its geometry. The measuring techniques can be divided into four principal ones, as shown in **Fig. 2** ,**Oskar, 2007.**

The instrument used these techniques is called ,**Rheometer. Leslie and Ji ,2001.** defined rheometer as the instruments for measuring flow behavior, which usually operate in rotation and measure torque and rotational speed and the rheological parameters of stress and strain rate are computed from these measurements.

According to **Hackley and Ferraris,2001.** rotational methods are generally better for concentrated suspensions, gels, and pastes despite the fact that capillary tube methods tend to be more precise in measuring viscosity.

"Impeller rheometers", can be defined as rotational rheometers which consist of an impeller that is rotated in a concrete specimen. Impeller rheometers can be simple to use; however, the shear rate and shear stress in the material around the impeller is unknown and the direct analytical calculation of fundamental rheological parameters is not possible. Although calibration procedures have been suggested to relate the intercept and slope of the torque versus rotation speed plot to yield stress and plastic viscosity, the accuracy of such procedures is debatable. Instead, results are often presented in terms of the slope *('h-value')* and intercept *('g-value')* of the torque versus rotation speed plot **Tattersall and Banfill,1983. Whorlow,1992. Ferraris ,1999. and Koehler and Fowler, 2006.**

3.1 Tattersall Two-Point Rheometer

The Tattersall two-point device was reportedly the first rheometer to measure concrete as a Bingham fluid. The device has been refined over the years by Tattersall and other researchers and continues to be widely used in research, **Tattersall and Bloomer,1979; Cabrera and Hopkins, 1984; Tattersall 1990; Bartos, Sonebi, and Tamimi, 2002; Ferraris and Brower,2004; Koehler and Fowler, 2006 and Josef , 2006.**

The original version of the two-point device, the MK I apparatus, was first presented in 1971 and consisted of a Hobart food mixer with a hook-shaped impeller moving in a planetary motion. The device, however, could not be used for high workability mixes.

Based on additional research, the MK I apparatus was later replaced by the MK II apparatus **Fig.3** for high workability mixes and the MK III for low to medium workability mixes.

MK II measures the pressure in a variable hydraulic transmission when turning an impeller in concrete at different speeds. Torque/Pressure calibration constant should be determined, **Tattersall and Banfill 1983.**

3.2 Laskar and Talukdar Rheometer

The rheometer which is designed by **Laskar and Talukdar , 2007. .Fig. 4** has the same concept of Tattersall two-point device. However, they used flat circular vane plate impeller, and the circuit for the purpose of calibration consists of a wattmeter, voltmeter, ammeter, and a 10 A variac. A spring balance anchored to a fixed object is fitted to the pulley of the spindle. When the motor is switched on, the spring balance blocks its rotor and the spring balance reading is noted. This arrangement gives the braking torques at different voltages. Thus for a set of voltages, braking forces or torques can be obtained.

4. ARTIFICIAL NEURAL NETWORKS

A neural network consists of a number of interconnected processing elements, commonly referred to as neurons. The neurons are logically arranged into two or more layers and interact with each other via weighted connections. These scalar weights determine the nature and strength of the influence between the interconnected neurons. Each neuron is connected to all the neurons in the next layer. There is an input layer where data are presented to the neural network and an output layer that holds the response of the network to the input. It is the intermediate layers, also known as hidden layers, which enable these networks to represent and compute complicated associations between patterns. Each hidden and

output neuron processes its inputs by multiplying each input by its weight, summing the product, and then passing the sum through a nonlinear transfer function to produce a result, **Goh ,1995.**
The neural network "learns" by modifying the weights of the neurons in response to the errors between the actual output values and the target output values. At the end of the training phase, the neural network should correctly reproduce the target output values for the training data, provided the errors are minimal, i.e., convergence occurs, **Kwan , 2000.**

5. NEW RHEOMETER DESIGN

Through searching in local engineering colleges, no available concrete rheometer exists in Iraq. Therefore, it is decided to adopt one of the available rheometer designs and fabricates a concrete rheometer. The modified design of Tattersall two-point device MK II is chosen for this purpose. The simple design and its continuously development through researches are the main are the main reasons for this choice.

5.1 First Adopted Design

The design of the Tattersall two-point device MK II that was donated for research purpose of **Josef, 2006.** work's **Fig. 5** is the first adopted design for current research purpose. This design consists of:

1. Electrical Motor which is used to generate the required rotation.
2. Variable Hydraulic Transmission Unit which is used to generate a pressure when turning the impeller in concrete.
3. Speed Control which is used to control and measure the speed of rotation.
4. Reduction Gear Box which is used to reduce the speed of motor rotation and increase the generated torque.
5. Pressure Gauge which is used to measure the generated pressure in the variable hydraulic transmission unit.
6. Interrupted Helical Impeller which is used to rotate the concrete sample.
7. Sample Holder which is used to hold the concrete sample.
8. Torque Calibration System **Fig. 6** which is used to determine the torque/pressure calibration constant. This system consists of an adjustable metal clamp with a copper sleeve, fixed so that the impeller drive shaft passes through it, and is used.

5.2 Modified Adopted Design

The first design and all of its components are studied carefully. The next step is going to be search for the availability of those components and the possibilities of fabrication. Through this search two important notes are recorded:

1. Instead of using an electrical motor and a reducing gear box as a separator device, a one unit that consists of both devices can be used. This has a big benefit of reducing the problems of coupling between the electrical motor and the reducing gear box.
2. Instead of using the variable hydraulic transmission unit, pressure gauge, and the torque calibration system which are used to measure and calibrate the generated torque, a Rotary Torque Transducer that measures the speed and torque strain in a rotating shaft can be used.

Taking previous two notes in consideration, the design is modified. The sketch of the modified adopted design is shown in **Fig.7**. The completed fabricated rheometer is shown in **Fig.8**. This design consists of below parts.

5.3 Electrical Motor and the Redaction Gearbox Vertical Unit (Figure 9):
This unit is chosen from Web-Drive which is a European company. The specifications of this unit are listed in **Table 1**.

5.4 Rotary Torque Transducer
This component is chosen from a British company, and it consists of three units; M420 Rotary Torque Transducer, Transducer Interface, and software package "TorqueLog". The specifications of these units are:

A - M420 Rotary Torque Transducer:

The Series M420 Rotary Torque Transducer **Fig.10**. measures the speed and torque strain in a rotating shaft. Signal output is transmitted directly from the shaft as serial data and providing clean and definitive data transmission. M420 rotary torque transducer is connected with the gearbox by a locally made stainless steel connector see **Fig. 11**. The specifications of M420 rotary torque transducer and its dimensions according to **Fig.12** are listed in **Table 2**. The purchased M420 rotary torque transducer is calibrated by Datum Electronics Ltd, and a Torque Calibration Certificate **Fig.13** is supplied with the device.

B - Transducer Interface:

This unit **Fig.14** receives the signal output from the transducer and converts it digitally through a USB converter to PC. The Transducer interface requires 15-24Volts dc supply power. The M420 connects directly to this interface.

C - Software Package "TorqueLog":

Datum Electronics TorqueLog software is an easy and convenient way of collecting data. This software provides a direct readout of Torque, Speed and Power on a PC with additional facilities to read peak torque and log data to other applications including Microsoft Excel. The features of this software include:

• Calibrated Display of Torque in Nm or lb/ft

• Display of Speed (rpm)

• Display of Power in kW or HP

• Peak Torque, Speed and Power Capture Facility

• Data logging of Torque (or Torque, Speed and Power)

Fig. 15. shows the interface window for this software.

D - AC Frequency Conversion Speed Regulator:

AdvanCon-SID32-G-S2 series **Fig.16** high functional conversion regulator is chosen to be the speed controller.

E - Interrupted Helical Impeller:

An axial stainless steel impeller with four angled blades set in a helical pattern around a central shaft which imparts a stirring and mixing action to the concrete is designed, fabricated and used for the purposes of this study. This type of impeller is chosen because it is suitable for slumps in excess of about 100 mm as referred to by **Ferraris and Brower , 2001.** The impeller is made in two parts. The first upper part is fixed to the body by a stainless steel ring that contains a bearing fixture in the middle and through this bearing it connects with the torque transducer **Fig.7.** This arrangement provides good support and free movement to the impeller and assures no direct load on the transducer. The other (lower) end of this part is externally threaded See **Fig.18**. The second lower part of this impeller is a free part that can be screwed to the upper part during running the rheometer or it can be removed out for cleaning. The lower end of this part contains four trapezoidal blades, right angled in its position, set and welded in a helical pattern around the central shaft. Total length of the shaft is (850 mm) and its diameter is (50 mm). Larger base of the blade is (65 mm), while smaller base is (35 mm), and the height of the base is (55 mm).

F - Sample Holder Fig. 9.

This is a metal cylindrical container with (254 mm) diameter and (305 mm) height. It is provided with vertical metal ribs at a pitch of 60 mm along the circumference. Ribs are welded at the wall of the cylinder. The effective gap between the bottom and the shearing surface is 60 mm. The effective concrete height above the vane plate is 75 mm. The no-slip condition at top of the cylinder is achieved by providing the mesh of blades.

5.5 Calibration of the Rheometer

Since it is shown through the literature that the flow properties of concrete conform to the Bingham model, the flow curves are taken as linear, the intercept on the torque axis and the reciprocal slope can also be calculated using the least squares method. The flow curve is represented by:

$$T = g + hN \qquad \text{Eq. (2)}$$

Where *(T)* is the torque at speed *(N)*, *(g)* is a measure of the yield value and *(h)* is a measure of plastic viscosity.

The values of *(g)* and *(h)* are calculated mixer viscometry method. Extensive work has been conducted on mixer viscometry **Castell and Steffe 1992.** This technique has been used mostly for non-reacting biological materials. But also it is applied in evaluating the workability of fresh concrete **Tattersall and Banfill , 1983** , and to chemo-rheological studies involving starch gelatinization **Dolan and Steffe 1990 and Steffe et al., 1989.**

The specific technique used in the current study for applying the matching viscosity method was developed by **Mackey et al 1987**and later described as the torque curve method by Castell-Perez and **Steffe 1990.** The following analysis is based on the work of those researchers.

5-6 Power Number (N_{Po}) & Reynolds Number (N_{Re})

Those dimensionless numbers are defined to the impeller, which takes the power *"P"* whose diameter is *"d"* whose rotational speed is *"N"* in fluid, and whose density and viscosity are *"ρ"* and *"η"*, by following equations:

$$N_{Po} = \frac{P}{N^3 d^5 \rho} \quad (3) \qquad \text{and} \qquad N_{Re} = \frac{N d^2 \rho}{\eta} \quad (4)$$

The power is equal to the product of torque and angular velocity: $= T * N$, where T is the torque. Thus, the Eq. (3) can be written with respect to the torque, rotational speed, effective diameter, density, and viscosity as:

$$N_{Po} = \frac{T}{N^2 d^5 \rho} \quad (5)$$

With a single phase fluid operating at low speed, or in a baffled system, the power number can be expressed with the impeller Reynolds number alone:

$$N_{Po} = f(N_{Re})$$

$$N_{Po} = A * (N_{Re})^B \quad (6)$$

Where *"A"* and *"B"* are constants depending on the geometry of the system and the flow regime present during mixing. *"B= -1"* when *"N_{Re} < 10"*, and *"B= 0"* when *"N_{Re} > 10 000"*. The values of *"A"* and *"B"* in the intermediate region will depend on the particular mixing system under consideration.

5.7 Apparent Viscosity

Apparent viscosity has a precise definition. It is shear stress divided by shear rate:

$$\eta = f(\dot{\gamma}) = \frac{\tau}{\dot{\gamma}} \quad (7)$$

With Newtonian fluids, the apparent viscosity and the Newtonian viscosity (μ) are identical but for a power law fluid is:

$$\eta = f(\dot{\gamma}) = \frac{\tau}{\dot{\gamma}} = \frac{K(\dot{\gamma})^n}{\dot{\gamma}} = K(\dot{\gamma})^{n-1} \quad (8)$$

Apparent viscosity for Bingham plastic fluids is determined in a like manner:

(9)

$$\eta = f(\dot{\gamma}) = \frac{\tau}{\dot{\gamma}} = \frac{\mu_{pla}(\dot{\gamma}) + \tau_o}{\dot{\gamma}} = \mu_{pla} + \frac{\tau_o}{\dot{\gamma}}$$

5.8 Average Shear Rate

Newtonian fluid viscosity (μ) is replaced by an apparent viscosity (η) evaluated at an average shear rate *($\dot{\gamma}_a$)* defined as:

$$\dot{\gamma}_{av} = k' * N \quad (10)$$

where *(k′)* is the mixer viscometer constant having units of 1/rad or 1/rev. *(k′)* is unique for any particular physical system and must be determined from experimental data.

In mixer viscometry, there are two primary techniques for determining *(k′)* the "Slope Method" and the "Viscosity Matching Method." Viscosity Matching Method is a technique that involves the comparison of power curves for Newtonian and non-Newtonian fluids using the idea of matching viscosities. The

phrase "matching viscosities" refers to the assumption that the average shear rate for a non-Newtonian fluid is equal to the average shear rate for a Newtonian fluid when the Newtonian viscosity equals the apparent viscosity of the non-Newtonian fluid. The technique is excellent for determining the average shear rate in a mixer and is also useful to rheological process engineers in evaluating the performance of commercial equipment (Rheometers) having poorly defined shear fields.

5.9 Derivation of Mixer Viscometry Relations

1- Power Flow Fluids: Working equations are developed starting with the assumption that surface tension, elastic, and vortexing effects are insignificant, the physical variables involved in mixing Newtonian and Non- Newtonian fluids in the laminar flow regime where *(N_{Re} < 10)*, then:

$$N_{Po} = \frac{A}{N_{Re}} \tag{11}$$

Substituting with **Eqs. (4)** and **(5),** gets

$$N_{Po} = \frac{\eta A}{Nd^2\rho} \tag{12}$$

using the definition of apparent viscosity for a power flow fluid **Eq. (8)**

$$N_{Po} = \frac{AK(\dot{\gamma})^{n-1}}{Nd^2\rho} \tag{13}$$

using the definition of average shear rate

$$N_{Po} = \frac{AK(\dot{\gamma}_{av})^{n-1}}{Nd^2\rho} \tag{14}$$

and solve for the average shear rate:

$$\dot{\gamma}_{av} = \left(\frac{Nd^2\rho N_{Po}}{AK}\right)^{1/n-1} \tag{15}$$

2- Bingham Plastic Fluids: Using the same assumption in above paragraph and the Eq**. (11)** and **(12)** and the definition of apparent viscosity for a Bingham plastic fluid (Eq.(9)):

$$\frac{T}{N^2d^5\rho} = \frac{A(\mu_{pla} + \tau_o/\dot{\gamma})}{Nd^2\rho} \tag{16}$$

using the definition of average shear rate and **Eq. (10)**

$$\frac{T}{N^2d^5\rho} = \frac{A(\mu_{pla} + \tau_o/k'N)}{Nd^2\rho} \tag{17}$$

then simplifying the resulting equation gives an expression relating torque and speed in a mixer viscometer:

$$T = \frac{Ad^3}{k'}\tau_o + Ad^3\mu_{pla}N \tag{18}$$

Collecting mixer rheometer data of torque versus angular velocity for a Bingham plastic and plotting the result will provide a slope ($Ad^3\mu_{pla}$) and an intercept ($Ad^3\tau_o/k'$) that reflect the rheological properties of the fluid. If *(A)* and *(k′)* are known, plastic viscosity and the yield stress can be calculated. Comparing between Equation (1) and Equation (18):

$$g = \frac{Ad^3}{k'}\tau_o \qquad (19)$$

then

$$\tau_o = \frac{gk'}{Ad^3} \qquad (20)$$

$$h = Ad^3\mu_{pla} \qquad (21)$$

then

$$\mu_{pla} = \frac{h}{Ad^3} \qquad (22)$$

5.10 Determination of Parameters

1- Using Water as a Newtonian fluid in the mixer rheometer, the constant *(A)* is determined from the experimental data.

a. Involving **Eq.(4)** to determine (N_{Re}), where, "ρ" for water is (1000 kg/m3), "η" for water is (0.001 kg/m.s), "N" the rotational speed in (rad/sec.), and the effective diameter for the impeller (d) is (0.16 m). **Table 3** shows that the average value of (N_{Re}) is about (120637).

b. Involving **Eq.(5)** to determine (N_{Po}), where, "T" units is (Nm), "ρ" for water is (1000 kg/m3), "N" is the rotational speed in (rad/sec.), and the effective diameter for the impeller (d) is (0.16 m). **Table 3** also, shows that the average value of (N_{Po}) is (0.095).

c. Since "N_{Re} > 10000", then "B= 0". Substituting this value in **Eq. (6)** yields (A) equal to (N_{Po}). Then (A = 0.09499).

2- Determination value of (k′), a non-Newtonian power flow fluid (or pseudo-plastic fluid) should be tested in a routine viscometer (like a concentric cylinder or cone and plate system). Through the traditional rheological techniques, the properties (K) and (n) of a power law fluid can be determined. This reference power law material is then tested by the rheometer (under study), and mixed at a several speeds. Next, the matching viscosity assumption is applied and an average shear rate ($\dot{\gamma}_{av}$) and (k′) values are calculated. (k′) is calculated {as it is equal to ($\dot{\gamma}_{av}/N$)} at numerous impeller speeds to determine how (k′) may vary with (N). An average value of (k′) may be taken to represent the constant required in **Eqs. (19)** and **(20).**

a. Cement slurry (cement + water) with w/c ratio equal to (0.442) is used as a power flow fluid. This slurry is tested in "Petroleum Research and Development Center". Their "OFITE Model 800 Viscometer" which is a Coaxial Cylinder Viscometer. The cement slurry is tested at seven speeds (6, 30, 60, 100, 200, 300, and 600 rpm). Obtained shear stress and shear rate values are plotted in Figure (20). This power flow curve show that (K) is equal to (10.63) and (n) is equal to (0.305). The shape of the curve and (n) value which is less than (1) indicates that the tested cement slurry is a "Shear Thinning" fluid.

b. The cement slurry with same materials and proportions that used in the previous paragraph is tested by this study's rheometer. The specimen is sheared at seventeen speeds **Table 4**. Values of ($\dot{\gamma}_{av}$) and (k′) at those seventeen speeds and their averages are determined by using **Eq.s (10) and (15)** and listed in **Table 4**, also.

3- As (A= 0.09499) and (k′ ≈ 0.0958) values are calculated, and as (d = 0.16 m), then (Ad^3 ≈ 0.000389), by using Equations (20) and (22):

$$\tau_o \approx 246\, g \qquad (23) \qquad \text{and} \qquad \mu_{pla} \approx 2570\, h \qquad (24)$$

6.EXPERIMENTAL PROGRAM

In order to evaluate and verify the rheological properties of SCC mixtures by the new Rheometer, (16) mixes of SCC are designed, mixed and tested. A detailed description of the experimental work carried out in the present study is demonstrated below.

6.1 Materials

1- Iraqi ordinary Portland cement (Taslogah) type (I). This cement is tested and checked according to IOS 5:1984. **Table 5** shows the chemical and physical properties of this cement and the criteria of IOS 5:1984 for each one.
2- Natural sand is used in this work. **Table 6** shows the grading of the fine aggregate and the limits of the Iraqi specification No.45/1984; and the physical properties of the fine aggregate.
3- Rounded gravel of nominal size (5-14) mm is used. **Table 7** shows the grading of this aggregate which conforms to the Iraqi specification No.45/1984, the specific gravity, sulfate content and absorption of coarse aggregate.
4- Tap water is used for both mixing and curing of concrete.
5- A third generation admixture for concrete and mortar named Sika ViscoCrete Hi-Tech 32 is used.

6.2 Concrete Mix Design

Initially EFNARC (2005) first approach for mix design method is used, and then the proportions of materials modified after the evaluation by fresh tests is done. The modifications are made according to EFNARC (2005) also.

6.3 Mix Proportions

In order to achieve the scopes of this study, the mixes are categorized into five groups. Each group represents one of the factors that affects rheology and strength of SCC. These groups are listed in **Table 8. Tables 9 and 10** show mix proportions. All proportions are based on volumetric mix design procedure.

6.4 Mixing Procedure

The mixing procedure that used in this study is briefly stated in the following:

1. The fine aggregates are added to the mixer with 1/3 quantity of water and mixed for 1 minute.
2. The cement and mineral admixtures are added with another 1/3 quantity of water. Then the mixture is mixed for 1 minute.
3. After that, the coarse aggregate is added with the last 1/3 quantity of water and 1/3 dosage of superplasticizer, and the mixing lasts for 1 ½ minute then the mixture is left for ½ minute for rest.
4. Then, the 2/3 leftover of the dosage of superplasticizer is added and mixed for 1 ½ minute.
5. The mixture is then discharged, tested and cast.

6.5 Workability (Empirical) Measurements

These tests include slump-flow (SFD), L-box, U-box and V-funnel (TV) tests. All of these tests are used to verify the filling ability, passing ability, and segregation resistance of all mixes of this study. The apparatus and the tests procedure are made according to the specifications and requirements mentioned in **Efnaec, 2005.** These apparatus are made from steel plate in the local market.

6.6 Procedure of Rheological Tests

Before testing can be done, the hardware (the torque transducer and its interface) should be connected and installed on the PC. Also, the TorqueLog software should be installed on the PC. The apparatus must be set up to be leveled. The procedure for testing is as follows:

1. Turn on the power source and let the impeller to rotate at speed of 15 rpm.
2. Fill the sample holder gradually with concrete to about 75 mm from the rim while the impeller rotates.
3. Increase the speed each 1 minute by steps 25, 35, 45, 55, 65, and 75 rpm.
4. The results are automatically fed to the PC in Microsoft Excel spreadsheet.

6.7 Verifying Reliability of Rheometer

In order to verify the reliability of the new rheometer, the following steps are followed:

1- Construct an ANN model with a well selected bank of data. This bank of data should have a suitable volume (number of mixes) that the better performance of the model can be achieved. Experimental data from (35) different sources is used to check the reliability of the model. In all about (700) SCC samples are evaluated. The evaluation processes are done in two stages. The first stage is involved with the input parameters, while the second stage is involved with the input and output parameters. After these two stages of evaluation, only (541) sets are adopted to be the model data base. (22) Variables (masses of constituents) are chosen to be as the input variables. While (8) variables represent the rheology, fresh and hardened properties of SCC are considered as the output variables.

2- These (16) sets of mixes are used as a validation set in the ANN model. This validation set does not have any effect on the training of the model. The predicated results of the validation set are compared with the experimentally measured results of the rheological tests.

6.8 Results of ANN Model

ANN model is fed forward neural network, which are trained by the (BFGS) optimization algorithm. The topography and training parameters obtained through trial and error for the ANN model thus developed are done with the aid of a commercial analytic software package called “StatSoft Statistica version 8” which is used to analyze, design and execute these models.

ANN model is constructed to predict yield stress and viscosity. The best performance is found to be the architecture of Multi Layers Perceptron (MLP) 22-35-8 (one input layer that contains 22 elements; one hidden layer that contains 35 elements; and one output layer that contains 8 elements).

Results of this model are listed in **Table 11**, and **Figs. 21 and 22** show correlation diagrams between train and test values for this model. The results show, very good percentages of correlation between target and output values with very low values of errors, and high percentage of matching between targets and outputs, and no clear trend to overestimation or underestimation. The results proved that these models are able to predicate SCC rheological parameters effectively, and the ANN model can be a good tool to verify the performance of the new rheometer.

6.9 Results of Experimental Rheological Tests

According to the procedure of testing with rheometer, every specimen is sheared under (7) speeds. However, the first and lowest speed is not adopted as a factor. The rest six speeds are (25, 35, 45, 55, 65, and 75 rpm). The specimen is sheared for (1) minute at each interval of speed. The output file of “TorqueLog” software provides about (5400) readings of (T) and (N) for each minute. Average readings for (T) and (N) at each speed are adopted and plotted as scatter-plots. Square of correlation coefficient “R^2” values and equation of linear regression fit are listed in Table (12). The intercept and

slope values of each linear regression equation are respectively used as *(g)* and *(h)* values in Equations (23) and (24). The calculated values of Yield Stress (τ_o) and Viscosity (μ) are listed in **Tables 13 and 14,** respectively, which also showed the predicted values of those two properties.
Figs. 23 and 24 show the correlation diagrams between predicted and measured results. The correlation coefficient between results of yield stress and viscosity are ($R^2 \approx 0.91$) for both of them. These figures demonstrate that the values of parameters of Bingham model (yield stress and viscosity) can be determined with high accuracy with correlation coefficients. The arrangements of points of results and the nature of predicted and measured results are displayed in **Figs. 25 and 26.** These figures show a very high percentage of matching between predicted and measured results.

7.CONCLUSIONS

The conceptual and new design of Tattersall two-point rheometer suitable for concrete has been outlined. The rheometer has been built up and used to obtain Bingham parameters related to SCC.
The proposed rheometer considers frictional resistance between concrete and vertical wall of cylindrical container. An expression for shear stress has been derived in terms of torque and average shear strain rate in terms of rotational speed have been obtained for given geometrical parameters of the rheometer. Torque and rotational speed have been measured using a Rotary Torque Transducer. The rheometer has been validated by testing (16) mixes of SCC and compared their measured results with the predicted measures that obtained by ANN predicting model. Very good percentages of correlation coefficient (0.91for both) are shown between measured and predicted results of yield stress and viscosity. All of the results indicate that the new rheometer able to be relied on.

REFRENCES

Bartos, P.J.M., Sonebi, M., Tamimi, A.K. (Eds.), 2002. *Workability and Rheology of Fresh Concrete* Compendium of Tests," Cachan Cedex, France: RILEM.

Cabrera, J.G., and Hopkins, C.J. , 1984. *A modification of the Tattersall Two-Point Apparatus for Measuring Concrete Workability,* Magazine of Concrete Research, 36(129), 237-240.

Castell-Perez, M. E., and Steffe, J. F, 1990 *Evaluating Shear Rates for Power Law Fluids in Mixer Viscometry*, J. Texture Stud.21:439-453.

Castell-Perez, E.M. and J.F. Steffe, 1992. *Using Mixing to Evaluate Rheological properties*, In: Rao, A.M. and J.F. Steffe (editors). Viscoelastic Properties of Food. Elsevier Applied Sci. Pub., Ltd., Barking, England. pg. 247-284.

Dolan, K.D. and J.F. Steffe, 1990. *Modeling the Rheological Behavior of Gelatinizing Starch Solutions using Mixer Viscometry Data*, J. Texture Stud. 21: 265-294.

Eric P. Koehler and David W. Fowler, 2006. *Development and Use of a Portable Rheometer for Concrete*, Eighth CANMET/ACI International Conference on Recent, Advances in Concrete Technology, , Montreal, Canada, June.

Eric P. Koehler and David W. Fowler, 2007. *Aggregates in Self Consolidating Concrete*. International Center for Aggregates Research (ICAR) .

Ferraris, C. F , 1999. *Measurement of the Rheological Properties of High Performance Concrete: State of the Art Report*, J. Res. Natl. Inst. Stand. Technol., Vol. 104, No. 5, pp. 461–478.

Ferraris C. F., Larrard F. and Martvs N , 2000. *Fresh Concrete Rheology: Recent Developments*, National Institute of Standards and Technology.

Ferraris, C.F., and Brower, L.E. (Eds.), 2001. *Comparison of Concrete Rheometers* International tests at LCPC (Nantes, France) in October 2000. (NISTIR 6819). Gaithersburg, MD: National Institute of Standards and Technology .

Ferraris, C. F., and Brower, L. E. (Eds.), 2004. *Comparison of Concrete Rheometers: International Tests at MB (Cleveland OH, USA) in May 2003*, NISTIR 7154, National Institute of Standards and Technology Gaithersburg, MD.

Goh, A. T. C, 1995. *Neural Networks for Evaluating CPT Calibration Chamber Test Data*, Microcomputers in Civil Engineering, Vol. 10, pp. 147-151 .

Josef Petrus Jooste, 2006. *Approaches to Mix Design and Measurement of Workability for Self-Compacting Concrete*, M.Sc. Thesis, University of the Witwatersrand, Johannesburg.

Kwan, A. K. H, 2000. *Use of Condensed Silica Fume for Making High-Strength, Self-Consolidating Concrete,* Canadian Journal of Civil Engineering, Vol. 27, No. 4, pp. 620-627.

Leslie J. Struble and Xihuang Ji, 2001. *Handbook of Analytical Techniques in Concrete Science and Technology*. Institute for Research in Construction National Research Council Canada .

Laskar A. I., and Talukdar S , 2007 *Design of a New Rheometer for Concrete*, Journal of ASTM International, Vol. 5, No. 1).

Mackey, K. L., Morgan, R. G., and Steffe, J. F 1987. *Effects of Shear-Thinning Behavior on Mixer Viscometry Techniques*, J. Texture Stud. 18:231-240.

Oskar Esping, 2007. *Early Age Properties of Self Compacting Concrete*, Department of Civil and Environmental Engineering, Chalmers University Of Technology, Göteborg, Sweden.

Steffe, J.F., F.A. Osorio and R.Y. Ofoli, 1989."*Dynamic and Steady Rheological Properties of Starch based Pie Filling. In: Ang, H.G. (editor). Trends in Food Science. Part Six, Rheological Studies*, pg. 128-130, The Singapore Inst. Food Sci. and Technol., Republic of Singapore.

Tattersall, G.H., and Bloomer, S.J, 1979,*Further Development of the Two-Point Test for Workability and Extension of its Range,* Magazine of Concrete Research, 31(109), 202-210.

Tattersall, G.H., and Banfill, P.F.G, 1983. *The Rheology of Fresh Concrete*. Marshfield, MA: Pitman Publishing.

Tattersall,G.H., 1990. *Progressin Measurement of Workability by the Two-Point Test,* H.-J. Wierig, Ed., Properties of Fresh Concrete, Proc of the Coll. RILEM, Chapman and Hall, 203-212.

Vincent A. Hackley and Chiara F. Ferraris, 2001. *Guide to Rheological Nomenclature: Measurements in Ceramic Particulate Systems*, NIST Special Publication 946.

Whorlow,R.W, 1992. *Rheological Techniques*. Chicheser, West Sussex, England: Ellis Horwood Limited.

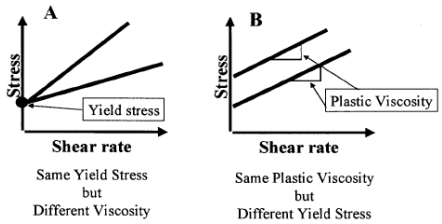

Figure 1. Concrete Rheology.

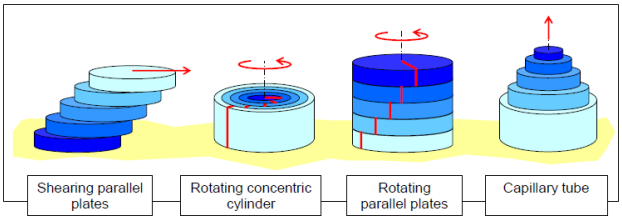

Figure 2. Four Main Rheological Techniques **.**

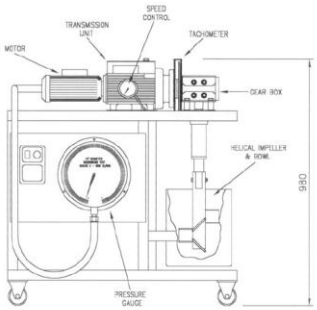

Figure 3. Mk II Apparatus.

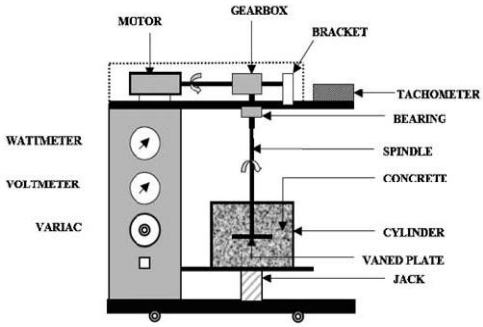

Figure 4. Schematic diagram of Laskar and Talukdar Rheometer.

Figure 5. First adopted design of Mk II apparatus.

Figure 6. Side view of torque calibration equipment.

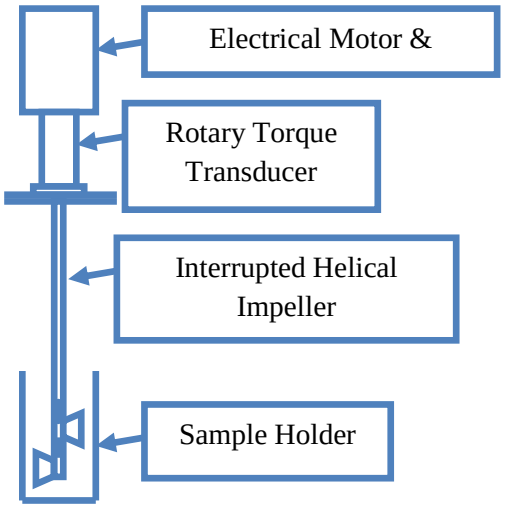

Figure 7 . Sketch of modified design**.**

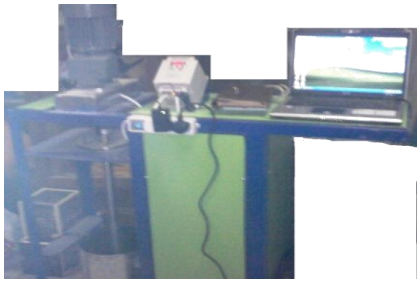

Figure 8. Completed new Rheometer

Figure 9. Vertical unit of electrical motor & reduction gearbox.

Figure 10. M420 rotary torque transducers.

Figure 11. Connection between M420 rotary torque transducers and gearbox**.**

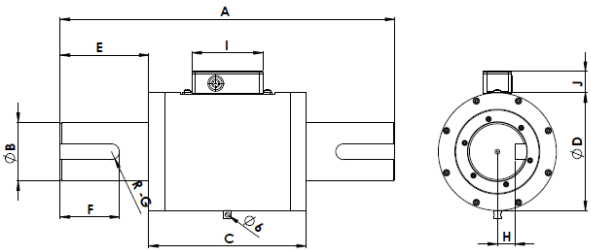

Figure 12. Front and side diagrams of M420 rotary torque transducers.

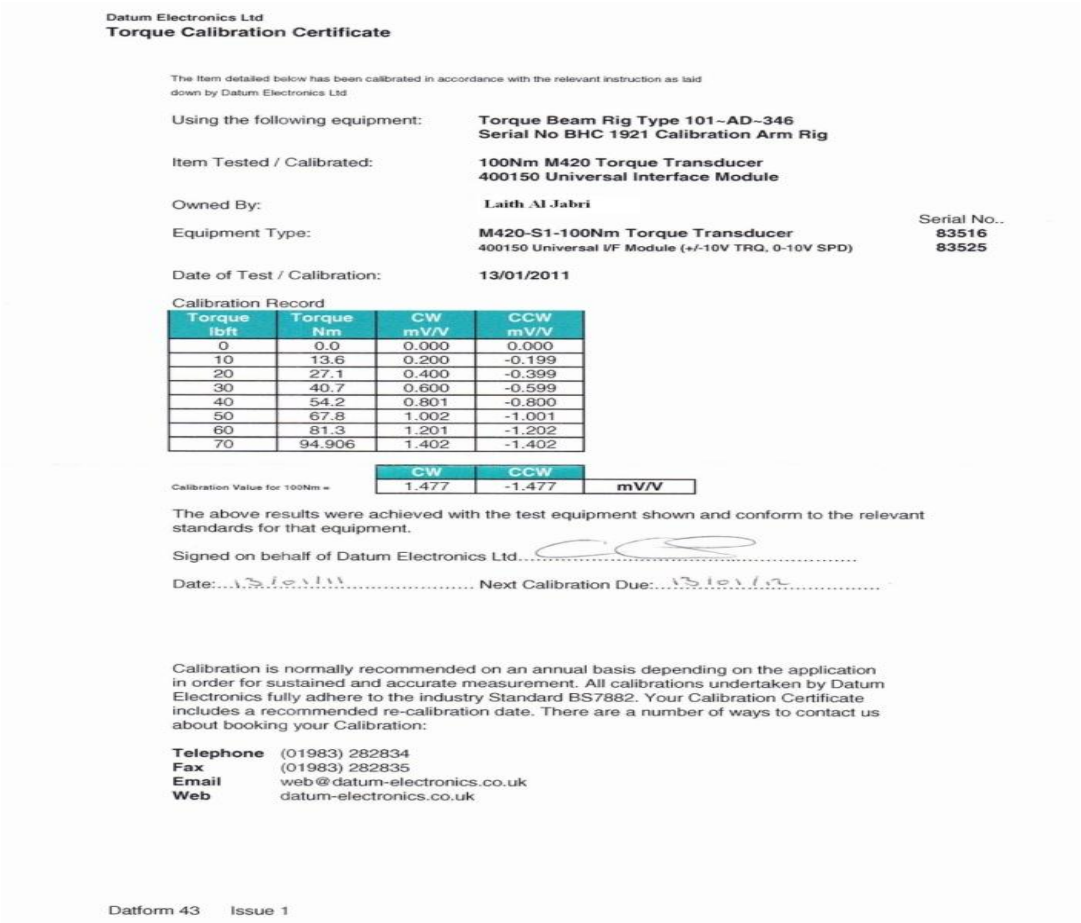

Datum Electronics Ltd
Torque Calibration Certificate

The Item detailed below has been calibrated in accordance with the relevant instruction as laid down by Datum Electronics Ltd

Using the following equipment: **Torque Beam Rig Type 101~AD~346 Serial No BHC 1921 Calibration Arm Rig**

Item Tested / Calibrated: **100Nm M420 Torque Transducer 400150 Universal Interface Module**

Owned By: **Laith Al Jabri**

Equipment Type: **M420-S1-100Nm Torque Transducer** Serial No.. **83516**
400150 Universal I/F Module (+/-10V TRQ, 0-10V SPD) **83525**

Date of Test / Calibration: **13/01/2011**

Calibration Record

Torque lbft	Torque Nm	CW mV/V	CCW mV/V
0	0.0	0.000	0.000
10	13.6	0.200	-0.199
20	27.1	0.400	-0.399
30	40.7	0.600	-0.599
40	54.2	0.801	-0.800
50	67.8	1.002	-1.001
60	81.3	1.201	-1.202
70	94.906	1.402	-1.402

Calibration Value for 100Nm =	CW	CCW	
	1.477	-1.477	mV/V

The above results were achieved with the test equipment shown and conform to the relevant standards for that equipment.

Signed on behalf of Datum Electronics Ltd.....

Date:...13/01/11..... Next Calibration Due:...13/01/12.....

Calibration is normally recommended on an annual basis depending on the application in order for sustained and accurate measurement. All calibrations undertaken by Datum Electronics fully adhere to the industry Standard BS7882. Your Calibration Certificate includes a recommended re-calibration date. There are a number of ways to contact us about booking your Calibration:

Telephone (01983) 282834
Fax (01983) 282835
Email web@datum-electronics.co.uk
Web datum-electronics.co.uk

Datform 43 Issue 1

Figure 13. Torque calibration certificate.

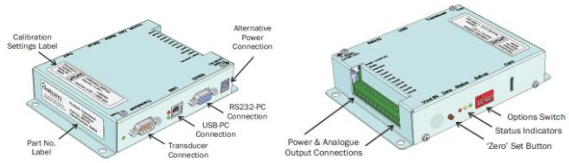

Figure 14. Transducers interface**.**

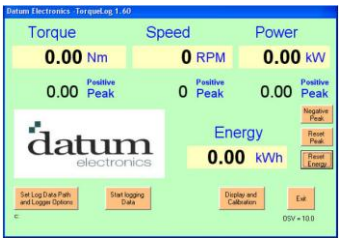

Figure 15. Torque log interface window.

Figure 16. Advanon AC frequency conversion speed regulator.

Figure 18. Lower part of impeller.

Figure 17. Upper part of impeller**.**

Figure 19. Sample holder.

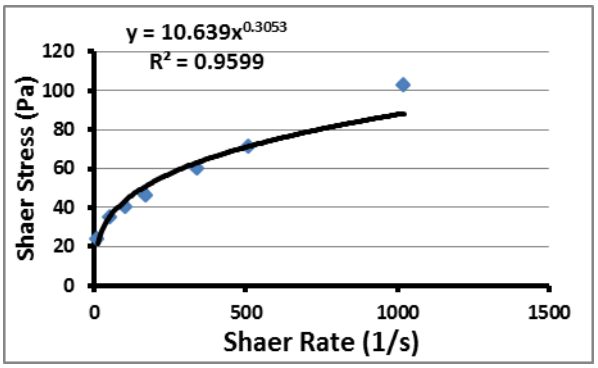

Figure 20. Shear stress vs. shear rate of cement slurry: OFITE model 800 viscometer.

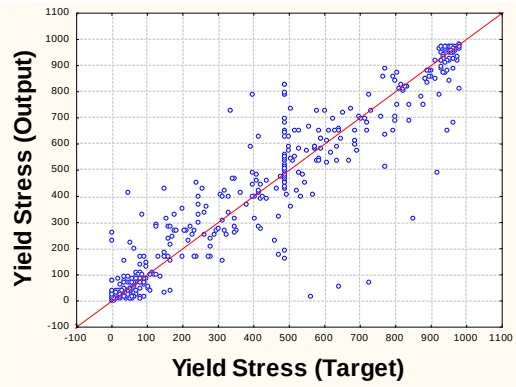

Figure 21. Correlations diagram of RP-CS model (Yield Stress)

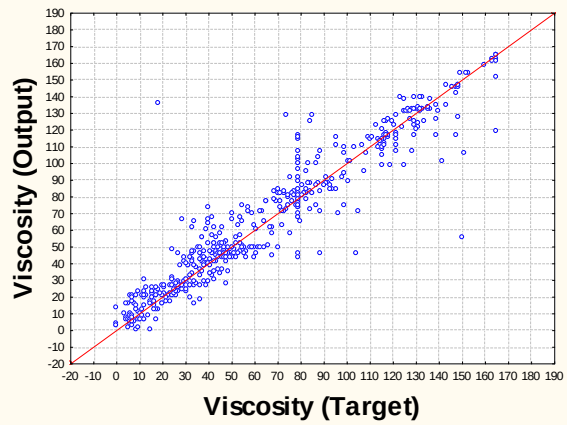

Figure 22. Correlations diagram of RP-CS model (Viscosity).

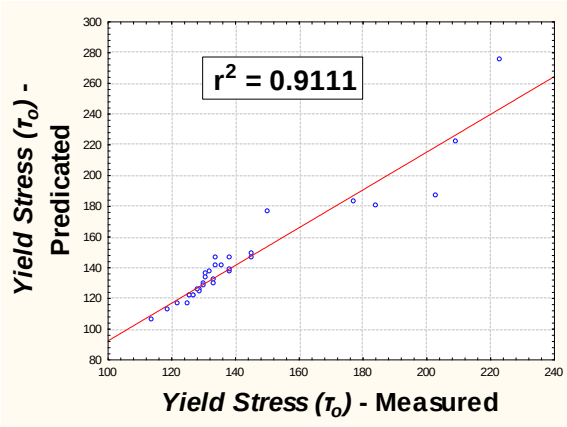

Figure 23. Correlations diagram between predicated and measured: yield stress (τ_o).

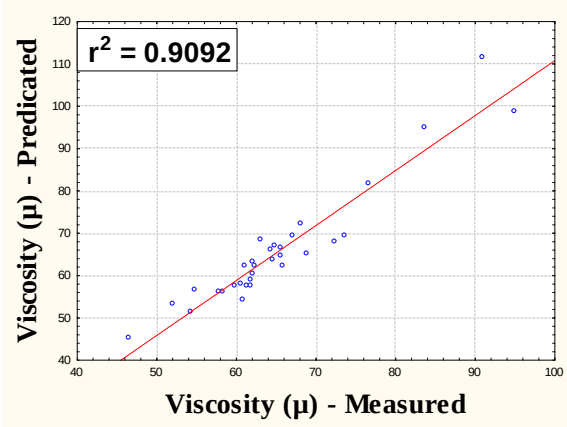

Figure 24. Correlations diagram between predicated and measured: Viscosity (μ).

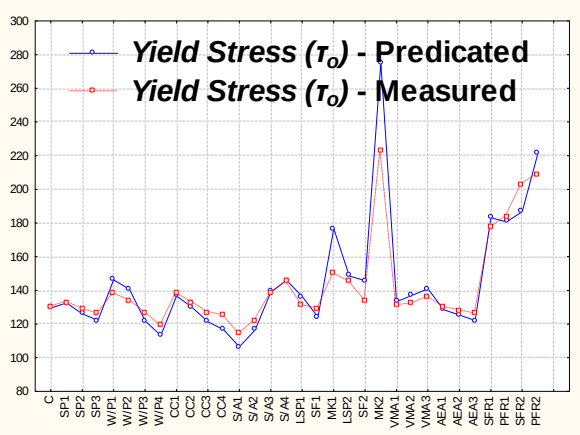

Figure 25. Points of predicated and measured results: Yield stress (τ_o)

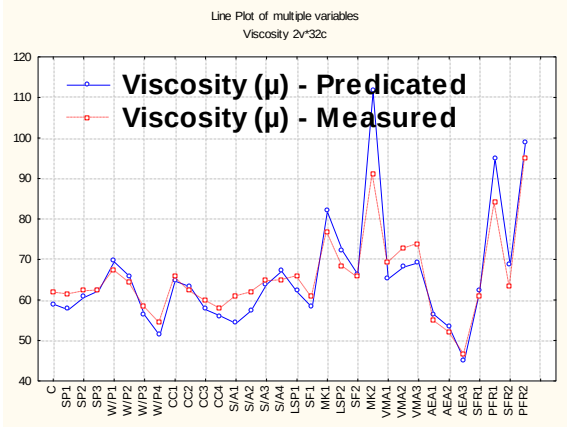

Figure 26. Points of predicated and measured results: Viscosity (μ).

Table 1. Specifications of Electrical Motor & Gearbox.

a- Electrical Motor:	
Power	0.75 kw
Amp.	3.6 – 2.1
Voltage	220 – 380
Frequency	50 Htz
Speed	1645 RPM
b- Gearbox:	
Power	0.75 kw
Speed	126 RPM
Reduction Ratio	1:14

Table 2. Specifications and dimensions of M420 rotary torque transducer (Size1).

Specifications	
Torque Ratings	0-100Nm
Max Rotation Speed	0-10,000 rpm
Accuracy	0.1%
Operating Temp	0-70ºC
Supply Voltage	15-24VDC
Cable Length	4 metre to interface (Standard)
Dimensions	
A: Overall Length	184 mm
B: Shaft Diam	15 mm
C: Body Length	129 mm
D: Body Diam	60 mm
E: Exposed Shaft Length	27.5 mm
F: Keyway Length	22.5 mm
G: Keyway Width	5 mm
H: Keyway Depth off centre	4.3 mm

Table 3. Experimental data for water test: (N_{Re}) & (N_{Po}) values.

N(rad/s)	d (meter)	ρ (kg/m^3)	η (kg/m.s)	T (Nm)	N_{Re}	N_{Po}
1.570796327	0.16	1000	0.001	0.070581	40212.39	0.272803
2.617993878				0.084697	67020.64	0.117851
3.665191429				0.105872	93828.9	0.07516
4.71238898				0.155278	120637.2	0.066685
5.759586532				0.176453	147445.4	0.0 0728
6.806784083				0.211743	174253.7	0.043584
7.853981634				0.247034	201061.9	0.038192
				Average	**120637.2**	**0.09499**

Table 4. Experimental data for cement slurry: Study's Rheometer.

N (rpm)	N (rps)	$\dot{\gamma}_a$ (1/s)	k' (1/rev)
25	0.416667	0.34229433	0.821506393
35	0.583333	0.210670077	0.361148704
45	0.75	0.146701589	0.195602119
55	0.916667	0.109885039	0.119874588
65	1.083333	0.086390424	0.079745007
75	1.25	0.070302799	0.05624224
85	1.416667	0.05870804	0.04144097
95	1.583333	0.050019442	0.031591227
105	1.75	0.043306018	0.024746296
115	1.916667	0.037988833	0.01982026
125	2.083333	0.03369073	0.01617155
135	2.25	0.03015645	0.013402867
145	2.416667	0.027207643	0.011258335
155	2.583333	0.024716285	0.009567594
195	3.25	0.017758693	0.005464213
225	3.75	0.014451669	0.003853778
235	3.916667	0.013574477	0.003465824
250	4.166667	0.012417301	0.002980152
275	4.583333	0.010824847	0.002361785
Average			0.095802311

Table 5. Chemical and physical composition of cement.

Chemical Composition					
Oxides	Test Results	IOS 5:1984 criteria	Oxides	Test Results	IOS 5:1984 criteria
SiO_2	19.22	-	SO_3	2.03	< 2.8
Fe_2O_3	3.34	-	L.S.F	1.01	0.66 - 1.02
Al_2O_3	4.51	-	L.O.I	3.72	< 4
CaO	63.26	-	I.R	0.84	< 1.5
MgO	2.62	< 5	C_3A	6.59	-

Physical Properties			
Properties	Test Results	IOS 5:1984	
Specific surface area (Blaine Method), m2/kg	352	> 230	
Mortar Compressive strength (MPa) at	3 days	20.8	> 15
	7 days	26.00	> 23
Setting Time(min)	Initial	141 min.	≥ 45 min.
	Final	320 min.	≤10 hours
Soundness: autoclave %	0.03		< 0.8

Table 6. Grading and physical properties of fine aggregate.

Sieve size (mm)	% Passing by weight	Limits of the Iraqi specification No.45/1984 (zone 3)
10	100	100
4.75	97	90-100
2.36	91	85-100
1.18	84	75-100
0.60	71	60-79
0.30	18	12-40
0.15	7	0-10
Physical Properties	Test Results	Limits of the Iraqi specification No.45/1984
Specific gravity	2.60	-
Sulfate content	0.17 %	≤ 0.50 %
Absorption	0.75 %	-

Table 7. Grading and physical properties of coarse aggregate.

Sieve size (mm)	% Passing by weight	Limits of the Iraqi specification No.45/1984
20	100	100
14	98	90-100
10	84.6	85-100
5	10.0	0-10
2.36	0	0-5
Physical Properties	Test Results	Limits of the Iraqi specification No.45/1984
Specific gravity	2.63	-
Sulfate content	0.06 %	≤ 0.1 %
Absorption	0.63 %	-

Table 8. Categories and description of variables in mixes.

Group No.	Mix Symbol	Description of Variables in Mixes
1	C	Reference Mix
2	SP1	0.8 % SP (by cement weight)
	SP2	1.2 % SP (by cement weight)
	SP3	1.4 % SP (by cement weight)
3	W/P1	w/p = 1 by volume
	W/P 2	w/p = 1.05 by volume
	W/P 3	w/p = 1.15 by volume
	W/P 4	w/p = 1.20 by volume
4	CC1	Decrease Cement Content by (4.58%); [w/p constant]
	CC2	Decrease Cement Content by (1.56%); [w/p constant]
	CC3	Increase Cement Content by (2.6%); [w/p constant]
	CC4	Increase Cement Content by (5%); [w/p constant]
5	S/A1	S/A = 0.425 by volume
	S/A 2	S/A = 0.450 by volume
	S/A 3	S/A = 0.500 by volume
	S/A 4	S/A = 0.525 by volume

Table 9. Details of C, SP1, SP2, SP3, W/P1, W/P 2, W/P 3 & W/P 4 mixes (Category 2).

		C	SP1	SP2	SP3	W/P 1	W/P 2	W/P 3	W/P 4
Materials	**Unit**	**Quantity**	**Quantity**	**Quantity**	**Quantity**	**Quantity**	**Quantity**	**Quantity**	**Quantity**
Water	Liter/m^3	168	168	168	168	168	168	168	168
Cement	Kg/m^3	480	480	480	480	529	504	460	441
Sand	Kg/m^3	814	814	814	814	795	805	822	830
Gravel	Kg/m^3	910	910	910	910	889	900	919	928
Super-Plasticizer	% of cement mass	1	0.80	1.20	1.40	1	1	1	1

Table 10. Details of CC1, CC 2, CC 3, CC 4, S/A 1, S/A 2, S/A 3 & S/A 4 mixes (Category 4).

		CC 1	CC 2	CC 3	CC 4	S/A 1	S/A 2	S/A 3	S/A 4
Materials	**Unit**	**Quantity**	**Quantity**	**Quantity**	**Quantity**	**Quantity**	**Quantity**	**Quantity**	**Quantity**
Water	Liter/m^3	160	165	172	176	168	168	168	168
Cement	Kg/m^3	458	472.5	492.5	504	480	480	480	480
Sand	Kg/m^3	833	821	805	795	728	771	857	900
Gravel	Kg/m^3	931	918	900	889	997	954	867	824
Super-Plasticizer	% of cement mass	1	1	1	1	1	1	1	1

Table 11. Results of RP-CS model.

Item	Value
Training Performance	0.950237
Test Performance	0.921961
Validation Performance	0.900702
Training Error	0.025069
Test Error	0.035493
Validation Error	0.051216
BFGS Algorithem Cycles	BFGS 106
Hidden Activation	Tanh
Output Activation	Logistic

Table 12. R^2 & Regression equations for (T) and (N) relations.

Mix	R^2	Regression Equation
Mix C	0.9570	T = 0.5285+0.024*N
Mix SP1	0.9554	T = 0.5391+0.0239*N
Mix SP2	0.9831	T = 0.5233+0.0241*N
Mix SP3	0.9578	T = 0.5128+0.0242*N
Mix WP1	0.9692	T = 0.5595+0.0262*N
Mix WP2	0.9787	T = 0.5454+0.025*N
Mix WP3	0.9877	T = 0.5167+0.0227*N
Mix WP4	0.9924	T = 0.4836+0.0211*N
Mix CC1	0.9778	T = 0.5559+0.0256*N
Mix CC2	0.9610	T = 0.5401+0.0241*N
Mix CC3	0.9560	T = 0.5182+0.0233*N
Mix CC4	0.9611	T = 0.5064+0.0225*N
Mix SA1	0.9943	T = 0.4651+0.0236*N
Mix SA2	0.9751	T = 0.4968+0.024*N
Mix SA3	0.9312	T = 0.5594+0.0251*N
Mix SA4	0.9690	T = 0.5885+0.0252*N

Table 13. Measured and predicted yield stress (τ_o)**.**

Mix	Yield Stress (τ_o) (Pa)	
	Measured	Predicted
C	129.558	130
SP1	132.594	133
SP2	126.082	129
SP3	122.233	126
W/P1	146.262	138
W/P 2	140.704	134
W/P 3	121.914	127
W/P 4	113.223	119
CC1	136.745	138
CC2	129.893	133
CC3	121.401	127
CC4	116.649	125
S/A1	106.440	114
S/A 2	116.584	122
S/A 3	138.880	138
S/A 4	146.041	145

Table 14. Measured and predicted viscosity (μ).

Mix	Viscosity (μ) (Pa s)	
	Measured	Predicted
C	59.005	61.75
SP1	57.553	61.25
SP2	60.579	62.00
SP3	62.282	62.25
W/P1	69.436	67.25
W/P 2	65.919	64.25
W/P 3	56.296	58.25
W/P 4	51.245	54.25
CC1	64.653	65.50
CC2	63.258	62.00
CC3	57.628	59.75
CC4	55.996	57.75
S/A1	54.206	60.75
S/A 2	57.375	61.5
S/A 3	63.808	64.50
S/A 4	67.087	64.75

Studying the Behavior of Asphalt Stabilized Gepseous Soil for Earth Embankment Model

Hussein Q. Kasim Abdulameer
M.Sc. Civil Engineering
college of Engineering-University of Baghdad
email:hussein83m@yahoo.com

Saad I. Sarsam
Professor
College of Engineering-University of Baghdad
email: Saadisasarsam3@yahoo.com

Mahmood D. Ahmed
instructor
College of Engineering-University of Baghdad
email:mahmoud_Baghdad@yahoo.com

ABSTRACT

The study presents the test results of stabilizing gypseous soil embankment obtained from Al- Faluja university Campus at Al-Ramady province. The laboratory investigation was divided into three phases, The physical and chemical properties, the optimum liquid asphalt (emulsion) requirements (which are manufactured in Iraq) were determined by using one dimensional unconfined compression strength test.in the first phase , The optimum fluid content was 11% (6% of emulsion with 5% water content).. At phase two, the effect of Aeration technique was investigated using both direct shear and permeability test. At phase three for the case of static load , the pure soil embankment model under dry test condition was investigated, The testing program included the determination of the unconfined compressive strength, direct shear strength, constant head permeability test, and one dimensional consolidation test for pure and asphalt stabilized gypseous soil. Testing was carried out in dry and absorbed conditions, the maximum pressure that can be supported before failure (ultimate sustained pressure) is 0.76 MPa with vertical settlement (0.21 mm) . However, For the pure soil embankment model under absorbed condition it was found that the maximum pressure before failure (ultimate sustained pressure) is 0.3 MPa with vertical settlement (12 mm), Which reflects the reduction in bearing capacity by (61%). Compression was made for absorbed stabilized soil and un-absorbed soil tested under hydraulic conductivity test for seven days, the results showed that a very low margin deffeneces in maximum pressure resistance and settlement were obtained (4.38 MPa , 0.11mm) and (4.11MPa , 0.12mm).

Key words: gypseous soil, Emulsion, hydraulic conductivity , soil stabilization.

دراسة تصرف التربة الجبسية المحسنة بالاسفلت لنموذج تعلية ترابية

حسين قاسم عبد الامير
ماجستير هندسة مدنية
كلية الهندسة-جامعة بغداد

سعد عيسى سرسم
أستاذ
كلية الهندسة- جامعة بغداد

محمود ذياب احمد
مدرس
كلية الهندسة- جامعة بغداد

الخلاصة

التربة الجبسية لهذا البحث احضرت من جامعة الفلوجة مدينة الرمادي, الفحوص المختبرية قسمت الى ثلاث اقسام: القسم الاول ايجاد الخواص الفيزياوية والكيمياوية, والنسبة المثلى لمستحلب الاسفلت المصنوع في العراق التي وجدت من فحص مقاومة الضغط الامحصور حيث كانت النسبة المثلى للسائل هي 11% (6% مستحلب الاسفلت + 5 % ماء) , وبرنامج

الفحوص العملية كانت ايجاد مقاومة الانضغاط, مقاومة القص المباشر, النفاذية و الانضمام بأتجاه واحد للتربة الجبسية في حالتها الجافة والرطبة. القسم الثاني استعملت تقنية التهوية من خلال فحص القص المباشر , اما القسم الثالث فقد تم تسليط حمل ساكن من خلال استعمال صندوق بأبعاد (35 * 35 * 30) سم بنفس الكثافة المحدولة المعدلة وايضاً خمس طبقات بمعدل (6) سم لكل طبقة , وتم فحص الانضغاط للتربة المحسنة و الغير محسنة بتسليط حمل ثابت بتأثير وعدم تأثير التوصيل الهايدروليكي وقد تم استعمال حساس رقمي لحساب الهطول العمودي. .

فقد وجد ان مقدار التوصيل الهايدروليكي للماء الى السطح خلال ثلاثة ايام للتربة الغير محسنة المغمورة فقد كان التشوه العمودي تحت ضغط اقصى مقداره (0.3) ميكا باسكال هو (12) ملم , و للتربة الغير محسنة والغير مغمورة تحت تأثير ضغط اقصى مقداره (0.76) ميكا باسكال هو (0.21)ملم, أي مقدار النقصان هم (61%). اما مقدار التوصيل الهايدروليكي للماء الى السطح خلال(7) ايام للتربة المحسنة المغمورة لم يتجاوز فتحات دخول الماء من الثلث السفلي فقد كان التشوه العمودي تحت ضغط اقصى مقداره (4.11) ميكا باسكال هو (0.12) ملم , و للتربة المحسنة والغير مغمورة تحت تأثير ضغط اقصى مقداره (4.38) ميكا باسكال هو (0.11)ملم, أي مقدار النقصان غير ملحوظ.

1. INTRODUCTION

The sandy soil with high gypsum content usually referred to as gypseous soil covers vast area in south, east, middle and west regions of Iraq, such soil possesses a type of cohesive forces when mixed with optimum amount of water and then compacted, but losses its strength when flooded with water again. Covering the soil particles with thin asphalt layer in a stabilization process will increase the cohesion, will limit the negative effect of water by blocking the voids, and will reduce the ability of water to traverse the soil layer through capillary action process.

The economic backfill material suitable for such embankments and roads could be the available local soil. When the soil is gypseous, it will be suitable for compaction use in the dry condition. There will always be a possibility for water to penetrate through the pavement cracks to the soil beneath. It may exhibit hazardous situation ,Then to prevent the soil from collapsing, the asphalt stabilization could provide a good remedy. for such case, theoretically, each particle of the gypseous soil will be surrounded by a thin film of asphalt which will act as a binding and a damp proofing agent. Stabilization of such soil with liquid asphalt will furnish waterproof layers with extra particles bond to serve for embankment construction. Two loading type subjected on embankment during the service life are the repeated load by vehicles and static loading due to its self weight.

2. BAGROUND

For the construction of any type of structure resting on problematic soils such as gypseous soils, there are many available methods to improve the behavior of soil. One of these methods is stabilization with asphalt which is used as addition to prevent water penetration that cause collapsibility potential and to improve the characteristics of the soil.

2.1 Gypseous Soils

In gypseous soils, collapse or compression occurs very quickly when the site is flooded with water during heavy rainfall, irrigation or breaking of sewerage and water pipes which may damage the engineering structures because the element of structure can not follow the sudden deformation occures by rearrangement of the inside forces or stresses , **Al-Mohammadi, 1987.** high strength of dry gypseous soil can be obtained, but great losses in strength and sudden increase in compressibility occur when these soils are fully or partially saturated. The dissolution of the cementing gypsum causes high softening of the soil. The problem becomes more complicated when the ground water flows through the gypseous soil causing leaching and movement of gypsum. In addition to softening, a loss in soil solids takes place. This causes a continuous collapse in the gypseous soil, **AL-Mufty, 1997.**

2.2 Asphalt Emulsion

It is simply a suspension of small asphalt globules in water assisted by an emulsifying agent such as soap. The emulsifying agent assists by imparting an electrical charge to the surface of the asphalt cement globules. Emulisified asphalts are divided into three major groups, namely, anionic, cationic and nonionic, on the basis of the electrical charges of the asphalt particle in the emulsion. Emulisified asphalts are further classified into three main groups namely, rapid-setting (RS), medium-setting (MS) and slow-setting (SS), on the basis of how quickly the suspended asphalt particles revert back to the asphalt cement, a form in which it is actually nedded as a binder **Olutaiwo, et al., 2008,** so **Table 2** shown the property of emulsion.

3. CHEMICAL TEST

The following chemical tests are conducted:

1- Total soluble salts (T.S.S.) (%).
2- Total (CO_3) (%).
3- Total (SO_3) (%).
4- Gypsum content (%).
5- pH value.

4. PHYSICAL TEST

Classification tests performed on the soil include particle sizedistribution, specific gravity, Atterberg limits, relative density, and compaction characteristics. Physical tests were conducted as described in **Table 1**.

5. MATERIAL TEST

Asphalt Emulsion used in the testing program was locally manufactured by Al- Zahf Al- Kabeer company with low cost, The specifications as supplied by the manufactured are as given in **Table 2.**

5.1 Design of Gypseous Soil-Asphalt Mixture

To prepare the specimen, the pulverized and homogenous gypseous soil passing sieve No.4 was oven dried at a temperature of (45°). The optimum moisture content and the maximum dry density of the soil that were found through modified compaction test was 17.7 kN/m^3(95% of modified compaction test) and was selected as a field target in compaction process. Such an issue is mostly considered as an acceptable relative compaction in most engineering requirements, It agrees well with procedure of **Hamdy, 2010**, **Al-Mohammadi, 1987**, **Al-Mufty, 1997, Al-Safarani, 2007**, so, **Fig 1** shown the Stress-Strain relationship for the unconfined compression test for soil with 11% fluid content.

The test was conducted on soil samples mixed by splitting the optimum moisture content into water and emulsion content which will be referred as to optimum fluid content obtained from modified compaction which was (11%), .The water contents were in a range from 4% to 8% with (1%) increment, while the emulsion was in different percentages of 3% to 7% with (1%) increment. Specimens were allowed to cure for seven days at room temperature of (27± 3)ºC and the average value of the unconfined compressive strength for each duplicate specimens were calculated, and **Fig. 2** shown the Unconfined compression strength – emulsion content (%) relationship.

5.2 Absorption technique

Unconfined compression test specimens were prepared using the same method, size and density as was described in the unconfined compression test. Duplicate specimens having the

same fluid content were prepared. Specimens were subjected to seven days curing at air dried condition. After an absorbed period of 7 days, The unconfined compressive strength of specimens was tested, same the results that obtained by **Ingles** and **Metcalf, 1972**. It is clear from **Table 4** that the effect of hydraulic conductivity on the unconfined compressive strength.

5.3 Direct shear test

Direct shear test was carried out on eleven groups of different specimens to determine the shear strength parameters, cohesion and angle of internal friction. The dry density was found to be 17.7 kN/m^3 as described in section(3.4, modified compaction). The optimum fluid content was determined from the unconfined compression strength test as (5% water + 6% emulsion) same the percentage that carried out by **Sarsam, 1979** and **Sarsam, 2008**. It is clear from **Fig. 3** to **Fig. 10**.

5.4 Aeration of asphalt soil

The Aeration technique was adopted before compaction by allowing the loose mix to be subjected to atmosphere condition at laboratory temperature of (30 ± 3)ºC for different times . The aeration periods were (30 ,60 , 90, 120, 240) minutes respectively with emulsion for direction shear test.

Eleven group of specimens were tested. The 1st and 2nd groups of specimens are not stabilized, It was pure soil. The specimens were tested in direct shear which was conducted in soaked and unsoaked conditions. The 3rd and 4th group of specimens are stabilized with optimum emulsion content and constructed without Aeration then the specimens were left for 7 days for curing. The period of soaking was (3-4)hrs. The 5th ,6th ,7th ,8th and 9th group of specimens were stabilized with optimum Emulsion content and subjected to Aeration for different time (30 ,60 , 90, 120, 240) minutes respectively and then the specimens were left for 7 days for curing. The 10th and 11th groups of specimens were stabilized with emulsion and subjected to Aeration condition as (120,140) minutes respectively and then tested under soaked condition. The effect of aeration on shear strength variable were examined. It is clear from **Fig. 9** and **Fig. 10**.

5.5 Static loading test

Four laboratory static loading tests were carried out on gypseous soil samples; the same procedure was applied for the four cyclic loads in the previous tests, but the new box was manufactured with dimension of (30cm x 30cm x 40cm) and had inlets in the bottom of box to allow the water touch the soil that put in the outer box under absorb condition. Same results are agreeing with **Al-Basri, 2012.**

The first test was on a non-stabilized gypseous soil embankment model cured for (24) hours in air.

The second test was carried out on a non-stabilized gypseous soil embankment model cured for (24) hours in air, then subjected to capillary rise with water through addition of water around the box that had inlets to allow the water touch the gyseous soil and then left for three days before applying the test.

The third test was carried out on stabilized gyseous soil with emulsion in dry condition; the mix was left for 2 hrs for aeration before the compact and then the model cured for (7) days before test. It is clear from **plate** 5 and **plate 6** are showing the set up of model.

The fourth test was for stabilized soil with under absorbed condition; the same procedure was applied for the third test by Aeration and curing, but the model was left with absorbed for 7 days. The model of dry pure soil of embankment model was considered as a reference to absorbed pure soil of embankment model as an improvement percentage, while the model of

absorbed stabilized soil was considered as a reference for the pure stabilized embankment model with emulsion as an improvement percentage.

5.5.1 Static loading test for the pure gypseous soil embankment model with dry condition

The pure gypseous soil was selected for this test; it was compacted in the model box and cured for 24 hours and then tested. Measurements of vertical settlements versus the applied vertical pressure were carried out. It is clear from **Fig. 11** that the load-vertical deflection characteristics of the pure gypseous soil sample, It is clear from **plate 6** that shows the test.

5.5.2 Static loading test for the pure gypseous soil embankment model under absorbed condition

The 2nd static loading test was for the pure gypseous soil embankment mode with observed condition. Hence, the model was allowed to face capillary rise of water for (3) days. It is clear from **Fig. 12** that the load-vertical deflection characteristics of the pure gypseous soil sample, and It is clear from **plate** 7 that shows the test.

5.5.3 Static loading test for the dry stabilized gypseous soil embankment model

The third test was carried out on a stabilized soil embankment model using emulsion asphalt for stabilization (based on 11 % of stabilizing material by weight, which is 6% Emulsion and 5% water. the mix was left for 2 hrs for aeration before the compact of 5 layers and then the model was cured for (7) days before test. The stabilized soil embankment model resists the pressure and less vertical displacement , Applied pressure - vertical settlement for stabilized gypseous soil with dry condition the vertical displacement at (0.77 Mpa) was (0.0037 mm), So the rate of decreased in vertical displacement was (- 69%) with compared to pure gypseous soil. This result is shows the strength and cementation added by emulsion to the soil. It is clear from **Fig. 13** that the load-vertical deflection characteristics of the pure gypseous soil sample, And it is clear from **plate 8** that shows the test.

5.5.4 Static loading test for the stabilized gypseous soil embankment model under absorbed condition

The fourth test was carried out for stabilized soil. In this test the same procedure was applied for the third test but after curing for 7 days. The model was absorbed for 7 days. The box was put in a container and the water was poured and left for 7 days to absorb condition from the inlet in the side bottom around the box. The applied pressure - vertical settlement for pure gypseous soil with absorbed condition the vertical displacement was (0.3 Mpa) with (12 mm), so when compared with absorbed stabilized gypseous soil, the vertical displacement was (0.0021 mm). Stabilization with emulsion was successfully as used to prevent the hydraulic conductivity and make blocking between the voids and add more strength and cementation for the soil particles especially for gypseous soil with a percent of gypsum that causes a collapse when touched by water or in wet state under road, embankment or another construction. It is clear from **Fig. 14** that the load-vertical deflection characteristics of the pure gypseous soil sample.

6. CONCLUSION

1. The unconfined compressive strength of the soil-emulsion mixture under dry and absorption test conditions increases with increasing emulsion asphalt content up to the optimum emulsion asphalt content of 6% and then decreases.
2. For pure gypseous soil tested at dry condition, the cohesion (c) was found to be 41 kPa, when the soil was stabilized by emulsified asphalt without Aeration condition; the cohesion was increased to 140 kPa which means an improvement by 250 %.
3. When the soil was stabilized by emulsified asphalt and aerated for two hours and tested under dry condition, the cohesion (c) was found to be 168 kPa , so the cohesion was improved by 21.5% improving on stabilized soil without Aeration.
4. When gypseous soil was tested at absorption condition, the cohesion (c) was found to be 29 kPa, But when the soil was stabilized with emulsified asphalt without aeration and tested at absorbed condition, the cohesion was 53 kPa which means an improvement by 83 %.
5. When the soil was stabilized by emulsified asphalt and aerated for two hours at absorbed condition , the cohesion (c) was found 64 kPa , so the cohesion was improved by 21 % , with respect to non aerated condition.
6. For the case of static load of the pure soil embankment model under dry test condition, the maximum pressure that can be supported before failure (ultimate sustained pressure) wass 0.76 MPa with vertical settlement (0.21 mm) . However, For the pure soil embankment model under absorbed condition, it was found that the maximum pressure before failure (ultimate sustained pressure) was 0.3 MPa with vertical settlement (12 mm).which means an decrease in bearing capacity (61%).
7. The hydraulic conductivity of gypseous soil was changed by asphalt stabilization. When tested under dry condition, a maximum pressure resistance of 4.38 MPa with vertical settlement (0.11 mm) was shown. But when stabilized soil was subjected to absorption for seven days, a maximum pressure resistance of 4.11 MPa with vertical settlement (0.12 mm) was shown;i.e. there was no difference in claim.

REFERENCE

- Al-Basri, M.F., 2012, *Assessing Frictional Behavior of Earth Reinforcement Embedded in Asphalt Stabilized Gypseous Soil*, M.Sc. Thesis, Civil Engineering Department, University of Baghdad.
- Al-Mohammadi, N.M., Nashat, I.H. and Bake, G.Y., 1987, *Compresibility and Collapse of Gypsiferous Soils*, 6th Asian Conference on Soil Mechanics, Tokyo.
- Al- Mufty, A.A. 1997, *Effect of Gypsum Dissolution on the Mechanical Behaviour of Gypseous Soils*, M.Sc. Thesis, Civil Eng Dep., Baghdad University.
- Al-Safarani, M.G., 2007, *Improvement Ability of Gypseous Soil Characteristics Using Cutback Aasphalt and Lime*, M. Sc. Thesis, Civil Engineering Department, University of Al – Mustansiria.
- Hamdy, B.H., 2010, *Implementation of Gypseous Soil-Asphalt Stabilization Technique for Base Course Construction*, M.Sc. Thesis, Dep.of Civil Engineering, University of Baghdad.
- Head, K.H., 1982, *Manual of Soil Laboratory Testing*, Vol. 2, Prentch, Press, London.

- Ingles, O.G., and Metcalf, J. B., 1972, *Soil Stabilization Principles and Practice*, Butter Worth Limited, Australia.

- Olutaiwo, A. O., Adedimila, A. S., and Sidiq, U., *An Examination of the Use of Liquid Asphalt Binders in Road Works in Nigeria*, Journal of Engineering and Applied Sciences, Vol. 3, No. 1, 2008 p 134-142.

- Sarsam, S. I., 1979, *Soil-Cutback Mix for Base Course Construction in Some Parts of Iraq*, M. Sc. Thesis, Civil Engineering Department, University of Sulaimaniah.

- Sarsam, S. I. and Ibrahim, S.W., 2008, *Contribution of Liquid Asphalt in Shear Strength and Rebound Consolidation of Gypseous Soil*, Engineering and Technology, Vol. 26, No. 4.

Table 1 Properties of gypseous soil.

Test result	Physical property
Gs=2.48	Specific gravity according [B.S-13377:I976, test No. (6)]
24 Non plastic Non plastic	Atterberg Limits: Liquid limit (%) according Plastic limit (%) according Plasticity Index (%)
17.17 kN/m^3 14%	Standard compaction properties according Max. standard dry density Optimum moisture content (%)
18.67 kN/m^3 11%	Modified compaction properties Max. modified dry density Optimum moisture content (%)
15.5 kN/m^3	Maximum dry density according to
11.7 kN/m^3	Minimum dry density according to ASTM
1.5	Coefficient of curvature
6.2	Coefficient of uniformity
SP-SM	Unified Classification System

Table 2 Properties of asphalt emulsion.

Test result	Property
+ve	Particles charge
45	Viscosity CSt
1.2	Cement mixing
19	Settling time (hr)
Good	Coating ability and water resistance
Fair	Coating dry & wet aggregate

- Al-zahf Al-Kabeer Co./Baghdad
-

Table 3. Chemical composition of the natural soil.

Percentage %	Chemical Composition
49	Gypsum content (CaSO4) (%)
46	Carbonate content (CaCo3) (%)
38	Total soluble salts (T.S.S.) (%)
22	Total (SO3) (%)
7.77	pH value

Table 4 Effect of hydraulic conductivity on the unconfined compressive strength.

Percent changing unconfined compressive strength (%)	Unconfined compressive strength (kPa) (under absorbed condition)	Unconfined compressive strength (kPa) with dry condition	Emulsion content (%)
-85.31	73	497	4
-87.59	80	645	5
-87.68	85	690	6

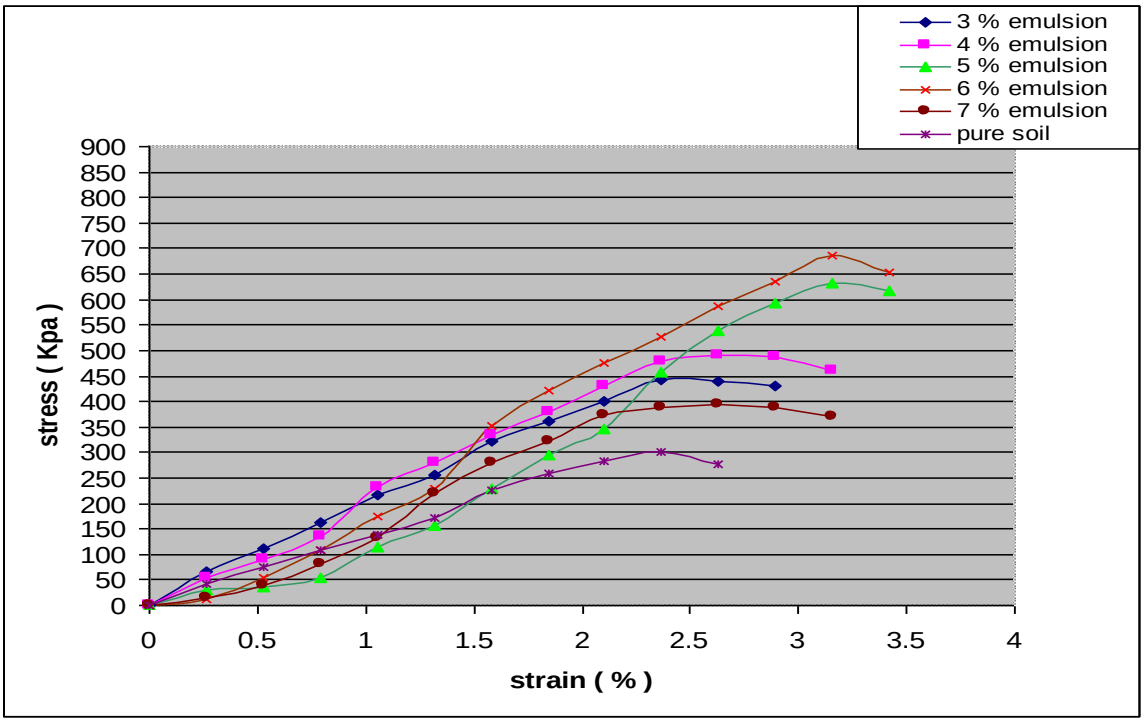

Figure 1. Stress-strain relationship for the unconfined compression test for soil with 11% fluid content.

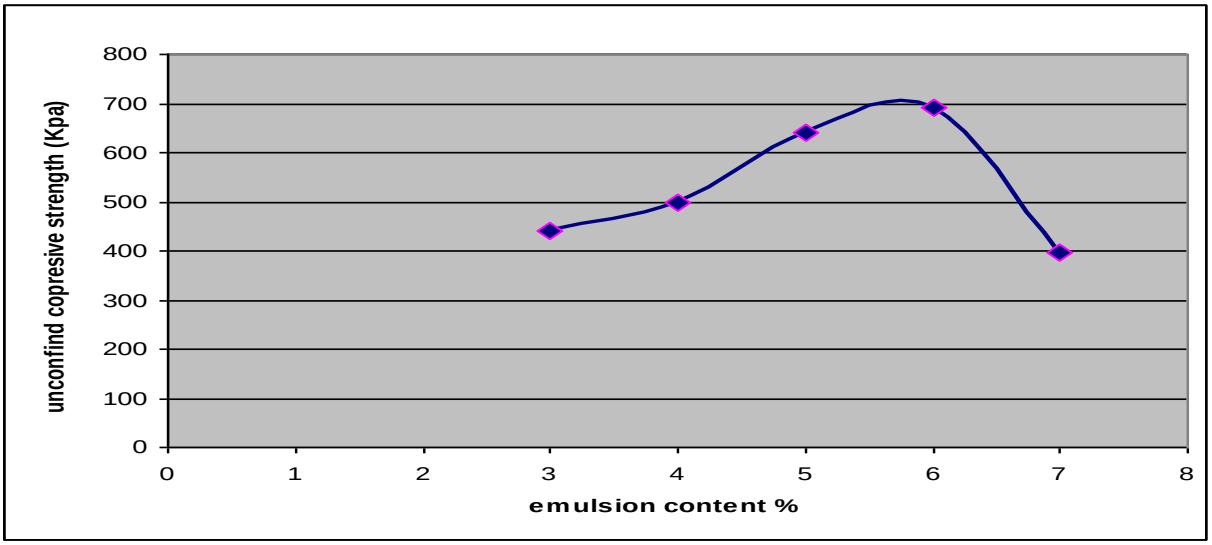

Figure 2. Unconfined compression strength – emulsion content (%) relationship.

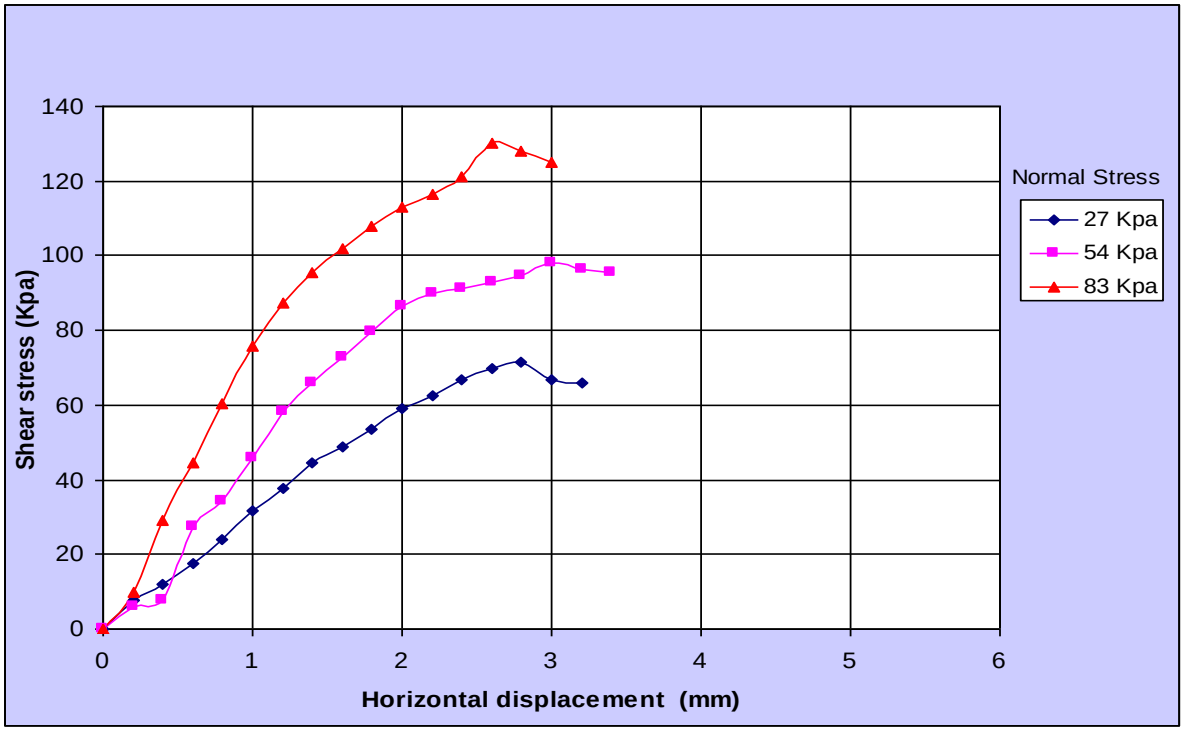

Figure 3. Shear stress- horizontal displacement relationship for non-stabilized gypseous soil (dry condition).

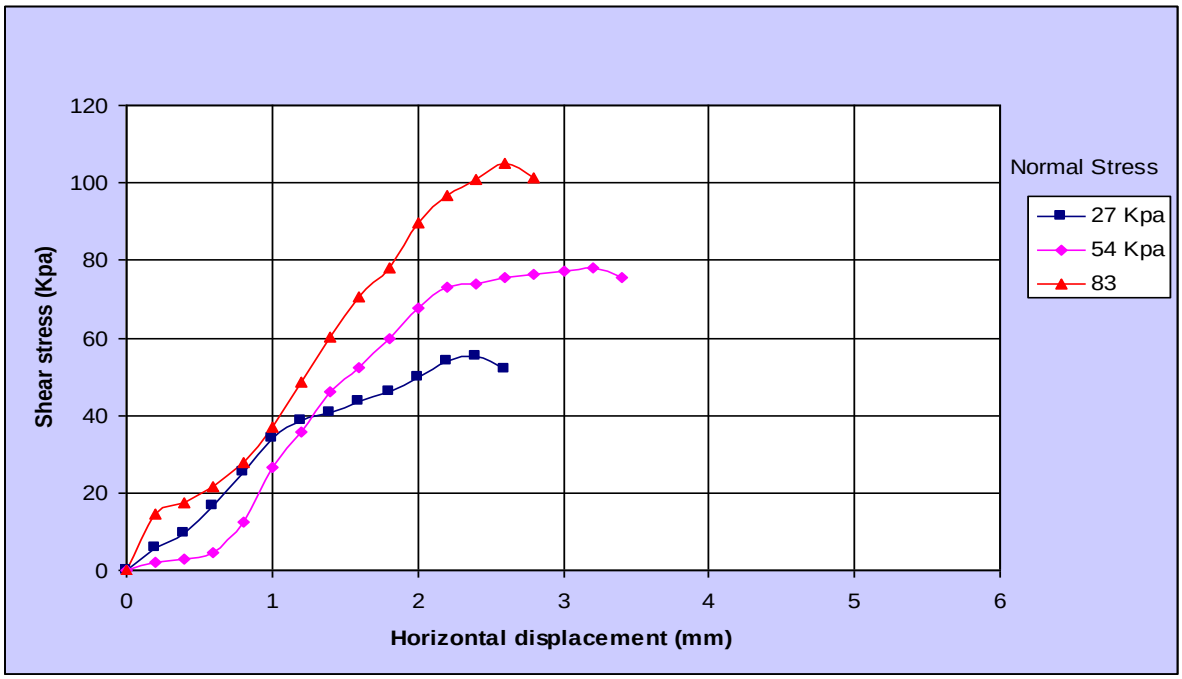

Figure 4. Shear stress- horizontal displacement relationship for non - stabilized gypseous soil (soaked condition) period time (3-4) hrs.

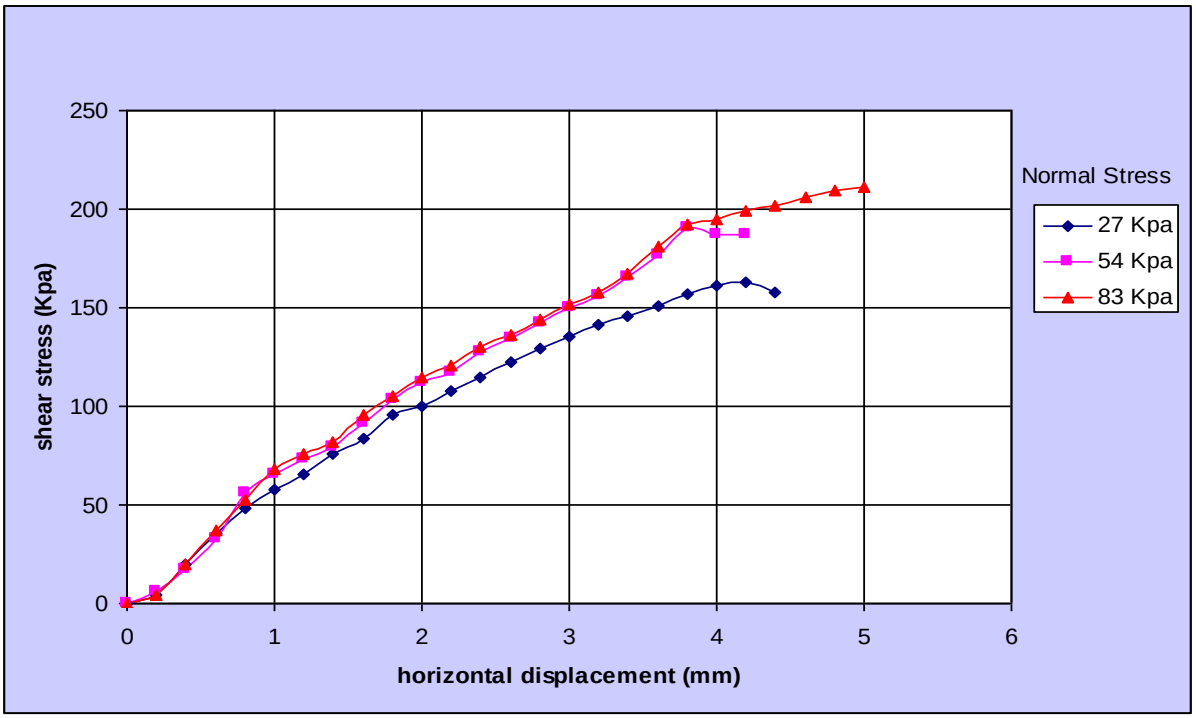

Figure 5. Shear stress- horizontal displacement relationship for stabilized gypseous soil with emulsion(dry condition). "0 aeration"

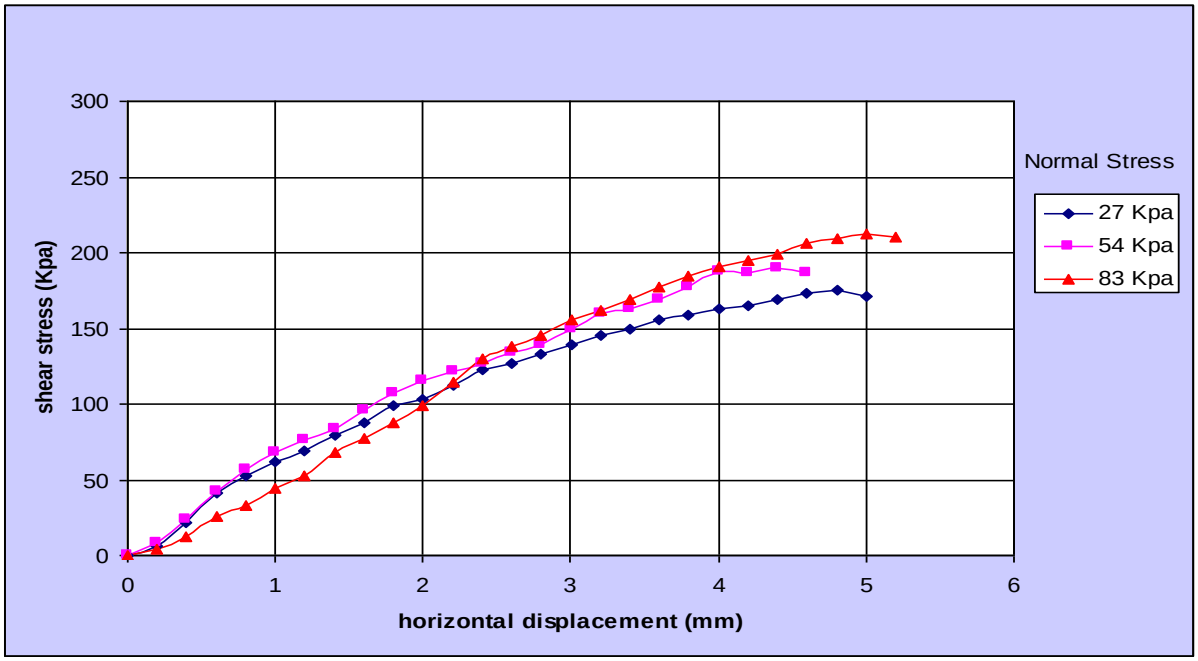

Figure 6. Shear stress- horizontal displacement relationship for stabilized gypseous soil with emulsion(dry condition). "½ hr aeration"

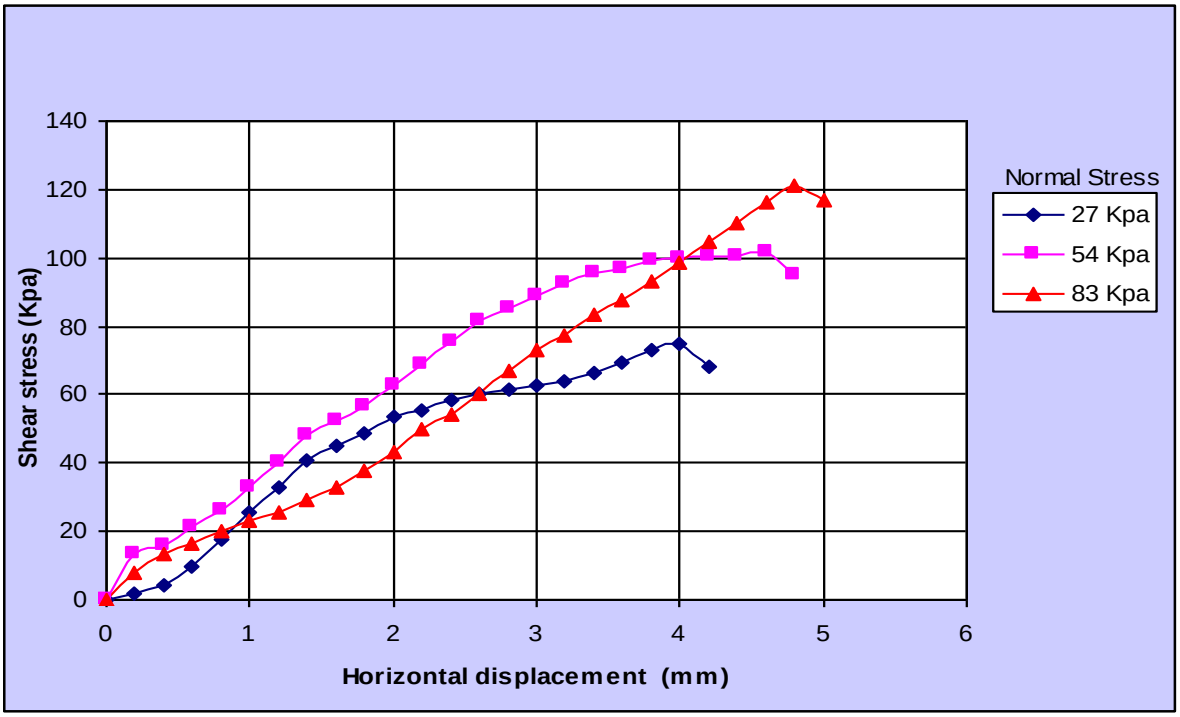

Figure 7. Shear stress- horizontal displacement relationship for stabilized gypseous soil with emulsion(soaked condition). " 0 aeration"

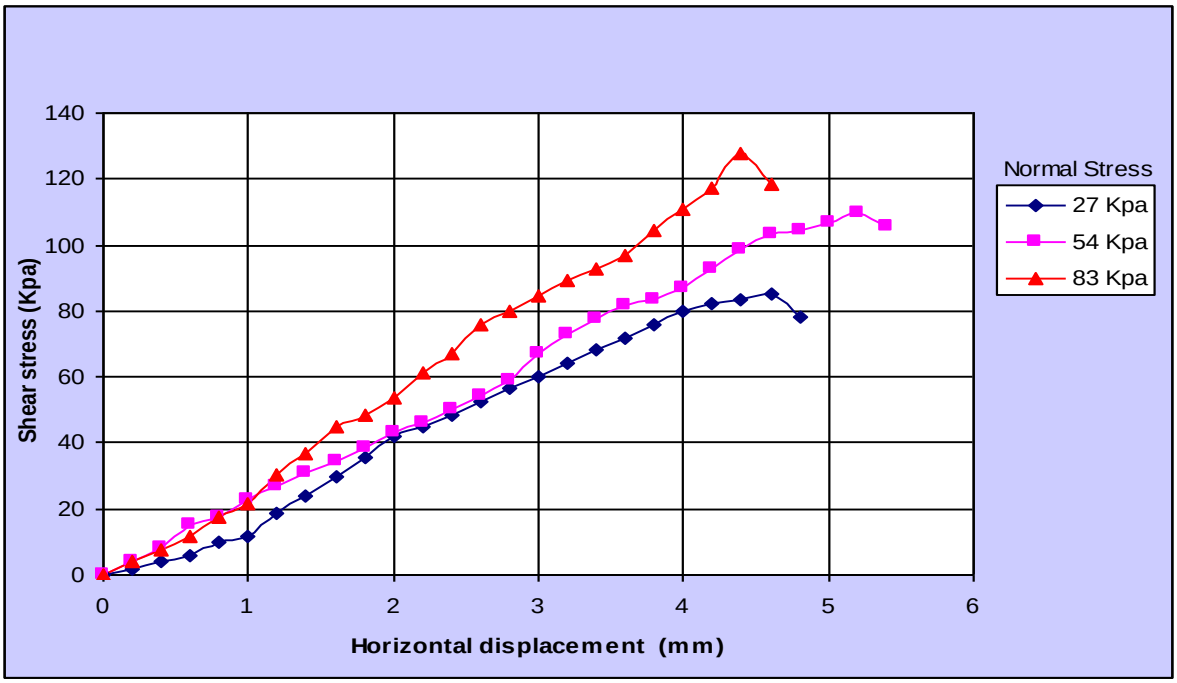

Figure 8. Shear stress- horizontal displacement relationship for stabilized gypseous soil with emulsion(soaked condition). " 2 hrs aeration"

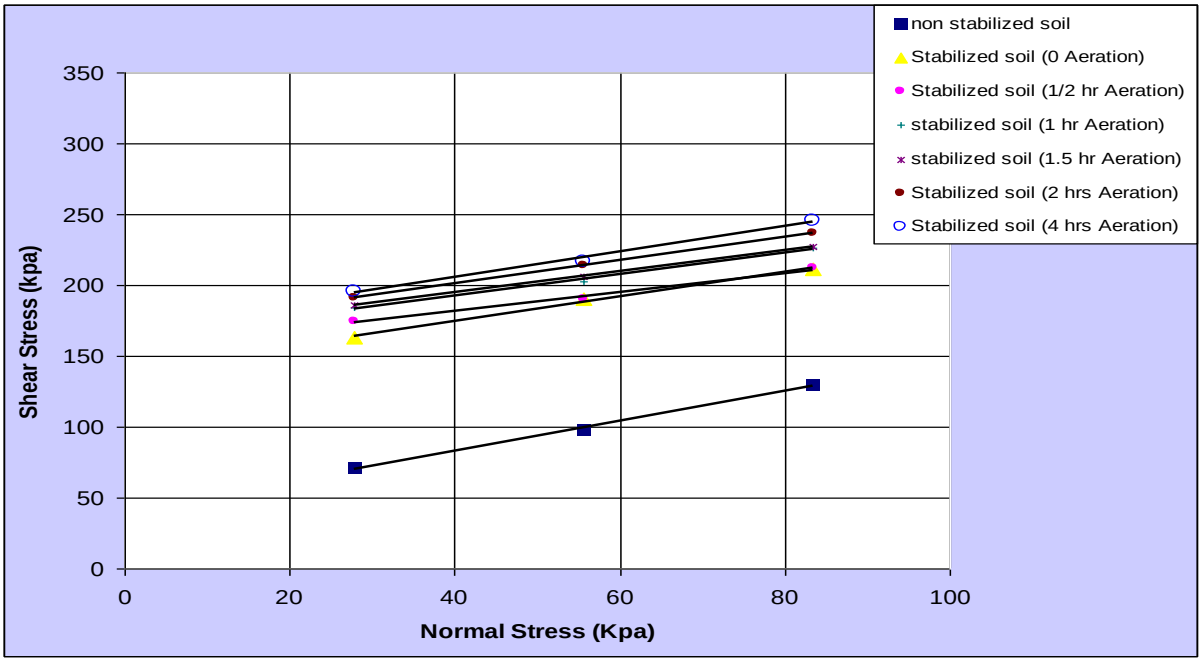

Figure 9. Direct shear test results for stabilized and non-stabilized.

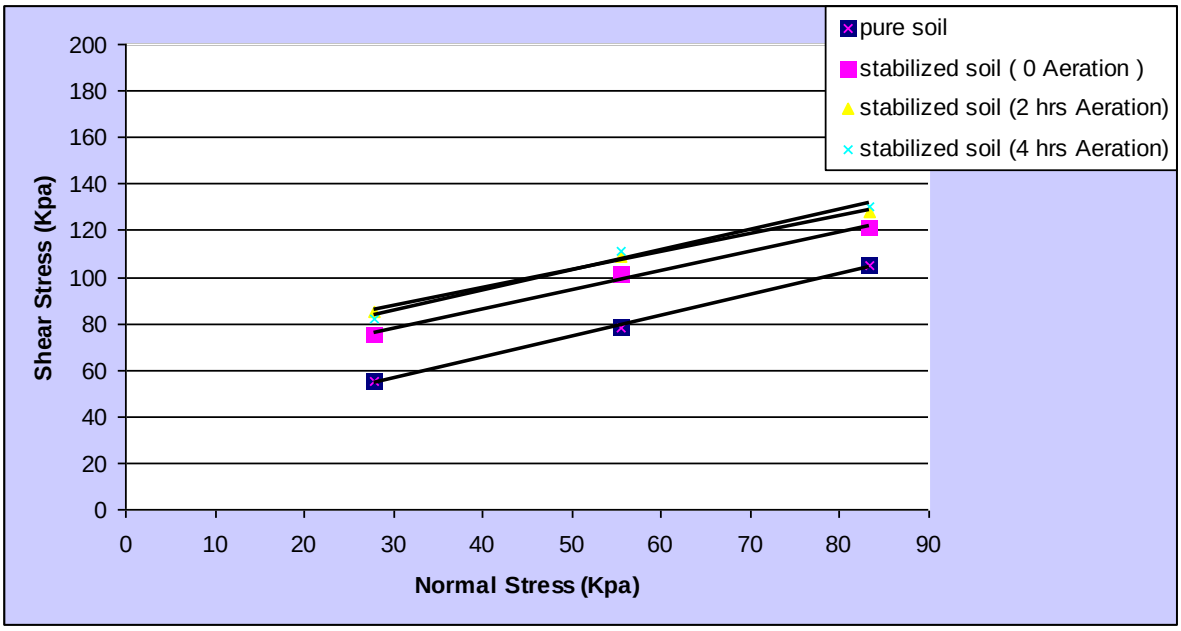

Figure 10. Direct shear test results for stabilized and non-stabilized gypseous soil under soaked condition with aeration technique.

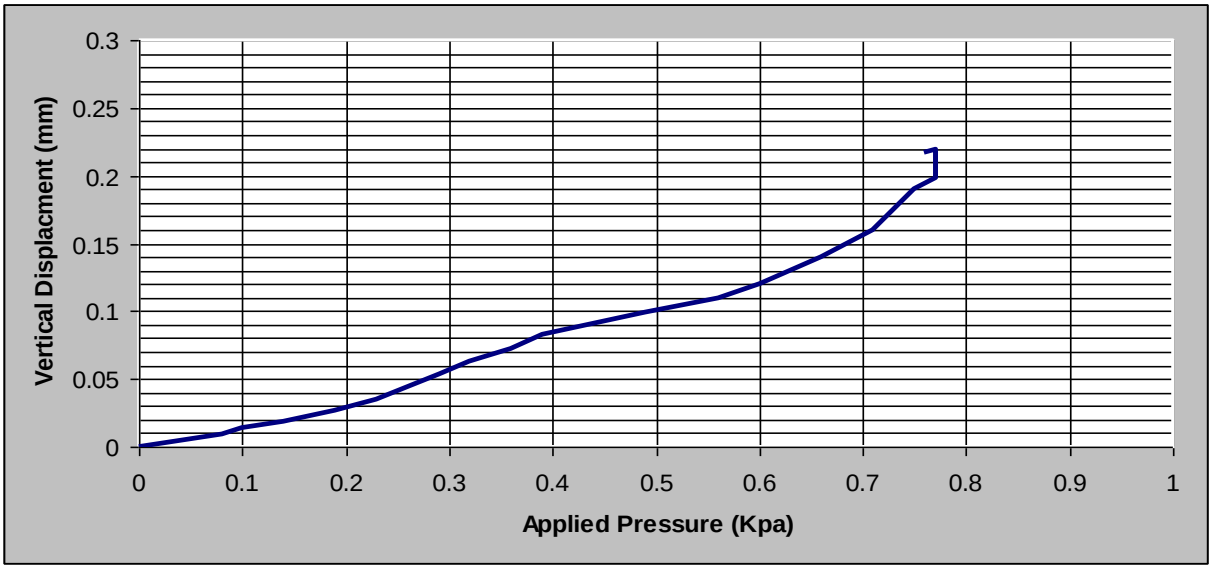

Figure 11. Applied pressure - vertical settlement for pure gypseous soil at dry condition.

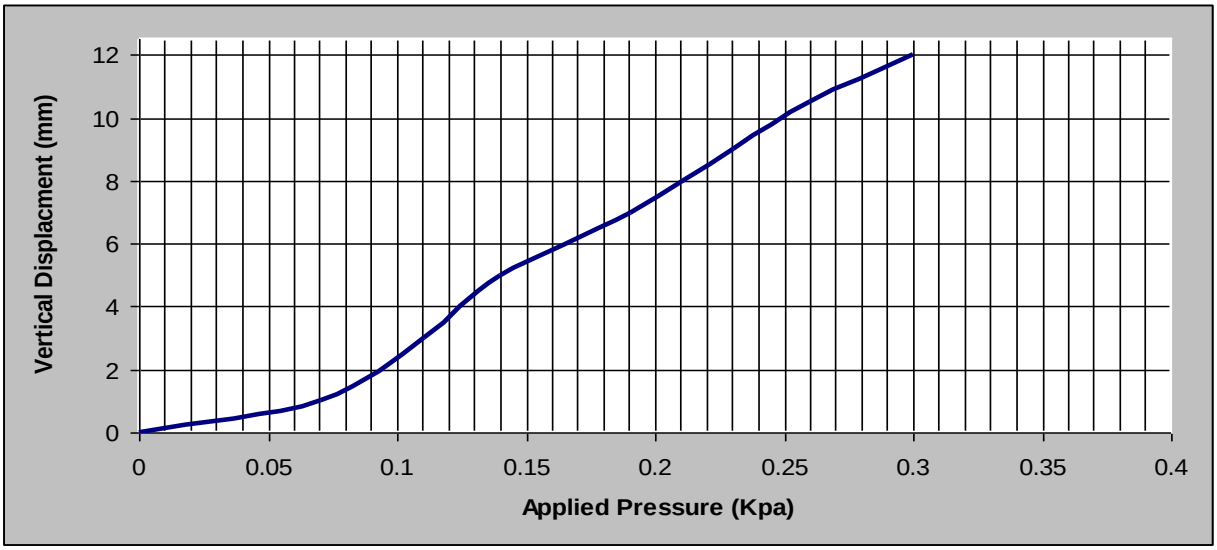

Figure 12. Applied pressure - vertical settlement for pure gypseous soil at hydraulic conductivity.

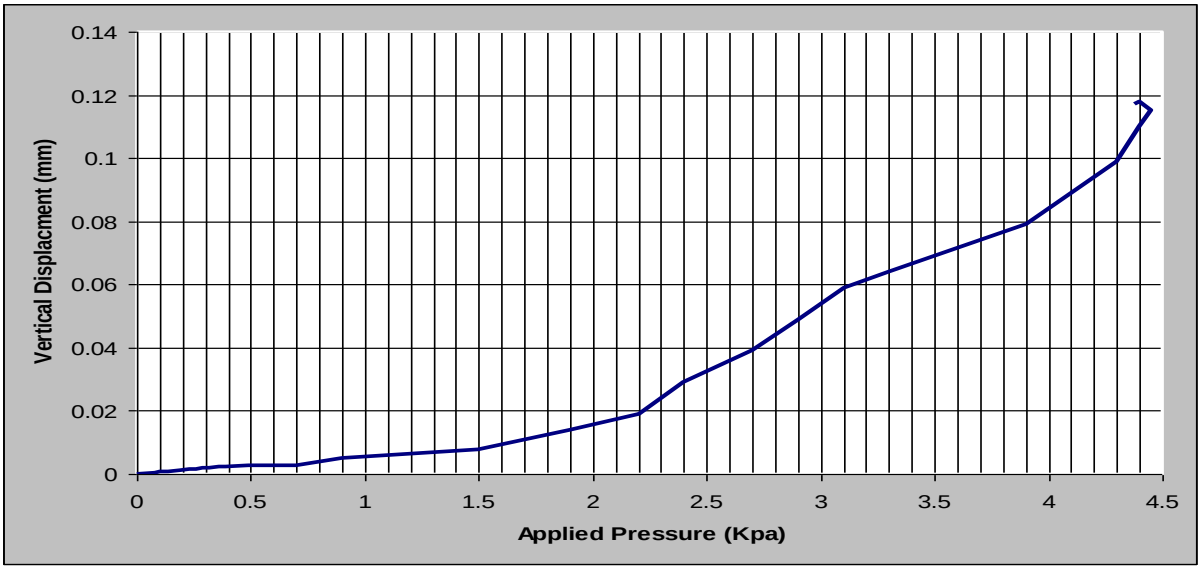

Figure 13. Applied pressure - vertical settlement for stabilized gypseous soil at dry condition.

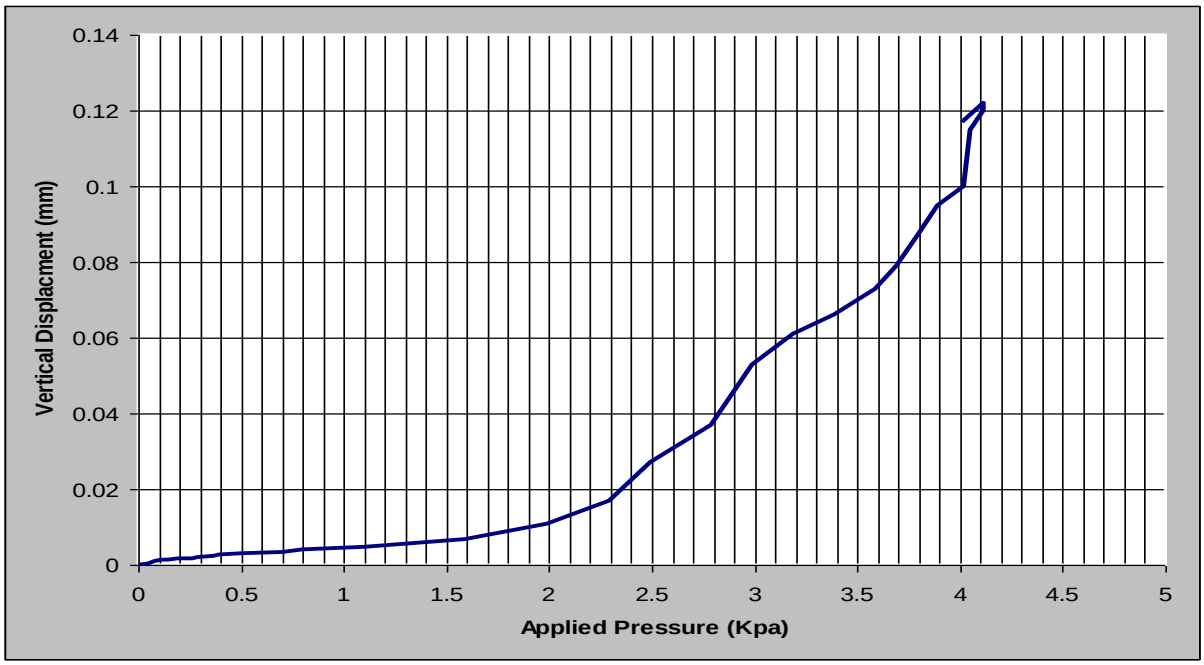

Figure 14. Applied pressure - vertical settlement for stabilized gypseous soil at absorbed condition.

Plate 1. Curing for specimens of soil stabilized with emulsion.

Plate 2. absorption technique for unconfined compression test.

Plate 3. Aeration technique in process.

Plate 4. Curing for specimens of soil stabilized.

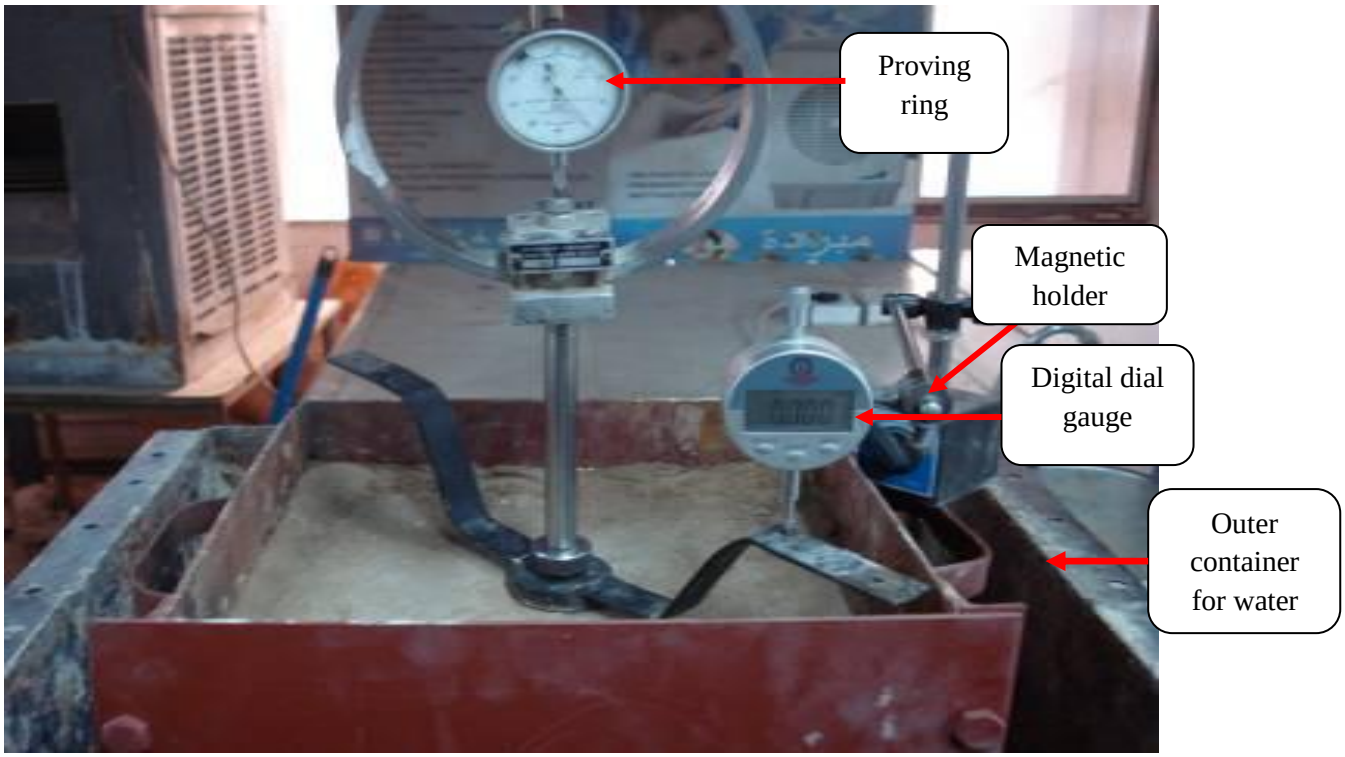

Plate 6. Set up of embankment model.

Plate 7. Punching failure after static loading test for the pure gypseous soil under absorbed condition.

Plate 8. Vertical deformation of tire print for stabilized embankment model.

Plate 9. Effect of hydraulic conductivity of asphalt stabilized soil on capillary rise of water after static loading application.

A Comparative Study of Various Intelligent Algorithms Based Nonlinear PID Neural Trajectory Tracking Controller for the Differential Wheeled Mobile Robot Model

Ahmed Sabah Al-Araji
Assistance Professor
Control and Systems Engineering Dept - University of Technology
E-mail:ahmedsas2040@yahoo.com

ABSTRACT

This paper presents a comparative study of two learning algorithms for the nonlinear PID neural trajectory tracking controller for mobile robot in order to follow a pre-defined path. As simple and fast tuning technique, genetic and particle swarm optimization algorithms are used to tune the nonlinear PID neural controller's parameters to find the best velocities control actions of the right wheel and left wheel for the real mobile robot. Polywog wavelet activation function is used in the structure of the nonlinear PID neural controller. Simulation results (Matlab) and experimental work (LabVIEW) show that the proposed nonlinear PID controller with PSO learning algorithm is more effective and robust than genetic learning algorithm; this is demonstrated by the minimized tracking error and obtained smoothness of the velocity control signal, especially when external disturbances are applied.

Key words: genetic algorithm, particle swarm optimization, nonlinear PID controller, NI mobile robots, trajectory tracking.

دراسة مقارنة لخوارزميات ذكية متنوعة أساسه مسيطر تتابع مسار عصبي لأخطي تناسبي تكاملي تفاضلي لنموذج التحرك التفاضلي لإنسان آلي متنقل.

أحمد صباح عبد الأمير الأعرجي
أستاذ مساعد دكتور
قسم هندسة السيطرة والنظم - الجامعة التكنولوجية

الخلاصة

يقدم هذا البحث, دراسة مقارنة لخوارزميتين لتعليم مسيطر تناسبي تكاملي تفاضلي عصبي لاخطي تتابعي لمسار عجلة الإنسان آلي متحرك لكي يتبع مسار مستمر معرف مسبقا.
كتقنيات سهله وسريعة التنغيم, لقد تم استخدام الخوارزمية الوراثية وخوارزمية حشد الجسيمات الامثلية لتنغيم عناصر المسيطر اللاخطي التناسبي التكاملي التفاضلي لإيجاد أفضل أشارة سرعة لعجلة للإنسان الآلي المتحرك الحقيقي. لقد تم استخدام الدالة الفعالة موجة البوليونك في هيكلية المسيطر العصبي.
من خلال نتائج المحاكاة والعمل التجريبي, أثبتت أن المسيطر التناسبي التكاملي التفاضلي العصبي اللاخطي المقترح تنغيمه بواسطة خوارزمية حشد الجسيمات الامثلية أكثر فعالية و متانة مقارنة بالمسيطرة الذي تم تنغيمه بواسطة الخوارزمية الوراثية, وهذا واضح من خلال تقليل الخطأ ألتتابعي لمسار الإنسان الآلي المتحرك مع توليد أشارة سرعة ناعمة, برغم من وجود التأثير الاضطرابي الخارجي.

الكلمات الرئيسية:
الخوارزمية الوراثية, حشد الجسيمات الأمثلية, المسيطر التناسبي التكاملي التفاضلي اللاخطي, الإنسان الآلي المتحرك, تتابع مسار.

1. INTRODUCTION

In the last decade, there has been an increasing amount of research on the subject of wheel-based mobile robots which have attracted considerable attention in various industrial and service applications. For example, room cleaning, lawn mowers, factory automation, transportation, nuclear-waste cleaning, **Wai,** and **Liu, 2009**.

These applications require mobile robots to have the ability to track specified path stably; therefore, several studies have been published for solving the mobile robot path tracking control problems which can be classified into three categories: The first category is the position estimation control approach for navigation problems of the mobile robot on interactive motion planning in dynamics environments and obstacle motion estimation, **Chang, et al., 2009**. The second category for navigation problems of the mobile robot is path planning and execution. The path planning is generated based on a prior map of the environment while the executed path is planned using certain optimization algorithms based on a minimal time, minimal distance or minimal energy performance index. Many methods have been developed for avoiding both static and moving obstacles as presented in, **Sahin,** and **Zergeroglu, 2007**. The third category for the navigation problems of mobile robot is the design and implementation of the driving control that the mobile robot must track to follow a desired path accurately and minimize the tracking error.

Tracking errors of mobile robot causes collisions with obstacles due to deviations from the planned path and also causes the robot to fail in accomplishing the mission successfully. It also causes an increase of the traveling time, as well as the travel distance, due to the additional adjustments needed to satisfy the driving sates. The major reasons for tracking error for mobile robot are the small rotation radius or not constant on the path such as the complex curvature or randomly curvature, **Takanori, et al., 2000**.

In, **Mnif,** and **Touati, 2005.** artificial intelligent controllers were carried out using neural networks or fuzzy inference in order to control the trajectory tracking for the mobile robot while the traditional control methods for path tracking have been used linear or non-linear feedback controller. There are other techniques for trajectory tracking controllers such as predictive control technique. Predictive approaches to path tracking seem to be very promising because the reference trajectory is known beforehand. Model predictive trajectory tracking control was applied to a mobile robot where linearized tracking error dynamics was used to predict future system behaviour and a control law was derived from a quadratic cost function penalizing the system tracking error and the control effort, **Klancar,** and **Skrjanc, 2007.**

In addition, an adaptive trajectory-tracking controller based on the robot dynamics was proposed in, **Park, et al. 2010**. Intelligent control architecture for two autonomously driven wheeled robot was developed in, **Su, et al. 2010**, that consists of the fuzzy inference as main controller and the neural network is an auxiliary part.

The fundamental essence of the contribution of this work can be understood considering the following points.

- The analytically derived control law which has significantly high computational accuracy to obtain the best control action and lead to minimum tracking error of the mobile robot based on genetic algorithm and particle swarm optimization.
- Investigation of the controller robustness and adaptation performance through adding boundary unknown disturbances.
- Verification of the proposed controller capability of tracking continuous trajectory is done by an experimental work using NI mobile robot model.

Simulation results and experimental work show that the proposed controller with PSO learning algorithm is more robust and effective than controller with genetic learning algorithm in terms of

minimum tracking error and in generating best velocity control action despite of the presence of bounded external disturbances.
The remainder of the paper is organized as follows: Section two is a description of the kinematics model of the differential wheeled mobile robot model and check controllability for the mobile robot. In section three, the proposed nonlinear PID neural controller is derived based on genetic algorithm and particle swarm optimization. The simulation results and experimental work of the proposed controller are presented in section four and the conclusions are drawn in section five.

2. DIFFERENTIAL WHEELED MOBILE ROBOT PLATFORM

The schematic of the differential drive mobile robot, shown in **Fig. 1**, consists of a cart with two driving wheels mounted on the same axis and one castor wheel as an omni-directional in the front of cart in order to carry the mechanical structure and keep the platform of the mobile robot more stable, **Al-Araji, et al, 2013**. Two independent analogous DC motors are the actuators of left and right wheels for motion and orientation. The two wheels have the same radius denoted by r, and L is the distance between the two wheels. The center of mass of the mobile robot is located at point c, center of axis of wheels.
The pose of mobile robot in the global coordinate frame $[O, X, Y]$ and the pose vector in the surface is defined as:

$$q = (x, y, \theta)^T \tag{1}$$

where $q(t) \in \Re^{3\times1}$,
x and y are coordinates of point c and θ is the robotic orientation angle measured with respect to the X-axis. These three generalized coordinates can describe the configuration of the mobile robot.
It is assumed that the mobile robot wheels are ideally installed in such a way that they have ideal rolling without skidding, **Yang, et al. 2004**, as shown in Eq. (2):

$$-\dot{x}(t)\sin\theta(t) + \dot{y}(t)\cos\theta(t) = 0 \tag{2}$$

Therefore, the kinematics equations in the world frame can be represented as follows **Han, et al. 2008**:

$$\dot{x}(t) = V_l(t)\cos\theta(t) \tag{3}$$

$$\dot{y}(t) = V_l(t)\sin\theta(t) \tag{4}$$

$$\dot{\theta}(t) = V_w(t) \tag{5}$$

where V_l and V_w, are the linear and angular velocities respectively.
In the computer simulation, the currently form of the pose equations are as follows:

$$x(k) = 0.5[V_R(k) + V_L(k)]\cos\theta(k)\Delta t + x(k-1) \tag{6}$$

$$y(k) = 0.5[V_R(k) + V_L(k)]\sin\theta(k)\Delta t + y(k-1) \tag{7}$$

$$\theta(k) = \frac{1}{L}[V_L(k) - V_R(k)]\Delta t + \theta(k-1) \tag{8}$$

where $x(k), y(k), \theta(k)$ are the components of the pose at the k step of the movement and Δt is the sampling period between two sampling times.
Using Jacobi-Lie-Bracket to check controllability of the nonlinear MIMO kinematic mobile robot system in Eqs. (3, 4, 5)**,** the accessibility rank condition is globally satisfied controllability. The mobile robot kinematics can be described by the left and right velocities as follows:

$$\begin{bmatrix} \dot{x}(t) \\ \dot{y}(t) \\ \dot{\theta}(t) \end{bmatrix} = \begin{bmatrix} 0.5\cos\theta(t) & 0.5\cos\theta(t) \\ 0.5\sin\theta(t) & 0.5\sin\theta(t) \\ 1/L & -1/L \end{bmatrix} \begin{bmatrix} V_R(t) \\ V_L(t) \end{bmatrix} \tag{9}$$

$$[\dot{q}] = [f]V_R(t) + [g]V_L(t) \tag{10}$$

and f and g can be defined as two vectors with components:

$$f = \begin{bmatrix} 0.5\cos\theta(t) \\ 0.5\sin\theta(t) \\ 1/L \end{bmatrix} \text{ and } g = \begin{bmatrix} 0.5\cos\theta(t) \\ 0.5\sin\theta(t) \\ -1/L \end{bmatrix} \tag{11}$$

$$[f,g] = \begin{bmatrix} [f,g]^1 \\ [f,g]^2 \\ [f,g]^3 \end{bmatrix} = \begin{bmatrix} \frac{-1}{L}\sin\theta(t) \\ \frac{1}{L}\cos\theta(t) \\ 0 \end{bmatrix} \tag{12}$$

$$rank\{f, g, [f,g]\} = rank\begin{bmatrix} 0.5\cos\theta(t) & 0.5\cos\theta(t) & \frac{-1}{L}\sin\theta(t) \\ 0.5\sin\theta(t) & 0.5\sin\theta(t) & \frac{1}{L}\cos\theta(t) \\ 1/L & -1/L & 0 \end{bmatrix} \tag{13}$$

The determent of the matrix in Eq. (13) is equal to $(1/L^2) \neq 0$, then the full rank of matrix is equal to 3, therefore, the system in Eqs. (3, 4 and 5) is controllable.

3. CONTROL METHODOLOGY

The proposed structure of the nonlinear PID neural controller can be given in the form of block diagram, as shown in **Fig. 2**. The approach to control the wheeled mobile robot depends on the available information of the unknown nonlinear system and can be known by the input-output data and the control objectives. The genetic algorithm and particle swarm optimization will generate the optimal parameters for the nonlinear PID neural controller in order to obtain best velocity control signal that will minimize the tracking error of the mobile robot in the presence of external disturbance.
The feedback PID neural controller is very important because it is necessary to stabilize the tracking error of the system when the output of the mobile robot is drifted from the desired point. The nonlinear PID neural controller for MIMO mobile robot system is shown in **Fig. 3**. The proposed nonlinear PID neural controller has the characteristics of control agility, strong

adaptability, good dynamic characteristic and robustness because it is based on a conventional PID controller that consists of three terms: proportional, integral and derivative where the standard form of a PID controller is given in the s-domain as Eq. (14), **Zhong, 2006** and **Omatu, 1995**.

$$Gc(s) = P + I + D = K_p + \frac{K_i}{s} + K_d s \tag{14}$$

where K_p, K_i and K_d are called proportional gain, integral gain and derivative gain, respectively. The proposed nonlinear PID neural controller scheme is based on the discrete-time PID as Eq. (15).

$$u_{1,2}(k) = u_{1,2}(k-1) + Kp_\gamma[e_\gamma(k) - e_\gamma(k-1)] + Ki_\gamma e_\gamma(k) + Kd_\gamma[e_\gamma(k) - 2e_\gamma(k-1) + e_\gamma(k-2)] \tag{15}$$

where $\gamma = x, y, \theta.$

Therefore, the tuning PID input vector consists of $e_\gamma(k)$, $e_\gamma(k-1), e_\gamma(k-2)$ and $u_{1,2}(k-1)$, where $e_\gamma(k)$ and $u_{1,2}(k)$ denote the input error signals and the PID output signal respectively.

The proposed control law of the feedback right and left velocity (u_1 and u_2) respectively can be proposed as follows:

$$u_1(k) = u_1(k-1) + o_x + o_y \tag{16}$$

$$u_2(k) = u_2(k-1) + o_\theta + o_y \tag{17}$$

o_x, o_y and o_θ are the outputs of the neural networks that can be obtained from non-linear Polywog wavelet activation functions, **Righeto, 2004,** as shown in **Fig. 4** and has nonlinear relationship as presented in the following function:

$$o_\gamma = (3(net_\gamma)^2 - (net_\gamma)^4)e^{-0.5(net_\gamma)^2} \tag{18}$$

net_γ is calculated from this equation:

$$net_\gamma(k) = Kp_\gamma[e_\gamma(k) - e_\gamma(k-1)] + Ki_\gamma e_\gamma(k) + Kd_\gamma[e_\gamma(k) - 2e_\gamma(k-1) + e_\gamma(k-2)] \tag{19}$$

The control parameters Kp_γ, Ki_γ and Kd_γ of the nonlinear PID neural controller are adjusted using genetic algorithm and particle swarm optimization.

3.1 Learning Genetic Algorithm (GA)

Genetic algorithm is an intelligent optimization technique that relies on the parallelism found in nature; in particular its searching procedures are based on the mechanics of natural selection and genetics, **Ali, et al, 2011**.

GAs includes three major operators: selection, crossover, and mutation, in addition to four control parameters: population size, selection pressure, mutation rate and crossover. Genetic algorithms start parallel searching from independent points of searching space in which the

solution knowledge is poor or not available. The solution depends on interaction of the surroundings and genetic operators. For that reason, obtaining the suboptimal solutions of genetic algorithm is a small probability, **Muhammet, 2010.**

In this paper, the first learning algorithm for determining the nonlinear PID neural controller parameters is genetic algorithm and the steps of the tuning these parameters can be described as follows:

- **Step1** GA makes the problem parameters into chromosomes then simulates evolutionary operation.
- **Step2** To determine the size of the population and to initialize. Set the population size 30, the evolution generation 100.
- **Step3** Decode the individual of the population into optimal parameters for calculating the value of fitness function.
- **Step4** Do population selection, crossover and mutation operations to produce the next generation population. The crossover probability is 0.75, mutation probability is 0.01.
- **Step5** Repeat steps 3 and 4 until the fitness function condition is achieved or the maximum number of generations is reached.

Mean square error (MSE) function for multi-input multi-output (MIMO) mobile robot system is chosen as a criterion for estimating the model performance and an objective function to be minimized with the GA as Eq. (20):

$$MSE = \frac{1}{pop}\sum_{j=1}^{pop}((x_r(k+1)^j - x(k+1)^j)^2 + (y_r(k+1)^j - y(k+1)^j)^2 + (\theta_r(k+1)^j - \theta(k+1)^j)^2) \tag{20}$$

Since the GA maximizes its fitness function, it is necessary therefore to map the objective function (MSE) to a fitness function. It is used objective –to- fitness transformation is of the form, **Al-Araji, 2005**.

$$fitness = \frac{1}{objectivefunction + \mu} \tag{21}$$

where μ is a constant chosen to avoid division by zero.

3-2 Learning Particle Swarm Optimization Algorithm

Particle Swarm optimization (PSO) is a kind of algorithm to search for the best solution by simulating the movement and flocking of birds. PSO algorithms use a population of individual (called particles) “flies” over the solution space in search for the optimal solution.

Each particle has its own position and velocity to move around the search space. The particles are evaluated using a fitness function to see how close they are to the optimal solution, **Derrac, et al, 2005**. The previous best value is called as *pbest*. Thus, *pbest* is related only to a particular particle. It also has another value called *gbest*, which is the best value of all the particles *pbest* in the swarm.

The nonlinear PID neural controller with nine weights parameters and the matrix is rewritten as an array to form a particle. Particles are then initialized randomly and updated afterwards according to Eqs. (22, 23, 24, 25, 26 and 27) in order to tune the PID parameters:

$$\Delta Kp_{\gamma,m}^{k+1} = \Omega(\Delta Kp_{\gamma,m}^{k}) + c_1 r_1 (pbest_{\gamma,m}^{k} - Kp_{\gamma,m}^{k}) + c_2 r_2 (gbest^{k} - Kp_{\gamma,m}^{k}) \tag{22}$$

$$Kp_{\gamma,m}^{k+1} = Kp_{\gamma,m}^{k} + \Delta Kp_{\gamma,m}^{k+1} \tag{23}$$

$$\Delta Ki_{\gamma,m}^{k+1} = \Omega(\Delta Ki_{\gamma,m}^{k}) + c_1 r_1 (pbest_{\gamma,m}^{k} - Ki_{\gamma,m}^{k}) + c_2 r_2 (gbest^{k} - Ki_{\gamma,m}^{k}) \tag{24}$$

$$Ki_{\gamma,m}^{k+1} = Ki_{\gamma,m}^{k} + \Delta Ki_{\gamma,m}^{k+1} \tag{25}$$

$$\Delta Kd_{\gamma,m}^{k+1} = \Omega(\Delta Kd_{\gamma,m}^{k}) + c_1 r_1 (pbest_{\gamma,m}^{k} - Kd_{\gamma,m}^{k}) + c_2 r_2 (gbest^{k} - Kd_{\gamma,m}^{k}) \tag{26}$$

$$Kd_{\gamma,m}^{k+1} = Kd_{\gamma,m}^{k} + \Delta Kd_{\gamma,m}^{k+1} \tag{27}$$

$m = 1,2,3,.....pop$

where

pop is number of particles,

$K_{\gamma,m}^{k}$ is the weight of particle *m* at *k* iteration,

c_1 and c_2 are the acceleration constants with positive values equal to 1.47,

r_1 and r_2 are random numbers between 0 and 1,

$pbest_{\gamma,m}$ is best previous weight of mth particle.

$gbest$ is best particle among all the particle in the population.

Ω is the inertia weight factor and it is equal to 0.75,

The number of dimension in particle swarm optimization is equal to nine because the proposed nonlinear PID controller has nine parameters. The mean square error function is chosen as a criterion for estimating the model performance as given in Eq. (20).

In this paper, the second learning algorithm for determining the nonlinear PID neural controller parameters is PSO algorithm and the steps of the tuning these parameters can be described as follows:

- **Step1** Initial searching points $Kp_{\gamma}^{0}, Ki_{\gamma}^{0}, Kd_{\gamma}^{0}, \Delta Kp_{\gamma}^{0}, \Delta Ki_{\gamma}^{0}$ and ΔKd_{γ}^{0} of each particle are usually generated randomly within the allowable range. Note that the dimension of search space consists of all the parameters used in the nonlinear PID neural controller as shown in **Fig. 2**. The current searching point is set to *pbest* for each particle. The best-evaluated value of *pbest* is set to *gbest* and the particle number with the best value is stored.
- **Step2** The objective function value is calculated for each particle by using Eq. (20). If the value is better than the current *pbest* of the particle, the *pbest* value is replaced by the current value. If the best value of *pbest* is better than the current *gbest*, *gbest* is replaced by the best value and the particle number with the best value is stored.
- **Step3** The current searching point of each particle is update by using Eqs. (22, 23, 24, 25, 26 and 27).
- **Step4** If the current iteration number reaches the predetermined maximum iteration number, then exit. Otherwise, return to step 2.

The fundamental essences for applying the proposed control algorithms are minimizing tracking error and obtaining smoothness of the velocity control signal through speed up the process of getting the optimal parameters of the nonlinear PID controller.

4. SIMULATION RESULTS

The kinematic model of the differential wheeled mobile robot described in section 2 is used and the proposed controller is verified by means of computer simulation using MATLAB package. The simulation is carried out by tracking a desired position (x, y) and orientation angle (θ) with continuous trajectory in the tracking control of the NI mobile robot. The parameter values of the NI robot model are taken from, **Al-Shibaany, 2012**: L=0.36 m, r=0.05 m and sampling time is equal to 0.5 second.

The proposed nonlinear PID neural controller scheme as in **Fig. 2** is applied to the mobile robot model and it uses the proposed learning algorithms steps of genetic algorithm and particle swarm optimization for tuning the nonlinear PID controller's parameters. The fist stage of operation is to set the following parameters of the GA and PSO:

Population size is equal to 30 and number of iteration is equal to 100 for GA.

Population of particle is equal to 30 and number of iteration is equal to 100 for PSO.

Number of weight in each chromosome and particle is 9 because there are nine parameters of the nonlinear PID controller.

The desired path which has explicitly continuous gradient with rotation radius changes can be described by the following equations:

$$x_r(t) = -0.5 \times \sin(\frac{2\pi t}{30}) \tag{28}$$

$$y_r(t) = 0.5 \times \sin(\frac{2\pi t}{20}) \tag{29}$$

$$\theta_r(t) = 2\tan^{-1}(\frac{\Delta y_r(t)}{\sqrt{(\Delta x_r(t))^2 - (\Delta y_r(t))^2} + \Delta x_r(t)}) \tag{30}$$

For simulation purposes, the desired path is chosen as described in Eq. (28) and Eq. (29) while the desired orientation angle is taken as expressed in Eq. (30).

The mobile robot model starts from the initial posture $q(0) = [-0.1,0,0]$ as its initial conditions. A disturbance term $\overline{\tau d} = [0.01\sin(2t) \quad 0.01\sin(2t)]^T$ **Al-Araji, et al, 2013**, is added to the mobile robot system as unmodelled kinematics disturbances in order to prove the adaptation and robustness ability of the proposed controller. The mobile robot trajectory tracking obtained by the proposed nonlinear PID neural controller is shown in **Fig. 5**.

The adaptive learning and robustness of nonlinear PID neural controller based on PSO show excellent position and orientation tracking performance and small effect of the disturbances than learning GA because the PSO algorithm has capability to obtain smooth values of the nonlinear PID controller's parameters with smoothness convergence behaviour in the parameters values that depend on previous values without using mutation and crossover processes for GA technique.

Table 1. shows the tuning values of the nonlinear PID neural controller parameters (k_x, k_y, k_θ) which are based on genetic and particle swarm optimization learning algorithms.

The effectiveness and robustness of the proposed nonlinear PID neural control algorithm based on PSO is clear by showing the convergence of the pose trajectory and orientation errors for the robot model motion, as shown in **Fig. 6**.

MSE of the pose trajectory and orientation errors for the robot model motion at 100 iterations is shown in **Fig. 7**.

The simulation results demonstrated the effectiveness of the proposed controller based on PSO technique by showing its ability to generate small smooth values of the control input velocities for right and left wheels without sharp spikes.

The actions described in **Fig. 8** show that smaller power is required to drive the DC motors of the mobile robot model.

The mean linear velocity of the NI mobile robot is equal to 0.0897 m/sec, and the maximum peak of the angular velocity is equal to ± 0.42 rad/sec. Both are shown in **Fig. 9**.

In order to validate the applicability of the proposed nonlinear neural PID control methodology, experiments have executed by using mobile robot from National Instrument Company type differential wheeled mobile robot shown in **Fig. 10**. The wheeled mobile robot is equipped with Lab VIEW package guided.

In the experiments, PSO technique control methodology of the simulation has been applied on real NI mobile robot because the controller was robust and effective in terms of minimum tracking error and in generating best velocity control action despite of the presence of bounded external disturbances in comparison with the GA simulation results. Therefore, these control data has transmitted to the NI mobile robot model, which admits right wheel velocity and left wheel velocity as input reference signals by using wireless communication after has been converted the data format from MATLAB file of simulations to LabVIEW package version 2010 format as a lookup table in the NI mobile robot.

Velocities commands sent by the computer are coded messages which are recognized by microcontroller. Based on received characters, the microcontroller creates control actions for servo motors. The output voltages of the two encoder sensors are converted to coded messages by microcontroller and sent to the personal computer in order to calculate the tracking error of the mobile robot during motion. Wireless communication technique has been used for transmitting the data between the NI mobile robot and main computer.

The velocities of the simulation results for right and left wheels have been downloaded to the memory of the NI mobile robot as commands which have smooth values without sharp spikes, as shown in **Fig. 8**.

The initial pose for the NI mobile robot starts at position (-0.1 and 0) meter and orientation 0 radian and should follow desired continuous trajectory, as show in **Fig. 11**. The desired trajectory starts at position (0, 0, 0).

After 61 seconds, the real mobile robot has followed and finished the tracking of the desired path, as shown in **Fig. 12a** with small drifted from the desired trajectory and the distance of the trajectory did not exceed 5.47m. **Fig. 12b** shows the actual orientation of the mobile robot with small error. As shown in **Fig. 12c** the tracking error in x-coordinate and y-coordinate were reasonably accurate because the mobile robot was trying to correct the pose and orientation errors.

The mean-square error for each component of the state error vector $[ex, ey, e\theta]$ for simulation results and experimental work for two control algorithms are calculated, as shown in **Table 2**.

Table 2. shows the effectiveness and robustness of proposed controller based on PSO in terms of minimum tracking error and excellent position and orientation tracking performance than genetic learning algorithm because the PSO learning algorithm has capability to obtain best values of the parameters of the proposed controller with smoothness convergence behaviour in these parameters that depend on previous values without using mutation and crossover processes for GA technique.

The percentage of the mean square error between simulation results and experimental work can be shown in **Table 3**.

Table 3. shows the difference between simulation results and experimental work which caused by the residual errors in the experimental results due to the inherent friction present in the real system, especially during tracking the continuous gradient path and modelling errors, due to the difficulty of estimating or measuring the geometric, kinematics or inertial parameters, or from incomplete knowledge of the system components.

5. CONCLUSIONS

The nonlinear PID neural trajectory tracking control methodology with two learning algorithms for the differential drive mobile robot model have been presented in this paper. It has been designed and tested using Matlab package and carried out on real NI mobile robot using LabVIEW package.

The simulation results and experimental work show evidently the capability of adaptation and robustness of the proposed nonlinear PID neural controller that based on PSO learning algorithm which has excellent position tracking performance and it has the capability of generating smooth and suitable velocity commands than the controller based on genetic learning algorithm because the PSO algorithm has capability to obtain best values of the nonlinear PID controller's parameters as well as smooth parameters convergences behaviour which depends on previous values and this with few parameters adjustment unlike GA which depends on more evolutionary operators such as mutation and crossover.

REFERENCES

Al-Araji, A., Abbod, M. and Al-Raweshidy, H., 2013, *Applying Posture Identifier in Designing an Adaptive Nonlinear Predictive Controller for Nonholonomic Mobile Robot*. Neurocomputing, Vol. 99, pp. 543-554.

Al-Araji, A., 2005, *Genetic Algorithm and Elman Neural Network Used for Tuning the Parameters of the PID Neural Controller Based Model Reference.* Iraqi journal of computers, communication, control and systems engineering by University of Technology Vol. 5, No.1, pp. 111-126.

Ali, O. M., Koh, S. P., Chong, K. H., Hamoodi, A. S., 2011, *Design a PID Controller of BLDC Motor by Using Hybrid Genetic-Immune*, Modern Applied Science .Vol. 5, No. 1, pp. 56-63.

Al-Shibaany, Z., Hedley, J. and Bicker, R., 2012, *Design of an Adaptive Neural Kinematic Controller for a National Instrument Mobile Robot System*, IEEE International Conference on Control System, Computing and Engineering, Penang, Malaysia, pp. 623-628.

Chang, Y-C, Lwin, Y.Y. and Yamamoto, Y., 2009, *Sensor-Based Trajectory Planning Strategy for Nonholonomic Mobile Robot with Laser Range Sensors*, IEEE International Symposium on Industrial Electronics, Seoul Olympic Parktel, Seoul, Korea. pp. 1755-1760.

Derrac, J., Garc, S., Molina, D. and Herrera, F., 2011, *A Practical Tutorial on the Use of Nonparametric Statistical Tests as a Methodology for Comparing Evolutionary and Swarm Intelligence Algorithms*, Journal of Swarm and Evolutionary Computation, Vol.1, pp. 3–18.

Han, S., Choi, B. and Lee, J., 2008, *A Precise Curved Motion Planning for a Differential Driving Mobile Robot*. Mechatronics, Vol. 18, pp. 486-494.

Klancar, G. and Skrjanc, I., 2007, *Tracking Error Model-Based Predictive Control for Mobile Robots in Real Time*, Robotics and Autonomous Systems, Vol. 55, pp. 460-469.

Mnif, F. and Touati, F., 2005, *An Adaptive Control Scheme for Nonholonomic Mobile Robot with Parametric Uncertainty*, International Journal of Advanced Robotic Systems, Vol. 2, No. 1, pp. 59-63.

Muhammet, U., 2010, *Trajectory Tracking Performance Comparison Between Genetic Algorithm and Ant Colony Optimization for PID Controller Tuning on Pressure Process*, Wiley Periodicals Inc.

Omatu, S., Khalid, M. and Yusof, R., 1995, *Neuro-Control and its Applications*. London: Springer-Velag.

Park, B. S., Yoo, S. J., Park, J. B. and Choi, Y. H., 2010, *A Simple Adaptive Control Approach for Trajectory Tracking of Electrically Driven Nonholonomic Mobile Robots*, IEEE Transactions on Control Systems Technology, Vol. 18, No. 5, pp. 1199-1206.

Righeto, E., Grassi, L-H M. and Pereira, J. A., 2004, *Nonlinear Plant Identification by Wavelet*, Proceeding of ABCM Symposium Series in Mechatronics, Vol. 1, pp. 392-398.

Sahin, T. and Zergeroglu, E., 2007, *A Computationally Efficient Path Planner for a Collection of Wheeled Mobile Robots with Limited Sensing Zones*, IEEE International Conference on Robotics and Automation, Roma, Italy, pp. 1074-1079.

Su, K-H., Chen, Y-Y. and Su, S-F., 2010, *Design of Neural-Fuzzy-Based Controller for Two Autonomously Driven Wheeled Robot*, Neurocompting. Vol. 73, pp. 2478-2488.

Takanori, F., Kiroshi, N. and Norihiko, A., 2000, *Adaptive Tracking Control of a Nonholonomic Mobile Robot*, IEEE Trans Robotic Autonomous, Vol. 16, No. 2, pp. 609-615.

Wai, R-J and Liu, C-M, 2009, *Design of Dynamic Petri Recurrent Fuzzy Neural Network and its Application to Path-Tracking Control of Nonholonomic Mobile Robot*, IEEE Transactions on Industrial Electronics. Vol. 56, No. 7, pp. 2667-2683.

Yang, S. X., Yang, H., Max, Q. and Meng, H., 2004, *Neural Dynamics Based Full-State Tracking Control of a Mobile Robot*, IEEE International Conference on Robotics & Automation, New Orleans, LA, pp. 4614-4619.

Zhong, Q., 2006, *Robust Control of Time-delay Systems*, Springer – Verlag London Limited.

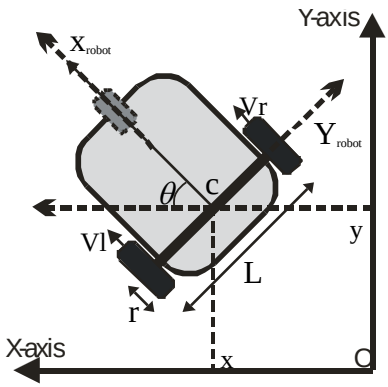

Figure 1. Mobile robot platform.

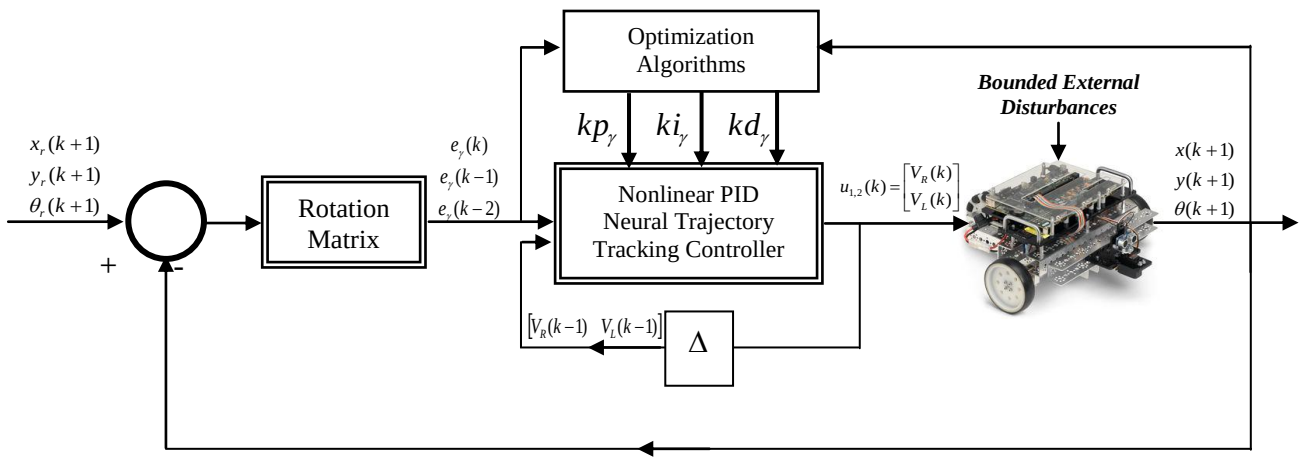

Δ is defined as a delay mapping.

Figure 2. Nonlinear PID Neural trajectory tracking controller structure for mobile robot.

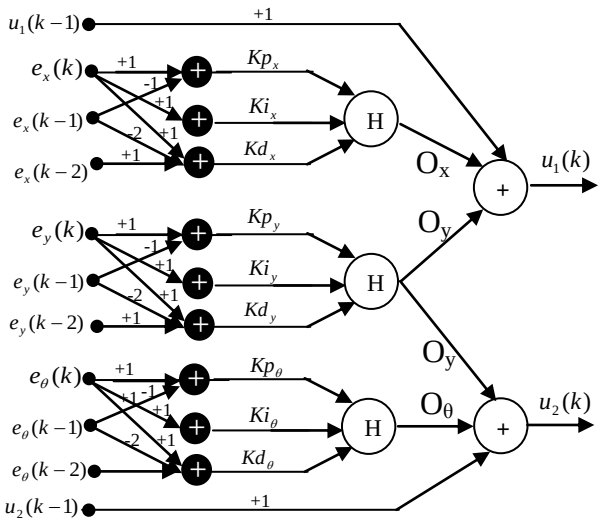

Figure 3. The nonlinear PID neural feedback controller structure.

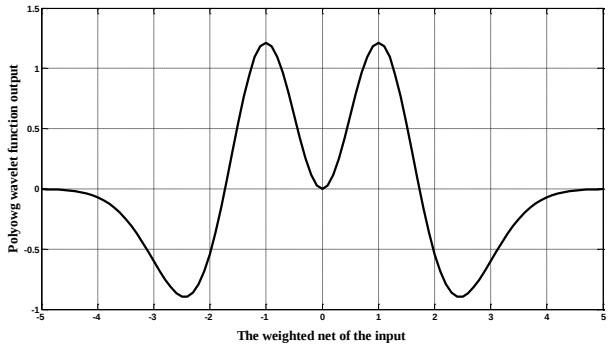

Figure 4. Polywog wavelet function.

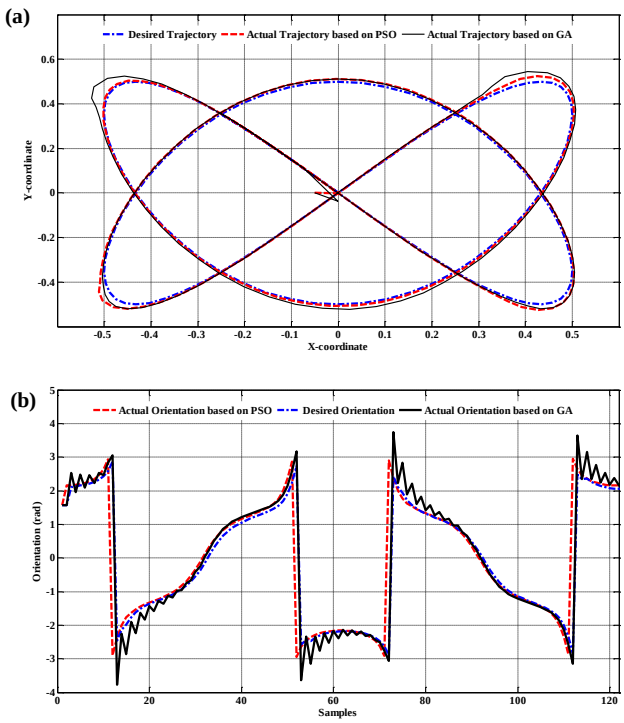

Figure 5. Simulation results (a) desired trajectory and actual mobile robot trajectory; (b) desired orientation and actual mobile robot orientation.

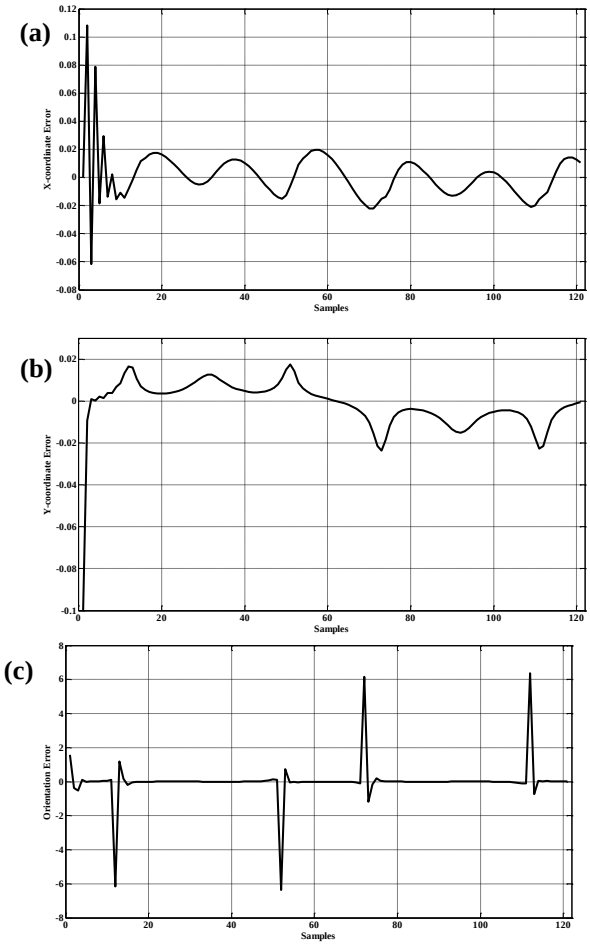

Figure 6. Position tracking error (a) in X- coordinate; (b) in Y-coordinate; (c) Orientation tracking error.

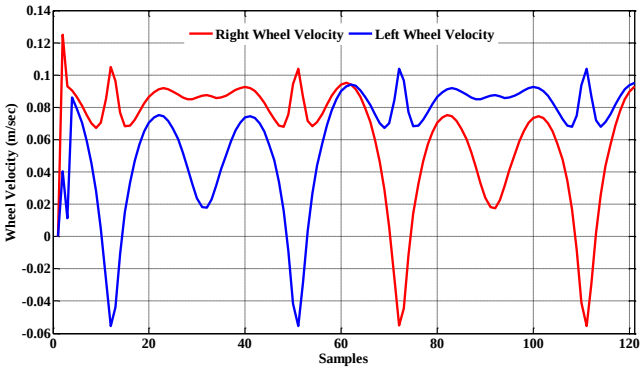

Figure 7. The right and left wheel action velocity.

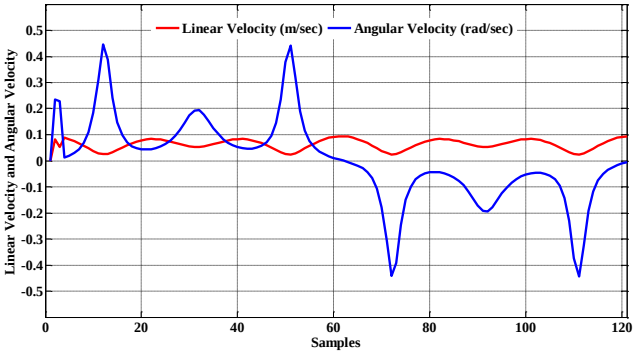

Figure 8. The linear and angular velocity.

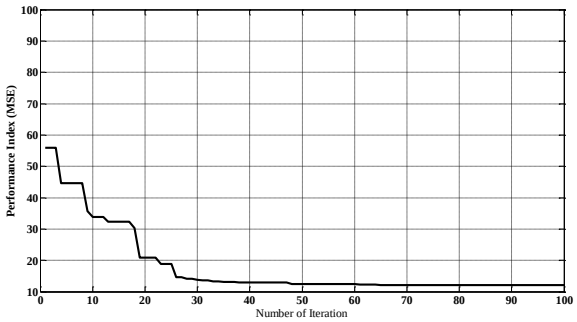

Figure 9. The performance index (MSE).

Figure10. NI mobile robot for the experiments.

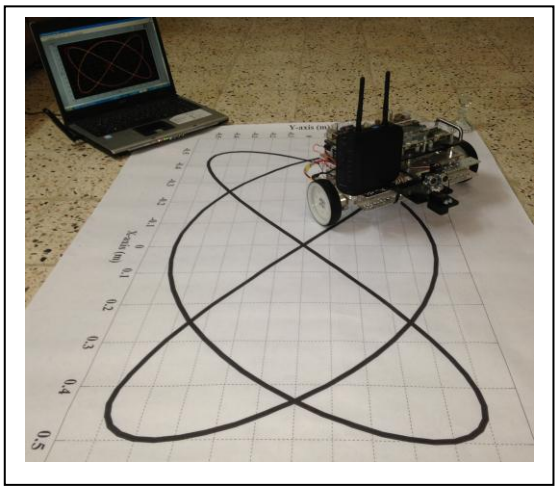

Figure 11. Real set-up experiment of NI mobile robot for continuous

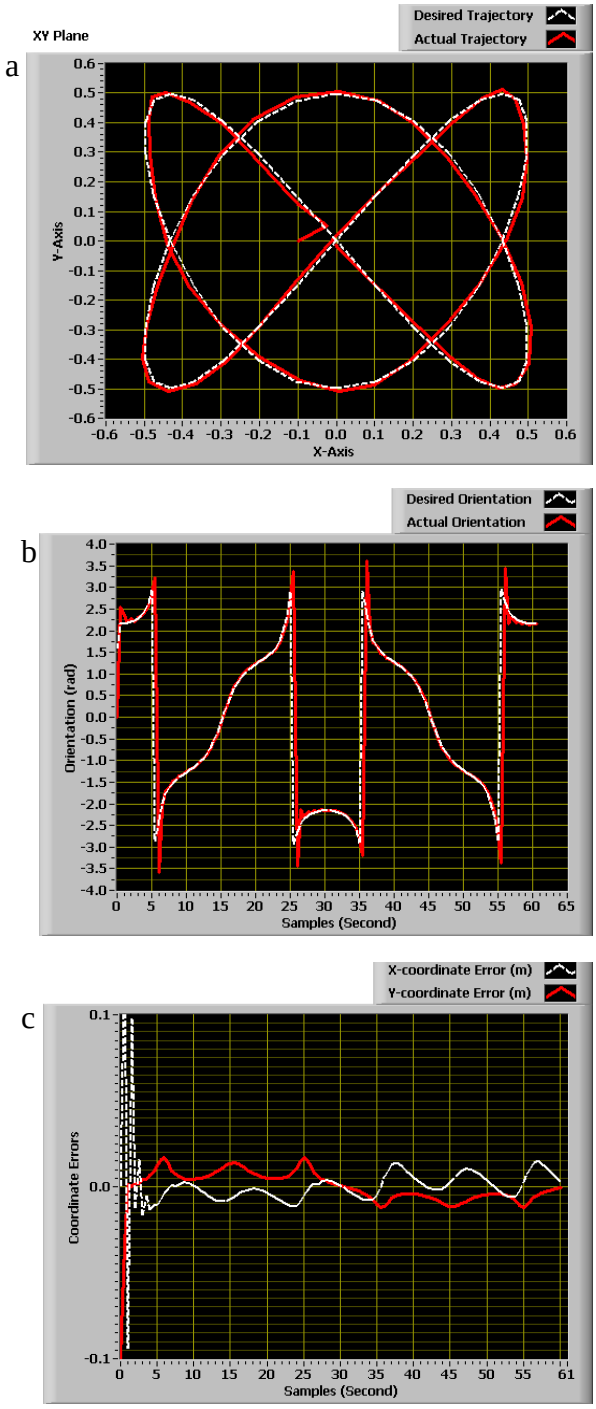

Figure 12. Practical results (a) desired trajectory and actual mobile robot trajectory; (b) desired orientation and actual mobile robot orientation; (c) X-coordinate and Y-coordinate errors.

Table 1. The nonlinear PID neural controller parameters.

Tech	kp_x	ki_x	kd_x	kp_y	ki_y	kd_y	kp_θ	ki_θ	kd_θ
PSO	0.75	0.72	0.131	-0.307	-0.36	1.039	-0.08	2.78	0.014
GA	0.007	0.42	0.460	0.316	0.407	0.554	0.242	0.454	0.5261

Table 2. The MSE for simulation results and experimental work.

PID Control Algorithm	**GA**			**PSO**		
MSE	(ex)	(ey)	(eθ)	(ex)	(ey)	(eθ)
Simulation Results	0.0021	0.0059	1.46	0.0013	0.0038	1.18
Experimental work	0.0032	0.0074	1.77	0.0019	0.0047	1.23

Table 3. The percentage of MSE between simulation results and experimental work.

PID Control Methodology	**GA**	**PSO**
(MSE of X-coordinate) 100%	34.3%	31.5%
(MSE of Y-coordinate) 100%	20.3%	19.1%
(MSE of Orientation) 100%	17.5%	4%

Analysis of Mosul and Haditha Dam Flow Data

Ahmaed Mohammed Ali
Professor
College of Engineering - University of Baghdad
Email:-drahmedmali@yahoo.com

Maryam Naeem Odaa
Instructor
Ministry of Water Resources
Email:-Eng_Maryam.Odaa@yahoo.com

ABSTRACT

The expansion in water projects implementations in Turkey and Syria becomes of great concern to the workers in the field of water resources management in Iraq. Such expansion with the absence of bi-lateral agreement between the three riparian countries of Tigris and Euphrates Rivers; Turkey, Syria and Iraq, is expected to lead to a substantially reduction of water inflow to the territories of Iraq. Accordingly, this study consists of two parts: first part is aiming to study the changes of the water inflow to the territory of Iraq, at Turkey and Syria borders, from 1953 to 2009; the results indicated that the annual mean inflow in Tigris River was decreased from 677 m^3/sec to 526 m^3/sec, after operating Turkey reservoirs, while in the Euphrates River the annual mean inflow was decreased from 1006 m^3/sec to 627m^3/sec after operating Syria and Turkey reservoirs. Second part is forecasting the monthly inflow and the water demand under the reduced inflow data. The results show that the future inflow of the Tigris River is expected to decrease to 57%, and reaches 301m^3/sec. The Mosul reservoir will be able to supply 64% only of the water requirements to the downstream. The share of Iraq from the inflow of the Euphrates River is expected to be 58%, therefore the future inflow will reach 290 m^3/sec. The Haditha reservoir will be able to supply 46% only of the water requirements to the downstream, due to reduced inflow at Iraqi border in the future.

Keywords: Time series; Reservoir operation; Tigris –Euphrates River; Dam; and Forecasting.

تحليل تدفق البيانات لسدي الموصل وحديثة

احمد عبد الصاحب محمد علي
البرفسور
كلية الهندسة - جامعة بغداد

مريم نعيم عودة
مهندس
وزارة الموارد المائية

الخلاصة

ان التوسع في انشاء مشاريع المياه في كل من تركيا وسوريا تقلق العاملين في حقل ادارة المياه في العراق حيث ليس هناك اتفاقية ثنائية بين الدول المتشاطئة (تركيا وسوريا والعراق) للاشتراك في مياه هذان النهران الدوليان دجلة والفرات مما سبب في انخفاض كميات المياه الواردة للعراق.

هذه الدراسة تتكون من جزءين :الجزء الاول هو دراسة التغير في كمية الواردات المائية القادمة للعراق عبر الحدود التركية والسورية للفترة من عام 1953 الى عام 2009. واشارت النتائج الى ان المعدل السنوي للوارد عند الحدود لنهر دجلة انخفض من 677 م^3/ ثا الى 526 م^3/ ثا بعد تشغيل السدود التركية. اما بالنسبة لنهر الفرات فأن المعدل السنوي للوارد عند الحدود انخفض من 1006 م^3/ ثا الى 627 م^3/ ثا بعد تشغيل السدود التركية والسورية. الجزء الثاني هو تخمين الوارد المائي الشهري والاحتياجات المائية في ضوء قلة الواردات المائية, حيث ان الوارد المستقبلي لنهر دجلة سيصل بنسبة 57% ليصل الوارد الى301م^3/ثا وان سد الموصل سيلبي 64% من الاحتياجات المائية لنهر دجلة. ان الوارد المستقبلي لنهر الفرات سيصل الى 290 م^3/ ثا على اساس ان الحصة المائية العراقية من نهر الفرات هي 58% وعليه سيلبي سد حديثة 46% من الاحتياج الكلي لنهر الفرات.

كلمات رئيسية : السلسلة الزمنية ; تشغيل الخزانات ; نهري دجلة والفرات ; سدود ; التخمين.

1. INTRODUCTION

The Tigris River is the second longest river in southwest Asia (1,840 km). The Tigris River rises in eastern Turkey near Lake Hazar and flows southeast to Iraqi borders at PaishKabur city, some of 400km from its source in Turkey **Kolars and Mitchell, 1991**. Through Iraq, numerous tributaries enter the lift bank of The Tigris River from the Zagros Mountains. Among these tributaries are the Greater Zab, the Lesser Zab, the Adhaim, and Diyala Rivers. While, the Euphrates River is one of the largest rivers of the Middle East; it originates in the mountainous areas of Turkey where up to 80% of the entire run off volume is formed, thenit crosses the territories of Turkey, Syria, and Iraq. The Euphrates River enters Iraq border at Hussaiba town. Many researchers have studied the Euphrates River and Tigris River basins and the Turkish Great Atatourk Project (GAP). **Kolars and Mitchell ,1991** introduced a chart for projected sequential depletion of the Euphrates River for the period 1990-2040. **Ishaq ,1998** studied the monthly optimal operation for the Iraqi water resources system for the periods (1962-1996)by a adopting an objective function to minimize the release and storage penalty. The result of optimization and simulation model indicated a deficiency in water supply for the periods (1974-1976) and (1989-1992).

El-obaidy ,2006 studied the effect of Turkish future projects implementation on Tigris River, this study consist of three parts; the first is to find synthetic time series. The second covers operating the existing and proposed reservoirs on Tigris River in Turkey. The third is to find the future expected water quality in accordance with the operation of the reservoirs. The optimum operational policies, from the Turkish point of view, show that the minimum flow irrigation requirements equal to 200 cumecs at the borders with Iraq.

Al-Bedyry ,2009 considered the Ilisu-Cizre reservoirs system as the case study, aiming at predict the effect of its optimal operation (from a Turkish point of view) on the flow of the Tigris River at the Turkish-Iraqi boarders, based on 51 years of real inflow data of the Tigris River recorded at Ilisu. The objectives were to test and remove a non- homogeneity from a historical monthly inflow data for Mosul, Dokan, and Haditha reservoir from 1952 to 2009, to analyze and forecast flow data of Tigris and Euphrates Rivers and to correct the monthly inflow coming to Iraqi borders, and the water demand according to reduced inflow data. The result of the study show that the annual flow at Iraqi borders will be equal to 9498MCM after operating Ilisu-Cizre reservoir.

2. THE STUDY AREA

The control system was divided into two sub systems. The first sub system consists of Mosul reservoir on Tigris River. The second sub system consists of Haditha reservoir on Euphrates River.

A- Mosul Dam is an embankment dam, it is the largest dam in Iraq. It is located on the Tigris River at the west of Ninawa governorate, approximately 50 km northwest of the town of Mosul, Iraq. The project is located approximately 65 km south from Iraq- Turkish border. The reservoir of the dam has been operated since 1986. it's a multi- purposes reservoir used mainly for flood control, supply water to Jazira irrigation projects and downstream river and generating hydro- power with a maximum capacity of 750MW **,Swiss Consultants, 1979**.

B- Haditha reservoir is located in the western part of Iraq about 140 Km from the Iraqi – Syrian border. The location of the reservoir is characterized by a dry and hot summer and a mild winter with low precipitation. It is an embankment reservoir, with a multi-purpose project intended for the control of the Euphrates River run off in order to meet the demands of irrigation,

electrical power generation and flood control to a certain extent. The reservoir has been operated since 1986.

3. HYDROLOGICAL TIME SERIES

Hydrologic time series is defined as continuous sequential observations which is usually expressed as an average value over specific intervals of time such as mean daily, mean monthly, or mean annual flows. Hydrologic time series may consist of four components depending on the type of variable and the average time interval **Yevjevich ,1972**. In seasonal stream flow series four components exist as shown in Eq. (1):

$$Q_t = J_t + T_t + P_t + E_t \quad (1)$$

where:

$\mathbf{Q_t}$ is the time series value (actual data) at period t,
$\mathbf{J_t}$ is the jump component at period t,
$\mathbf{T_t}$ is the trend-cycle component at period t,
$\mathbf{P_t}$ is the periodic component at period t, and
$\boldsymbol{E_t}$ is the irregular (or remainder) component at period t.

For the test and removal of non-homogeneity, the suitability of the historical data must be checked. The homogeneity definition requires at least two conditions: -

1. The hydrological data series must not contain any systematic error.
2. All the hydrological conditions should be constant.

If these conditions are satisfied then the series may be considered as homogeneous. These two conditions imply that homogenous series should be free from trend and jump component respectively; therefore homogeneity should be insured at the beginning of the analysis by the detection and removal of jump and trend components.

1. ***Jump*** is a sudden considerable change in the parameters of historical data such as mean and standard deviation of the stream flow data. A sudden increase is called a positive jump, while a sudden decrease is called a negative jump.

2. ***Trend*** component is defined as a systematic and continuous change over an entire sample in any parameter of the series. The causes of trend are either sequential man-made changes within the catchments area, extensive urban or natural causes or inconsistency (systematic errors).

There are many methods to detect the existence of jump components, such as statistical tests (t-test, F-test, etc.), which can be used to check for any significant changes in means or standard deviations of two samples at the desired percent probability level of significant. If those tests indicate significance changes then it means that the two sub-samples are from different populations and a jump and/or trend components exist. Trend can also be detected by regression analysis and described mathematical by means of polynomial function. The most powerful method for testing homogeneity is suggested by **Yevjevich ,1972**. where the test for homogeneity is made by using the spilt-sample approach to ascertain whether or not the differences between the mean and standard deviation of the two sub-samples are significantly different from zero at the 95% confidence interval. This test requires that the sample be divided into two sub-samples.

4. ANALYSIS AND FORCASTING OF FLOW DATA

4.1 Mosul Dam

There is a gauge station at upstream Mosul dam on Tigris River. The mean monthly discharge data sample (1953-2009) is divided into two sub-samples; the first is (36) years long, (1953-1988), and the second is (21) years long, (1989-2009). **Fig. 1 and 2** show the annual means and standard deviations of the original time-series The solid line of those Figures represents the average of the annual means and standard deviations of the series. The results of Split – Sample Test of original data are shown in **Table 1**. From this table, the jump component exists in the annual mean and annual standard deviation.

The jump component on the data of the first sub-sample is removed by applying Eq. (2).

$$Y(j,t) = \frac{X(j,t) - 677}{588} * 460 + 526 \qquad (2)$$

where:

j,t = the annual and seasonal positions of observations, respectively. The overall mean and standard deviation of the last 21 years (1989-2009), were 460 m^3/sec and 526 m^3/sec, respectively.

The test is repeated using [Y (j, t)] series as the new first sub-sample, and the original second sub-sample, the result are shown in **Figs. (3) and (4)** for the annual means and standard deviations respectively. These Figures indicated the removal of the jump component from the hydrological data. Trend was detected by fitting linear regression equations for annual means and standard deviations against years. The correlation coefficients after removing the jump component are shown in **Figs. (1) and (2)** Those Figures show the existence of the trend component in the annual mean and annual standard deviation. The trend component on the data of the sample is removed by applying Eq. (3):

$$Y(j,t) = \frac{Y(j,t) + 540. - 0.5(i + j/12)}{478 - 0.6(i + j/12)} * 460 + 526 (3)$$

where:

j, t = the annual and seasonal positions of observations, respectively. The overall mean and standard deviation of the last 21 years (1989-2009), were 460 m^3/sec and 526 m^3/sec, respectively.

After that the test was repeated using [Y (j, t)] series as the new series for all sample, the results are shown in **Figs. (3) and (4)** for the annual means and standard deviations, respectively. Those figures show that the correlation coefficients are very small for linear trends, which indicates the absence of linear trend component. As shown in **Figs. (3) and (4)**, the slopes of these lines are mild enough to be attributed to sample fluctuations, which indicate that the trend component is removed from the hydrological data. The series now may be considered homogeneous, i.e. free from jump and trend components.

The Results of Split – Sample Test of data after removing the jump and trend components are shown in **Table 2**, which indicates that the jump and trend component does not exist anymore in the annual mean and annual standard deviation.

The expansion in water projects implementations in Turkey and Syria is reduces the water inflow to the territory of Iraq. Therefore, the inflow data under the developement of the construction of additional reservoir and increase of the irrigation projects since 1952, must be corrected to find the optimal monthly operation rules for Mosul, and Haditha reservoirs. The method used to correct the inflow data was by applying the annual flow at Iraqi border which is equal to 9498MCM **,Al-Bedyry, 2009**. The annual mean of 57 years were 16587 MCM. So, K (factor) from Eq. (4) is 57.3%, the future annual mean from Eq. (5) is 301.4 m^3/s and the future annual standard deviation from Eq. (6) is 264m^3/sec.

K (factor) = annual flow at Iraqi border / annual mean at this time in Iraqi (4)

New annual mean = Annual mean inflow after Removing the jump and trend K (factor)* (5)

New annual standard Deviation= Annual standard Deviation after Removing the jump and trend K (factor)* (6)

The corrected data inflow calculated by Eq. (7) as follow.

$$Y(j,t) = \frac{X(j,t) - 526}{461} * 264.15 + 301.39 \qquad (7)$$

where:

Y (j, t): new monthly inflow data (1953-2009).

X (j, t): old monthly inflow data (1953-2009).

The new corrected [Y (j, t)], as new series for all samples, are shown in **Figs. 5 and 6** for the annual means and standard deviations, respectively.

4.2 Haditha Dam

A gauge station is existed at Hesaiba town upstream of Haditha dam on the Euphrates River. A mean monthly discharge data sample (1953-2009) was divided into two sub-samples; the first is (20) years long (1953-1972), and the second is (37) years long (1973-2009). **Figs. 7 and 8** show the annual means and standard deviations of the original time-series. The solid line of those Figures represents the average of the annual means and standard deviations of the series. **Figs. 7 and 8** show is the presence of jump in the annual flow data of Haditha dam.

The results of Split–Sample Test of original data are shown in **Table 1**. From this table it is clear that the jump component exists in the annual mean and annual standard deviation.

The jump component on the data of the first sub-sample was removed by applying Eq. (8):

$$Y(j,t) = \frac{X(j,t) - 1006}{867} * 241 + 627 \qquad (8)$$

where

j,t = the annual and the seasonal positions of observations, respectively, the number 241 m^3/sec and 627 m^3/sec are the overall mean and standard deviation of the last 37 years (1973-2009), respectively.

The test repeated using [Y (j, t)] series as the new first sub-sample, and the original series as the second sub-sample, as shown in **Figs. 9 and 10** for the annual means and standard deviations, respectively. Those Figures indicate that the jump component was removed from the hydrological data.

Trend was detected by mean of regression analysis. That was made by fitting linear regression equations for annual means and standard deviations against years. The correlation coefficients after removing the jump component are shown **in Figs. 7 and 8.** Those figures show that the trend component was existed in the annual mean and annual standard deviation. The trend component was removed by applying Eq. (9):

$$Y(j,t) = \frac{Y(j,t) + 695.3 - 2.3(i + j/12)}{258.4 - 0.6(i + j/12)} * 241 + 627 \quad (9)$$

where:

j, t = the annual and seasonal positions of observations, respectively, the numbers 241 m^3/sec and 627 m^3/sec are the overall mean and standard deviation of last 27 years (1973-2009), respectively.

The test repeated using [Y(j,t)] series as the new series for all samples, the result for the annual means and standard deviations are shown in **Figs. 9 and 10**. Those figures show that the correlation coefficients were very small for linear trends, which indicates the absence of linear trend component. As also shown in **Figs. 9 and 10**, the slopes of these lines are mild enough to be attributed to sample fluctuations, which indicate that the trend component was removed from the hydrological data. Accordingly, the series can be considered homogeneous, i.e. free from jump and trend components.

The results of Split–Sample Test of the data after removing the Jump component are shown in **Table 2**. This table show that the jump and trend components do not exist in the annual mean and annual standard deviation.

Considering that the total inflow of Euphrates River at the Turkish-Syrian border as 500m 3/sec, and the share of Iraq from this inflow is equal to 58% (**Ministry of Water Resources)**, then

*Annual flow at Iraqi border =500 * 0.58 =290m^3/sec, and*

Annual Standard Deviation =134.0 m^3/sec.

$$Y(j,t) = \frac{X(j,t) - 626.4}{241.1} * 134.0 + 290.0 \quad (10)$$

Accordingly, the correct inflow data is calculated by Eq. (10).

where:

Y (j, t): new monthly inflow data (1953-2009).

X (j, t): old monthly inflow data (1953-2009).

The new corrected [Y (j, t)], as new series for all samples, are shown in **Figs. 11 and 12** for the annual means and standard deviations, respectively.

5.RESULTS AND CONCLUSIONS

- The analysis of the 57 years (for the period 1953-2009) of historical monthly stream flow downstream Mosul , and Haditha reservoirs indicate significant changes occurred through the period of the record, which means that the series is not homogenous. There was jump and trend

components exist in the data and indicated by the mean and the standard deviation. The annual inflow at further of Tigris River will be decreased to 57%, meaning reduction from (526 m^3/sec to 301m^3/sec).

- The annual inflow at further of Euphrates River will be decreased to 58%, meaning reduction from (626 m^3/sec to 290m^3/sec).
    - Mosul reservoir can supply 64% of the water requirements downstream with an actual value of 469 m^3/sec, while the adopted value is 301 m^3/sec due to the expected reduction of the inflow at Iraqi border in the future.
    - Haditha reservoir Mosul reservoir can supply 76.3%, of the water requirements downstream with actual value of 723m^3/sec, while the adopted value is 551m^3/sec at current study and will supply 46.3% with actual value of 551 m^3/sec where the adopted value is 255m^3/sec due to future inflow reduction at Iraqi border.

6. RECOMMENDATIONS

- This study recommended that statistical analysis should be done from time to time to monitor the drops in the annual inflow due to the operation of the new dams and irrigation projects in Turkey and Syria to improve the quality of the data in order to be taken into consideration in the operation of Iraqi reservoirs system.
- The operating rules for Iraqi reservoirs must be reviewed to account for the inflows reduction.
- New researches that focus on the operation of Turkish and Syrian future projects implementation on Tigris, Euphrates, Grater Zab and Less Zab River will be required to determine the future inflow and salinity at Iraqi borders.
- Optimization of the operation of Mosul, Haditha, Dokan, Hemreen, Derbendikhan and Al-Tharthar reservoirs after operating new reservoirs in Turkey and Syria.

REFERENCES

- Al-Bedyry, N. K. 2009, *Application of Genetic Algorithm to Proposed Operation Scenario of Ilisu Dam*, Ph. D. Thesis, Irrigation and Drainage Department, College of Engineering, University of Baghdad, Iraq.

- El-Obaidy, A. I. F. ,2006, *Effect of Turkish Future Projects Implementation on Tigris River*, Ph. D. Thesis, College of Engineering, University of Baghdad.

- Ishaq, M. B. ,1998, *Optimum Operation Rules for Tigris-Euphrates System in Iraq*, Ph.D. Thesis, Irrigation and Drainage Department, College of Engineering, University of Baghdad, Iraq.

- Kolars, J. and Mitchell W. ,1991, *The Euphrates River and the Southeast Anatolia Development Project*, Southern Illinois University Press, Carbondale and Edwardsville.

- Swiss Consultants ,1979, *Planning Report for Mosul Dam Project, Iraq.*

- Yevjevich, W. M. ,1972, *Structural Analysis of Hydrologic Time Series*. Colorado State University, Hydrology Paper No. 56, Fort Collin, Colorado.

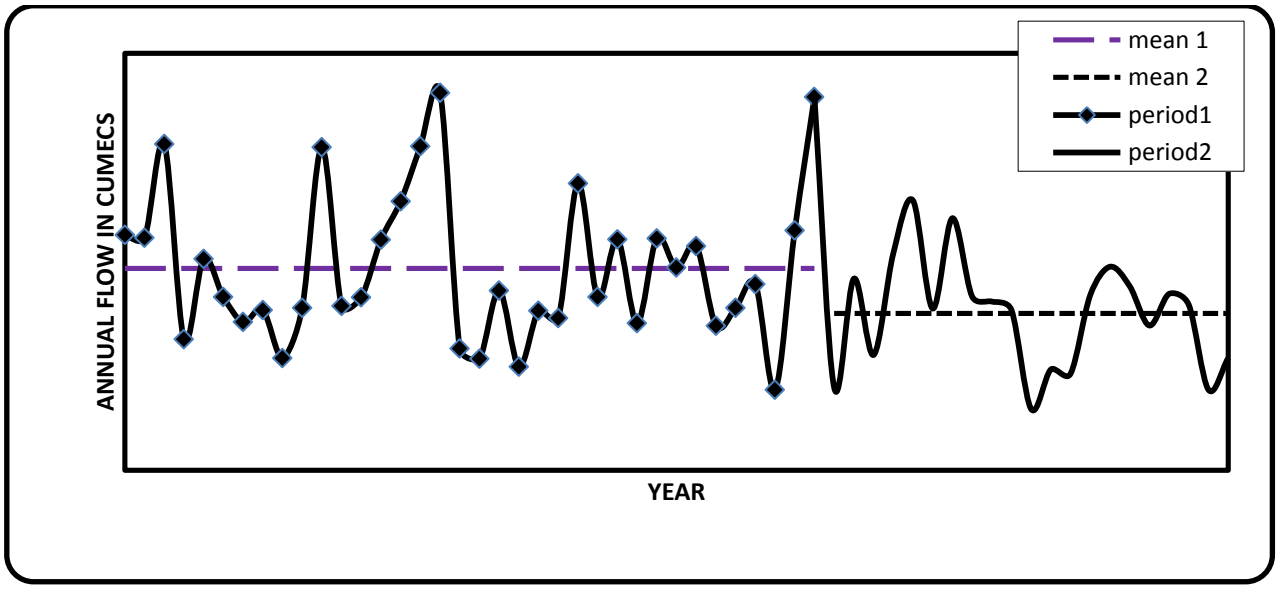

Figure 1. Annual flow upstream Mosul Dam (m^3/sec).

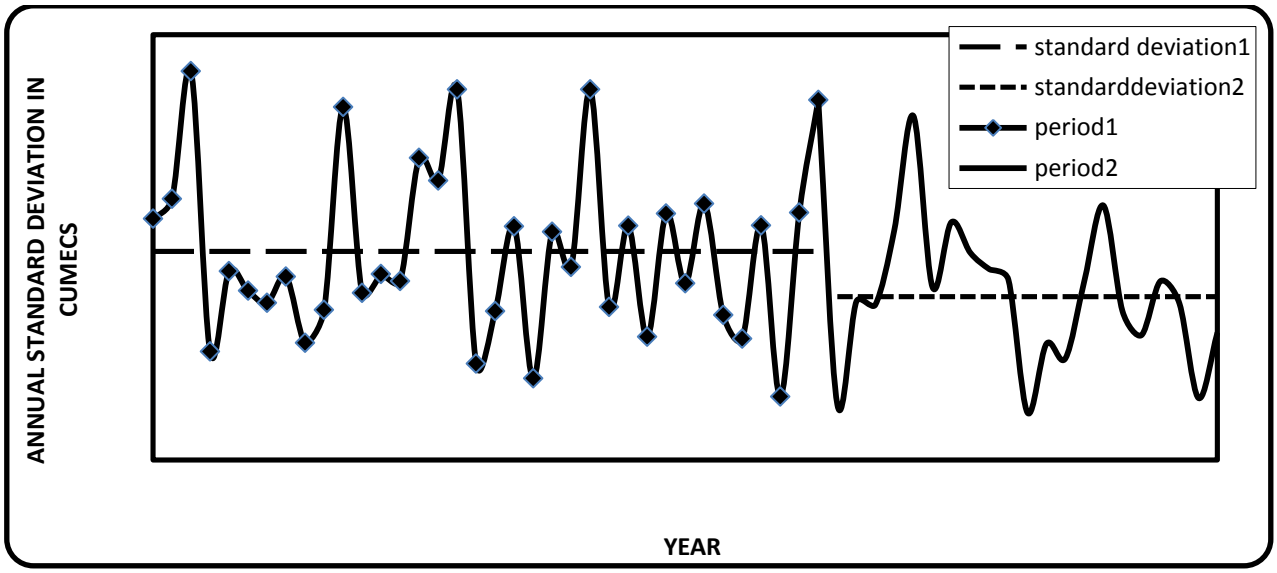

Figure 2. Annual standard deviation of the flow upstream Mosul Dam.

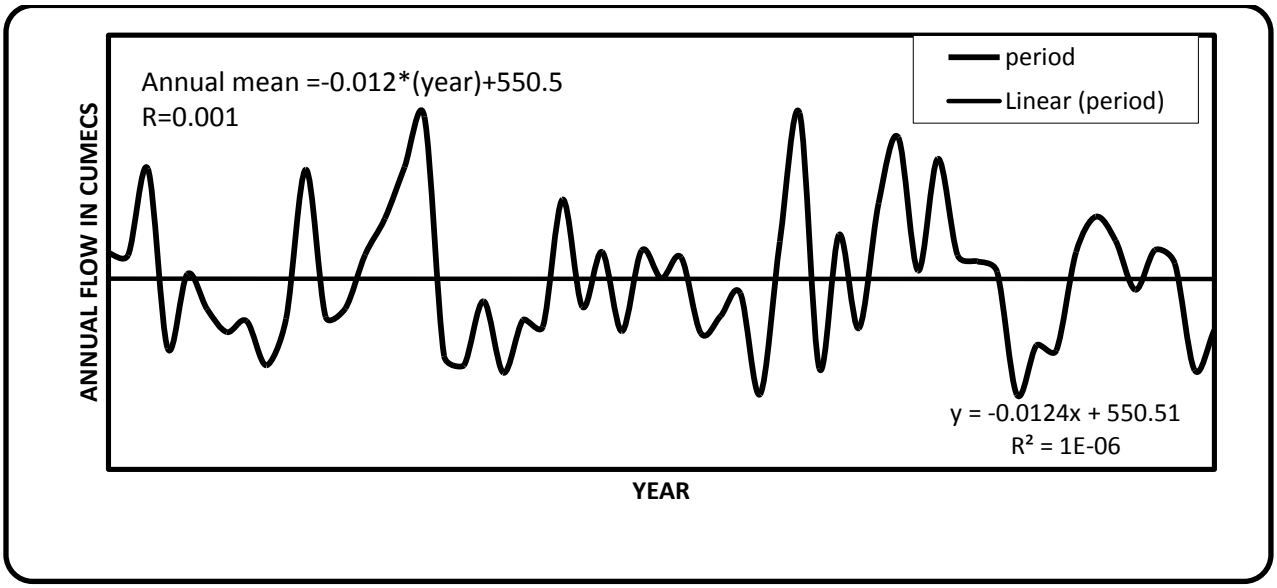

Figure 3. Annual flow at upstream Mosul Dam (m^3/sec), (After removing the jump and trend components).

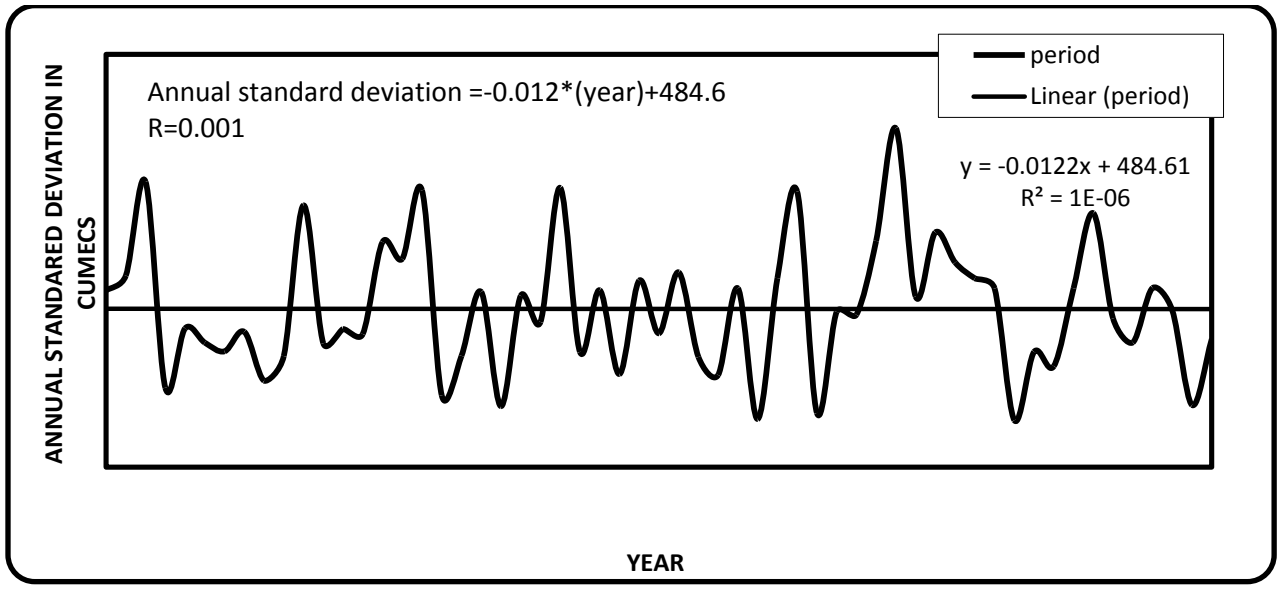

Figure 4. Annual standard deviation of the flow at upstream Mosul dam (m^3/sec). (After removing the jump and trend components).

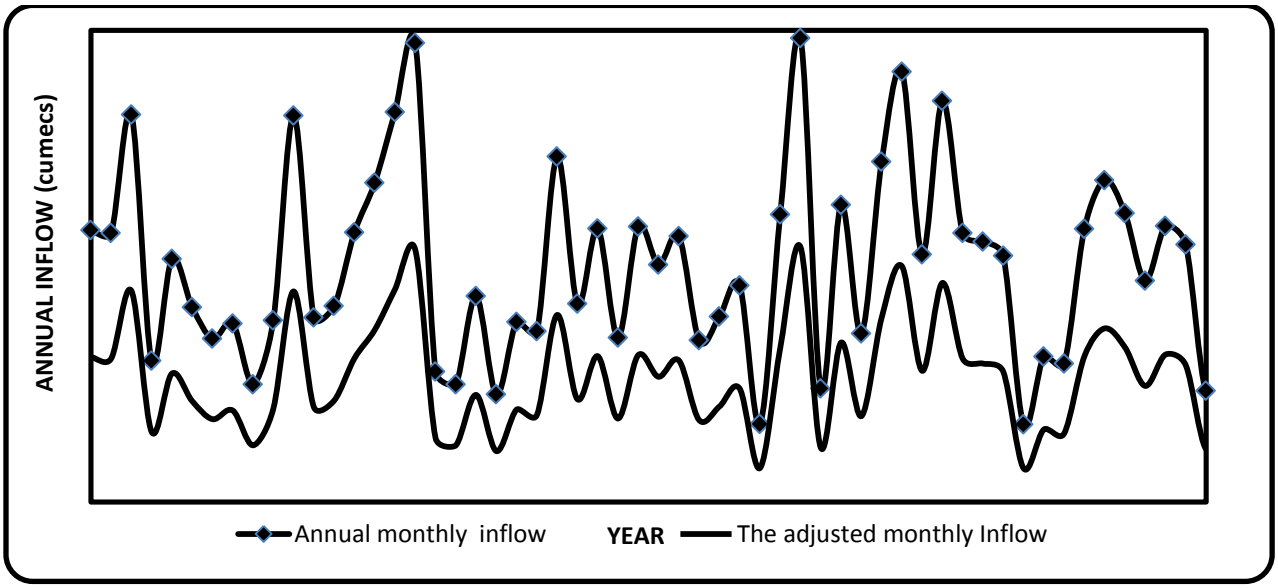

Figure 5. The adjusted monthly inflow (m^3/sec) of Tigris River up stream Mosul dam.

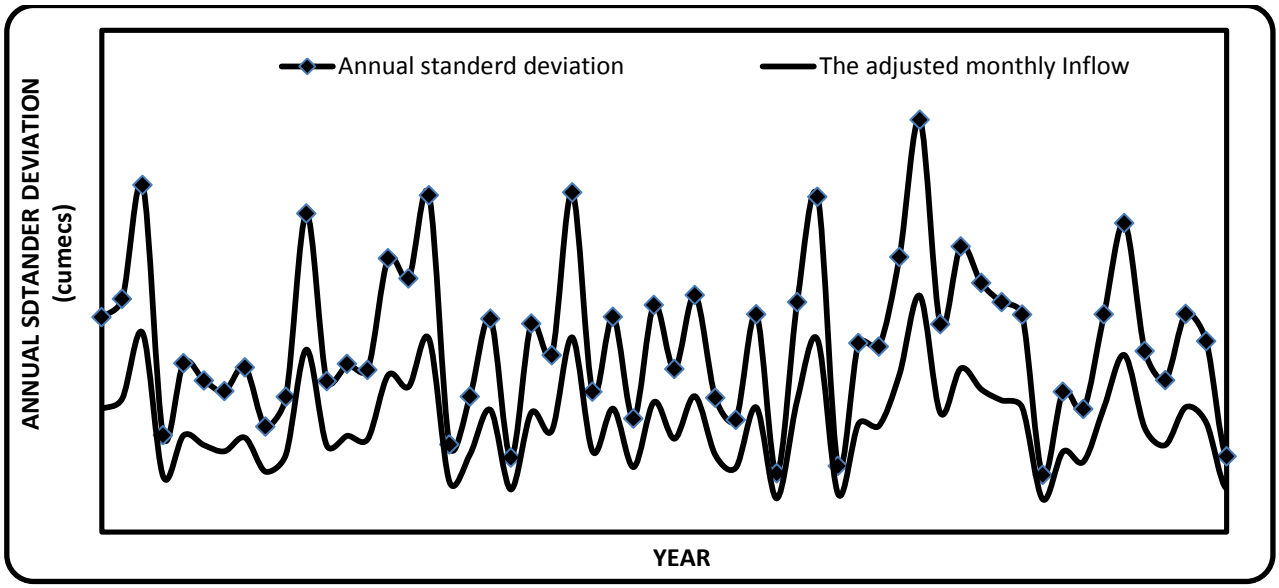

Figure 6. The adjusted monthly standard deviation (m^3/sec) of Tigris River up stream Mosul dam.

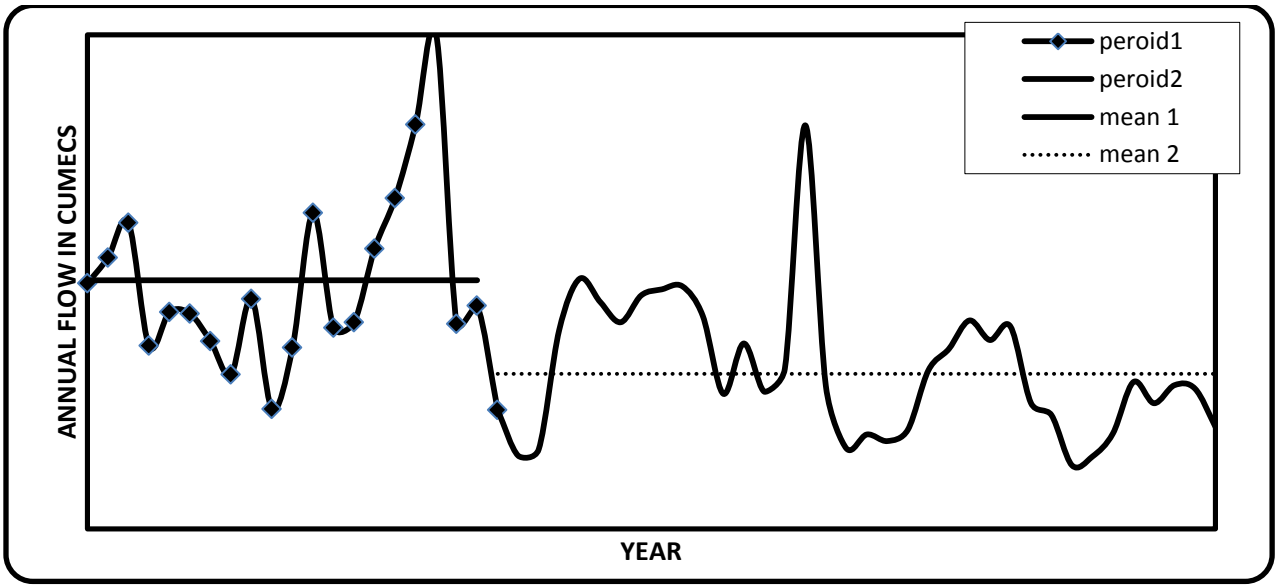

Figure 7. Annual flow at Haditha dam (m^3/sec).

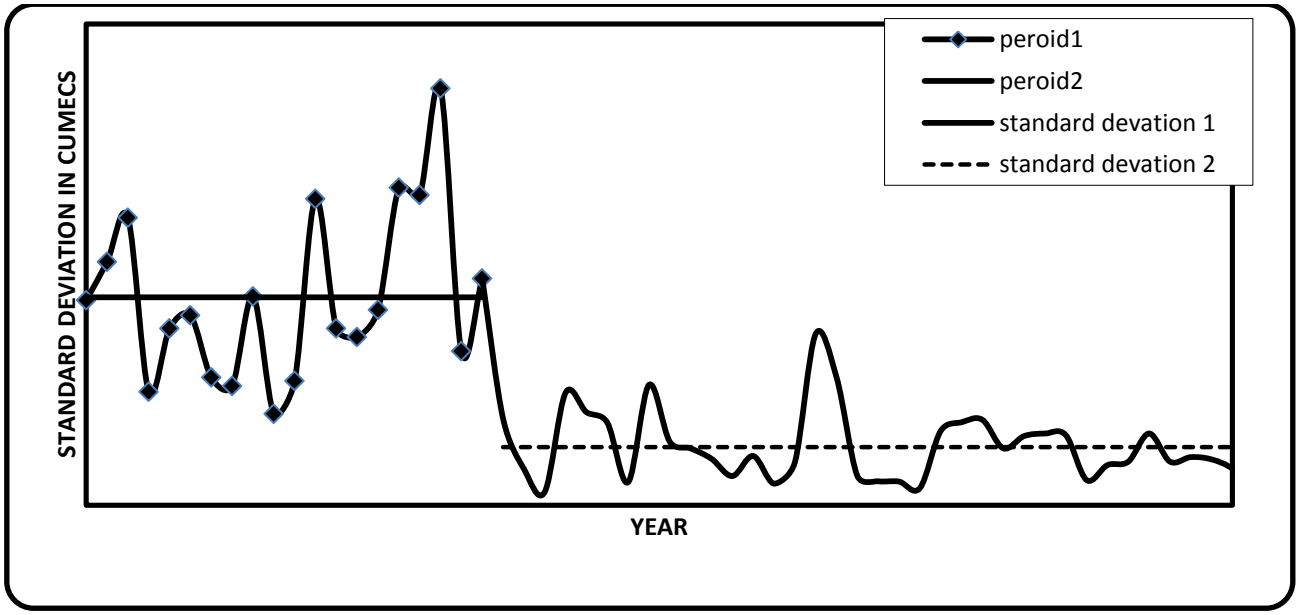

Figure 8. Annual standard deviation of the flow at Haditha dam (m^3/sec).

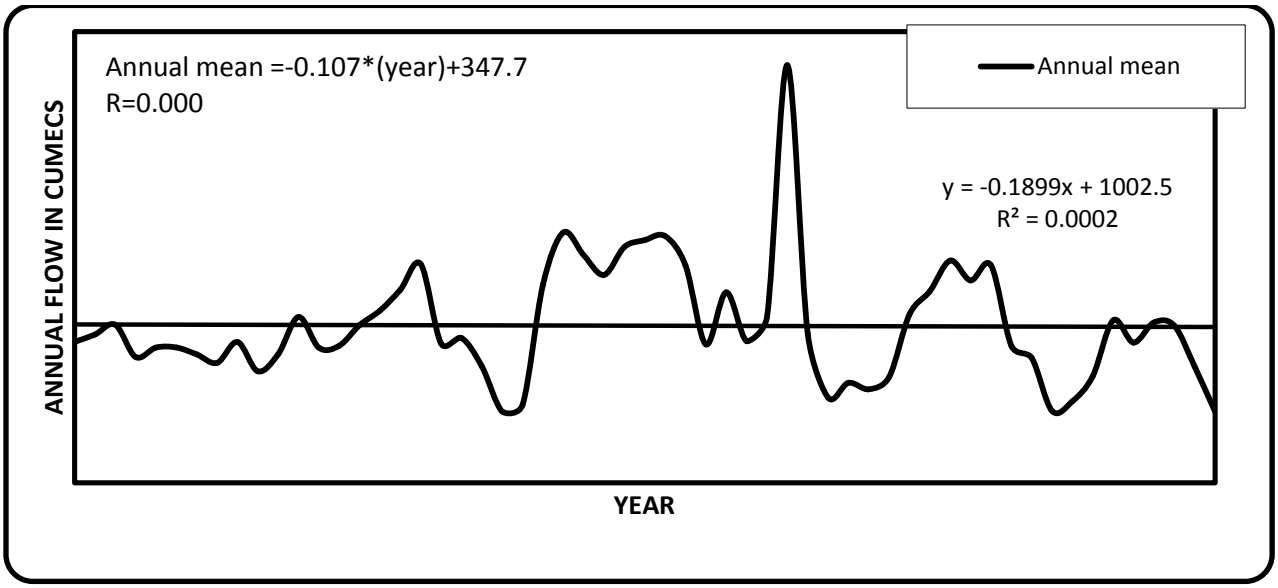

Figure 9. Annual flow at Haditha Dam (m^3/sec), (After removing the jump and trend components).

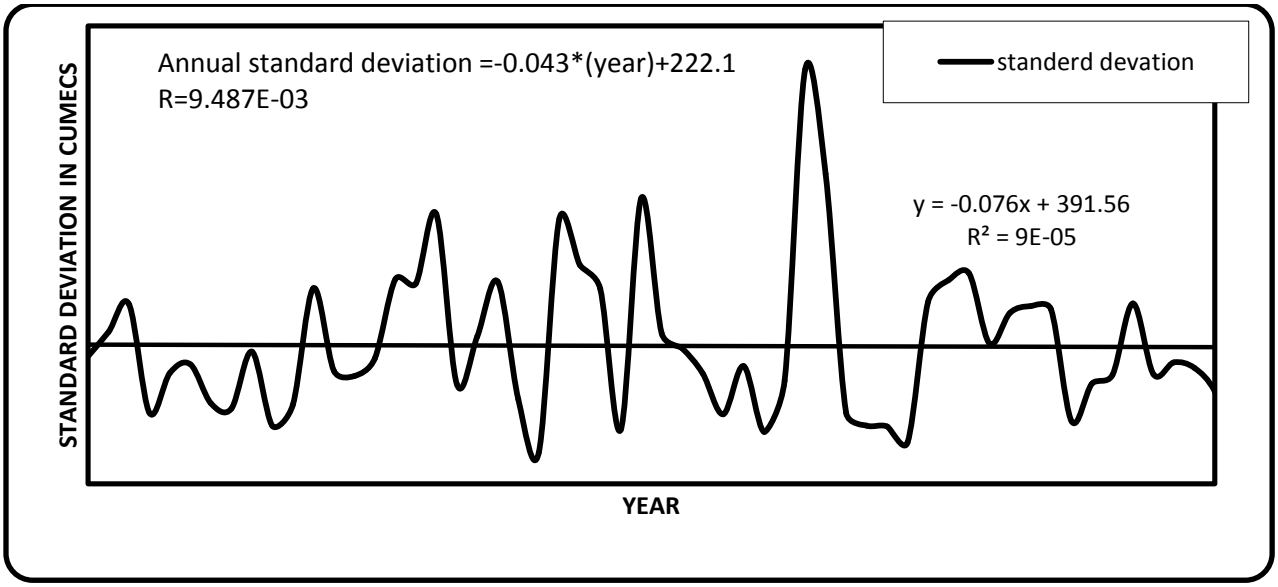

Figure 10. Annual standard deviation of the flow at Haditha dam (m^3/sec), (After removing the jump and trend components).

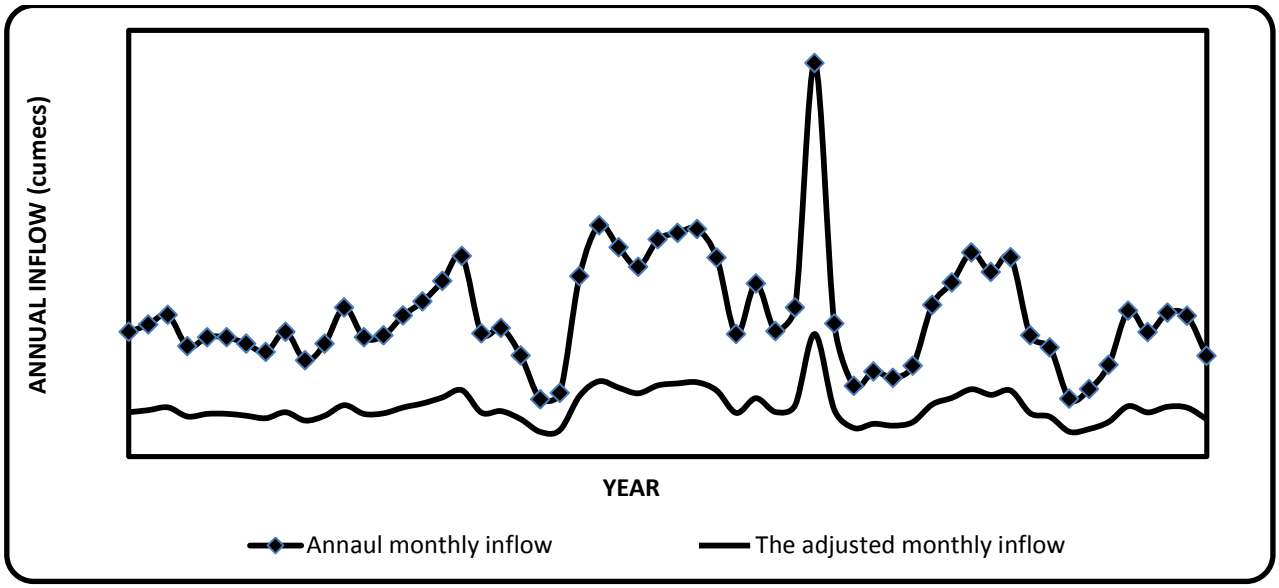

Figure 11. The adjusted monthly inflow (m^3/sec) of Euphrates River up stream Haditha dam.

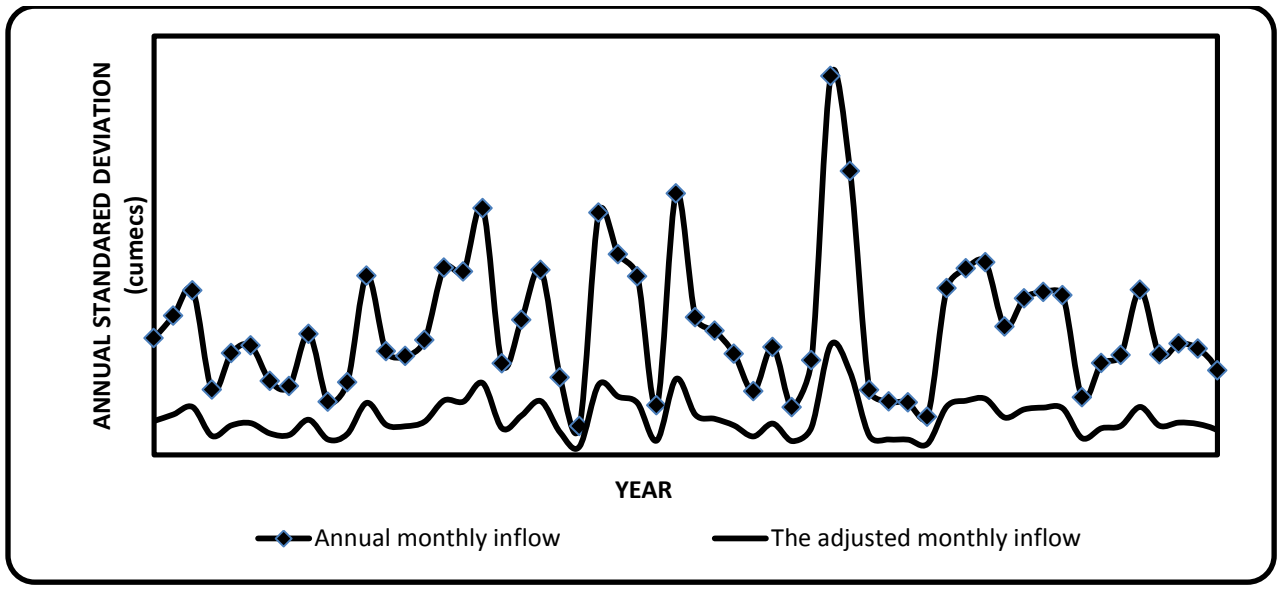

Figure 12. The adjusted monthly standard deviation of the flow at Haditha dam (m^3/sec).

Table 1. Results test of original data.

Reservoir	Statistical Parameters	Annual Mean m^3/sec	Annual Standard Deviation m^3/sec	
Mosul	No. of Years	36	36	1st. Periods (19531988)
	Average	677.46	588.44	
	Standard Deviation	252.83	240.10	
	No. of Years	21	21	2nd. Periods(19892009)
	Average	526.44	460.76	
	Standard Deviation	186.76	193.79	
	t-value	2.381	2.072	
	t-table	2.002	2.002	
	Jump Component	Exist	Exist	
Haditha	No. of Years	20	20	1st. Periods (19531988)
	Average	1006.57	867.32	
	Standard Deviation	357.44	340.75	
	No. of Years	37	37	2nd. Periods(19892009)
	Average	627.62	241.47	
	Standard Deviation	285.24	145.14	
	t-value	2.508	4.375	
	t-table	2.002	2.002	
	Jump Component	Exist	Exist	

Table 2. Results test of data after removing the jump and trend component.

Reservoir	Statistical Parameters	Annual Mean m^3/sec	Annual Standard Deviation m^3/sec	
Mosul	No. of Years	36	36	1st. Periods (19531988)
	Average	521.20	454.33	
	Standard Deviation	195.20	185.40	
	No. of Years	21	21	2nd. Periods(19892009)
	Average	534.82	471.11	
	Standard Deviation	189.90	196.84	
	t-value	-0.256	-0.322	
	t-table	2.002	2.002	
	Jump Component	Not Exist	Not Exist	
Haditha	No. of Years	36	36	1st. Periods (19531988)
	Average	502.00	191.42	
	Standard Deviation	119.45	125.28	
	No. of Years	21	21	2nd. Periods(19892009)
	Average	515.05	262.51	
	Standard Deviation	217.92	127.45	
	t-value	-0.293	-2.054	
	t-table	2.002	2.002	
	Jump Component	Not Exist	Not Exist	

Dynamic Behavior of Pb(II) and Cr(III) Biosorption onto Dead Anaerobic Biomass in Fixed-Bed Column, Single and Binary Systems

Abbas Hameed Sulaymon
Professor
College of Engineering
University of Baghdad
inas@yahoo.com

Shahlaa Esmail Ebrahim
Assistant Professor
College of Engineering
University of Baghdad
shahlaaaga@yahoo.com

Mohanad Jasim Mohammed Ridha
Instructor
College of Engineering
University of Baghdad
muhannadenviro@yahoo.com

ABSTRACT

The biosorption of lead (II) and chromium (III) onto dead anaerobic biomass (DAB) in single and binary systems has been studied using fixed bed adsorber. A general rate multi- component model (GRM) has been utilized to predict the fixed bed breakthrough curves for single and dual-component system. This model considers both external and internal mass transfer resistances as well as axial dispersion with non-liner multi-component isotherm (Langmuir model). The effects of important parameters, such as flow rate, initial concentration and bed height on the behavior of breakthrough curves have been studied. The equilibrium isotherm model parameters such as maximum uptake capacities for lead (II) and chromium (III) were found to be 35.12 and 23.84 mg g^{-1} respectively. While pore diffusion coefficients (D_p) were obtained to be 7.23×10^{-11} and 3.15×10^{-11} m^2 s^{-1} for lead (II) and chromium (III) respectively from batch experiments. The results show that the general rate model was found correct for describing the biosorption process of the dynamic behavior of the DAB adsorber column.

Key words: biosorption, DAB, lead (II), chromium (III), GRM, fixed bed, pore diffusion

السلوك الديناميكي من الرصاص (II) والكروم (III) الامتزاز الحيوي على الكتلة اللاهوائية الحيوية الميتة في عمود ثابت الكتلة، نظام مفرد و ثنائي

عباس حميد سليمون
استاذ
كلية الهندسة
جامعة بغداد

ا.م.د. شهلاء اسماعيل ابراهيم
استاذ مساعد
كلية الهندسة
جامعة بغداد

م.د. مهند جاسم محمد وَضا
مدرس
كلية الهندسة
جامعة بغداد

الخلاصة

تم دراسة الامتزاز الحيوي لايونات كل من االرصاص (II) والكروم (III) على الكتلة الحيوية اللاهوائية الميتة (DAB) في نظام مفرد وثنائي وباستخدام نظام الكتلة الثابتة الممتزة. وقد استخدم النموذج العام المتعدد العناصر (GRM) للتنبؤ بمنحنيات اختراق نظام الكتلة الثابتة الممتزة المفرد والثنائي. وقد تم الاخذ بنظر الاعتبار في هذا النموذج كل من مقاومة نقل المادة على الاسطح الخارجية والداخلية للمادة الممتزة، فضلا عن التشتت والانتشار المحوري خلال الانتقال داخل العمود الحيوي مع موديل متعدد المكونات (Langmuir mode). وقد تم دراسة تاثير المتغيرات، مثل معدل التدفق، وتركيز وارتفاع المادة الممتزة داخل العمود على سلوك منحنيات الاختراق لتركيز معين. ومن تجارب الدفعة الواحدة تم الحصول على ثوابت نموذج الاتزان حيث وجد ان اعظم امتزاز كان 35.12 و23.84 mg g^{-1} لكل من ايونات الرصاص(II) و الكروم(III) على التوالي. ومعاملات الانتشار المسامي (D_P) كانت 7.23×10^{-11} و 5×10^{-11} m^2s^{-1} لكل من ايونات الرصاص(II) و الكروم(III) على التوالي. وأظهرت النتائج أن النموذج المعدل العام صحيح لوصف عملية الامتزاز الحيوي من السلوك الديناميكي.

الكلمات الرئيسية : الامتزاز الحيوي، الكتلة اللاهوائية الميتة، والرصاص (II)، الكروم (III)، النموذج العام المتعدد العناصر عمود الكتلة الثابتة، الانتشار المسامي

1. INTRODUCTION

Metallic species mobilized and released into the environment by the technological activities of humans tend to persist indefinitely, circulating and eventually accumulating throughout the food chain, thus posing a serious threat to the environment, animals, and humans. It is essential to realize that the metal is only "removed" from the solution when it is appropriately immobilized **Sekomo et al., 2011**. The continuous use of heavy metals in industrial applications with the production of contaminated wastewaters is a serious environmental problem these biomass types serve as a basis for newly developed metal biosorption processes foreseen particularly as a very competitive mean for the detoxification of metal-bearing industrial effluents **Van et al., 2006**. Only within the past decade has the potential of metal biosorption by biomass materials been well established. For economic reasons, biomass produced as a waste byproduct of large-scale industrial could be used as biosorbents **Prasad et al., 2008**. Lead (II) has been found together with other compounds including Chromium (III) at high concentrations in a number of contaminated sites **Naseem** and **Tahir, 2001**. Lead (II) and Chromium (III) are released from industrial sources such as the iron-steel, petroleum, wood preserving chemicals dye and pigment **Prasad et al., 2008**.

The use of natural biomass as adsorbent will involve the same concept of separation as in adsorption which is termed as biosorption **Fiol et al., 2004**. Biosorption is a well-established and powerful technique for treating domestic and industrial effluents **Sulaymon et al., 2012 b**. DAB is the new and effectively used adsorbent. Biosorbent for the removal of metals/dyes mainly come under the following categories: bacteria, fungi, algae, industrial wastes, agricultural wastes and other polysaccharide materials. In general, all types of biomaterials have shown good biosorption capacities towards all types of metal ions **Vijayaraghavan** and **Yun, 2008**. The surface chemistry of biomass and the chemical characteristics of adsorbate, such as polarity, ionic nature, functional groups, and solubility, determine the nature of bonding mechanisms as well as the extent and strength of adsorption **Sulaymon** and **Ebrahim, 2010**. A variety of physicochemical mechanisms/forces, such as van der Waals, ion exchange, dipole interactions, H-binding, cation bridging, covalent bonding, and water bridging, can be responsible for the biosorption of inorganic compounds in biomass. **Sulaymon et al., 2012**. Metal uptake is caused by physico-chemical interaction between the metal and the functional groups present on the microbial cell surface, which is not dependent on the cells' metabolism **Vijayaraghavan** and **Yun, 2008**. Cell walls of microbial biomass, mainly composed of polysaccharides, proteins and lipids have abundant metal binding groups such as carboxyl, sulphate, phosphate and amino groups. This type of biosorption, i.e., non-metabolism dependent is relatively rapid and can be reversible **Sulaymon et al., 2012 b**.

Fixed bed adsorber is a continuous flow operation adsorption process for industrial applications in wastewater treatment **Ahmed, 2006**. The design of an adsorption column depends on various important parameters such as flow rate, initial concentration and bed height (mass of biomass). The sorption bed has to be porous to allow the liquid to flow through it with minimum resistance but allowing the maximum mass transfer into the particles as small as practical 0.7-1.5 mm **Sulaymon et al., 2012 b** Understanding of biosorption characteristics, determination of break point time for biosorption operation and effective utilization of the column is possible by carrying out the mathematical modeling of fixed-bed biosorption columns. Continuous biosorption studies are required to collect the experimental data for the design of biosorption column and for subsequent scale-up from pilot plant to industrial scale operation **Ahmed, 2006**. Past studies mainly focused on

analytical approach of solving the dynamics of fixed-bed adsorption columns. These models, exclude some of the important physical aspects such as axial dispersion and intra-particle resistances along the bed length and linear isotherm such as: second-order reversible reaction model (SRRM) and quasichemical kinetic model (QKM) and homogenous surface diffusion model (HSDM) described by **Pérez et al.,2013**. In the present study, a general multi-component model is used to predict the breakthrough curves of metal ions mixture in fixed bed column for single and binary components onto DAB and compare the experimental results with that simulated by a numerical solution of the model which includes film mass transfer, pore diffusion resistance, axial dispersion and nonlinear isotherm **Sulaymon et al., 2012 a**.

2. MATHEMATICAL MODELING AND SIMULATION

In the present study, a mathematical model for the fixed bed column is proposed by incorporation of important parameters such as external mass transfer resistance, internal mass transfer resistance and nonlinear multi-component isotherm **Ahmed, 2006**. The proposed model can be extensively used for understanding the dynamics of the fixed bed adsorption column for the biosorption of multi-inorganic (metal ions) compounds. To formulate a generalized model for the fixed bed adsorption column, the following assumptions are made **Sulaymon et al., 2012 a**:

- Equilibrium of adsorption is described by the nonlinear multi-component Langmuir isotherm.
- Mass transfer across the boundary layer surrounding the solid particles is characterized by external-film mass transfer coefficient (k_f).
- Intra-particle mass transfer is characterized by pore diffusion coefficient (D_p)
- Macro-porous adsorbent particles are spherical and homogeneous in size and density.
- Compressibility of the mobile phase is negligible.
- Fluid inside particles (macropores) is stagnant, i.e., there is no convective flow inside macropores.
- The adsorption process is isothermal. There is no temperature change during a run.
- The concentration gradients in the radial direction are negligible.
- All mechanisms which contribute to axial mixing are lumped together into a single axial dispersion coefficient.

Based on the assumptions of the model, the governing equations for a multi-component system can be obtained from differential mass balance of the bulk-fluid phase and the particles phase respectively:

Continuity equation in the bulk-fluid phase Eq.(1):

$$-D_{bi}\frac{\partial^2 C_{bi}}{\partial Z^2}+V_i\frac{\partial C_{bi}}{\partial Z}+\frac{\partial C_{bi}}{\partial t}+\frac{3k_{fi}\left(1-\varepsilon_b\right)}{\varepsilon_b R_p}\left[C_{bi}-C_{pi,R=R_p}\right]=0 \qquad (1)$$

Continuity equation inside the particle phase Eq.(2):

$$\left(1-\varepsilon_p\right)\frac{\partial C_{pi}^*}{\partial t}+\varepsilon_p\frac{\partial C_{pi}}{\partial t}-\varepsilon_p D_{pi}\left[\frac{1}{R_p^2}\frac{\partial}{\partial R_p}\left(R_p^2\frac{\partial C_{pi}}{\partial R_p}\right)\right]=0 \quad (2)$$

Initial and Boundary Conditions:
The initial and boundary conditions may be represented by Eq.(3) to Eq.(8):

Initial Condition (t = 0):

$$C_{bi}=C_{bi}(0,Z)=0$$
(3)

$$C_{pi}=C_{pi}(0,R,Z)=0 \quad (4)$$

Boundary Conditions:
Z = 0:

$$\frac{\partial C_{bi}}{\partial Z}=\frac{v}{D_{bi}}\left(C_{bi}-C_{oi}\right) \quad (5)$$

Z =L:

$$\frac{\partial C_{bi}}{\partial Z}=0 \quad (6)$$

R = 0:

$$\frac{\partial C_{pi}}{\partial R}=0 \quad (7)$$

$R = R_p$:

$$\frac{\partial C_{pi}}{\partial R}=\frac{k_{fi}}{\varepsilon_p D_{pi}}\left(C_{bi}-C_{pi,R=R_p}\right) \quad (8)$$

Dimensionless Groups:
Defining the following dimensionless variables:

$$c_{bi}=\frac{C_{bi}}{C_{oi}},\ c_{pi}=\frac{C_{pi}}{C_{oi}},\ c_{pi}^*=\frac{C_{pi}^*}{C_{oi}},\ \tau=\frac{vt}{L},\ r=\frac{R}{R_p},\ z=\frac{Z}{L}$$

Also, the dimensionless parameters are defining as:

$$Pe_i = \frac{vL}{D_{bi}},\ Bi_i = \frac{k_{fi}R_p}{\varepsilon_p D_{pi}},\ \eta_i = \frac{\varepsilon_p D_{pi} L}{R_p^2 v},\ \zeta_i = \frac{3Bi_i \eta_i (1-\varepsilon_b)}{\varepsilon_b}$$

The model equations can be transformed into the following dimensionless Eq. (9) and Eq.(10):

$$-\frac{1}{Pe_i}\frac{\partial^2 c_{bi}}{\partial z^2} + \frac{\partial c_{bi}}{\partial z} + \frac{\partial c_{bi}}{\partial \tau} + \zeta_i \left(c_{bi} - c_{pi,r=1}\right) = 0 \tag{9}$$

$$\frac{\partial}{\partial \tau}\left[(1-\varepsilon_p)c_{pi}^* + \varepsilon_p c_{pi}\right] - \eta_i \left[\frac{1}{r^2}\frac{\partial}{\partial r}\left(r^2 \frac{\partial c_{pi}}{\partial r}\right)\right] = 0 \tag{10}$$

In these equations, the Peclet number (Pe_i) reflects the ratio of the convection rate to the dispersion rate, while the Biot number (Bi_i) reflects the ratio of the external film mass transfer rate to the intra-particle diffusion rate.
Initial conditions become ($\tau = 0$) **Ahmed, 2006** Eq.(11) and Eq.(12):

$$c_{bi} = c_{bi}(0, z) = 0 \tag{11}$$

$$c_{pi} = c_{pi}(0, r, z) = 0 \tag{12}$$

And boundary conditions become Eq(15) to Eq(16);

z = 0: $$\frac{\partial c_{bi}}{\partial z} = Pe_i \left(c_{bi} - 1\right) \tag{13}$$

z =1: $$\frac{\partial c_{bi}}{\partial z} = 0 \tag{14}$$

r = 0:

$$\frac{\partial c_{pi}}{\partial r} = 0 \tag{15}$$

r = 1:

$$\frac{\partial c_{pi}}{\partial r} = Bi_i \left(c_{bi} - c_{pi,r=1}\right) \tag{16}$$

The concentration c_{pi}* in Eq.(10) is the dimensionless concentration of component *i* in the solid phase of the particles. It is directly linked to a multi-component isotherm, which is the extended Langmuir model Eq.(17) and Eq.(18):

$$C_{pi}^{*} = \frac{q_{mi}\rho_p b_i C_{pi}}{1+\sum_{j=1}^{N_s} b_j C_{pj}} = \frac{\rho_p a_i C_{pi}}{1+\sum_{j=1}^{N_s} b_j C_{pj}} \tag{17}$$

And in dimensionless form:

$$c_{pi}^{*} = \frac{\rho_p a_i c_{pi}}{1+\sum_{j=1}^{N_s} \left(b_j C_{oj}\right) c_{pj}} \tag{18}$$

Because of nonlinear multi-component Langmuir isotherm is considered, finite element method (Galerkin weighted residual method) is used for the discretization of the bulk-fluid phase partial differential equation and the orthogonal collocation method for the particle phase equation is produced. The ordinary differential equation system with initial values can be readily solved using an ordinary differential equation solver such as the subroutine "ODE15S" of MATLAB V-7.3 which is a variable order solver based on the numerical differentiation formulas (NDFs**) Sulaymon** and **Ahmed, 2008**.

3 EXPERIMENTAL MATERIALS AND PROCEDURE

3.1 Adsorbate

Standard stock solutions of 1000 mg/l of lead (II) and chromium (III) were prepared by dissolving $Pb(NO_3)_2$ and $Cr(NO_3)_3$ (BDH, England with minimum purity 99.5 %). The salts obtained from a local market with specifications are shown in **Table1**. Lead nitrate of 0.1599 g and 4.577 g of chromium nitrate were dissolved in 1 L distilled water. Metal concentrations were determined by a flame atomic absorption spectrophotometer Buck, Accusys 211, USA

3.2 Adsorbent

Heterogeneous cultures including mostly anaerobic bacteria, yeast fungi and protozoa of sorbents were taken from Al-Rustomia third extension drying bed Baghdad-Iraq. The physical, chemical and biological properties were measured and listed in **Table 2**. Anaerobic and facultative anaerobic microorganisms (*Aeromonas species, E-coli, Pseudomonas aerginrsa, Clostridium, Staphylococcus sp and Salmonella sp, Rhizopusarrhizus, Saccharomyces erevisiae)* were found in the biomass from the drying beds using API Instrument (Biomerieux, France). Preparation (DAB) using heterogeneous culture of live anaerobic biomass (LAB) was dried at temperature (37-45°C) for 5 days crushed, sieved, washed with distilled water and dried at 70°C for 6 h.

3.3 Procedure

Solutions pH were adjusted to the desired value (pH=4) using 0.1 M NaOH or 0.1 M HNO_3. With pH higher than 5.5, solubility of metal complexes decreases sufficiently allowing precipitation, which may complicate the sorption process and do not bind to the adsorption sites on the surface of DAB. These flasks were then placed on a shaker (HV-2 ORBTAL, Germany) and agitated continuously for 4 h at 200 rpm and (33±3°C). The samples were filtered by no. 42

Whatman filter paper. Few drops of 0.1 M HNO_3were added to the samples to decrease the pH below 2 in order to fix the concentration of the heavy metals during storage before analysis **APHA, 1995**.The final equilibrium concentrations were measured by means of atomic absorption

The fixed bed adsorber was made of an acrylic column of 0.05 m inner diameter and 0.5 m height **Fig. 1**. The DAB bed is confined in the column by fine stainless steel screen and glass cylindrical packing at the bottom and also at the top of the bed to ensure a uniform distribution of influent through the biomass bed. A perforated plate is fixed at the top of the column where the influent solution is introduced to the column.
For determination of the biosorption isotherm, different weights (0.05, 0.1, 0.15… to 0.6 g) of dry dead anaerobic biomass were used, (electronic balance Sartorius BL 210S); biosorbent were placed in 12 volumetric flasks of 250 mL. A volume of 100 mL of solution with concentration of 50 mg/L was added to each flask for single systems of Pb(II), Cr(III) ions respectively. The experiment was performed at sufficiently high metal concentrations so that maximal uptake would be achieved. The adsorbed amount was calculated using Eq. (19) **Sulaymon et al., 2012 b**

$$q_e = \frac{V_L(C_o - C_e)}{W_A} \tag{19}$$

The necessary dosage of DAB used for kinetic study, to reach equilibrium related concentration of C_e/C_o equal to 0.05, were calculated from Langmuir isotherm model and mass balance equation Eq.(20) With Eq.(21)

$$W_A = \frac{V_L(C_o - C_e)}{q_e} \tag{20}$$

$$q_e = \frac{q_m b C_e}{1 + b C_e} \tag{21}$$

The important characteristic of the Langmuir isotherm can be expressed in terms of the dimensionless constant separation factor for equilibrium parameter R_L. This is defined by:

$$R_L = \frac{1}{1 + bC_e} \tag{22}$$

The adsorption isotherms were obtained by plotting the weight of solute adsorbed per unit weight of biomass q_e, mg/g against the equilibrium concentration of the solute in the solution C_e, mg/L, and R_L Separation factor Eq. (22) **Sulaymon** and **Ebrahim 2010**. Reaction pathways were found using 2L pyrex beaker fitted with variable speed mixer. The beaker was filled with 1 L of 50 mg/L concentration and the agitation started before adding value of DAB. At time zero, the accurate weight of DAB where added and samples were taken at specified time intervals. Pore diffusion coefficient (D_p) of Pb(II) and Cr(III) was obtained using a batch model by matching the concentration decay curve obtained from the experimental data. At the beginning the pore diffusion coefficient is assumed and the model is solved numerically using MATLAB program. This process continued until obtaining perfect matching between the theoretical and experimental concentration

decay curve. The principle parameter required for solving the batch model is the external mass transfer coefficient (k_f) Eq.(23) and the assumed pore diffusion coefficient (D_p). Eq.(24) The external mass transfer coefficient kf and Molecular diffusivity D_m in the fixed bed column model were calculated using the correlation of Crittenden Eq.(25) **Sulaymon** and **Ahmed, 2008**.

$$k_f=2.4V_s/(Sc^{0.58}\,R_e^{0.66}) \quad (23)$$

The liquid diffusivity coefficient was calculated using Eq.(24):

$$D_m=2.74*10^{-9}\,(MW)^{-1/3} \quad (24)$$

The axial dispersion coefficient D_b of the liquid flowing through fixed beds was obtained from the following correlation **Urban** and **Gomezplata, 2009**:

$$\frac{D_z}{D_m}=0.67+1.15\left[\frac{V_s d_p}{D_m}\right]^{1.2} \quad (25)$$

4 RESULTS AND DISCUSSION

4.1 Adsorption Isotherm

The equilibrium isotherm for the investigated solutes (Pb^{+2} and Cr^{+3}) onto DAB using multi-component Langmuir model are presented in **Fig.2**. The correlation coefficient (R^2) between the experimental data and the theoretical model is 0.958 and 0.999 for lead and chromium respectively. The Langmuir parameters are as follows:

- Pb^{2+}: q_m= 35.12 mg g^{-1}, b= 0.311 L mg^{-1}, R^2 = 0.958
- Cr^{+3}: q_m= 23.84 mg g^{-1}, b= 0.165 L mg^{-1}, R^2 = 0.999

To compare these results obtained by DAB with other absorbents, **Table 3** comparison of metal adsorption capacities (mg/g) onto different adsorbents

4.2 Pore Diffusion Coefficient

Pore diffusion coefficients (D_p) of chromium and lead are obtained using the batch model by matching the concentration decay curve obtained from the experimental data at optimum agitation speed 400 rpm with that obtained from the batch model as shown in **Fig. 3**. The pore diffusion coefficients for each solute are evaluated from batch experiments to be:

- Pb^{2+}: $D_p = 7.23\times10^{-11}$ m^2s^{-1}, R^2 = 0.994
- Cr^{+3}: $D_p = 3.15\times10^{-11}$ m^2s^{-1}, R^2 = 0.971

With $k_f=4.73\times10^{-5}$ m/s for Pb^{+2} and $k_f=2.4\times10^{-5}$ m/s for Cr^{+3}

4.3 Breakthrough Curves of The Binary System

The experimental and predicted breakthrough curves for single and binary systems for adsorption of lead and chromium ions onto DAB at different flow rates, bed height and initial concentration are shown in **Figs. 4 to 8**.

5 DISCUSSION

1. The adsorption capacity order for lead and chromium onto DAB was as follow:

Pb^{+2} (35.12 mg g^{-1}) > Cr^{+3} (23.84 mg g^{-1}). This behavior of the capacity of the adsorbate in batch system seems to influence the adsorption capacity of DAB in fixed bed adsorber. This can be explained by:

a- Lead nitrate has less solubility (520000 mg L^{-1}) in water in comparison with chromium nitrate (810000 mg L^{-1}).

b- Hydrated ion radius for lead is greater than chromium (4.01 $Å^2$ for lead and 4.13 $Å^2$ for chromium).

c- Lead can be adsorbed by means of electrostatic attraction between positively charged and binding sites. Physical adsorption by means of Vander Waals, and dipole-induced dipole has been the main way to adsorb lead ions with high electronegativity (2.33) in comparison with chromium (1.66) **Table 1**. However, lead and chromium ions biosorption depended on the activity and availability of functional groups onto DAB (electrostatic attraction) with the mean of competitive biosorption **Sulaymon et al, 2012 b**.

2. The effect of flow rate:

Figs.4,5 and 6 shows the experimental and predicted breakthrough curves for Pb^{+2} and Cr^{+3} in single and binary systems at different flow rates (1.39×10^{-6}, 2.78×10^{-6}, 4.17×10^{-6} $m^3s^{-1}$and 5.56×10^{-6} m^3s^{-1}) in terms of C_e/C_o. It's clear from these figures that as the flow rate increases, the time of breakthrough point decreases. This is because that the residence time of solute in the bed decreases. Therefore there is not enough time for adsorption equilibrium to be reached which results in lower bed utilization and the adsorbate solution leaves the column before equilibrium. It is expected that the change in flow rate will affect the film diffusion but not the intra-particle **diffusion Sulaymon** and **Ahmed, 2008**. The higher the flow rates, the smaller film resistance to mass transfer and hence larger k_f results. Increasing the flow rate at constant bed height will increase the Bi number with slight increase in Pe number as listed in **Table 4**. When the Bi number is high the time of breakthrough point will appear early. The higher Bi number values indicate that the film diffusion is not dominating compared to the intra-particle mass transfer and the intra-particle mass transfer is the controlling parameter **Fig. 6**. These results agree with those obtained by **Sulaymon et al.,2012 .**

3. Effects of bed height:

Fig. 8 shows that at smaller bed height the effluent adsorbate concentration ratio increases more rapidly than that for a higher bed height. Furthermore, smaller bed heights will be saturated in less time. Smaller bed heights corresponds to lesser amount of adsorbent, at a given flow rate and increasing the bed height will increase the contact time of the solute within the bed, thus improving the three solute removal efficiencies

Increasing the bed height at constant flow rate will increase Peclet number (Pe). Pe is the ratio of axial convection rate to axial dispersion rate. When Pe is small the breakpoint appears early and the breakpoint increases with increasing Pe as listed in **Table 4**. Therefore both the internal and external resistances are considered as the major items controlling the adsorption kinetics as the bed height increases. A deep bed requires more time to reach saturation point or a breakpoint appearing later. Also, larger bed provide greater surface area or (adsorption sites) which causes increasing adsorption process and contact time. The bed height is one of the major parameters in the design of

fixed bed adsorption column **Sulaymon et al., 2012 a**. The experimental and predicted breakthrough curves obtained for different heights of DAB 0.05, 0.1, 0.15 and 0.2 m at constant flow rate and constant initial concentration are presented in **Fig.8**. Hence, the internal and external resistances are confirmed to be the main parameters that control the adsorption kinetics with the increase in bed height. Similar findings have been obtained by **Sulymoon et al., 2012 a**

4. Effect of initial concentration:

The change in initial concentrations of Pb^{+2} and Cr^{+3} will have a significant effect on the breakthrough curves. **Fig.7** shows the experimental and predicted breakthrough curves at different initial concentrations (25, 50, 75 and 100 mg L^{-1}). This figure shows that an increase in initial concentration causes a decrease in breakpoint time and makes the breakthrough curves much steeper, this would be anticipated with the basis of increasing driving forces for mass transfer with increasing the concentration of solutes. As the initial concentration increases the time of breakthrough point decreases. This may attribute to the diffusion rate and controlled by the concentration gradient, it will take a longer time to reach saturation in the case of low initial solute concentration. It is also clear that as the influent concentration increases, the adsorption capacity increases. These results are in agreement with that obtained by **Sulaymon** and **Ahmed, 2008**.

5. In multi-component system (binary system) for lead and chromium, it is clear from **Figs. 6,7**, and 8 that, at the initial stage, there are a lot of active sites of DAB, and the strongly (Pb^{+2}) and weakly (Cr^{+3}) adsorbed component take the active site freely. With increasing time, the weakly adsorbed component is not easily adsorbed but moves ahead with the bulk-fluid and the strongly adsorbed component tends to displace the sites that had been taken by the weakly adsorbed component. The result is that the local concentration of the weakly adsorbed component within the fixed bed adsorber is higher. These results are in agreement with that obtained by **Sulaymon et al., 2012 a.**

6 CONCLUSIONS

The simulated breakthrough curves for adsorption of lead and chromium both in single and binary systems onto dead anaerobic biomass are in close agreement with the experimental results. Thus, the mathematical model, which includes axial dispersion, film mass transfer, pore diffusion resistance and nonlinear isotherm, provides a good description of the single and competitive adsorption process in fixed bed adsorbed. As the flow rate increases, the Biot number arranges to for Pb(II) ions from 74.6 to 119, for Cr(III) ions from 155 to 249 for each solute, the rate of competitive adsorption will decrease and the shape of breakthrough curves will be sharp with lower breakpoint, due to the high intra-particle resistance and the decrease in contact time to reach saturation. Finally DAB was found to be more suitable adsorbent for removal of lead than chromium the same conclusions were obtain by **Sulaymon et al., 2012 a.**

REFERENCES

Ahmed, K. W., 2006, *Removal of Multi-pollutants from Wastewater by Adsorption Method*, Ph.D. Thesis, University of Baghdad

APHA, 1995, *Sta*ndard *Methods for the Examination of Water and Wastewater*, 19th edn. American Public Health Association,Washington, DC.

Fiol, N., Poch J., and Villaescusa I., 2004, *Chromium (VI) Uptake by Grape Stalks wastes Encapsulated in Calcium Alginate Beads: Equilibrium and Kinetics Studies*, Chemical Speciation and Bioavailability Vol.16, No.2, PP. 25-33.

Gupta, V. K., and Ali, I. 2004 *Removal of Lead and Chromium from Wastewater using Bagasse Fly Ash - A Sugar Industry Waste*. Journal of Colloid Interface, Vol.271, PP. 321-328.

Gupta, V. K., and Rastogi, A., 2009 *Biosoprtion of Hexavalent Chromium by Raw and Acid-Treated Green Alga Oedogonium Hatei from Aqueous Solutions*, Journal of Hazardous Materials, Vol. 163, PP. 396- 402.

Huifen, L., Yanbing, L., Wumeng, G., Jiali, C., Lin, X., and Junkang, G,. 2010, *Biosorption of Zn(II) by Live and Dead Cells of Streptomyces Ciscaucasicus Strain CCNWHX 72-14*. Journal of Hazardous Materials, Vol.179, PP. 151–159.

Lawrence, K., Wang, J. T., Stephen, T. T., and Yung, T., H., 2010, *Handbook of Environmental Engineering, Environmental Bioengineering*. Springer New York Dordrecht Heidelberg London.

Naseem, R., and Tahir, S., S., 2001, *Removal of Pb(II) from Aqueous Solution By using Bentonite as an Adsorbent*. Journal of Water Research, Vol. 35, PP. 3982 – 3986.

Pérez, F., A., Casoni, E., and Huerta A., 2013, *Dimensionless Analysis of HSDM and Application to Simulation of Breakthrough Curves of Highly Adsorbent Porous Media*, Journal of Environmental Engineering, Vol. 139, No.5, PP. 667–676.

Prasad, M., Xu, H., Y., and Saxena, S., 2008, *Multi-Component Sorption Of Pb(II), Cu(II) and Zn(II) Onto Low-Cost Mineral Adsorbent*, Journal of Hazardous Materials, Vol. 154, PP. 221 – 229.

Sekomo, C. B., Kagisha, V., Rousseau, D., P., and Lens, P., N., 2011, *Heavy Metal Removal by Combining Anaerobic Upflow Packed Bed Reactors with Water Hyacinth Ponds*. Environmental Technology, Vol. 32, No.1, PP.87-95.

Sulaymon, A., H., Abbood, D., W., and Ali, A., H., 2012 a, *Removal of Phenol and Lead from Synthetic Wastewater by Adsorption onto Granular Activated Carbon in Fixed Bed Adsorbers: Prediction of Breakthrough Curves*, Desalination and Water Treatment, Vol.40, No.1-3, PP. 244-253.

Sulaymon, A., H., and Ahmed, K., W., 2008, *Competitive Adsorption of Furfural and Phenolic Compounds onto Activated Carbon in Fixed Bed Column*, Environmental Science Technology, Vol. 42, No.2, PP.392-7.

Sulaymon, A., H., and Ebrahim, S., E., 2010, *Removal of lead, cadmium, and mercury ions using biosorption*, Desalination Water Treatment, Vol. 24, PP.44–352.

Sulaymon, A., H., Ebrahim, S., E., and Ridha, M., J., 2012 b, *Equilibrium, kinetic, and thermodynamic biosorption of Pb(II), Cr(III), and Cd(II) ions by dead anaerobic biomass from synthetic wastewater*, Environmental Sciences Pollution Research, Vol. 20, No.1, PP.75-187.

Tuzun, I., Bayramoglu, G., Alcin, Y., E., Basaran, G., Celik, G., and Arica, M., Y., 2005, *Equilibrium and kinetic studies on biosorption of Hg(II), Cd(II) and Pb(II) ions onto microalgae Chlamydomonas reinhardtii*. Journal Environmental Management, Vol.77, PP. 85-92.

Urban, C., and Gomezplata, A., 2009, *Axial Dispersion Coefficients in Packed Beds at Low Reynolds Numbers*, The Canadian Journal of Chemical Engineering, Vol. 47, No. 4, PP.353–359.

Van-Hullebusch, E., D., Gieteling, J., Zhang, M., Zandvoort, M., H., Daele, W., V., Defrancq, J., and Lens, P., N., L., 2006, *Cobalt sorption onto anaerobic granular sludge: isotherm and spatial localization analysis*, Journal of Biotechnology, Vol. 121, No. 2, PP. 227 – 240.

Vijayaraghavan K., and Yun, Y-S., 2008, *Bacterial biosorbents and biosorption*, Biotechnology Advance, Vol. 26, PP.266–291.

NOMENCLATURE

Å	Angstrom, 1×10^{-10} m
b	Adsorption equilibrium constant relate to affinity between adsorbent and adsorbate, L mg^{-1}
Bi	Biot number
C	Fluid phase concentration, mg L^{-1}
C_e	Equilibrium liquid phase concentration, mg L^{-1}
C_o	Initial liquid phase concentration, mg L^{-1}
D_b	Axial dispersion coefficient m^2/s
D_m	Molecular diffusivity, m^2 s^{-1}
D_p	Pore diffusion coefficient, m^2 s^{-1}
d_p	Particle diameter, m
k_f	External mass transfer coefficient, m s^{-1}
MW	Molecular weight, g mol^{-1}
L	Length of the column, m
P_e	Peclet number
Q	Flow rate, m^3 s^{-1}
q_e	Adorption capacity at equilibrium, mg g^{-1}
q_m	Langmuir constant related to maximum adsorption capacity, mg g^{-1}
r	Radial coordinate, m
R	Radial coordinate, m
Re	Renold number,$Re=\rho_w \upsilon d_p/\mu_w$
R_p	Radius of particle, m
Sc	Schmidt number, $Sc= \mu_w/\rho_w D_m$
Sh	Sherwood number, $Sh=k_f d_p/D_m$
t	Time, s
V_L	Volume of solution, L

W_A	Mass of dead anaerobic biomass, g
Z	Axial distance, m
ε_b	Bed porosity
ε_p	Particle porosity
μ_w	Viscosity of water
υ	Interstitial velocity, $\upsilon=Q/\pi R^2{}_p\varepsilon_b$
ρ_w	Density of water, kg/m^3
ρ_p	Particle density, kg/m^3
Subscript	
b	Bulk fluid phase
e	Equilibrium
DAB	Dead anaerobic biomass
i	Component number, 1,2,…
L	Liquid Phase
o	Initial phase
p	Particle phase
Cr^{3+}	Chromium
Pb^{2+}	Lead

Table 1. Main physicochemical properties of the metals tested.

Properties	Lead	Chromium
Formula	Pb(II) from $Pb(NO_3)_2$	Cr(III) from $Cr(NO_3)_3$
Appearance	White colorless crystals	blue-violet crystals
Molar mass, g/mole	331.2	238.011
Standard atomic weight	207.2	51.99
Solubility in water, g/100 mL	52	81
Molecular diffusion, $m^2/s\times10^{-8}$	4.98	4.22
Hydrated ion radius (Å)	4.01	4.13
Crystal radius (Å)	1.19	0.75
Electronegativity	2.33	1.66
Charge	2	3
Density, g/cm^3	4.53	1.85
Wavelengths used by AA, nm	283.3	357.9
Company	BDH (England)	BDH (England)

Table 2. Physical chemical and biological characteristic of DAB.

Biomass			
Physical characteristic (dead biomass)		Biological characteristic (live biomass)	
Particle diameter, mm	0.775	*Bacteria*	
Surface area, m^2/g	94.53[(a)]	*Aeromonas species, CFU/mL*	222000
Actual density, kg/m	1741.6	*E-coli, CFU/mL*	430000
Bulk density, kg/m	609.9[(b)]	*Pseudomonas aerginrsa, CFU/mL*	703500
Particle porosity	0.584	*Klebsiella species, CFU/mL*	210000
Total Suspended Solid, mg/L	153950	*Clostridium, CFU/mL*	370000
Volatile Suspended, mg/L	78126	*Staphylococcus sp., CFU/mL*	210000
Chemical characteristic (dead biomass)		*Streptococcus sp., CFU/mL*	490000
pH	5.5-6.3	*Salmonella sp., CFU/mL*	190000
CEC, meq/100g	51.2	*Shiglla dysente, CFU/mL*	410000
Lead, mg/L	0. 02	*Fungi*	
Chromium, mg/L	0.01	*Penicillium sp., CFU/mL*	180000
Cadmium, mg/L	0.02	*Yeast*	
		Candida albicans, CFU/mL	460000
		Protozoa	
		Entamoeba species, CFU/mL	16000
		Giardia lambihia, CFU/mL	90000

(a) Surface area analyzer, BET method, Quantachrome.com.(USA), (b) Apparent density instrument, Autotap, Quantachrome.(USA), CEC Cat ion Exchange Capacity, CFU Colony-forming unit

Table 3. Comparison of metal adsorption capacities (mg/g) onto different adsorbents.

Adsorbent	pH	Other information	Pb(II)	Cr(III)	Reference
Granular Activated Carbon	7.5	M=30 g/L, t_{eq}= 30 h	45(L)	23(L)	Lawrence et al. 2010
Waste sorbent Sugar beet pulp	5.5	M=1 g/L, t_{eq}= 8 h	74(E)	36(E)	Lawrence et al. 2010
bagasse fly ash	5-6	M=10 g/L,	3.8(E)	1.8(E)	Gupta and Ali
		t_{eq}= 1 h			2004
Green algae *Spirogyra sp.*	5	M=10 g/L, t_{eq}= 1.8 h	93.5(E)	----	Gupta and Rastogi 2009
Fungus *Sargassum natans*	3.5	M=1 g/L, t_{eq}= 1 h	252.5(L)	----	Huifen et al. 2010
Macrolagae Chlamydomonas reinhardtii	5	M=1 g/L, t_{eq}= 24 h	24.9 (L)	----	Tuzun et al. 2005
This study (binary system)	4	M=0.5 g/L, t_{eq} = 4 h	35.12 (E)	23.84 (E)	

E Experimental uptake, L uptake predicted by the Langmuir model, M biosorbent dosage, t_{eq} equilibrium time, ----- not available

Table 4. Values of Biot no. and Peclet no. at different flow rates and bed heights.

Pollutants	Flow rate, m^3s^{-1}	Biot no. (Bi)	Peclet no.(Pe)	Bed height, m	Biot no. (Bi)	Peclet no.(Pe)
Pb^{+2}	1.39×10^{-6}	74.6	131	0.05	74.6	32.7
	2.78×10^{-6}	93.3	134	0.10	74.6	65.4
	4.17×10^{-6}	108	137	0.15	74.6	98.0
	5.56×10^{-6}	119	139	0.20	74.6	131
Cr^{+3}	1.39×10^{-6}	115	131	0.05	155	32.7
	2.78×10^{-6}	197	134	0.10	155	65.4
	4.17×10^{-6}	226	137	0.15	155	98.0
	5.56×10^{-6}	249	139	0.20	155	131

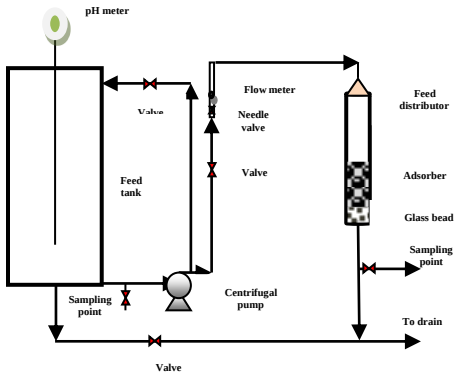

Figure1. Fixed bed biosorption column.

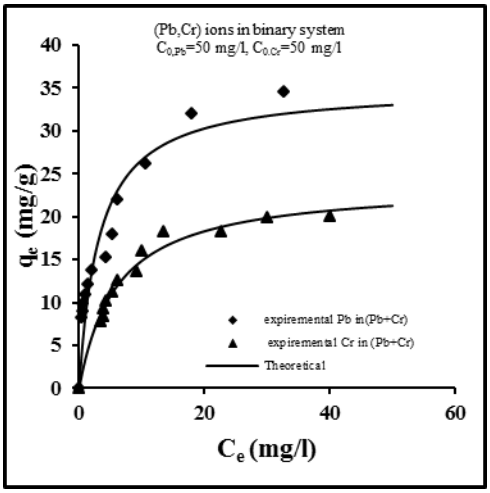

Figure 2. Biosorption isotherm for (Pb^{+2}, Cr^{+3}) onto DAB**.**

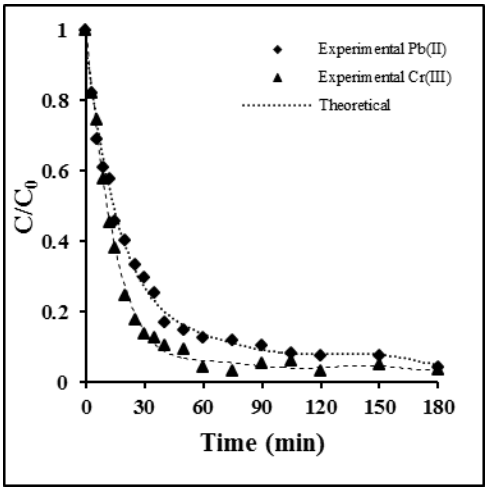

Figure 3. Comparison of the measured concentration-time decay data with that predicated by pore diffusion model for Pb^{+2} and Cr^{+3}. k_f=4.73×10^{-5} m/s for Pb^{+2} and k_f=2.4×10^{-5} m/s for $Cr^{+3.}$

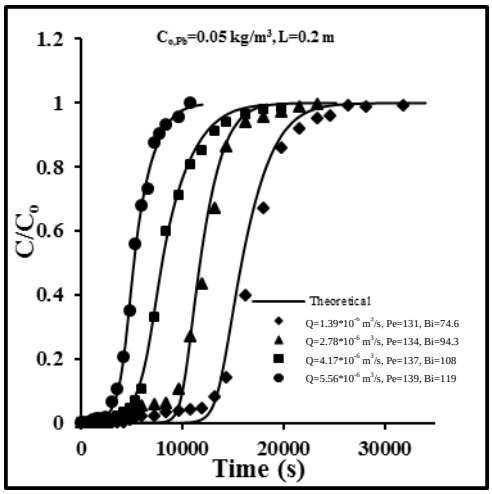

Figure 4. Experimental and predicted breakthrough curves for biosorption of lead onto DAB at different flow rate.

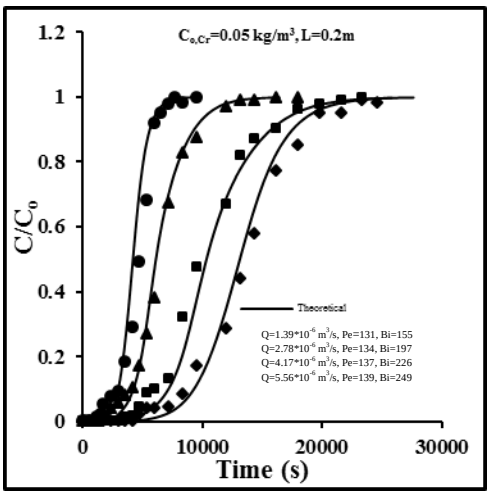

Figure 5. Experimental and predicted breakthrough curves for biosorption of chromium onto DAB at different flow rates.

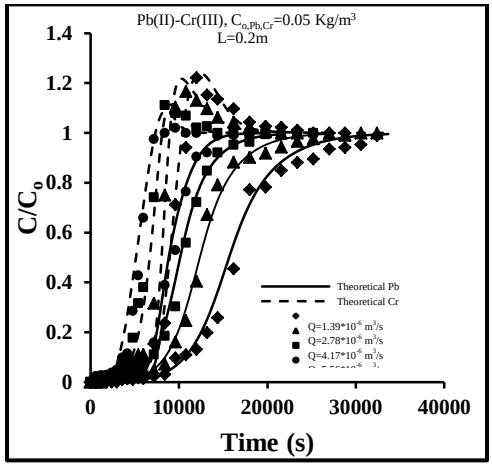

Figure 6. Experimental and predicted breakthrough curves for biosorption of Pb(II)-Cr(III) system onto DAB at different flow rates.

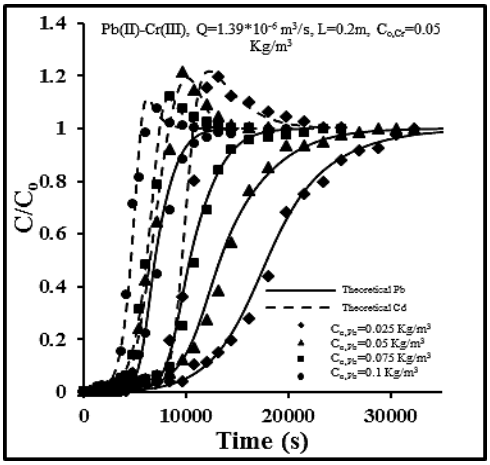

Figure 7. Experimental and predicted breakthrough curves for biosorption of Pb(II)-Cd(II) system onto DAB at different initial concentrations of Pb(II) ions.

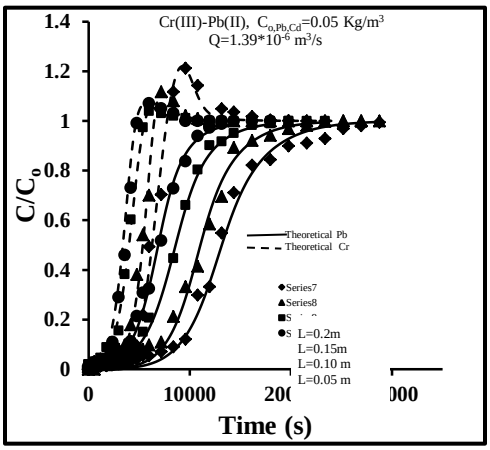

Figure 8. Experimental and predicted breakthrough curves for biosorption of Cr(III)-Pb(II) system onto DAB at different bed heights.

Biogas Recovery from Anaerobic Co-Digestion of Poultry House Wastes for Clean Energy Production

Dr. Zainab Ziad Ismail
Assistant professor
Department of Environmental Engineering
College of Engineering- University of Baghdad
Email: zismail9@gmail.com

Ali Raad Talib
Department of Environmental Engineering
College of Engineering- University of Baghdad
Email: aliraad201089@gmail.com

ABSTRACT

Anaerobic digestion is a technology widely used for treatment of organic waste for biogas production as a source for clean energy. In this study, poultry house wastes (PHW) material was examined as a source for biogas production. The effects of inoculum addition, pretreatment of the substrate, and temperature on the biogas production were taken into full consideration. Results revealed that the effect of inoculum addition was more significant than the alkaline pretreatment of raw waste materials. The biogas recovery from inoculated waste materials exceeds its production from wastes without inoculation by approximately 70% at mesophilic conditions. Whereby, the increase of biogas recovery from pretreated wastes was by 20% higher than its production from untreated wastes at mesophilic conditions. The thermophilic conditions improved the biogas yield by approximately 73%. The kinetic of bio-digestion process was well described by modified Gompertz model and the experimental and predicted values of biogas production were fitted well with correlation coefficient values > 0.96 suggesting favorable conditions of the process.

Key Words: biogas, anaerobic digestion, lignocellulosic waste, clean energy.

استخلاص الغاز الحيوي من الهضم اللاهوائي المشترك لمخلفات الدواجن لانتاج الطاقة النظيفة

د. زينب زياد اسماعيل
أستاذ مساعد
قسم الهندسة البيئية
كلية الهندسة/ جامعة بغداد

علي رعد طالب
قسم الهندسة البيئية
كلية الهندسة/ جامعة بغداد

الخلاصة

تعد عمليات الهضم اللاهوائي من اكثرالتقنيات استخداما لمعالجةِ النفايات العضويةِ لاغراض انتاجِ الغاز الحيوي كمصدر للطاقةِ النظيفةِ. في هذه الدراسة تم استخدام مخلفات الدواجن كمصدر لانتاج غاز الميثان حيث تم دراسة تأثيرات بعض العوامل التشغيلية كأضافةِ براز الحيوانات (تحديدا الدجاج)، المعالجة الكيمياوية التمهيدية للمخلفات قبل اجراء عملية الهضم اللاهوائي، و درجة حرارة على إنتاجِ الغاز الحيوي. بينت النَتائِجَ بأنّ تأثيرَ إضافةِ براز الحيوانات كَانَ أكبر من تأثير المعالجةِ التمهيدية القلويةِ للفضلاتِ الخامِ. الغازَ الناتج مِنْ المخلفات بعد اضافة براز الحيوانات اكثرُ من الغاز الناتج مِنْ المخلفات بدون اضافة بما يقارب 70% تحت ضروف الحرارة المعتدلة .(Mesophilic) اما الغاز الناتج مِنْ المخلفات التي تمت معالجتها بشكل اولي فقد كان معدلُ انتاجه اعلى من المخلفات التي بدون معالجة تمهيدية بما يقارب 20% تحت ظروف حرارة معتدلة (Mesophilic) اما في الظروف الحرارية الاعلى (Thermophilic) فقد بينت النتائج ان كميات الغاز الحيوي الناتج قد ارتفعت الى 73%. تم تطبيق نموذج رياضي لعملية الهضم وهو (Modified Gompertz Model) على القيم الناتجة من التجارب المختبرية, وقد بينت النتائج وجود تطابق بين النتائج المختبرية والنظرية بمعامل ارتباط > 0.96.

الكلمات الرئيسية : الغاز الحيوي، الهضم اللاهوائي، المخلفات اللكنوسيليلوزية، الطاقة النظيفة.

1. INTRODUCTION

Renewable energy is a socially and politically defined category of energy sources. Renewable energy is generally defined as energy that comes from resources which are continually replenished on a human timescale such as sunlight, wind, rain, tides, waves and geothermal heat. About 16% of global final energy consumption comes from renewable resources, with 10% of all energy from traditional biomass, mainly used for heating, and 3.4% from hydroelectricity. Renewable energy sources play a key role in the current European Union strategies to mitigate the impact of global warming. Among the different forms of renewable sources, biomass is undoubtedly one of the most promising**, Messineo, et al., 2012.** When biomass is burn or digested, the emitted CO_2 is recycled into the atmosphere, so not adding to atmospheric CO_2 concentration over the lifetime of the biomass growth, **Twidell,** and **Weir, 2006.**

Anaerobic digestion has been, and continues to be, one of the most widely used processed for the stabilization of biosolid waste, such as from the agro and municipal waste to industrial waste. The widespread use of this technology stems from its potential advantages. These advantages include the production of energy of methane (in excess of that required for process operation), a reduction of 30–50% of waste volume requiring ultimate disposal, and a rate of pathogen destruction-particularly in the thermophilic process. The anaerobic digestion technology, properly implemented in an agro, municipal or industrial technical reality, can also be used to control malodorus emissions. The stabilized biomass can also be utilized as an excellent soil conditioner after appropriate treatment**, Converti, et al., 1999.**

Biogas is a gas mixture mainly composed of methane. The composition of biogas varies depending upon the types and relative contents of different raw materials, as well as upon the different conditions and fermenting phases. The quality of biogas generated by organic waste materials does not remain constant but varies with the period of digestion**, Abdel-Hadi, 2008.**

Yunqin, et al., 2009 developed an alkali pretreatment process prior to anaerobic digestion of pulp and paper sludge (PPS) to improve the methane productivity. Different concentrations of sodium hydroxide solution were used to pre-treat the pulp and paper sludge (PPS). The process efficiency of PPS with and without pretreatment was evaluated. The highest methane yield under optimal pretreatment condition was $0.32m^3$ CH_4/kg VS removal. The results indicated that alkali/NaOH pretreatment could be an effective method for improving methane yield with PPS.

Kafle, et al., 2013, studied the use of fish waste (FW) obtained from a fish processor for biogas production. The FW silages were prepared by mixing FW with bread waste (BW) and brewery grain waste (BGW), and the quality of the prepared silages were evaluated. A first-order kinetic model and the modified Gompertz model were used to predict methane yield. The biogas and methane yield for FW silages after 96 days was calculated to be 671–763 mL/g VS and 441–482 mL/g VS, respectively.

Current study, aimed to study the biogas production and recovery from the anaerobic co-digestion of poultry house wastes. This type of solid waste materials is abundantly available in Iraq without proper consideration and management.

2. MATERIALS AND METHODS

2.1 Materials

Poultry houses wastes (PHW) used in this study included a mixture of chicken feather, chicken feet, egg cartons and boxboard. Samples were freshly collected from local poultry houses. These materials are available in enormous quantities as a discarded waste material of no economic value. Inoculum, chicken dung which is known to be rich in methanogenic anaerobic bacteria was used to inoculate the bio-digesters. These materials were freshly collected from local

slaughter and poultry houses, prepared as slurry, and then added to the digesters as a supplementary material to enrich the bacterial activity and enhance the anaerobic bio-digestion process. All chemical reagents used in this study were of analytical grade as given in **Table 1.**

2.2 Methods of Analysis

2.2.1 Total, volatile solids and pH

The measurement of total solids (TS) and volatile solids (VS) were carried out in triplicate according to the procedure outlined in the *standard met*hods**, APHA, 1998.** pH was measured using pH meter (Model: WTW, Inolab 720). The average measured values of total solids (TS), volatile solids (VS), and pH for the examined poultry house waste samples were found to be 24.28 ± 1.20, 23.32 ± 1.08, and 7 ± 0.4, respectively.

2.2.2 Biogas production

The produced biogas was measured by three different methods including the followings:

Manometer, a simple apparatus consisted of glass U-tube shape with 10 mm internal diameter filled with potassium hydroxide solution. The U-tube hitched with tap to adjust the level of solution with atmospheric pressure after CO_2 removal. The tube was provided with two ports, one for a biogas injection, and the other for gas outlet after removal of CO_2. Methane percentage was measured using potassium hydroxide solution in the laboratory scale investigation. The released gas was fractioned in a percentage (i.e. methane and CO_2 percentage) using the 4% potassium hydroxide. All measurements were carried out at room temperature and atmospheric pressure. The volume of gases was recalculated for standard temperature and pressure (STP: 0^oC and 1 bar)**, Hansen, et al., 2004**.

Water displacement method, the gases were first passed through an airtight washing bottle containing 1 molar sodium hydroxide solution in order to eliminate the carbon dioxide. Then the remaining methane passed to a 500-ml glass container; displacing the water which overflowed into a measuring cylinder. The volume of displaced colored water represents the volume of produced methane.

Gas chromatography (GC), was used to determine the major components of the biogas produced as a byproduct of the anaerobic digestion process.

2.3 Experimental Procedure

The experimental work consisted of the main following steps:

Pretreatment of waste materials, the pretreatment of poultry house wastes was carried out to facilitate the hydrolysis of cellulose component existing in the substrate. Cellulose has a highly crystalline structure due to the presence of an extensive hydrogen bond and inter-chain in the cellulose structure. There are various methods of pretreatment to destruct the lignin component and to reduce the crystalline nature of the cellulose structure. After manual cleaning by removing dirt dust, the clean materials were crushed, and sieved to different particle sizes. Chemical pretreatment included the addition of $Ca(OH)_2$ to the sieved waste materials at concentrations ranged from 0.1 to 0.2 g $Ca(OH)_2$/g TS of waste was carried out then the mixtures were autoclaved at 120 °C for 20 min. The calcium will precipitate and removed as $CaCO_3$ by flushing the autoclaved mix with CO_2, **Forgács, 2012**.

Inoculum preparation, Inoculum slurry was prepared by mixing either 50 g of chicken dung with 400 mL distilled water. The mixed slurry was manually homogenized with glass rod.

Experimental setup and digesters start-up, in this study, a series of lab scale-digesters were operated in batch mode to study the biogas production from the poultry houses wastes. The apparatus used to carry out the processes of anaerobic biological degradation, basically

comprised of 500-mL Pyrex borosilicate heatproof code glass bottles act as the anaerobic bio-digesters. The components of each digester were maintained at 1:10 which is equivalent to 40 g solid waste material: 400 mL (inoculum slurry or distilled water). Each digester was tightly plugged with rubber stopper contains 2 holes each of 4mm diameter through which a piece of glass tube was submersed into the digester and the other end of the glass tube was connected with rubber tube for the produced biogas transfer to the gas measuring section. The rubber stoppers were tightly wrapped with parafilm to prevent any release of the produced gas. Digesters were immersed in a thermostatic water bath to maintain the required temperature conditions. Manual shaking of digesters were daily performed to insure that substrate molecules and bacterial come into close. The experiments were divided into two groups labeled I for mesophilic tests at 38º C, and II for thermophilic tests at 55º C. Group I consisted of 3 digesters, while group II consisted of 1 digester as given in **Table 2**. To achieve anaerobic conditions in the digesters, they were flushed with nitrogen for 10 min to provide anaerobic environment conditions.

Soil fertilization with digested sludge of lignocellulosic waste materials, to examine the overall efficiency, feasibility, and sustainability of the selected treatment approach, the sludge resulted from the digestion process was further processed and a decision was made to examine the validity of utilizing this sludge as a fertilizer. Cress seeds were selected for this test. The seeds were planted in suitable pots, fertilized with the sludge. The pots were irrigated and observed on a daily basis for a period of one week.

3. RESULTS AND DISCUSSION

The results of operating 4 anaerobic bio-digesters in duplicate with (190) sample tests and measurements proved a sustainable and environmentally friendly approach for biogas recovery from the selected agro-industrial waste materials as well as reduction of the waste volume.

3.1 Biogas Production

Results of anaerobic digestion process were used to analyze the quality of biogas with respect to its major component, methane (CH_4). In order to determine the best conditions for maximum volume of the recovered biogas from the waste materials, the effect of several key parameters including inoculum addition, chemical pretreatment of the digestive waste materials, and temperature were carefully considered in this study.

3.1.1 The influence of inoculum addition

This part of work was carried out to study the effect of inoculum on biogas production. The biogas production in digester No. 1 for pretreated PHW with inoculum and digester No. 2 for pretreated PHW without inoculum was monitored for 160 day. The effect of inoculum addition on biogas yield is given in **Figs. 1-3.** However, results of the specific biogas production **Table 3** indicate that the use of inoculum improved the co-digestion process and anaerobic biodegradation of waste materials. The increase of biogas production associated with the inoculum addition is significantly related to the increase of cultures populations since the chicken dung is a rich source for bacteria. However, the existence of cellulose digestive bacteria could be another potential assumption for the increase of biogas generation rates, this type of bacteria is capable to attack the tight association between lignin and cellulose bond. These results are in a good agreement with the previously outlined findings reported by **Budiyono, et al., 2010,** for biogas production from anaerobic digestion of inoculated with rumen fluid. Results revealed that biogas production rate increased two to three times compared to the digestion of cattle manure without rumen fluid.

3.1.2 The influence of chemical treatment

This section was devoted to investigate the effect of chemical pretreatment on biogas production for each type of waste materials. Results of the chemical pretreatment effect on biogas production in digester No. 1 for pretreated inoculated PHW and digester No. 3 for untreated inoculated PHW is given in **Figs. 4-6.** Anaerobic digestion of lignocellulosic materials is a challenge because of the complex, rigid, and fibrous structure of these matters which under anaerobic conditions degrades poorly. Therefore, the addition of alkaline buffer based on total solid contents increased the biodegradability of the organic fraction of solid waste, **Abdulkarim,** and **Evuti, 2010**. However, plots given in **Figs. 4-6** indicate that the effect of alkaline pretreatment for this waste material was significant with respect to the enhancement of co-digestion process and the subsequent biogas production. **Table 4** presents the effect of pretreatment on the biogas produced from the co-digestion process of the lignocellulosic waste materials in this study.

3.1.3 The influence of temperature

Results revealed a significant effect of temperature on biogas production as given in **Fig. 7**. The biogas recovery at thermophilic conditions was relatively higher than at mesophilic conditions in all digesters. This is due to the general rule that temperature is a very important operational parameter in anaerobic digestion processes. **Zinder, et al., 1984,** suggested that methanogensis are optimal at 55 to 60°C and completely inhibited at 65°C. **Table 5** summarizes the effect of temperature condition on the specific biogas production during 90 days-period observation indicating that biogas production at thermophilic conditions exceeds its production at mesophilic conditions by 73%. In conclusion, biogas yield with respect to methane content produced at thermophilic conditions is more favorable than its quality produced at mesophilic temperature range in this study **Fig. 8**. These observations are in a good agreement with the previously reported data regarding the biogas production at mesophilic and thermophilic conditions. **Vindis, et al, 2009,** reported a decrease in solid retention time and increase in biogas production from anaerobic digestion of maize silage under thermophilic conditions. **Achu,** and **Liu, 2010,** realized higher biogas productivity under thermophilic conditions.

3.2 Kinetic Model

Biogas production rate in batch condition is corresponding to specific growth rate of methanogenic bacteria in the bio-digester. Accordingly, the predicted biogas production rate will obey Modified Gompertz Model Eq. (1)**, Nopharatana, et al., 2007,** as follows:

$$G_{(t)} = G_0 . exp\{- exp [((R_{max}.e)/G_0) (\lambda - t) + 1]\} \quad (1)$$

Where:

$G_{(t)}$ = the cumulative biogas yield at a digestion time (mL/g VS)
G_0 = the biogas potential of the substrate (mL/g VS)
R_{max} = maximum methane production rate (mL/g VS-d)
λ = lag phase (day)
t = time (day)
e = exp (1) = 2.7183.

A nonlinear least-square regression analysis was performed using SPSS [IBM SPSS statistics 18 (2009)] to determine λ, R_{max}, and the predicted biogas and methane yield **Table 6** at 90 day. Plots of the measured and predicted values of biogas production are given in **Figs. 9-11**. It is well observed that the predicted values of biogas production using modified Gompertz model is well fitted with the measured values. Results of this section are in a good agreement with the

previously outlined findings. **Kafle, et al., 2013,** reported that the measured values of biogas produced from the bio-digestion of fish waste are well fitted with the predicted values using modified Gompertz model. **Budiyono, et al., 2010,** proved that the measured values of biogas produced from the digestion of cattle manure in batch mode are well fitted with the predicted data obtained by modified Gompertz model.

3.3 Soil Fertilization with Residual Digestates

The results of this part of work demonstrated that the selected process is a potential approach to treat residues of digestion process of poultry house waste materials. **Fig. 12** presents the growth progress of cress seeds after one week's observation period. As shown in this Figure, healthy favorable growth of fertilized crop was observed compared to the non-fertilized crop indicating that this approach is potential method to treat residues of digestive process.

4. CONCLUSIONS

This study was devoted to investigate the potential of anaerobic co-digestion for biogas production using abundantly available lignocellulosic waste materials of no economic value as the substrate. The co-digestion process was evaluated using poultry houses wastes (PHW). The main conclusions that can be drawn from this study are as follows:

● The experimental work demonstrated that the volume of produced biogas significantly affected by inoculum addition, pretreatment of waste materials, temperature conditions (mesophilic or thermophilic).

● The ultimate biogas yield from co-digesting of inoculated wastes was estimated to be 99.058 ± 3.8 mL/g VS, whereby without waste inoculation it was 58.261 ± 4.7 mL/g VS for PHW. These results indicate the potential effect of inoculum addition on the digestion process.

● Maximum biogas production from co-digestion of alkaline pretreated wastes was estimated to be 99.058 ± 3.8 mL/g VS, whereby, it was 82.246 ± 6.3 mL/g VS for untreated PHW.

● During 90 days observation period, maximum biogas production from pretreated inoculated PHW were 87.173 mL/g VS at mesophilic temperature condition. However, higher rate of methane production was observed at thermophilic condition which were 150.870 mL/g VS.

● kinetic of bio-digestion process was well described by Modified Gompertz Model and the experimental and predicted values of biogas production were fitted well with correlation coefficient values > 0.96 for the PHW suggesting favorable conditions of the process.

REFERENCES

- Abdel-Hadi, M.A., 2008, *A Simple Apparatus For Biogas Quality Determination*, Misr Journal Agriculture Engineering, Vol.25, PP. 1055- 1066.

- Abdulkarim, B.I., Evuti, A. M., 2010, *Effect of Buffer ($Nahco_3$) and Waste Type in High Solid Thermophilic Anaerobic Digestion*, International Journal of ChemTech Research, Vol. 2, PP. 980-984.

- Achu N.I., Liu, J., 2010, *Effects of Solid Retention Time on Anaerobic Digestion of Dewatered-Sewage Sludge in Mesophilic and Thermophilic Conditions*, Renewable Energy, Vol. 35, PP. 2200-2206.

- American Public Health Association (APHA), 1998, Standard methods of the examination of water and wastewater, Washington, DC.

- Budiyono, I N. Widiasa, S. Johari, and Sunarso, 2010, *The Kinetic of Biogas Production Rate from Cattle Manure in Batch Mode*, International Journal of Chemical and Biological Engineering, Vol. 3, PP. 39–44.

- Converti, A., Del Borghi, A., Zilli, M., Arnì, S., Del Borghi, M., 1999, *Anaerobic Digestion of the Vegetable Fraction of Municipal Refuses: Mesophilic Versus Thermophilic Conditions*, Bioprocess Engineering, Vol. 21, PP. 371–376.

- Forgács, G., 2012, *Biogas Production from Citrus Wastes and Chicken Feather: Pretreatment and Co-digestion*, PhD Thesis, Borås University.

- Hansen, T. L., Schmidt, J. E. Angelidaki, I., Marca, E., Jansen, J., Mosbaek, H., Christensen, T. H., 2004, *Method For Determination of Methane Potentials of Solid Organic Waste*, Waste Management, Vol. 24, PP. 393–400.

- Kafle, G., K., Kim, S., H., Sung, K., 2013, *Ensiling Of Fish Industry Waste For Biogas Production: A Lab Scale Evaluation of Biochemical Methane Potential (BMP) And Kinetics*, Bioresource Technology, Vol. 127, PP. 326–336.

- Messineo, A., Volpe, R., Marvuglia, A., 2012, *Ligno-Cellulosic Biomass Exploitation for Power Generation: A Case Study In Sicily*, Energy,Vol. 45, PP. 613-625.

- Nopharatana, A., P., Pullammanappallil, C.W., Clarke, P., 2007, *Kinetics and Dynamic Modeling of Batch Anaerobic Digestion Of Municipal Solid Waste In A Stirred Reactor*, Waste Management, Vol. 27, PP. 595–603.

- Twidell, J. and Weir, T., 2006, *Renewable Energy Resources*, 2nd edition, New York: Taylor & Francis.

- Vindis, P., Mursec, B., Janzekovic, M., Cus, F., 2009, *The Impact of Mesophilic And Thermophilic Anaerobic Digestion on Biogas Production*, Journal of Achievements in Materials and Manufacturing Engineering, Vol. 36, PP. 192-198.

- Yunqin, L., Dehan, W., Shaoquan, W., Chunmin, W., 2009, *Alkali Pretreatment Enhances Biogas Production in the Anaerobic Digestion of Pulp and Paper Sludge*, Journal of Hazardous Materials, Vol. 170, PP. 366–373.

- Zinder, S.H., Anguish, T., Cardwell, S. C., 1984, *Effects of Temperature on Methanogensis in a Thermophilic (58°C) Anaerobic Digestor*, Applied and Environmental Microbiology, Vol. 47, PP. 808-813.

NOMENCLATURE

$G_{(t)}$= the cumulative biogas yield at a digestion time , mL/g VS.
G_0= the biogas potential of the substrate, mL/g VS.
R_{max}= maximum methane production rate, mL/g VS-d.
λ= lag phase, day.
t= time, day.

Table 1. Chemical reagents detail**.**

Chemical Reagent	Chemical Formula	Purity %	Provided by	Purpose of Use
Sodium bicarbonate	$NaHCO_3$	99	BDH, England	pH adjustment
Phenolphthalein	$C_{14}H_{14}N_3NaO_3S$	99	BDH, England	To color the water in the displacement bottle
Calcium hydroxide	$Ca(OH)_2$	99	BDH, England	Pretreatment of waste
Sodium hydroxide	NaOH	98	BDH, England	CO_2 removal
Potassium hydroxide	KOH	98	BDH, England	CO_2 removal

Table 2. Digesters setup with waste material at different temperature condition.

Poultry houses waste (PHW)	Digester No.	Waste materials mix in digester	Temperature condition
Group (I)	1	Pretreated waste inoculated with chicken slurry	Mesophilic
	2	Pretreated waste with distilled water	
	3	Untreated waste inoculated with chicken slurry	
Group (II)	4	Pretreated waste inoculated with chicken slurry	Thermophilic

Table 3. Effect of inoculum addition on biogas production.

Digester No.	Inoculum	Maximum specific biogas production (mL/g VS)	Maximum specific CH_4 production (mL/g VS)	Biogas increase (%)
1	Applicable	99.058 ± 3.8	63.367	70.02
2	NA*	58.261 ± 4.7	35.932	

* Not applicable

Table 4. Effect of pretreatment process of waste materials on biogas production.

Digester No.	Pretreatment	Maximum specific biogas production (mL/g VS)	Maximum specific CH_4 Production (mL/g VS)	Biogas increase (%)
1	Applicable	99.058 ± 3.8	63.367	20.44
3	NA*	82.246 ± 6.3	51.879	

* Not applicable

Table 5. Effect of temperature on specific biogas production from pretreated inoculated PHW.

Digester No.	Temperature condition	Specific biogas production (mL/g VS)	Specific CH_4 production (mL/g VS)
1	Mesophilic	87.173	55.635
4	Thermophilic	150.870	110.225

Table 6. Results of a kinetic study using Gompertz model at mesophilic conditions.

Digester No.	$G_{(t)}$ exp. (mL CH_4/g VS)	Gompertz model parameters				R^2
		λ (day)	R_{max}. (mL CH_4/g VS)	G_0 (mL CH_4/g VS)	$G_{(t)}$ model (mL CH_4/g VS)	
1	55.635	8.475	0. 877	63.367	55.830	0.981
2	32.320	18.018	0. .544	35.932	31.220	0.986
3	44.745	13.280	0. 701	51.879	44.100	0.983

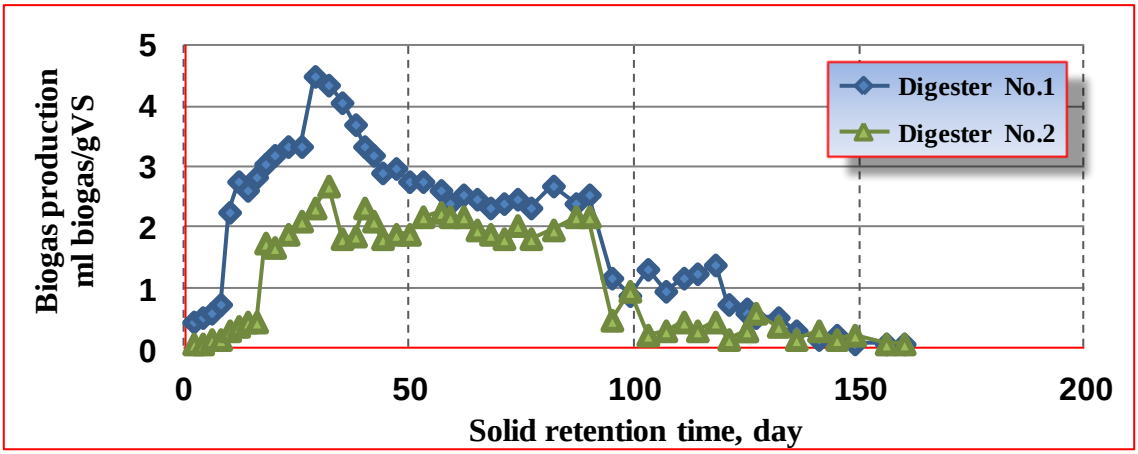

Figure 1. Biogas production profile for digesters No.1 and 2.

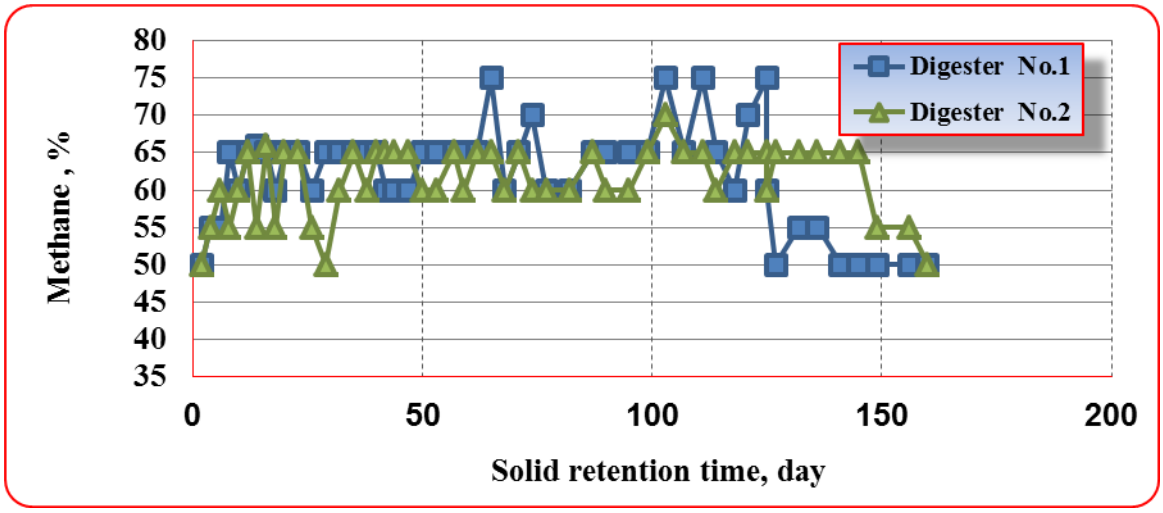

Figure 2. Percentages of CH_4 production digesters No. 1 and 2.

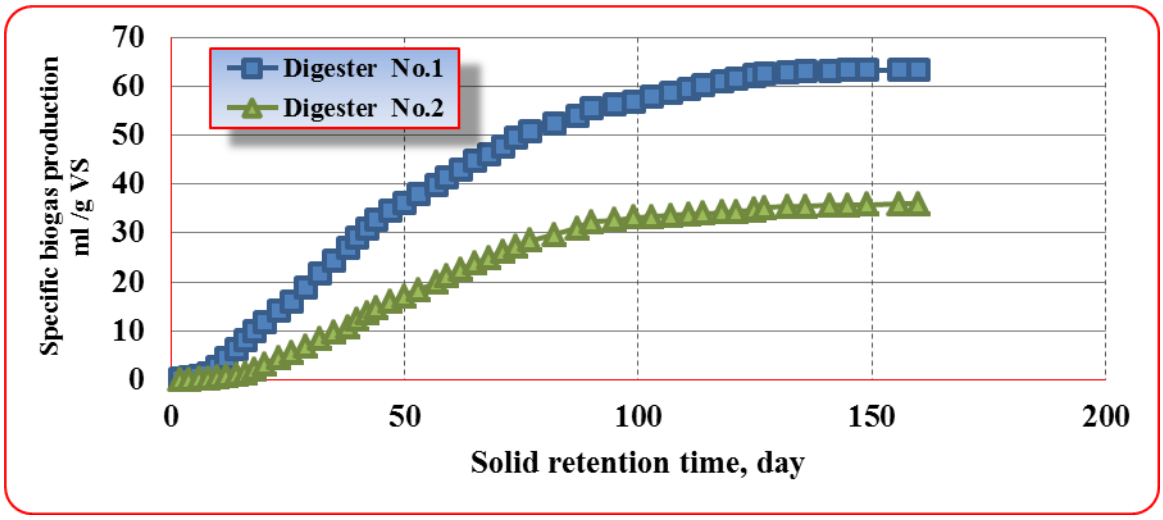

Figure 3. Specific and cumulative biogas production profiles for digesters No. 1 and 2.

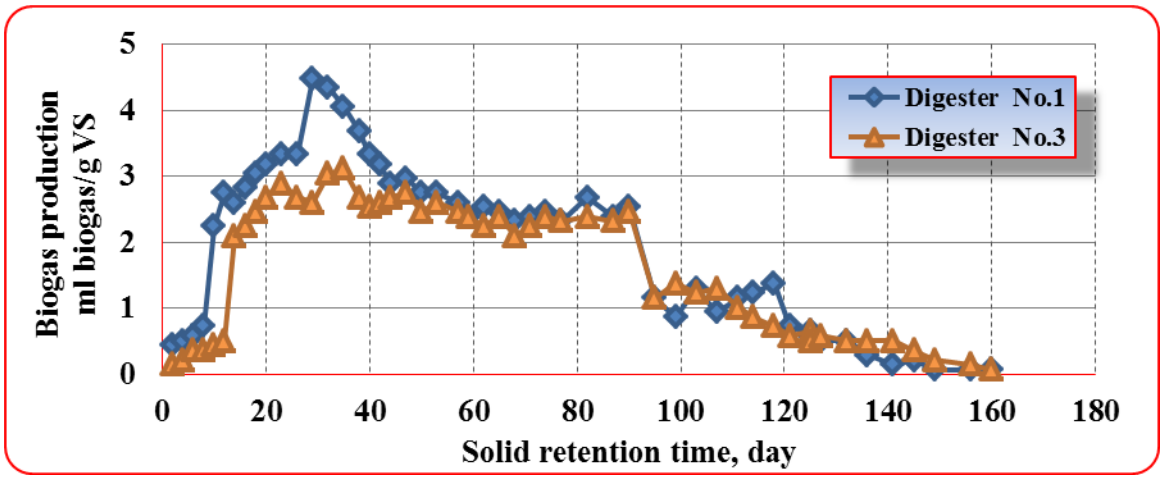

Figure 4. Biogas production profile for digesters No.1 and 3.

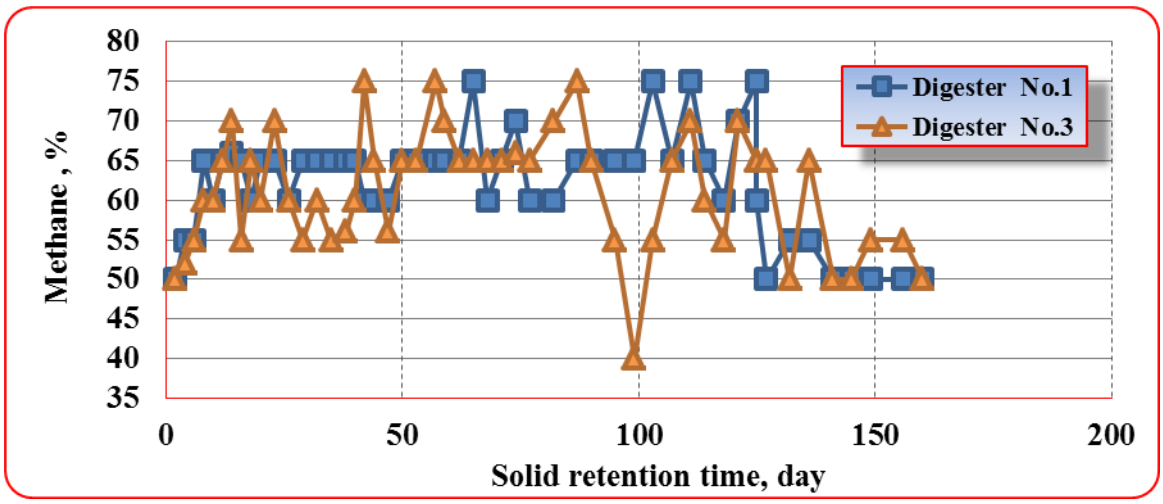

Figure 5. Percentages of CH_4 production digesters No. 1 and 3.

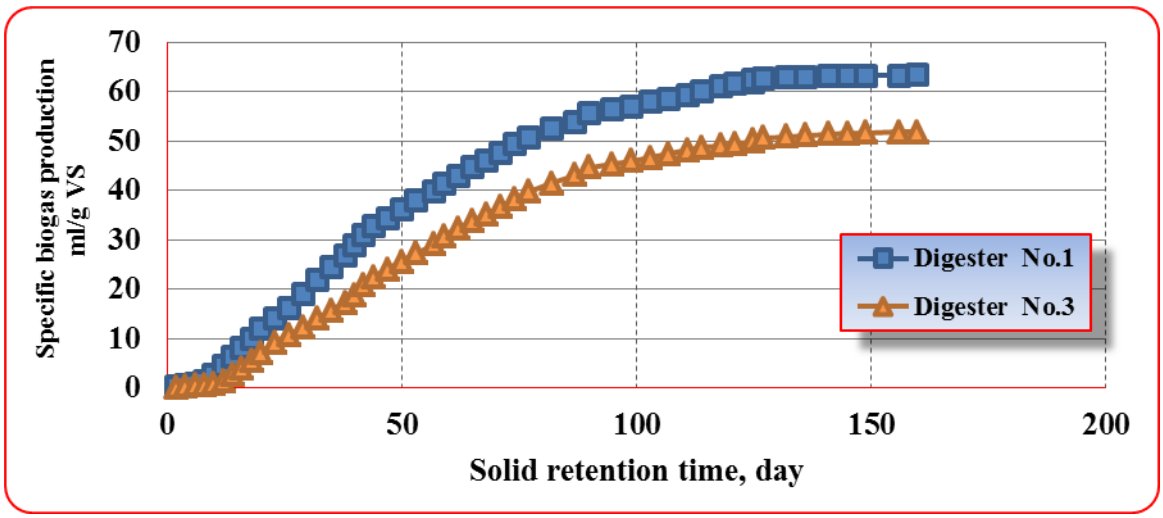

Figure 6. Specific and cumulative CH_4 production profiles for digesters No. 1 and 3.

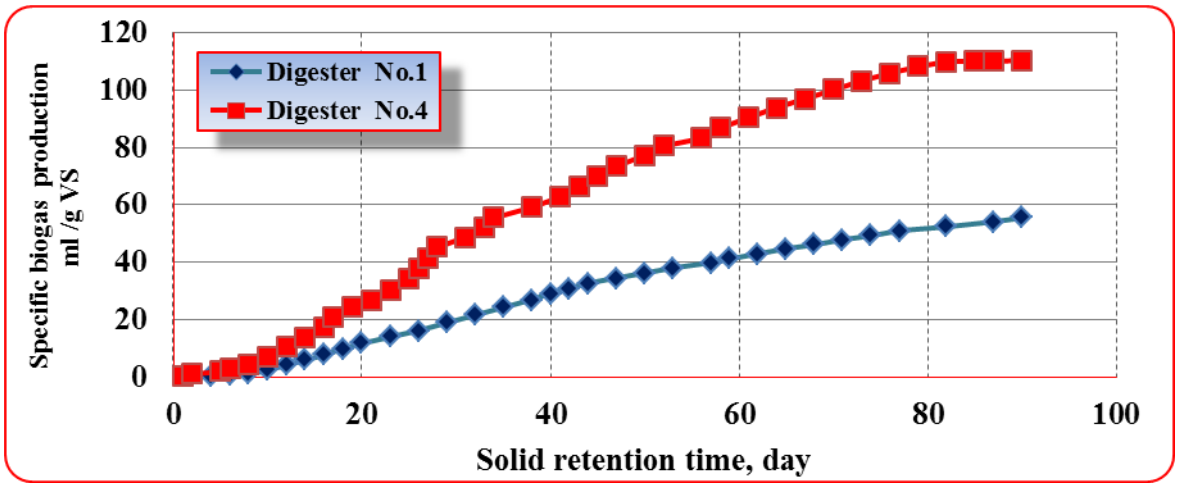

Figure 7. Specific and cumulative biogas production profiles in digesters No.1 and 4.

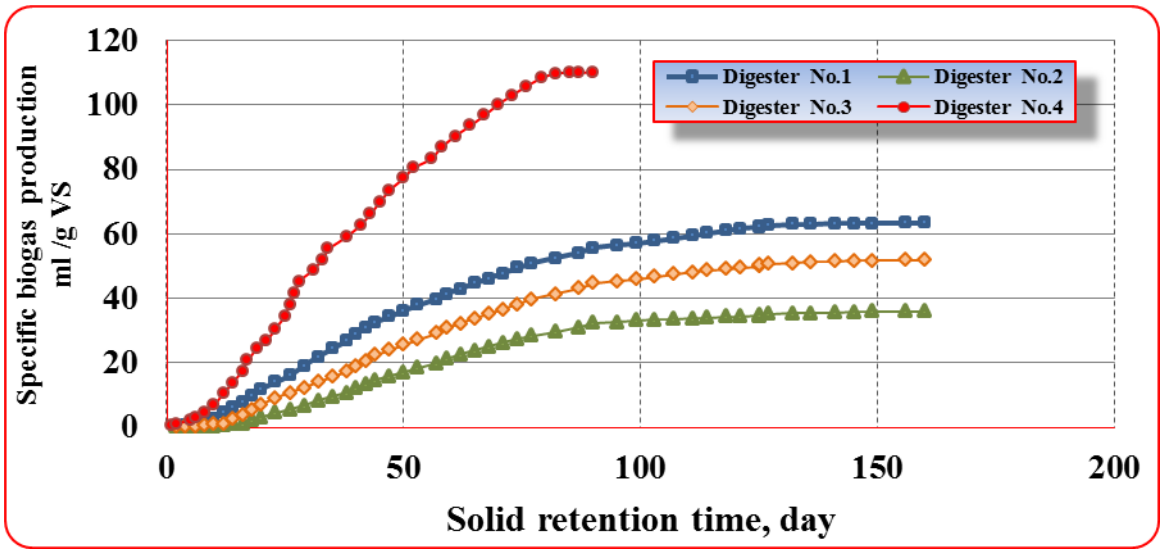

Figure 8. Potential effect of temperature on the specific biogas production for the four cases.

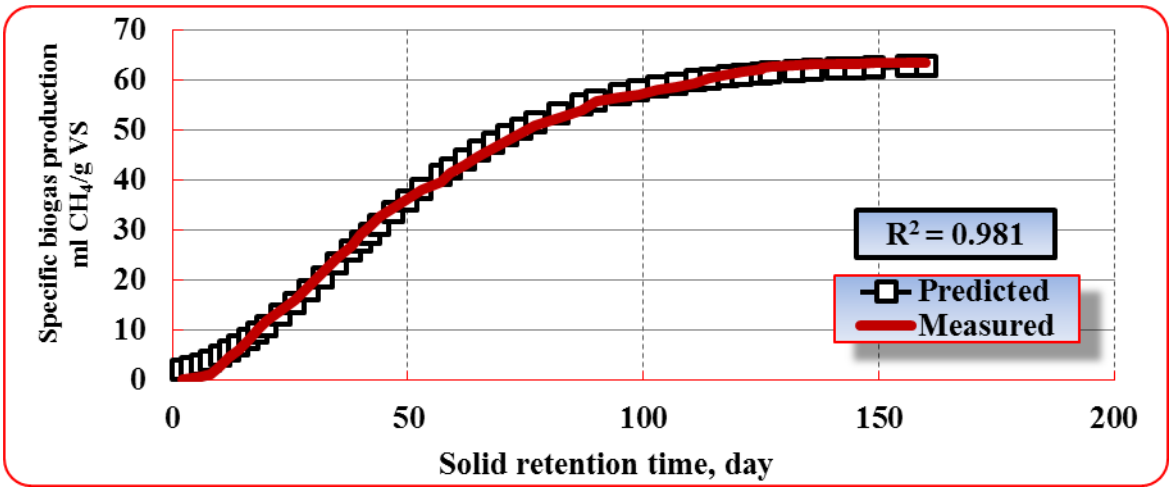

Figure 9. Measured and predicted data for pretreated inoculated PHW.

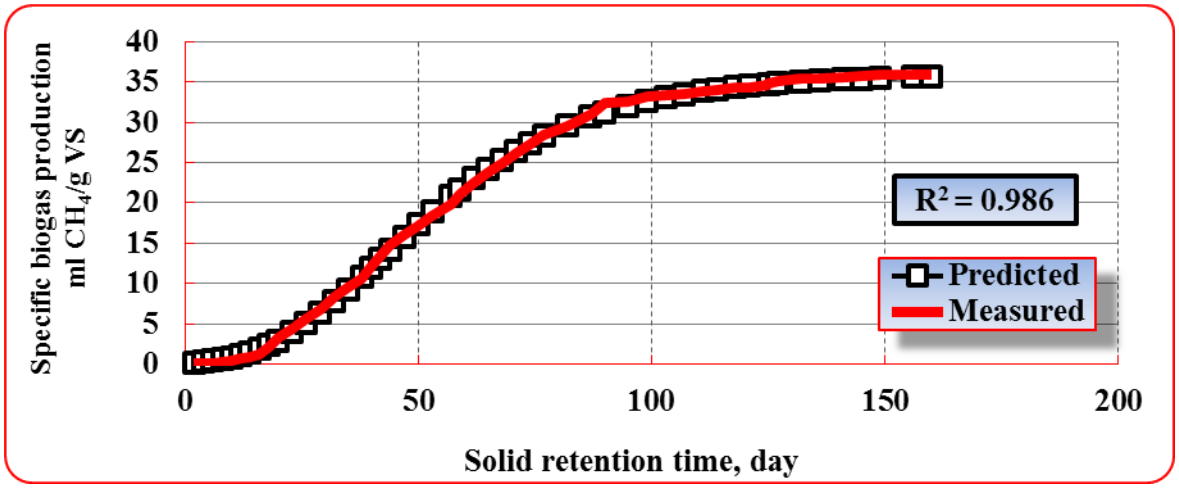

Figure 10. Measured and predicted data for pretreated PHW with distilled water.

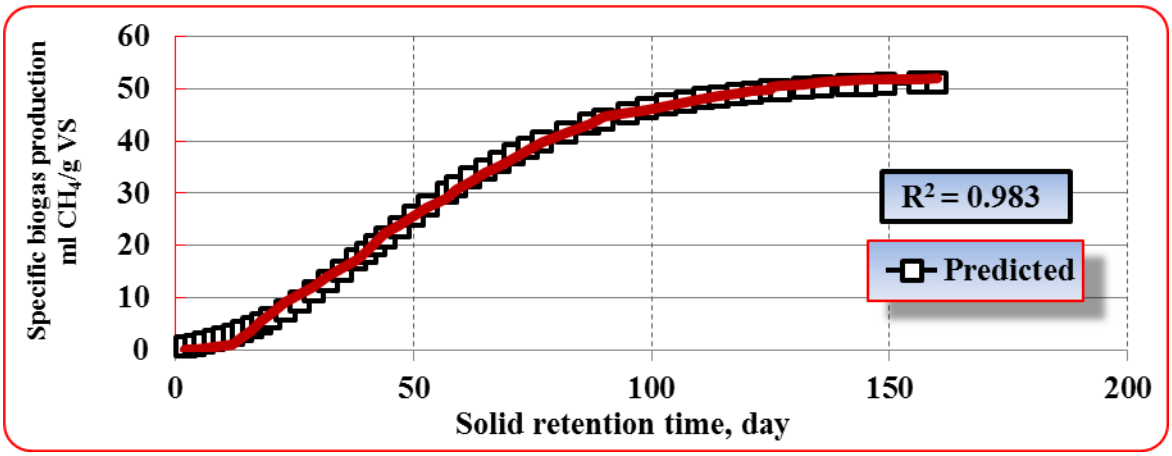

Figure 11. Measured and predicted data for untreated inoculated PHW.

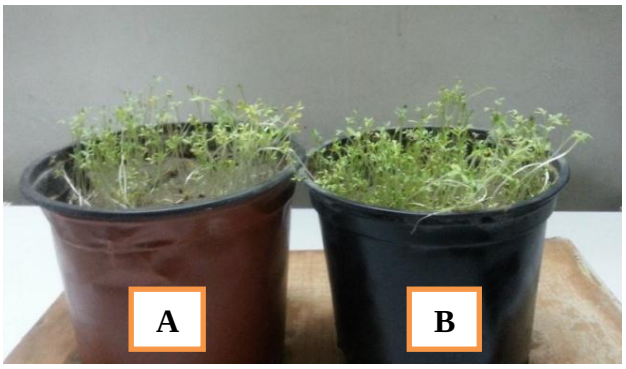

Figure 12. Growth observations for the planted cress seeds after one week, red pot (A) is for non-fertilized soil, black pot (B) for fertilized soil with digestate.

A study of the Effect of Air Inlet and Exit on Indoor Air Movement

Abdual Hadi Nema Khalifa
Assistant Professor
Technical College-Baghdad
email:ahaddi58@yahoo.com

Ahmed Jasim Hamad
Lecturer
Technical College-Baghdad
email:ahmed.elhamad@yahoo.com

Johain Joudet Faraj
Lecturer
Technical College-Baghdad
mail:Johaintech@yahoo.com

Ahmed Qasim Ahmed
Assistant Lecturer
Technical College-Baghdad
email:en_ahmed82@yahoo.com

ABSTRACT

This work consists of a numerical simulation to predict the velocity and temperature distributions, and an experimental work to visualize the air flow in a room model. The numerical work is based on non-isothermal, incompressible, three dimensional, $(k-\varepsilon)$ turbulence model, and solved using a computational fluid dynamic (CFD) approach, involving finite volume technique to solve continuity, momentum and energy equations, that governs the room's turbulent flow domain. The experimental study was performed using (1/5) scaled room model of the actual dimensions of the room to simulate room air flow and visualize the flow pattern using smoke generated from burnt herbs and collected in a smoke generator to delivered through the prototype room. The numerical results were compared with those obtained from experiments, the correspondence between numerical and experimental was fairly good and also, a fair comparison was found with other workers in this field.

Key words: visualization, air flow, indoor air, climate, numerical

دراسة تأثير مدخل ومخرج الهواء على حركة الهواء داخل غرفه

عبد الهادي نعمه خليفه
استاذ مساعد
الكلية التقنية - بغداد

أحمد جاسم حمد
مدرس
الكلية التقنية - بغداد

جهين جودت فرج
مدرس
الكلية التقنية - بغداد

أحمد قاسم أحمد
مدرس مساعد
الكلية التقنية - بغداد

الخلاصة

يهدف هذا البحث الى تحسين المعرفة ببعض الوسائل التي يمكن ان تستخدم في حساب توزيع السرع ودرجات الحرارة واظهار هيئه جريان الهواء خلال الفضاء المكيف للغرفه وهذه الخطوه لايمكن الاستغناء عنها عند تصميم انظمة تكييف بنوعيه جيدة. تضمنت الدراسه اجراء محاكاة عدديه لحساب توزيعات السرع ودرجات الحراره وعمل تجريبي لاظهار هيئه جريان الهواء في انموذج الغرفه. المحاكاة العدديه للجريان اعتمدت على انموذج الجريان ثلاثي الابعاد المضطرب غير المنضغط وبدرجات حراره مختلفه وباسلوب المعادلتين $k-\varepsilon$ واستخدم في الحل احدى طرائق ديناميك الموائع الحسابي. اجريت الدراسه التجريبيه على انموذج مصغر لغرفه صمم ونفذ خلال هذه الدراسه وفق معامل قياس مناسب 5\1 لمحاكاة جريان الهواء للفضاء الحقيقي (الغرفه) لاظهار هيئه الجريان باستخدام دخان منتج من احتراق حبوب نباتيه يجمع في مولد دخان و يوجه الى انموذج الغرفه. مقارنة النتائج العدديه مع النتائج التجريبيه ومع نتائج باحثين اخرين اظهرت توافق مقبول.

1. INTRODUCTION

The major objective of the heating, ventilation and air-conditioning system is to provide comfort and suitable indoor air quality within the occupied zone of building. An important step in the process is to furnish air to each space, in such a way that any natural air current or irradiative effect within the space are counteracted, and assure that temperature, humidity and air velocities within the occupied zones, are held at acceptable condition. The challenge is to provide good mixing without creating uncomfortable drafts, and assure that there is reasonable uniformity, without unacceptable changes in the room conditions as the load requirements of the room change. **Awbi, 1989.** studied the results of computer programs developed for solving 2-D and 3-D ventilation problems, the problems were solved by finite difference form, steady state conservation equations of mass, momentum, and thermal energy. Preservation of fluctuating velocity components is made using the $(k-\varepsilon)$ turbulence model. Predicted result of air velocity and temperature distribution in the room, were corrected by experimental measurements, a CFD method has been described and applied to predict the air flow and heat transfer in 2-D enclosure and the 3-D flow of wall jet over surface with mounted obstacles. The CFD solution produced reasonably good predictions of the air velocity and temperature distribution in the test room. **Bartak , et el.,2001.** studied the room with mixing ventilation, focused on the local mean age of air. The measurements were performed, using the tracer gas concentration decay method. The numerical predications were obtained from CFD model. Two numerical grids, coarse and fine, have been used to compare the accuracy of the results. **Hanibuchi, and Hokoi,2001.** studied the distribution properties of room air temperature, velocity and heat loss, which were investigated experimentally and analytically. Measurements under heating condition were made in a full-scale model room, in order to investigate the influence of air conditioner location on the velocity and temperature fields in steady state, as well as unsteady heating load. The following results were obtained, the influence of the direction in which the jet was blown from the air conditioner is clearly seen in regions of different temperature distribution adjacent to the floor; the heat loss calculated from those experimental results showed several difference characterized by the direction of the blown jet, and the difference between the maximum and minimum heat loss obtained from the experimental results is roughly 15%, and, results from numerical analysis agree with the experimental results. **Zhang,** and **Chen,2005**. studied the particle transport and other distributions in ventilated rooms, by both experimental investigation and numerical simulation. The numerical simulation was achieved by $(k-\varepsilon)$turbulence model, the Lagrangian particle tracked method, and the particle source in cell scheme. The Lagrangian method was introduced, evaluated and then used to analyze particle dispersion in rooms, with three different ventilation systems. The Lagrangian method introduced uncertainty in the particle concentration calculation. The uncertainly level is associated with Lagranging sample size, number of computational cells for concentration, and even particle source position in the turbulent flow. **Nielsen, 2006.** conducted the experiments with room air distribution that is generated by a radial ceiling-mounted diffuser and a diffuser generating flow with swirl then compared with the air distribution obtained by mixing ventilation from a wall-mounted diffuser, vertical ventilation, and displacement ventilation. The air distribution generated by a radial diffuser is partly controlled by the momentum flow from the diffusers and partly from gravity forces where the thermal load and the temperature difference between room air and supply air deflect the radial wall jet down into the occupied zone. The ceiling diffuser with swirling flow generates a flow pattern in the room that is rather uninfluenced by the thermal load. The flow is highly mixed above the occupied zone, and the air movement penetrates the occupied zone close to the walls. All systems were tested in the same room with a load consisting of two manikins, each sitting at a desk with two PCs and two desk lamps, producing a total heat load of 480 W. In all five cases, the design of the air distribution system was based on flow elements from the diffuser, a maximum velocity assumption, and a critical vertical temperature gradient in the room. **Chen,** and **Zhang,2008.**

introduced two categories of flow models, Reynolds Average Navier stoke equation model (RANS modeling), and Large Eddy Simulation (LES), as well as two popular particle models (Lagrangian and Eulerian). Both RANS and LES modeling have been used to predict air flow in rooms. The performance of RANS modeling was similar to that of LES for the case studied. However, LES provide more detailed information than RANS modeling and used only one or no empirical coefficient. LES is considered as a powerful tool for multiple scale studies. **Kwang, et al., 2008**. studied the effect of the airflow discharge rate of the ceiling type air-conditioner on ventilation performance in a lecture room with mixing ventilation. Experiments and CFD were conducted for analyzing ventilation performance. The concepts of mean air age and indoor CO_2 concentration were used for evaluating ventilation performance. A CO_2 generation model was used in the simulation and calculation a lot of cases with respect to the airflow rate of air-conditioner and the mechanical ventilation rate. A selected experimental measurements were performed in the lecture room of the same layout as the numerical one for verifying simulation results. Mean air age is gradually increased, but CO_2 concentration is oppositely decreased in the occupied zone with the increment of the discharge airflow rate of the ceiling type air-conditioner. This result shows that both mean air age and residual life time must be considered for evaluating ventilation performance when the contaminants are generated indoors. And the increment of discharge airflow of the ceiling type air-conditioner can induce the piston effect and push the contaminants out of the occupied zone. From this result, it is found out that ventilation performance can be increased when the momentum source like an air-conditioner is used in the room with the mixing ventilation.

2. ROOM AIR MODELING

The successful prediction of room air flow or air movements in enclosure has recently been based on two approaches. The first approach depends on the measurements of air velocity, and temperature distribution in a physical model of building in a laboratory, for pre-design evaluation or actual site measurements for post design investigation. The second approach depends on numerical predication by considering the room air flow simulation model solved using computational fluid dynamic (CFD) techniques. The two approaches mentioned above were used in this work.

2.1 Numerical Solution

The equations that describe the flow of a fluid and heat within an enclosure are all based on **Awbi,1989**, and assume that the numerical simulation is based on non-isothermal, incompressible three- dimensional ($k-\varepsilon$) two - equations turbulent flow model:

2.1.1 Conservation of mass

$$\frac{\partial \rho}{\partial t}+\frac{\partial}{\partial x}(\rho u)+\frac{\partial}{\partial y}(\rho v)+\frac{\partial}{\partial z}(\rho w)=0 \qquad (1)$$

2.1.2 Conservation of momentum

For x direction, U momentum is:

$$\frac{\partial}{\partial t}(\rho u)+\frac{\partial}{\partial x}(\rho uu)+\frac{\partial}{\partial y}(\rho uv)+\frac{\partial}{\partial z}(\rho uw)=-\frac{\partial p}{\partial x}+\frac{\partial}{\partial x}\left(\mu\frac{\partial u}{\partial x}\right)+\frac{\partial}{\partial y}\left(\mu\frac{\partial u}{\partial y}\right)+\frac{\partial}{\partial z}\left(\mu\frac{\partial u}{\partial z}\right)+$$
$$\frac{1}{3}\frac{\partial}{\partial x}\left[\mu\left(\frac{\partial u}{\partial x}+\frac{\partial v}{\partial y}+\frac{\partial w}{\partial z}\right)\right]+\frac{\partial}{\partial x}(-\rho\overline{u'u'})+\frac{\partial}{\partial x}(-\rho\overline{u'v'})+\frac{\partial}{\partial x}(-\rho\overline{u'w'})+\rho g_x \qquad (2)$$

Similar equations are used for momentum in y and z directions.

2.1.3 Conservation of energy

$$\frac{\partial}{\partial t}(\rho T)+\frac{\partial}{\partial x}(\rho uT)+\frac{\partial}{\partial y}(\rho vT)+\frac{\partial}{\partial z}(\rho wT)=\frac{\partial}{\partial x}\left(\Gamma\frac{\partial T}{\partial x}\right)+\frac{\partial}{\partial y}\left(\Gamma\frac{\partial T}{\partial y}\right)+\frac{\partial}{\partial z}\left(\Gamma\frac{\partial T}{\partial z}\right)$$
$$+\frac{\partial}{\partial x}\left(-\rho\overline{u'T'}\right)+\frac{\partial}{\partial x}\left(-\rho\overline{v'T'}\right)+\frac{\partial}{\partial x}\left(-\rho\overline{w'T'}\right)+S_T \quad (3)$$

Where: $\Gamma=\frac{\mu}{\sigma}$, *and* $\sigma=\frac{\mu.cp}{\lambda}$ *and* $T=T+T'$

The term S_T is a source term allowing for the rate of thermal energy production.

2.1.4 $k-\varepsilon$ Turbulence model

Two equations $k-\varepsilon$ turbulent model is considered to simulate the turbulent flow numerically. The transport equation for turbulence kinetic energy (k) is given by [**Awbi, 1989**.]:

$$\frac{\partial}{\partial t}(\rho k)+\frac{\partial}{\partial x}(\rho uk)+\frac{\partial}{\partial y}(\rho vk)+\frac{\partial}{\partial z}(\rho wk)=\frac{\partial}{\partial x}\left(\Gamma_k\frac{\partial k}{\partial x}\right)+\frac{\partial}{\partial y}\left(\Gamma_k\frac{\partial k}{\partial y}\right)+\frac{\partial}{\partial z}\left(\Gamma_k\frac{\partial k}{\partial z}\right)+$$
$$\mu_t\{2[(\frac{\partial u}{\partial x})^2+(\frac{\partial v}{\partial y})^2+(\frac{\partial w}{\partial z})^2]+(\frac{\partial u}{\partial y}+\frac{\partial v}{\partial x})^2+(\frac{\partial u}{\partial z}+\frac{\partial w}{\partial x})^2+(\frac{\partial w}{\partial y}+\frac{\partial v}{\partial z})^2\}$$
$$-c_u\rho\frac{k^{1.5}}{L}+\beta g\frac{\mu_t}{\sigma_t}\frac{\partial T}{\partial y} \quad (4)$$

Where:

$$k=\frac{1}{2}\left[\left(\overline{u'}\right)^2+\left(\overline{v'}\right)^2+\left(\overline{w'}\right)^2\right] \quad (5)$$

is the turbulent Prandtl number (0.5 to 0.9) **Awbi,1989**, and c_u is constant $\Gamma_k=\frac{\mu_e}{\sigma_k}$, $\sigma_k\approx 1$, $\sigma_t \approx 0.09$, the last term of equation 4 represents the effect of buoyancy.

The body force in x and z direction ρg_x *and* ρg_z were omitted.

$$\frac{\partial}{\partial t}(\rho u)+\frac{\partial}{\partial x}(\rho uu)+\frac{\partial}{\partial y}(\rho uv)+\frac{\partial}{\partial z}(\rho uw)=-\frac{\partial p}{\partial x}+\frac{\partial}{\partial x}\left(\mu_e\frac{\partial u}{\partial x}\right)+\frac{\partial}{\partial y}\left(\mu_e\frac{\partial u}{\partial y}\right)+\frac{\partial}{\partial z}\left(\mu_e\frac{\partial u}{\partial z}\right)+$$
$$\frac{\partial}{\partial x}\left(\mu_e\frac{\partial u}{\partial x}\right)+\frac{\partial}{\partial y}\left(\mu_e\frac{\partial v}{\partial x}\right)+\frac{\partial}{\partial z}\left(\mu_e\frac{\partial w}{\partial x}\right) \quad (6)$$

The body force in the y direction has been written as a buoyancy force, where is the density at the flow reference temperature.

$$\frac{\partial}{\partial t}(\rho v)+\frac{\partial}{\partial x}(\rho uv)+\frac{\partial}{\partial y}(\rho vv)+\frac{\partial}{\partial z}(\rho vw)=-\frac{\partial p}{\partial y}+\frac{\partial}{\partial x}\left(\mu_e\frac{\partial v}{\partial x}\right)+\frac{\partial}{\partial y}\left(\mu_e\frac{\partial v}{\partial y}\right)+\frac{\partial}{\partial z}\left(\mu_e\frac{\partial v}{\partial z}\right)+$$
$$\frac{\partial}{\partial x}\left(\mu_e\frac{\partial u}{\partial y}\right)+\frac{\partial}{\partial y}\left(\mu_e\frac{\partial v}{\partial y}\right)+\frac{\partial}{\partial z}\left(\mu_e\frac{\partial w}{\partial y}\right)-g(\rho-\rho_o) \quad (7)$$

The transport equation for ε is given as:

$$\frac{\partial}{\partial t}(\rho\varepsilon)+\frac{\partial}{\partial x}(\rho u\varepsilon)+\frac{\partial}{\partial y}(\rho v\varepsilon)+\frac{\partial}{\partial z}(\rho w\varepsilon)=\frac{\partial}{\partial x}\left(\Gamma_\varepsilon\frac{\partial\varepsilon}{\partial x}\right)+\frac{\partial}{\partial y}\left(\Gamma_\varepsilon\frac{\partial\varepsilon k}{\partial y}\right)+\frac{\partial}{\partial z}\left(\Gamma_\varepsilon\frac{\partial\varepsilon k}{\partial z}\right)+$$

$$C_1\frac{\varepsilon}{k}\mu_t\{2[(\frac{\partial u}{\partial x})^2+(\frac{\partial v}{\partial y})^2+(\frac{\partial w}{\partial z})^2]+(\frac{\partial u}{\partial y}+\frac{\partial v}{\partial x})^2+(\frac{\partial u}{\partial z}+\frac{\partial w}{\partial x})^2+(\frac{\partial w}{\partial y}+\frac{\partial v}{\partial z})^2\}$$

$$-c_2\rho\frac{\varepsilon^2}{k}+C_1\beta g\frac{\varepsilon}{k}\Gamma_t\frac{\partial T}{\partial y} \qquad (8)$$

Where:

$\Gamma_k=\frac{\mu_e}{\sigma_\varepsilon}, \sigma_k$:is a constant equal to 1.22, C_1=1.44, C_2=1.92.

2.1.5 Boundary conditions

2.1.5.1 Inlet boundary conditions

The flow is assumed uniform at room inlet as shown in **Fig.1**. The tangential velocity is set to be zero, the normal velocity component (U_n) is determined depending on the desired air change per hour (ACH) as follows **Kwang, 2008**:

$$U_{jet}=\frac{ACH.V_r}{3600.A_{in}} \qquad (9)$$

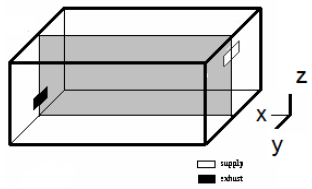

Figure1.

Where:

V_r =Room volume

A_{in} =Supply outlet area

The kinetic energy and dissipation rate at inlet are determined using the following equations **Awbi, 1989**:

$$k_{in}=\frac{2}{3}I_u^2.U_{jet}^2 \qquad (10)$$

$$\varepsilon_{in}=\frac{k_{in}^{\frac{2}{3}}}{\lambda_H} \qquad (11)$$

Where $\lambda=0.005$ and I_u^2=0.14

2.1.5.2 Outlet boundary conditions

A uniform velocity distribution is assumed over the room outlet. Tangential velocity is considered to equal zero (U_i=0), and the normal velocity is computed from the continuity equation.

$$U_{out}=U_{in}=\frac{(\rho.A)_{in}}{(\rho.A)_{out}} \qquad (12)$$

Exit temperature T_{out} is obtained from the energy equation for whole flow field. Due to the assumption of a uniform distribution of the forces in the exit plane, the gradient of k,ε and all scalar properties are zero **Kwang,2008**, hence

$$\frac{\partial T}{\partial x_n}=0,\quad \frac{\partial k}{\partial x_n}=0,\quad \frac{\partial \varepsilon}{\partial x_n}=0, \qquad (13)$$

2.1.5.3 Solid boundary conditions

The normal velocity U_n is considered equal to be zero at the wall. The simplest way of imposing the tangential velocity U_i is

$$\left.\frac{\partial U_i}{\partial x_n}\right|_{wall}=\frac{mU_i}{y_n} \qquad (14)$$

Where m is a constant equals to $\frac{1}{7}$.

Boundary conditions for turbulent energy may be imposed using the following equation **Nielsen, 2006**:

$$\varepsilon=\frac{(c_u^{\frac{1}{2}}.k)^{\frac{3}{2}}}{k_{y_n}} \qquad (15)$$

Where c_u is constant and equal to 0.09.

To impose the temperature B.C. on the wall, a heat balance concept is adopted, by assuming the heat conduction through the wall is equal to the heat convected a way from the wall.

$$k\frac{\partial T}{\partial x_n}=hc(T_2-T_w) \qquad (16)$$

2.1.6 Initial conditions

The initial values for all three velocities and pressure at every node inside the computational flow domain are set to zero, while, the initial value of temperature is assumed some suitable value depending of each case, and the initial values for the turbulent kinetic energy and turbulent dissipation rate are set at some percentage of the inlet values.

2.2 Numerical Procedure

A finite volume method has been used in discretization scheme with staggered grids and Semi Implicit Method for Pressure Linked Equation (SIMPLE) procedure to link the velocity filed to pressure filed **Shuzo, 1989** . The computational domain is divided into number of non-overlapping control volumes.

3. EXPERIMENTAL WORK

The experimental test rig consists of a typical prototype room (5m × 4m × 3m), and a suitably scaled (1/5) model room (1m × 0.8m × 0.6m). The minimum air changes per hour (ACH), for a room with side wall supply air, was calculated using the relation given by **Kwang,2008**:

$$N = 7.84\sqrt[3]{\frac{qB}{(3+H)\times L^2}} \qquad (17)$$

Where :

B,H,L= room dimension in m.

q: total heat load in W.

To produce N=6.913 ACH for the prototype room. Accordingly, other prototype related

parameters were calculated. The kinematical similarity, between the prototype and model rooms, was achieved by equating the Reynolds number, resulting in:

$U_m = 5\ U_p = 4.5$ m/s

Similarly, other model related parameters were calculated.

The reduced scale model was made from an aluminum frame with 4mm thick sliding plastic walls and ceiling. The ducting system were made from galvanized steel plates (gauge 24), with different dimensions. Two centrifugal fans (2825 rpm) were used; one to deliver the smoked air to the room and the other is for the exhaust. The supply and return air velocities were measured using digital anemometers (Model DA40). The smoke was traced out using Sony digital camera. **Fig.3** shows the complete test rig with the model room mounted.

4. RESULT AND DISCUSSIONS

The flow inside a room is affected by many parameters, mechanical and thermal. The amount of air flow, inlet temperature, supply velocity, location of opening, room geometry and the presence of obstacles are all important parameters. To add to the complexity, the buoyancy has many sources like computers, human, lights to name a few. Almost, all of the above parameters were considered in this work. **Fig.4** pictures the air distribution through the prototyped room, the swirl is clearly visible. The numerical results come close to the experimental outcome as shown in **Fig.5** for the same case of one supply opening and one outlet opening. The swirl persists even near side walls as shown in **Fig.6**.The swirl becomes more pronounced with the two supply openings and one outlet opening all located on the same wall as shown in **Fig.7**. While **Fig.8** shows that the pattern becomes more complicated for the three supply opening on the front wall and one outlet opening on the side wall. The flow pattern generated by air diffusers is simpler as can be seen from f**igures 9** and **10** for one and two diffusers respectively. When the ceiling contains an obstacle, stagnant zones will be generated behind them, also separation and reattachments of the air stream and the accompanying recirculation can be recognized. These flow patterns vary in strength depending on the proximity of these obstacles from the supply openings, as shown in **figures 11, 12** and **13** for (1/4), (1/2) and (3/4) room length proximity respectively. **Table 1** gives the summary of the variables under study. **Table 2** shows the properties of air and other numerical parameters used in simulation model.

5. VALIDITY OF CURRENT WORK

The results of the air velocity and temperature distribution that's obtained by using numerical solution method inside the room are validated with that obtained from experimental work. The comparison between the numerical and experimental work showed a good agreement, as shown in **Fig.2**. Also the numerical and experimental results obtained in current work are validated by

comparing with similar experimental and numerical work **Shuzo, 1989** and the comparison also showed a good agreement, as shown in **Fig.2**.

6. CONCLUSIONS

When inlets discharge horizontally near the ceiling, the warmest air in the room mixed immediately with cool air. Ceiling diffusers that designed for vertical downward air projection produce stagnant regions near the ceiling. When the supply jet encounters ceiling obstacles, it either completely separates from the ceiling or it may reattach downstream the obstacle.

Table1. Summary of variables that are studied in the present work.

Parameter	variation
Supply velocity	0.6 , 0.9 , 1.5 (m/s)
Flow type	Turbulent with all function
Room dimensions	$4\times5\times3$ (m)
Inlet air velocity profile	Uniform for all cases
Grid resolution	Uniform $40\times50\times30$

Table2. Fluid properties in simulation model.

Parameter	ρ kg/m^3	ν m^2/s	k W/mK	C_p J/kgK	T_{in} $^\circ C$	T_w $^\circ C$
Value	1.19	1.15×10^{-5}	0.026	1003.6	17, 25, 35	30

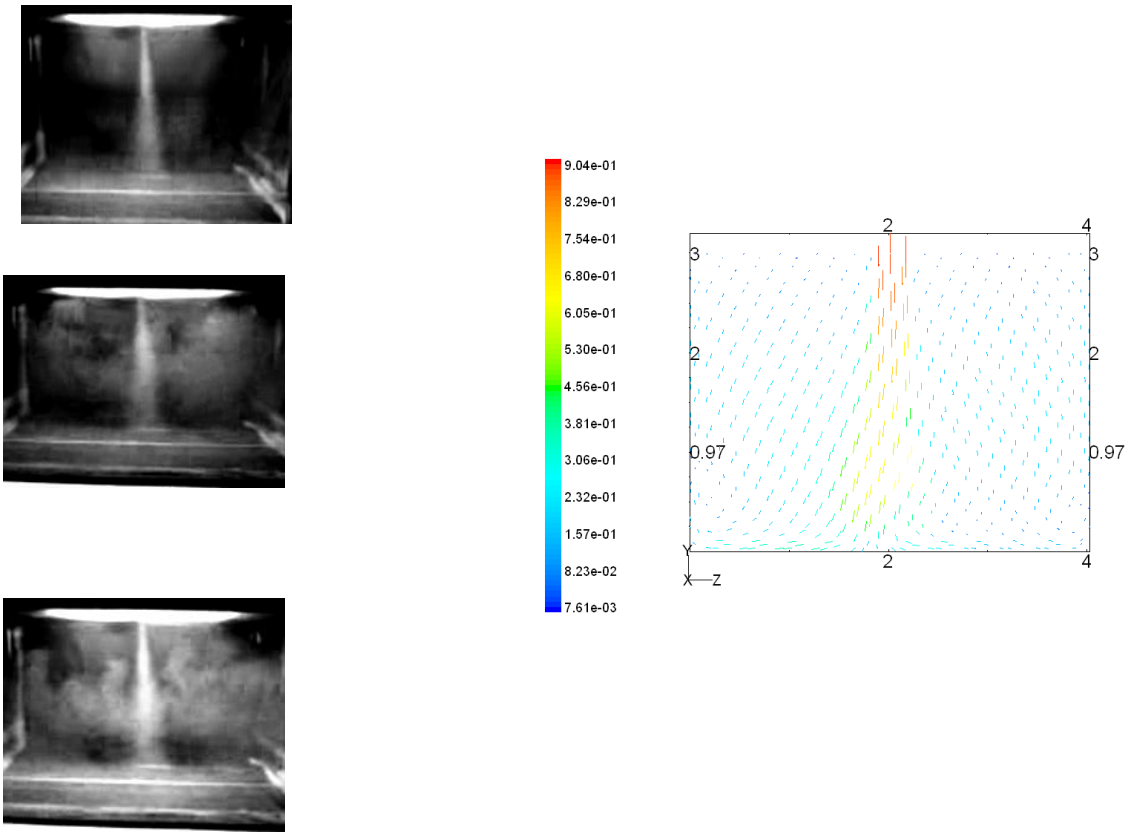

Visualization current work

Numerical current work

Numerical simulation ,**Shuzo, 1989**.

Experimental work, **Shuzo, 1989.**

Figure 2. Validity of current work**.**

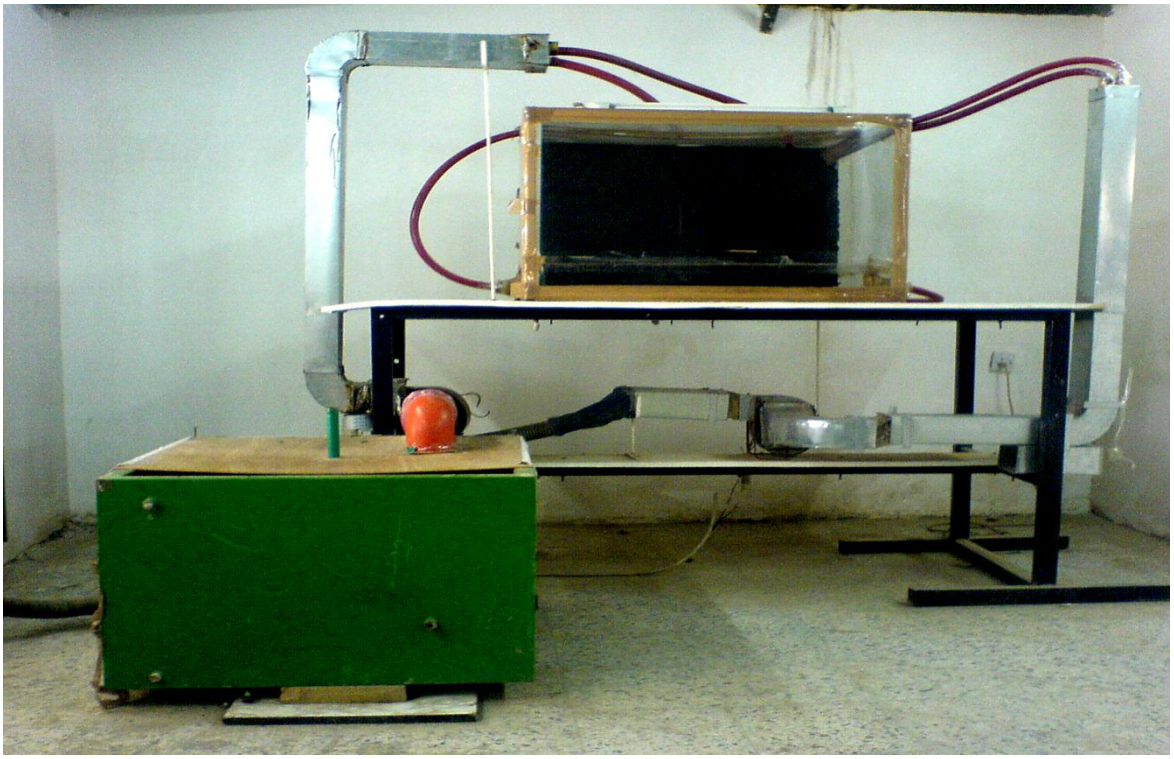

Figure3. Complete test rig with the model room mounted.

Figure4. Air distribution through the prototyped room.

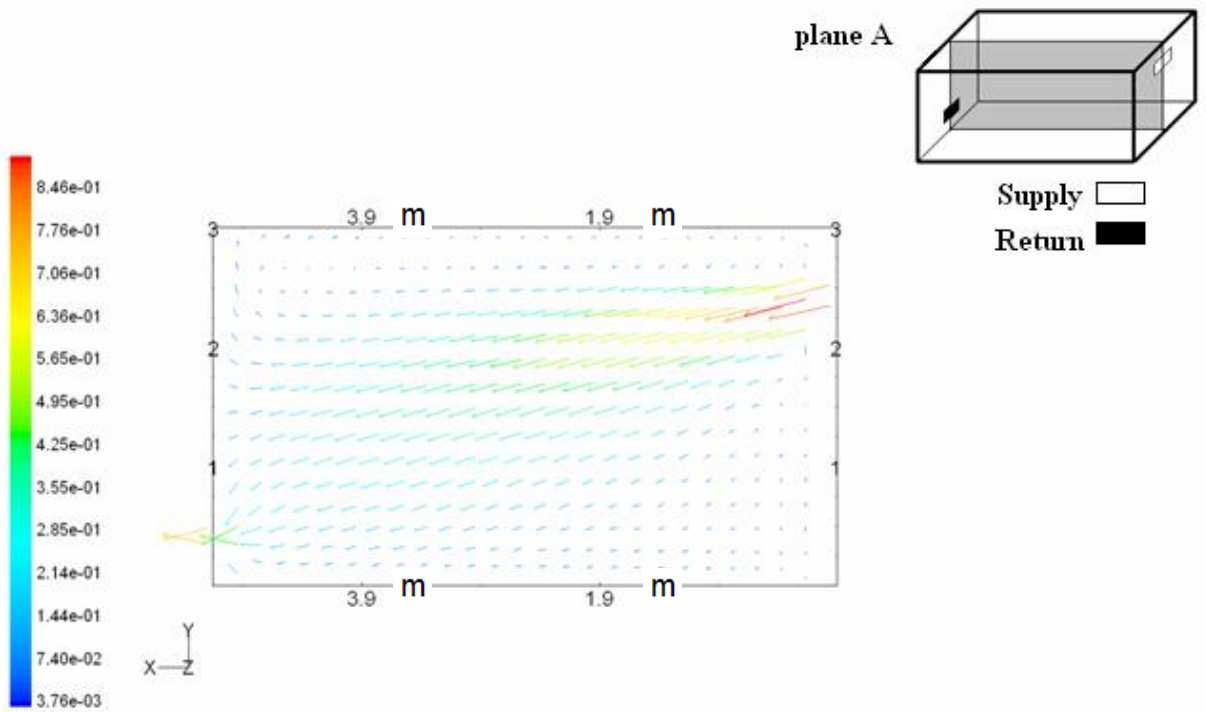

Figure 5. Velocity distribution in a room with single supply and single extract opening.

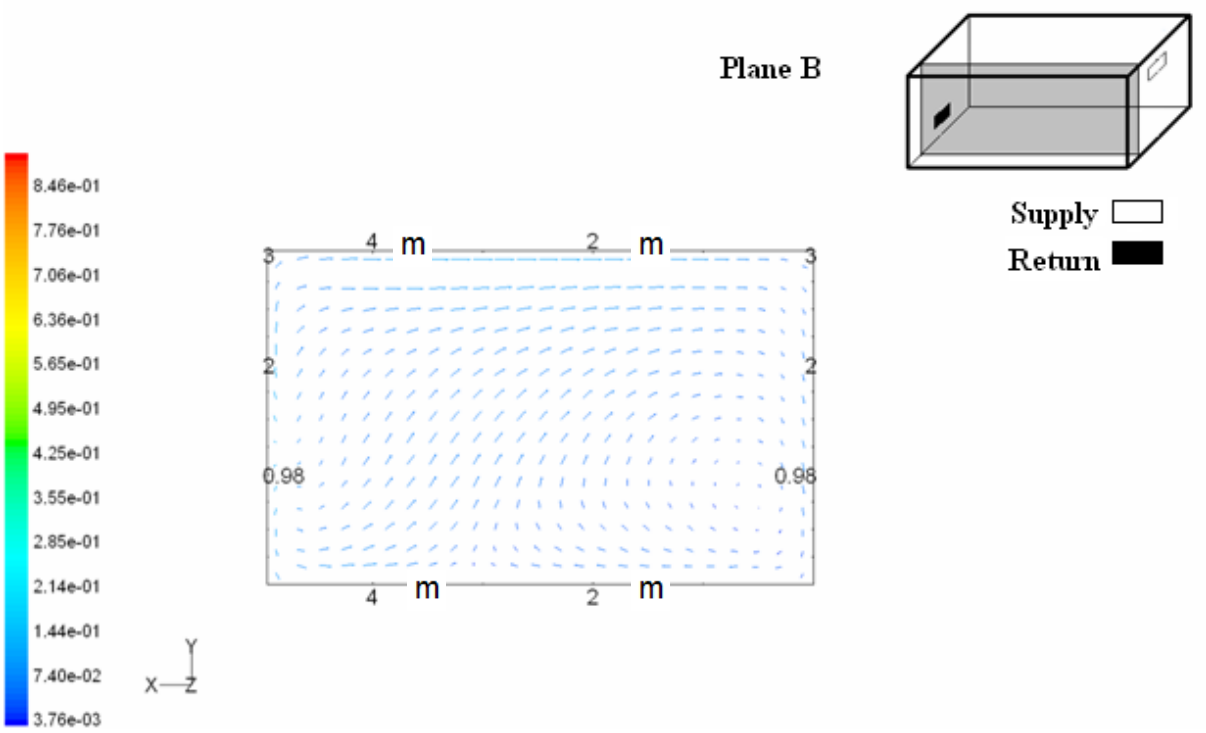

Figure 6. Velocity distribution in a room with single supply and single extract opening.

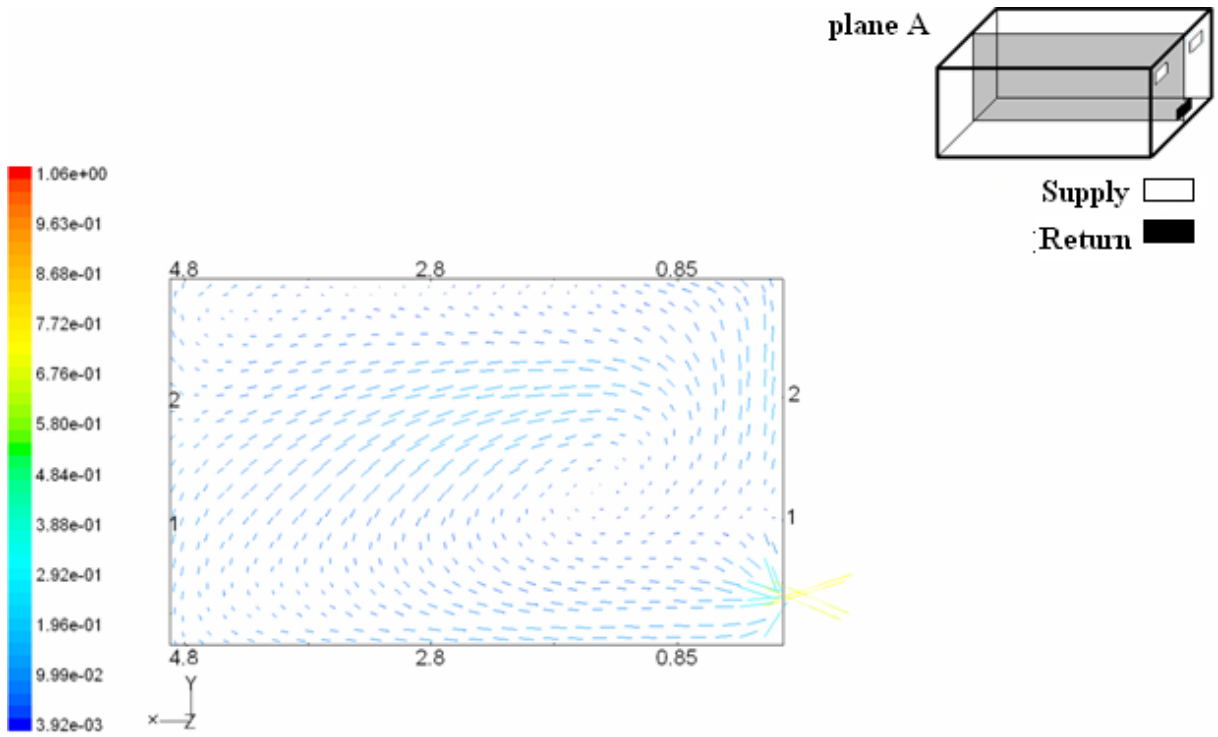

Figure7. Velocity (m/sec) distribution in a room with two supply and single extract opening.

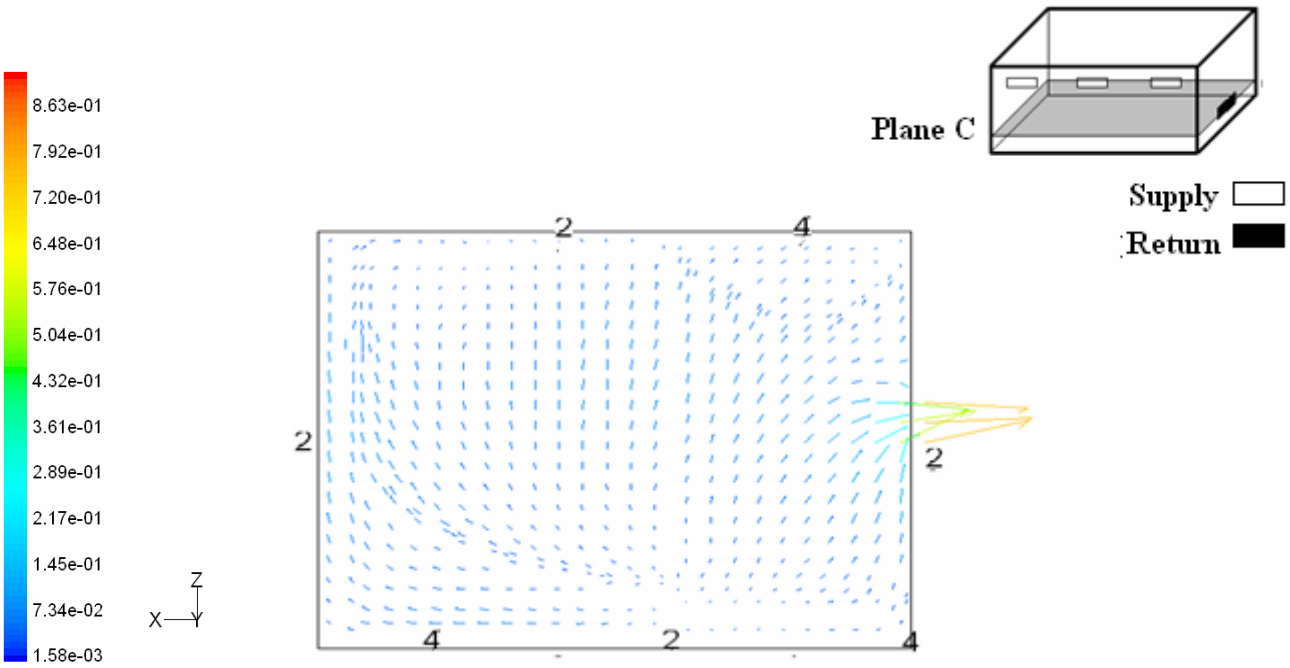

Figure 8. Velocity (m/sec) distribution in a room with three supply and single extract opening.

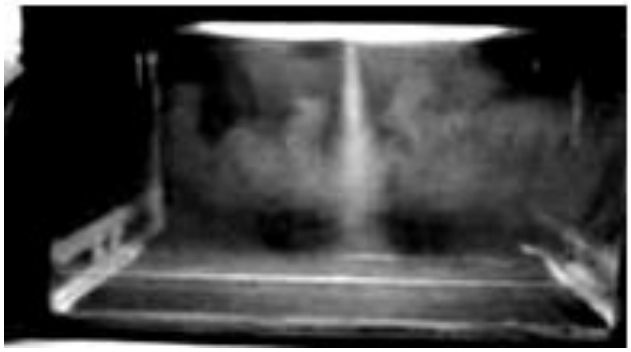

Figure 9. Pattern generated by single diffuser.

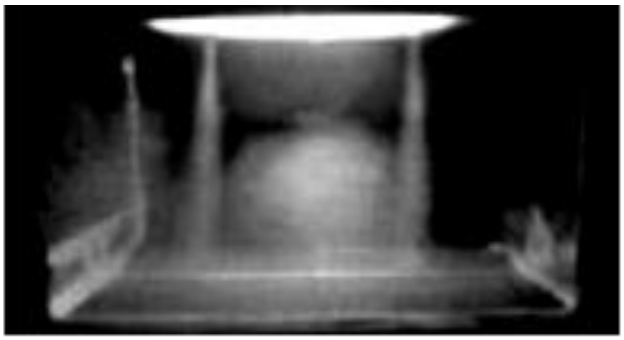

Figure10. Pattern generated by two diffusers.

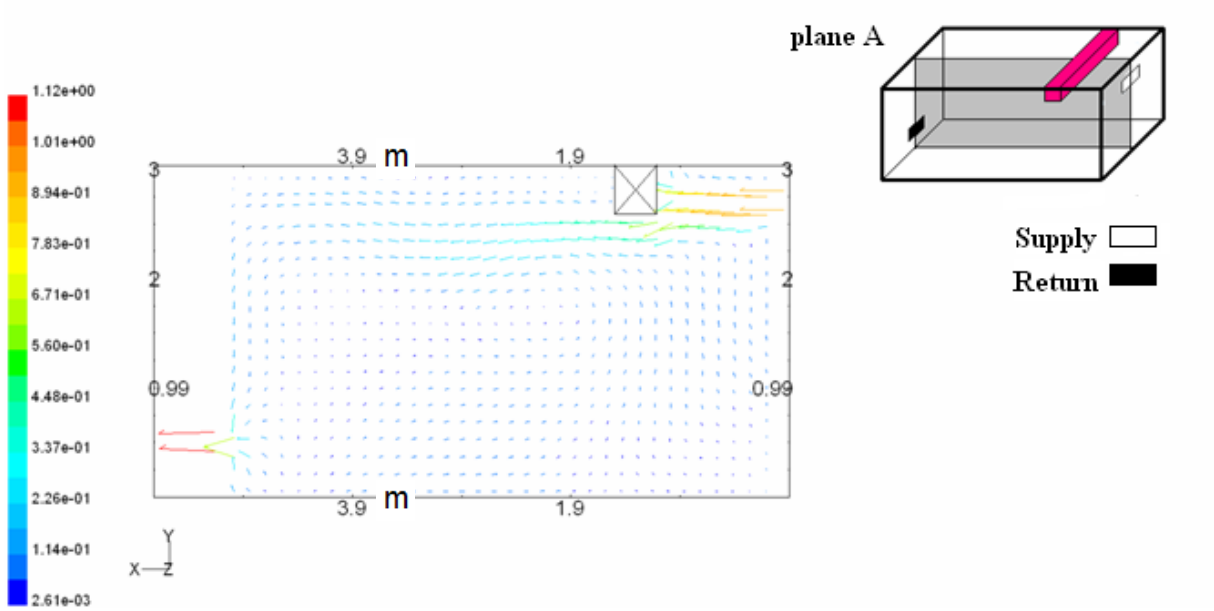

Figure11. Velocity distribution with velocity (U supply= 0.9 m/s) and constant supply temperature of (T=17 $^{\circ}C$) with ceiling obstacle at (1/4) of the room length.

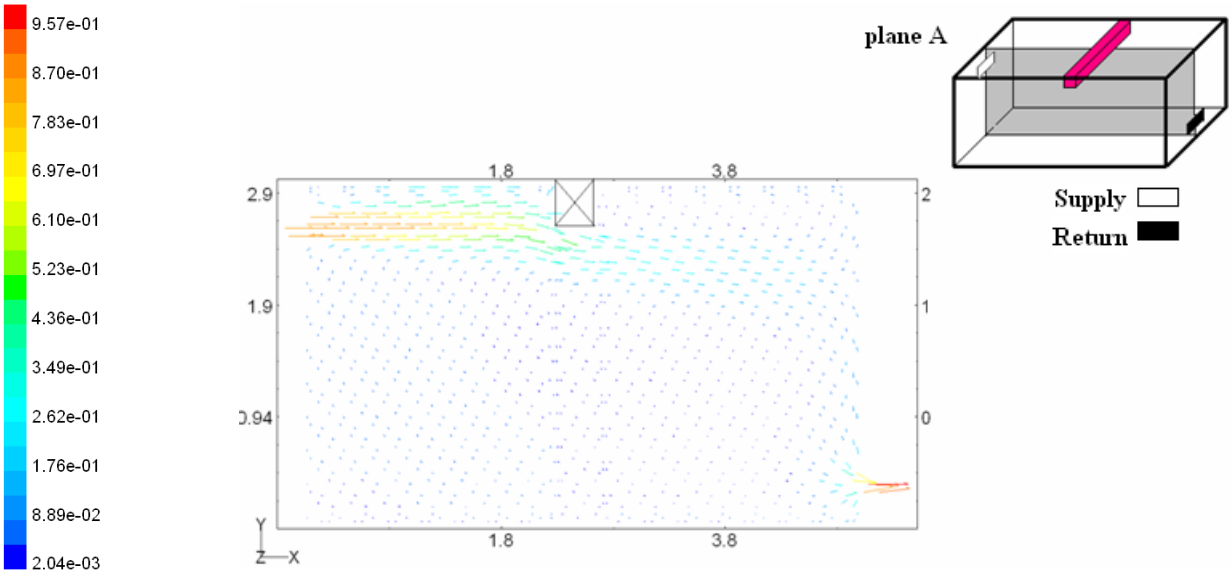

Figure 12. Velocity distribution with velocity (U supply=0.9 m/s) and constant supply temperature of (T=17 $^{\circ}C$) with ceiling obstacle at (1/2) of the room length.

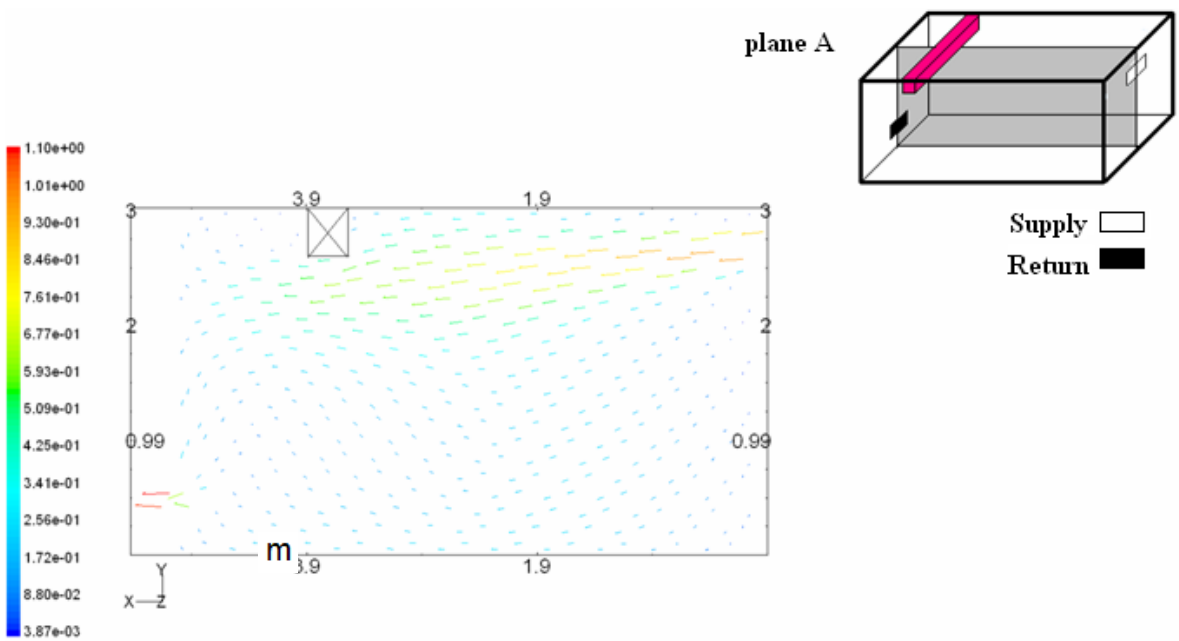

Figure 13. Velocity distribution with velocity (U supply=0.9 m/s) and constant supply temperature of (T=17 $^{\circ}C$) with ceiling obstacle at (3/4) of the room length.

REFERENCES

Awbi, H.B., 1989, *Application of Computational Fluid Dynamics in Room Ventilation,* Building and environment, Vol.24, No.1, PP.73-84.

Bartak, M., Cermak, M., Clarke, J. A., Denev, J., and Drkal, F., 2001, *Experimental and Numerical Study of Local Mean Age,* Seventh International IBPSA Conference, Rio de Janeiro, Brazil, PP. 773-780.

Chen, Q., and Zhang, Z., 2005, *Prediction of Particle Transport in Enclosed Environment*, China Particuology, Vol.3, No.6, PP. 364-372.

Hanibuchi, H., and Hokoi, S., 2001, *Experimental and Numerical Prediction of the Velocity and Temperature Field in a Room Heated by a Room Air-conditioner* , Ph.D. thesis- Kyoto University, Japan, PP. 606.

Kwang, C. N., Chang, W.H., and Myung, D. O., 2008, *Effect of the Airflow Rate of a Ceiling Type Air-Conditioner on Ventilation Effectiveness in a Lecture Room*, International Journal of Refrigeration Vol. 31, Issue 2, PP. 180-188.

Nielsen, P., 2006, *Air Distribution In A Room With Ceiling-Mounted Diffusers : Comparison With Wall-Mounted Diffuser, Vertical Ventilation, and Displacement Ventilation*, American Society of Heating, Refrigerating and Air-Conditioning Engineers. Annual meeting, Chicago, Vol. 112, No.2, PP. 498-504.

Shuzo, M., and Shinsuke, K., 1989,*Numerical and Experimental Study on Room Air Flow 3-D Predictions using the (K-E) Model*, Building and environment.Vol.24, No.1, PP 85-97.

Zhang, Z., and Chen, Q., 2006, *Experimental Measurements and Numerical Simulations of Particle Transport and Distribution in Ventilated Rooms*, Atmospheric Environment, Vol.40, No.18, PP. 3396-3408.

NOMENCLATURE

Symbols	Definition	Unit
a	Coefficient value	dimensionless
A_{in}, A_{out}	Inlet and outlet cross- section area	m^2
g_x, g_y, g_z	Gravitational acceleration	m/s^2
H	Room height	m
J	Flux due to both diffusion and convection	dimensionless
k	Thermal conductivity	$W/m.K$
k	Turbulent kinetic energy	m^2/s^2
k_{in}	Turbulent energy at room inlet	m^2/s^2
$k_{i,j,k}$	Turbulent energy at cell	m^2/s^2
p	Pressure	N/m^2
Pe	Peclet number	dimensionless
Re	Reynolds number	dimensionless
$T_\circ$	Reference temperature	K
T	Temperature	K
T'	Fluctuation temperature	K
$T_{i,j,k}$	Temperature at cell center	K
U, V, W	Velocity components in x ,y and z-direction	m/s
U_{jet}	Inlet velocity	m/s
U_n	Normal velocity	m/s
μ	Dynamic viscosity	$kg/m.s$
α	Diffusivity	m^2/s
β	Volumetric expansion coefficient	$1/K$

ε	Turbulent energy dissipation	m^2/s^3
ϕ	Generic scalar quantity	dimensionless
ρ	Density	kg/m^3
μ_e	Effective viscosity coefficient	$kg/m.s$
μ_t	Turbulent viscosity	$kg/m.s$
υ	Kinematics viscosity	m^2/s
υ_e	Effective kinematics viscosity	m^2/s
υ_t	Turbulent viscosity	m^2/s
$\sigma_k, \sigma_\varepsilon$	Constants for $k-\varepsilon$ model	dimensionless
$\Delta x, \Delta y, \Delta z$	Cell dimensions	m
Γ	Diffusion coefficient	dimensionless
Γ_t	Turbulent diffusion coefficient	dimensionless
μ_e, μ_t	Coefficients of effective viscosity and turbulent viscosity	$kg/m.s$

Experimental and Numerical Analysis of Incompressible Flow over an Iced Airfoil

Karima E. Amori
Professor
College of Engineering-University of Baghdad
drkarimaa@yahoo.com

Ethar Saad Ahmed
ethar_eng_87@yahoo.com

ABSTRACT

Determining the aerodynamic characteristics of iced airfoil is an important step in aircraft design. The goal of this work is to study experimentally and numerically an iced airfoil to assess the aerodynamic penalties associated with presence of ice on the airfoil surface. Three iced shapes were tested on NACA 0012 straight wing at zero and non-zero angles of attack, at Reynolds No. equal to ($3.36*10^5$). The 2-D steady state continuity and momentum equations have been solved utilizing finite volume method to analyze the turbulent flow over a clean and iced airfoil. The results show that the ice shapes affected the aerodynamic characteristics due to the change in airfoil shape. The experimental results show that the horn iced airfoil consumes more power than the other shapes of ice, its value was (44.4W). The horn iced shape has the worst effect on the airfoil than the other shapes. The present results are compared with previously reported results; it is found there is a very good agreement between them. A comparison between the experimental and computational results of the presented work were pursing the same behavior.

Keywords : Iced airfoil, computational fluid dynamics, turbulence model, drag, lift, aerodynamic.

التحليل التجريبي والعددي لجريان لاانضغاطي حول مطيار مثلج

أ.د. كريمة أسماعيل عموري **ايثار سعد أحمد**

الخلاصة

إن تحديد الخصائص الديناميكية الهوائيه لمطيار متكون عليه جليد هو خطوة هامة في تصميم الطائرات. الهدف من هذا العمل هو بناء تجارب عملية وعددية لجنيح متجمد وذلك لتقييم الاداء الايروديناميكي المرتبط بوجود ثلج على سطح الجنيح.تم اختيار ثلاثة اشكال لثلج متكون على مطيار من نوعNACA 0012 حيث اختبرت عند زاويا هجوم صفرية غير صفرية ولعدد رينولدز($3.36*10^5$). تم حل معادلات الاستمرارية والزخم ذات البعدين للحاله المستقرة باستخدام طريقة الحجوم المحددة وذلك لتحليل الجريان المضطرب حول جنيح بدون ومع وجود الثلج عليه.أظهرت النتائج إن اشكال الثلج المتولده على المطيار تؤثر على الخصائص الايروديناميكية وذلك بسبب تغير الشكل الانسيابي للجنيح. النتائج التجريبية بينت أن شكل الثلج بحافة حادة على الجنيح يستهلك طاقة اعلى من بقية اشكال الثلج, حيث كانت أعظم طاقة (44.4 واط). أظهرت النتائج ايضا أن الثلج ذو الحافة الحادة تأثيره الاسوء على الأجنحة من بقية الاشكال.قورنت النتائج الحالية مع نتائج لبحوث سابقة وكانت متوافقة معها بصورة جيدة جدا. قورنت النتائج العملية مع النتائج النظرية، حيث كانت تسلك نفس السلوك .

1. INTRODUCTION

Decades of operational experiences have revealed many situations in flight as well as on the ground when ice can accrete on ‘‘ice-protected’’ aircraft. With the very large variety of forms and sizes in which ice can accrete on aircraft surfaces in real operational conditions, the challenge facing researchers and aircraft designers has been to establish an effective process for defining the accretion process and physical characteristics of these ice shapes for any aircraft surface at any flight or meteorological conditions, and to determine which are the most harmful iced shape. Typically, some flight testing in natural icing conditions is required as part of the aircraft certification process for new aircraft designs in order to demonstrate the effectiveness of ice protection systems as well as overall aircraft performance and handling characteristics. In the late 80’s of the previous century, several studies have been completed of ice accretions and resulting performance losses for airfoil profiles by National Air and Space Administration (NASA) Lewis research which led to many important works. Many researchers investigated iced airfoils over the years from different perspectives; the following paragraphs summarize their works.

Bragg, 1986. studied the aerodynamics of a National Advisory Committee for Aeronautics (NACA) 0012 airfoil with a simulated glaze ice accretion and he found that there is a decreasing in lift and increasing in the drag. **Bragg, 1994.**studied experimentally the aerodynamics of a NACA 0012 of 30-degree swept and unswept semi-span wing with simulated glaze ice accretion on their leading edge. He found in the region of 2D flow that all small roughness produced by the presence of the dense mid-span tap row caused higher than expected (C_D) results for the clean wing when the wake probe was placed directly behind the mid-span tap row. **National technical information service (NTIS), 2000** reported an integrated experimental and computational investigation to determine the effect of simulated ridge ice shapes on airfoil aerodynamics. **Mateescu, 2004.**presented an efficient solution of steady and unsteady flows by solving the Euler and Navier-Stokes equations using finite difference and finite volume formulations. **Mateescu and Abdo, 2005.** studied analytically the velocity and pressure distributions on airfoils of arbitrary shapes, considering the rigorous boundary conditions. A second-order accurate method using velocity singularities in the expression of the fluid velocity is first developed for airfoils in inviscid incompressible flows, by simultaneously solving the symmetric and anti-symmetric flow components defined by coupled complex boundary conditions**. Broeren, et.al, 2006.**carried out the flow field measurements on the upper surface of a GLC-305 airfoil configured with glaze and rime ice-shape simulations. The separation region for the glaze ice configuration was much larger than those for the rime ice case, resulting from the differences in the ice horn geometry. Changes in Reynolds number did not significantly affect the separation region characteristics. A larger Mach number resulted in a slightly larger separation region for the glaze ice case at α equal to 6°. **Hasoun, 2007.** conducted to study the effect of simulated ice accreted on airfoil aerodynamics performance NACA 0012.

Bragg, et.al, 2008.conducted a major research program to improve the understanding of the aerodynamic scaling of ice accretions on airfoil NACA 23012. **Mirzaei,et.al,2008.**presented the icing phenomenon on surface of NLF-0414 airfoil experimentally using single element hot-wire and also using CFD calculations to solve Navier-Stokes equations, with 22.5 minute ice accretions at Reynolds number of 0.5×10^6. They concluded that Reynolds number variation did not affect seriously on the drag coefficient of iced airfoil. **Gord, et.al, 2009.** presented experimental and numerical analysis of incompressible flow around an airfoil NACA 0012.Numerical analysis combined vortex panel method techniques for solving potential flow around the airfoil and Von Karman boundary layer integral equation solver. Results show that this method has a good capability to predict velocity profile, pressure and drag coefficients over the surface. **Bortholin and Catalano, 2012.**analyzed two categories of icing accretions in NACA 0012 airfoil through the effects in the force as well as in pressure distribution via numerical simulations.

From above literature review, it can be seen that a rare of experimental investigations for iced symmetrical straight wings have been carried out for one ice shape (i.e. they didn't compared the effect of different shapes with each other on the same airfoil). Most of the reviewed researches were investigated numerically especially that of the glaze iced because it is natural complicated throughout the accretions on the airfoil. As a result concluded that aerodynamics performance of the airfoil affected by ice amount, shape and its location, also Angel Of Attack (AOA) and the geometry of the wing play important part as well. In addition most of previous studies indicated that ice accretion decreasing lift and increasing drag when the AOA increased.

The main objective of the present work is to investigate the aerodynamic characteristics of the iced and clean symmetrical wing (NACA0012airfoil) numerically and experimentally at zero and non-zero angle of attack. The CFD analysis of airfoil NACA 0012 is performed for a Reynolds number ($3.36*10^5$) at various angles of attack using a fully turbulent flow solution in ANSYS FLUENT software, where k-ε model and SIMPLE algorithm to solve the continuity and momentum equations of airflow over a 2D airfoil are adopted. Three shapes have been chosen as follow:

a. Horn iced shape (case A II).
b. Flat iced shape (case A III).
c. Quarter round forward iced shape (case A IV).

2. MATHEMATICAL MODEL ANDCOMPUTATIONAL METHODOLOGY

The two dimensional governing differential equations of external flow analysis in Cartesian coordinates with two equations for (k-ε) turbulence model **Verestage&Malalasekera, 1995.** can be written as:

- **Conservation of Mass**

$$\frac{\partial u}{\partial x} + \frac{\partial v}{\partial y} = 0 \qquad \dots (1)$$

where u, υ are velocity components in x and y direction respectively.

- **Momentum Equations**

$$\frac{\partial}{\partial x}(\rho u u) + \frac{\partial}{\partial y}(\rho u \upsilon) = -\frac{\partial p}{\partial x} + \frac{\partial}{\partial x}(\mu_{eff}\frac{\partial u}{\partial x}) + \frac{\partial}{\partial y}(\mu_{eff}\frac{\partial u}{\partial y}) + S_u \qquad (2)$$

v-momentum (y-direction)

$$\frac{\partial}{\partial x}(\rho \upsilon u) + \frac{\partial}{\partial y}(\rho \upsilon \upsilon) = -\frac{\partial p}{\partial y} + \frac{\partial}{\partial x}(\mu_{eff}\frac{\partial v}{\partial x}) + \frac{\partial}{\partial y}(\mu_{eff}\frac{\partial v}{\partial y}) + S_v \qquad (3)$$

μ_{eff} is the effective viscosity coefficient which can be evaluated as:

$$\mu_{eff} = \mu_l + \mu_t \dots \qquad (4)$$

where μ_l is the laminar viscosity, and μ_t is the turbulent eddy viscosity. S_u, is a source term of u in x-direction, while $S_v$is a source term of υ in y-direction.

The k-ε turbulence model is the two-equation model of kinetic energy (k) and its dissipation rate (**ε**) **Launder and Spalding1972**. This model relates the turbulent viscosity to the local values of ρ, k and ε by the expression.

$$\mu_t = \rho c_\mu k^2 / \varepsilon \qquad (5)$$

wherec_μ is an empirical constant. The distribution of k and ε over the flow field is calculated from the following semi-empirical transport equations for k and ε , **Ideriah1975.**

(i) Turbulence Energy, k

$$\frac{\partial}{\partial x}(\rho u k) + \frac{\partial}{\partial y}(\rho \upsilon k) = \frac{\partial}{\partial x}\left(\frac{\mu_{eff}}{\sigma_k}\frac{\partial k}{\partial x}\right) + \frac{\partial}{\partial y}\left(\frac{\mu_{eff}}{\sigma_k}\frac{\partial k}{\partial y}\right) + G - \rho\varepsilon \qquad (6)$$

(ii) Energy Dissipation Rate, ε

$$\frac{\partial}{\partial x}(\rho u \varepsilon) + \frac{\partial}{\partial y}(\rho \upsilon \varepsilon) = \frac{\partial}{\partial x}\left(\frac{\mu_{eff}}{\sigma_\varepsilon}\frac{\partial \varepsilon}{\partial x}\right) + \frac{\partial}{\partial y}\left(\frac{\mu_{eff}}{\sigma_\varepsilon}\frac{\partial \varepsilon}{\partial y}\right) + c_1\frac{\varepsilon}{k}G - c_2\rho\frac{\varepsilon^2}{k} \qquad (7)$$

In the turbulence transport equations, Grepresents production of the kinetic energy from mean velocity gradients and σ_ε, $\sigma_k$are the effective Prandtl number.

$$G = \mu_t \left\{2\left[\left(\frac{\partial u}{\partial x}\right)^2 + \left(\frac{\partial v}{\partial y}\right)^2\right] + \left(\frac{\partial u}{\partial x} + \frac{\partial v}{\partial y}\right)^2\right\} + S_G \qquad (8)$$

$S_G$given by **Ideriah1975**.

$$S_G = -\frac{2}{3}\mu_t\left[\frac{\partial u}{\partial x} + \frac{\partial v}{\partial y}\right]^2 - \frac{2}{3}\rho k\left[\frac{\partial u}{\partial x} + \frac{\partial v}{\partial y}\right] \qquad (9)$$

where S_G is source term of production of G.

The boundary conditions at the airfoil shown in **Fig. (1)** are:

- No slip boundary condition is applied on solid surface.
- Uniform and constant free stream velocity.
- The physical properties of air are constant.
- It is assumed that the ice formation is stretched from the wing root to the tip with no spanwise variations.

The Computational Fluid Dynamics (CFD) is adopted in this work by utilizing a finite volume method. Fluent software is used to solve the governing differential equations for air flow over a clean and iced airfoil. FLUENT does not contain an integrated meshing capability and must therefore be used with GAMBIT or other mesh generation software. Model construction, assembly and meshing require a trial and error approach that many times needs multiple iterations before a good geometry and mesh can be developed. **Fig. (2 a, b, c, and d**) represents the unstructured grid generated for airfoil with and without ice in Gambit, **Fluent Inc., 2009.**

3. EXPERIMENTAL WORK

The experimental investigation consisted of clean airfoil tests and ice shape castings (basically three shapes had been made) for aerodynamics testing. The aerodynamics characteristics investigation was made using a subsonic Low-Speed Wind Tunnel facility at the Mechanical engineering Dept.\ University of Baghdad. The wind tunnel used in the present work is a blowing type low speed, open circuit facility with solid walls and a maximum speed of 15.6 m\s. The general arrangement of this tunnel (experimental set up) is schematic in **Fig (3, a, b).** The test section is just downstream of the tunnel exit which its dimension is (450 mm high by 450 mm wide).The details of construction of the tunnel up to the test section are adopted from**, Hussain 1989.**

Aerodynamic considerations and facility size limitations determined the overall size of the wing model. Details of the symmetrical wing model and photograph for it are provided in **Fig (4, a, b).** The model is a symmetrical finite wing with a NACA 0012 two dimensional airfoil its coordinates are given in **Table (1),** airfoil section aligned in the streamwise direction. The airfoil section had manufactured from wood and had a maximum thickness to chord ratio of 0.12, the wing chord and span were 340 mm and 525 mm respectively. The model was instrumented with 16 pressure ports (suction and pressure side) distributed chordwise at one tap row spanwise locations corresponding to 50%, semispan which is aligned perpendicular to the stream direction and their coordinates are given in table (2)**,**

Bragg1994. The capillary tubes that are collected from the wing side face connected the pressure taps to the manometers.

Icing tests were conducted to document ice shapes formed on two-dimensional airfoils and to study the effects of the accreted ice on aerodynamic performance. The ice conditions were selected primarily from the Federal Aviation Administration's Federal Aviation Regulations **, Addy2000**. To verify the aerodynamic performance measurements, molds were made of selected ice shapes (three shapes were chosen) **, Addy2000.**and **FAA 2000**. Castings of the ice were made from wax and industrial clay because it is cheap and easy to form then horn ice shape and flat ice shape placed on the leading edge where the quarter round ice shape placed on the maximum thickness on the suction side of the symmetrical wing model in a dry low-speed wind tunnel, and precision aerodynamic performance measurements were taken. To illustrate how the castings look in general, **Fig (5, a, b)** shows the ice casting for the straight symmetrical airfoil.Pressure readings were obtained with a Pressure manometer System Inc. which by using the basic equation of pressure calculated to clean and iced airfoils at negative and positive angles of attack.

4. RESULTS AND DISCUSSION

The CFD analysis of airfoil NACA 0012 was performed for dimensionless chord section and Reynolds number ($3.63*10^5$) same as the experimental data at various angles of attack. To validate the adopted computational algorithm, the numerical results of this work are compared with previous work **, Rajakumar and Ravindran2012.** which analyze the flow over airfoil using the same boundary conditions. The maximum value of the percentage deviations obtained for lift and drag coefficient are (5.9%) at (17°) AOA and (7.5%) at AOA (2°). The coefficient of drag increases with the increase in angle of attack and it's not linear. Also the error percentage between the published results and present work was less than 10% of error.

Fig (6, a, b) shows pressure coefficient behavior over the upper and lower surfaces of the airfoil NACA 0012, it's obvious that there is a considerable decrease in pressure at the ice shape location on the upper surface because ice obstruct the streamline way and change the distribution of pressure over the airfoil. Also a reverse flow after ice location at the 35% of x/c on the upper surface of the airfoil NACA 0012 at angle of attack equal to (-12°).

Fig (7, a) shows the variation of drag coefficient at different AOA for clean and iced symmetrical airfoil NACA 0012. The maximum drag reported for clean airfoil was (0.139) at angle of attack equal to (12°). The most dangerous case is the horn iced (case A-II) which had the maximum percentage value of drag increased by (60%), while **Fig. (7, b)** presented C_l behavior for the clean and iced airfoil NACA 0012 at different angles of attack. It can be observed that lift coefficient of horn iced airfoil at AOA (12°) is decreased by (38%). Fig. (7, c) shows numerical lift to drag coefficients ratio for clean and iced airfoil. The minimum value is equal to (3.6) at positive angle of attack. Numerical results of percentage reduction of lift coefficient and percentage increase of drag coefficient for iced cases at different angles of attack are given in **Table3.**

The velocity distribution over clean and iced airfoil at angle of attack equal to (4°) is depicted in **Fig. 8.** No separation is indicated for case A-I (clean airfoil) and the maximum speed was (4 m/s) at the upper surface. For case (A-II) a reverse flow (bubble separation region) near ice location is indicated and the maximum speed at the upper surface was (4.3 m/s). This figure reveals two stagnation points for case A-IV one at the leading edge and the second at the quarter round iced shape.

Fig. 9. represents the distribution of computational pressure coefficient over clean and iced airfoil NACA 0012 at angle of attack (8°). In case A-I the pressure on the lower surface of the airfoil was greater than that of the incoming flow. Also a back flow is reported at iced shapes location especially for horn iced case and quarter round forward iced shape case because of the shape of the ice and its location which considerably affect on the stream line of flow.

Four experimental cases are tested on symmetrical airfoil NACA 0012 with chord equal to **340 mm**, these cases are:

- Case A-I: Symmetrical clean airfoil.
- Case A-II: Horn iced symmetrical airfoil.
- Case A-III: Flat iced symmetrical airfoil.
- Case A-IV: Quarter round forward iced airfoil.

The experimental results of lift and drag coefficient at different angles of attack for the four cases for NACA0012 airfoil are given in **Table 4.** The maximum C_l is (0.92) for clean case at AOA (12°). Horn iced airfoil produce the maximum drag at angle of attack equal to (12°).**Fig.(10,a , b)** shows a comparison between the experimental results for the four cases (clean, flat iced, horn iced and quarter iced airfoil cases) at AOA (12°). Case A-IV and case A-II reported the highest change in Cp distribution over the upper and lower surface of the airfoil compared to clean airfoil and this is due to the shape of the ice and the high AOA, where the maximum value of C_p is 0.51 at L.E., where x/c is equal to (0) for all cases.**Fig (11, a, b, c)** depicted the experimental conductance of the lift, drag coefficients and lift/drag ratio of NACA 0012 at different angles of attack for four cases. It shows that horn iced cause the maximum drag and minimum lift at positive angles of attack which is complies with previous literatures. The experimental percentage reduction and increase of lift coefficient and drag coefficient at different AOA for the studied cases above are given in **Table (5).**

Fig (12,a, b) represents the experimental power consumption due to drag force for clean and iced airfoil NACA 0012 at AOA (4°, 8°). The horn iced airfoil needs more power to avoid its effect than the other shapes of ice. It can be observed the maximum power is for horn iced airfoil, namely (44.4W) for NACA0012at AOA of (8°). It can be observed at AOA (-4°, -8°) that the maximum power were for horn iced airfoil as (126W) for NACA0012at (-8°) AOA. The power increases as the absolute value of negative AOA increase for each AOA.

A comparison between the numerical and experimental results of drag and lift coefficients are presented in **Fig. (13, a, b)** for clean airfoil (case A-I) at different angles of attack. It can be observed that experimental results had the same behavior of the numerical work with maximum deviation equal to (30%) and (10%) at AOA (12°) for drag coefficient and lift coefficient respectively.

Fig (14, a, b) depicted a comparison between computational and experimental results of drag and lift coefficients for horn iced airfoil case NACA 0012 (case A-II) at different angles of attack. The drag coefficient C_d was almost identical at the negative angles but it mismatched at the positive angles it was less than the numerical results with maximum deviation equal to (35%) at angle of attack equal to (12°), while the lift coefficient C_l had almost the same behavior of the numerical results with maximum deviation equal to (29%) at AOA (-12°).

5. CONCLUSIONS

Experimental and computational investigations of the aerodynamic characteristics of an iced airfoil NACA 0012 at zero and non-zero angles of attack has been carried in this work. According to the previous discussion the following conclusions can be deduced:

- Experimental tests show that the presence of ice on airfoil increases drag by 60% and reduces lift by 45%. Horn iced airfoil consumes more power than the other shapes of ice.
- The numerical results show that the lift coefficient is decreased by 38% and the drag coefficient is increased by 60% for horn iced NACA 0012 airfoil.
- A steep pressure decrease is reported for iced airfoil with quarter round forward iced case at the location of ice (which was at the maximum thickness of the upper surface of the airfoil.
- Drag coefficient increases much higher for horn iced case compared to other cases of iced clean airfoil.
- For negative angle of attack (0°, -4°) the pressure coefficient (Cp) at iced airfoil airfoil lower surface was less than that of the upper surface.
- Prominent pressure spikes can be seen at the location of ice droplet on the airfoil surface.

REFERENCES

Addy H. E., 2000 *Ice Accretions and Icing Effects for Modern Airfoils*, NASA/TP-2000-210031, DOT/FAA/AR-99/89, April.

Bortholin T., Catalano F. M., 2012 *Computational investigation of icing contamination on airfoil*, 28th International Congress of the Aeronautical Sciences (ICAS).

Bragg M., 1986 *An experimental study of the aerodynamics of a NASA 0012 airfoil with simulated glaze ice accretion*, The Ohio State University Research foundation Columbus, Ohio prepared for NASA Lewis Research Centre under Grant No. NAG 3-28 CR 179897, November.

Bragg M., 1994 , *An experimental study of the aerodynamics of a swept and unswept semispan wing with a simulated glaze ice accretion*, prepared for Lewis Research Centre under Grant NAG 3-1134 NACA CR195330, University of Illinois-Urbana, May.

Bragg M., Broeren A.P., Addy H. E., Potapczuk M. G., 2008 ,*Airfoil Ice-Accretion Aerodynamics Simulation*, NASA/TM—2008-214830, AIAA–2007–0085.

Broeren A. P., Bragg M., Addy, 2006, *Flow field Measurements About an Airfoil with Leading-Edge Ice Shapes*, journal of aircraft Vol. 43, No. 4, July–August.

Federal Aviation Administration (FAA)., 2000, office of Aviation Research Washington, D.C. 20591, U.S. Department of Transportation, *Effects of Large-Droplet Ice Accretion on Airfoil and Wing Aerodynamics and Control*, National Technical Information Service (NTIS), Springfield, Virginia 22161, DOT/FAA/AR-00/14, March.

Fluent Inc., 2009 Fluent User's Guide, Version 6.3.26. *Available free online on www.sharcnet.ca.*

Gord M. F., 2009 Alizadeh H. H., *Combined Experimental and Numerical Analysis of Incompressible Flow around an Airfoil*, Shahrood University of Technology, Shahrood, Iran, computational dynamics, part 41, part , pp. 793-798.

Hasoun, H. Q., 2007 ,*Effect of ice formation on airfoils performance*, PH.D. thesis, university of Baghdad, College of Engineering, Dept. of Mech. Engr.

Hussain, I.Y., 1989 *Computational and experimental investigation of three dimensional turbulent boundary layer*, M.Sc. thesis, university of Baghdad, college of Engineering, Dept. of Mech. Engr,.

Ideriah, F. J. K., 1975, *Review of equation solved in TEACH*, private communication.

Launder, B.E. and Spalding, D.B., 1972, *Mathematical models of turbulence*, Academic press, London.

Mateescu D., 2004 *Efficient solution of the Euler and Navier-stokes equations for external flow*, the 6th International Conference on Hydraulic Machinery and Hydrodynamics (H M H), Timisoara, Romania, October 21 - 22.

Mateescu D., 2005Abdo M., *Efficient second-order analytical solutions for airfoils in subsonic flows*, Aerospace Science and Technology 9 pp. 101–115. Also vailable online on www.sciencedirect.com.

Mirzaei M., Ardekani M. A., Doosttalab M., 2008 , *Numerical and experimental study of aerodynamic characteristics of an iced airfoil*, 5th WSEAS Int. Conf. on fluid mechanics (fluids'08) Acapulco, Mexico, January 25-27.

National technical information service (NTIS)., 2000 *Effects of Large-Droplet Ice Accretion on Airfoil and Wing Aerodynamics and Control*, spring field, Virginia 22161, March.

Rajakumar S., Ravindran D., 2012 ,*Iterative approach for optimising coefficient of power, coefficient of lift and drag of wind turbine rotor*, Anna university of technology, India, available online at Science Direct, Renewable energy 38, pp. 83-93.

Verestage, H. K., and Malalasekera, W., 1995 *An Introduction to Computational Fluid Dynamic-The Finite volume Method*, Longman Group Ltd.

Nomenclature

Latin symbols		**Greek symbols**	
AR	Aspect Ratio	α	Angle of attack Deg.
b	Span length of wingm	∞	Mainstream conditions
C_1, C_2, $C\mu$	constants for (k-ε) model	λ	Taper ratio
C_d	Drag Coefficient	ε	Rate of dissipation of kinetic energy m^2/s^3
C_l	Lift coefficient	μ	Dynamic viscosity $N.s/m^2$
Cp	Pressure coefficient [(P-Pa)/0.5ρV_∞^2]	μ_l	Laminar viscosity $N.s/m^2$
G	Production of the kinetic energy from mean velocity gradients	μ_t	Turbulent viscosity $N.s/m^2$
k	Kinetic energy of turbulence m^2/s^2	μ_{eff}	Effective kinematics viscosity $N.s/m^2$
		ρ	Density Kg/m3
p	PressurePa	σ_k, σ_ε	constants for (k-ε) model
q_∞	Reference pressure [0.5ρV_∞^2] N/m^2	**Abbreviations**	
Re	Reynolds number	AOA	Angle Of Attack
S	Surface wing area m^2	CFD	Computational Fluid Dynamics
SG	Source term of production of the kinetic energy from mean velocity gradients	CV	Control Volume
Su	Source term of u in x-direction,	2D	Two-Dimensional
		FAA	Federal Aviation Administration
Sv	Source term of υ in y-direction	FVM	Finite Volume Method
u ,v	Velocity component in x, y respectively m/s	IRT	Icing Research Tunnel
		L.E	Leading Edge
V∞	Free stream velocity m/s	NTIS	National Technical Information Service
x, y	Cartesian coordinates	SIMPLE	Semi-Implicit Method for Pressure Linked Equation
		T.E	Trailing Edge

Table 1. Symmetrical straight airfoil coordinates.

No.	x/c	y/c	No.	x/c	y/c	No.	x/c	y/c
1	1	0.00126	25	0.224552	0.058578	49	0.303487	-0.06001
2	0.997987	0.001542	26	0.188255	0.056645	50	0.345492	-0.05958
3	0.991965	0.002382	27	0.154469	0.053896	51	0.38874	-0.05843
4	0.981981	0.00376	28	0.123464	0.050351	52	0.432883	-0.05665
5	0.968117	0.005647	29	0.095492	0.046049	53	0.477568	-0.0543
6	0.950484	0.008002	30	0.070776	0.041043	54	0.522432	-0.05147
7	0.929224	0.010776	31	0.049516	0.0354	55	0.567117	-0.04824
8	0.904508	0.013914	32	0.031883	0.029189	57	0.61126	-0.0447
9	0.876536	0.017359	33	0.018019	0.022483	58	0.654508	-0.04092
10	0.845531	0.021049	34	0.008035	0.015347	59	0.696513	-0.03698
11	0.811745	0.024921	35	0.002013	0.007839	60	0.736934	-0.03295
12	0.775448	0.02891	36	0	0	61	0.775448	-0.02891
13	0.736934	0.032952	37	0.002013	-0.00784	62	0.811745	-0.02492
14	0.696513	0.036978	38	0.008035	-0.01535	63	0.845531	-0.02105
15	0.654508	0.040917	39	0.018019	-0.02248	64	0.876536	-0.01736
16	0.61126	0.044698	40	0.031883	-0.02919	65	0.904508	-0.01391
17	0.567117	0.048243	41	0.049516	-0.0354	67	0.929224	-0.01078
18	0.522432	0.051471	42	0.070776	-0.04104	68	0.950484	-0.008
19	0.477568	0.0543	43	0.095492	-0.04605	69	0.968117	-0.00565
20	0.432883	0.056646	44	0.123464	-0.05035	70	0.981981	-0.00376
21	0.38874	0.05843	45	0.154469	-0.0539	71	0.991965	-0.00238
22	0.345492	0.059575	46	0.188255	-0.05665	72	0.997987	-0.00154
23	0.303487	0.060014	47	0.224552	-0.05858	73	1	-0.00126
24	0.263066	0.059695	48	0.263066	-0.0597			

Table 2. Pressure taps coordinates.

No.	X mm	Y mm
1	0	0
2	10.37	9.7268
3	19	12.6537
4	36.7	16.3458
5	71.7	19.6895
6	105.19	20.375
7	140	19.5463
8	173.16	17.766
9	206.6	15.2648

Table 3. Numerical precentage reduction and incease of lift and drag coefficients for NACA 0012.

	Case A	AOA					
		4	8	12	-4	-8	-12
% reduction of lift coefficient	II	5	20	20.565	1.47	6.35	6.56
	III	3	3.5	6.6	4.52	7.338	12.85
	IV	6.6	12	13.5	2.68	4.961	3.7
% increase of drag coefficient	II	34.7	38.67	68	40.8	63	75.48
	III	9	15.4	26.1	17.78	22.98	28.9
	IV	6	7.37	38.2	11.66	28.11	39.6

Table 4. Experimental lift and drag coefficients for NACA 0012 airfoil.

	Case A	AOA						
		0	4	8	12	-4	-8	-12
Lift coefficient	I	0.017	0.29	0.614	0.92	-0.459	-0.74	-0.9
	II	0.001	0.259	0.537	0.769	-0.194	-0.597	-0.85
	III	0.011	0.27	0.61	0.89	-0.39	-0.71	-0.87
	IV	0.011	0.26	0.59	0.875	-0.35	-0.72	-0.885
Drag coefficient	I	0	0.019	0.045	0.085	0.051	0.083	0.125
	II	0	0.03	0.056	0.087	0.075	0.159	0.263
	III	0	0.022	0.049	0.074	0.069	0.135	0.185
	IV	0	0.02	0.046	0.085	0.04	0.135	0.235

Table 5. Experimental precentage reduction and incease of lift and drag coefficients.

	Case A	AOA					
		4	8	12	-4	-8	-12
% Reduction of lift coefficient	II	11.6	12.5	16.2	57.79	19.31	5.55
	III	2.54	2.39	3.1	15.18	4.05	3.3
	IV	3.57	4	4.7	23.87	2.7	1.66
% Increase of drag coefficient	II	16.35	15.6	23.27	45.13	48.1	52.18
	III	3.97	4.7	4.84	33.87	58.5	47.17
	IV	5.75	2.75	20.4	22.39	58.5	86.95

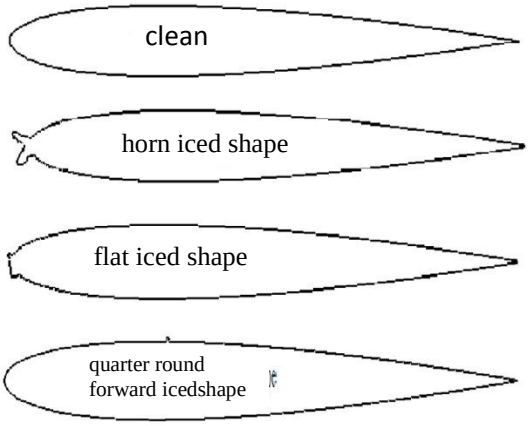

Figure 1. Airfoil profile with and without ice.

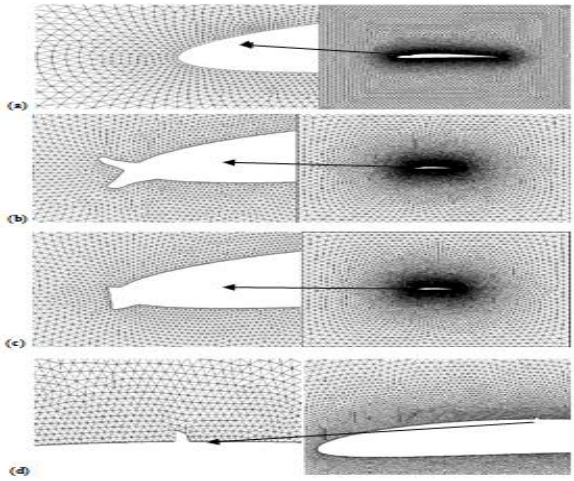

Figure 2. Mesh for airflows over airfoil NACA 4410. a) clean airfoil, b) horn iced airfoil, c) flat iced airfoil, d) quarter round forward iced airfoil.

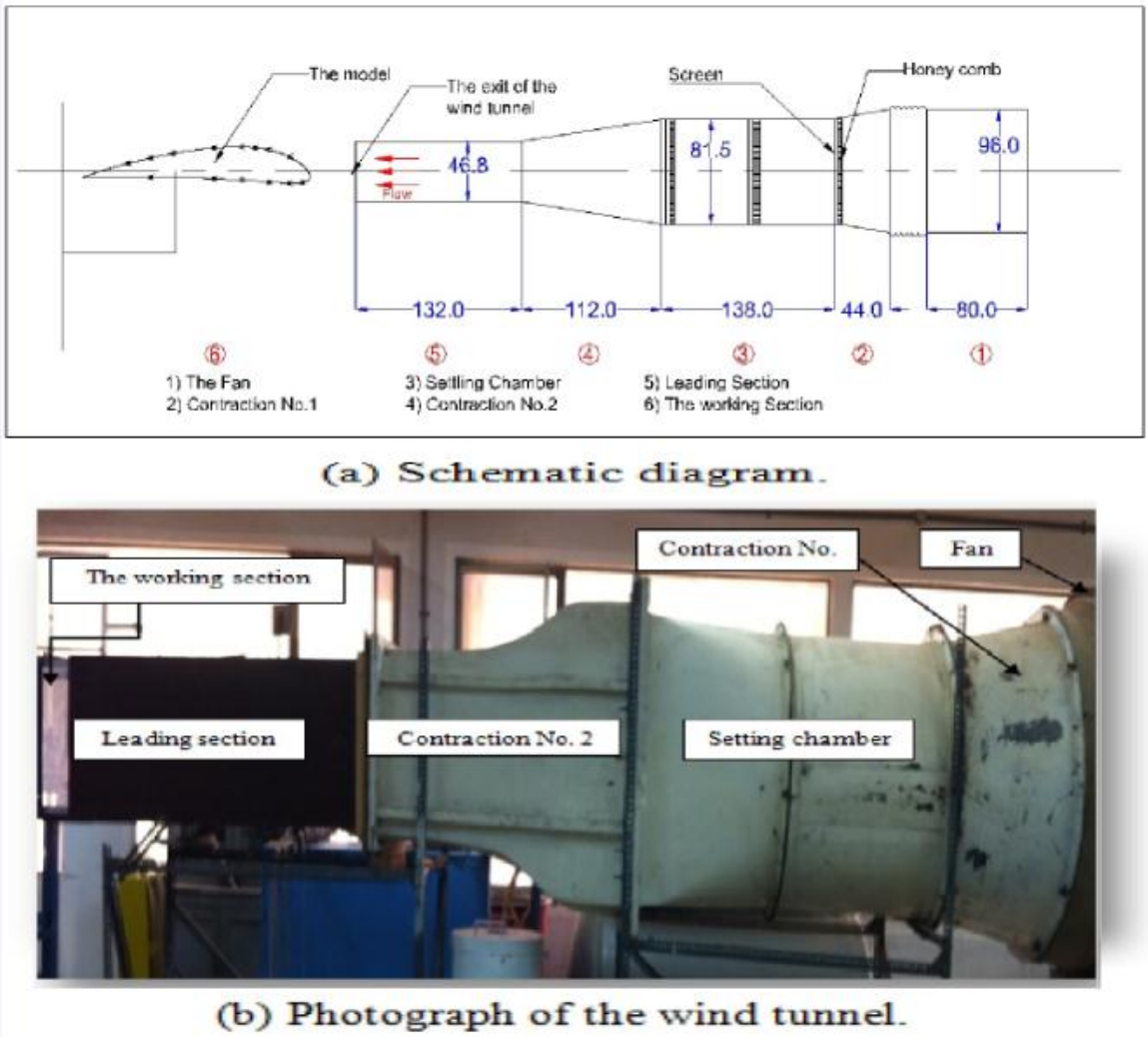

Figure 3. Subsonic wind tunnel at Mechanical Engr. Dept.

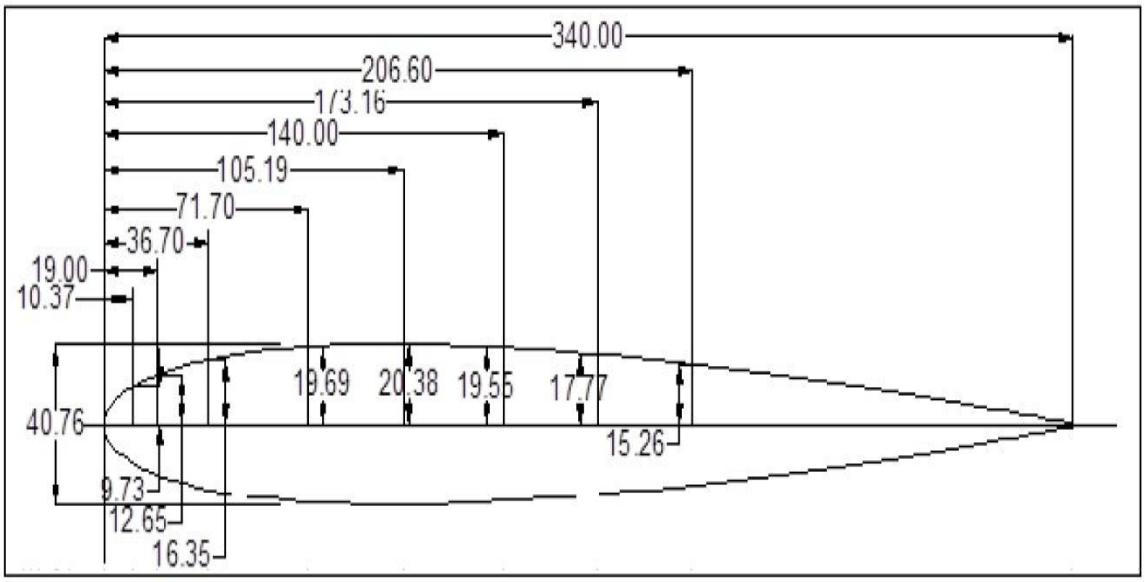

(a)

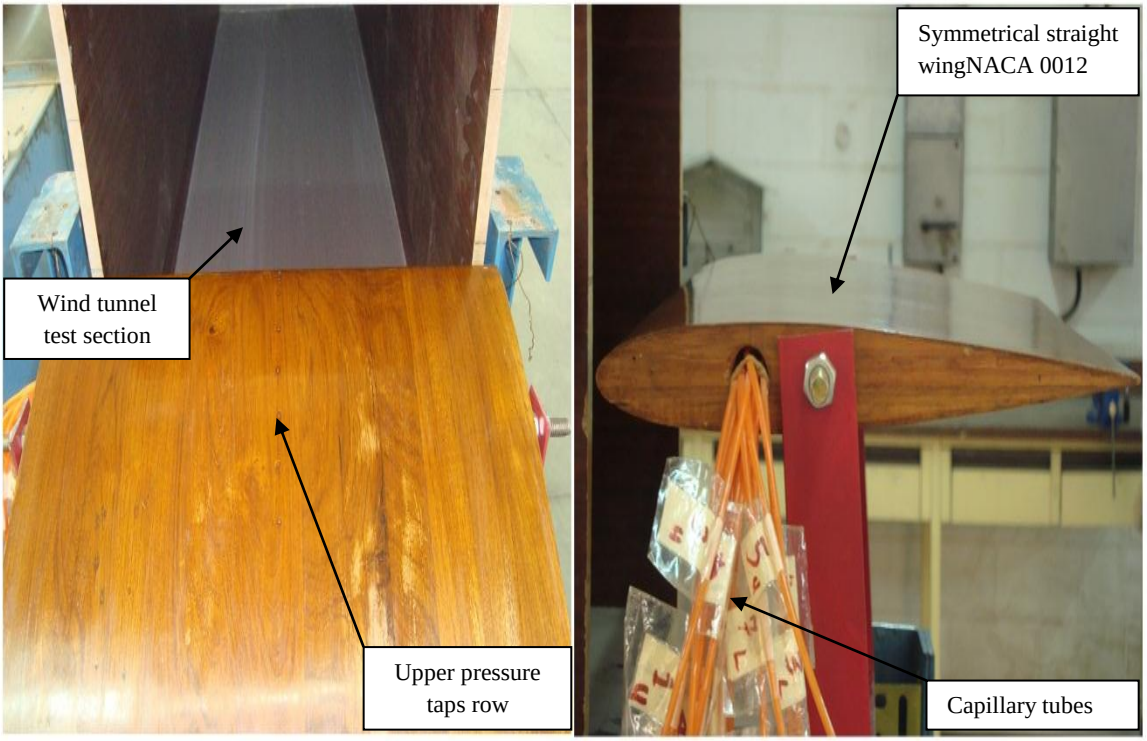

(b)

Figure 4. The symmetrical wing model, (a) Designed section and pressure taps arrangement(all dimensions in mm), (b) Photographs of the straight wing side and top view.

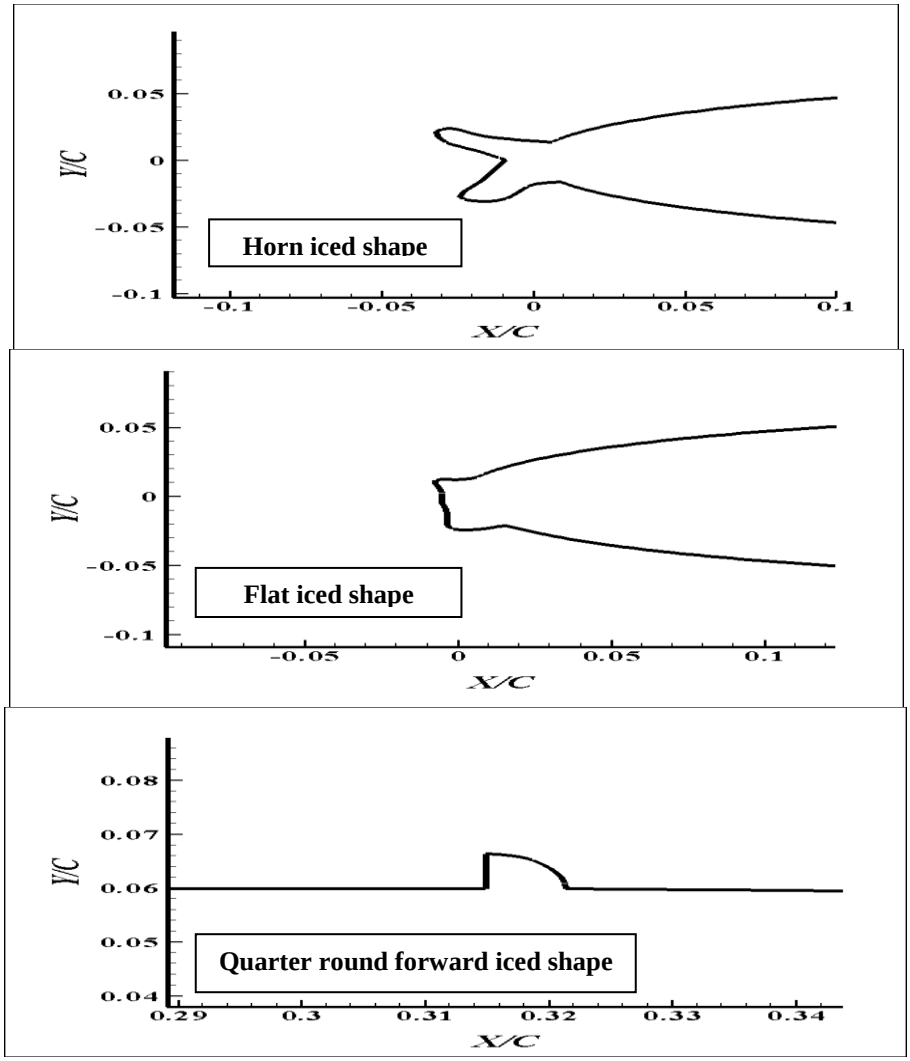

(a)

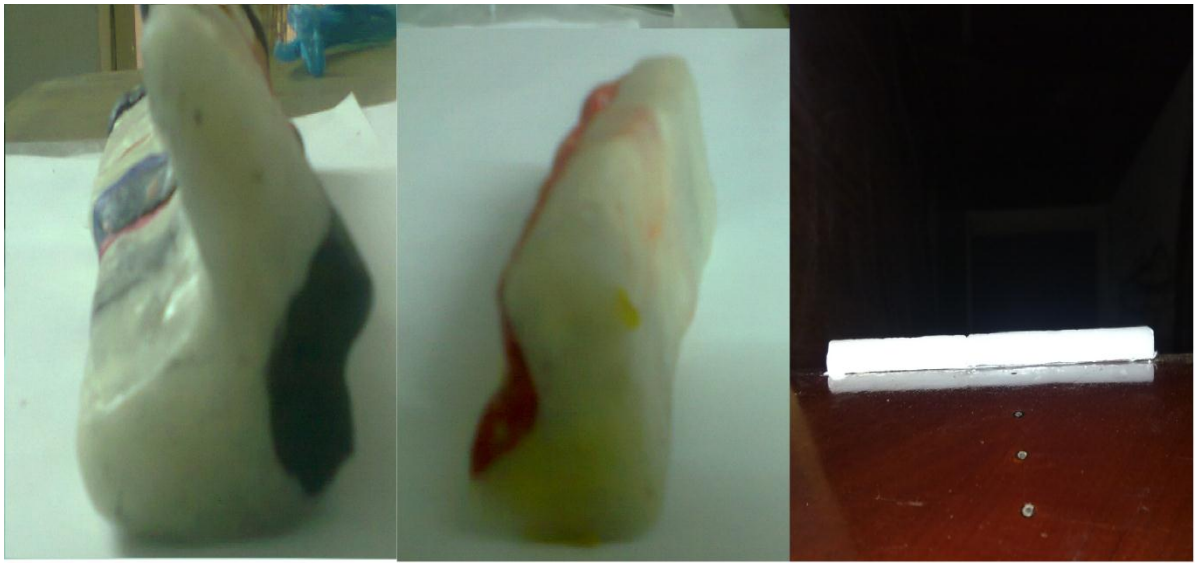

(b) **Figure 5.** The ice casting for the straight symmetrical airfoil, (a) Typical iced shapes, (b) photographs for three iced shapes.

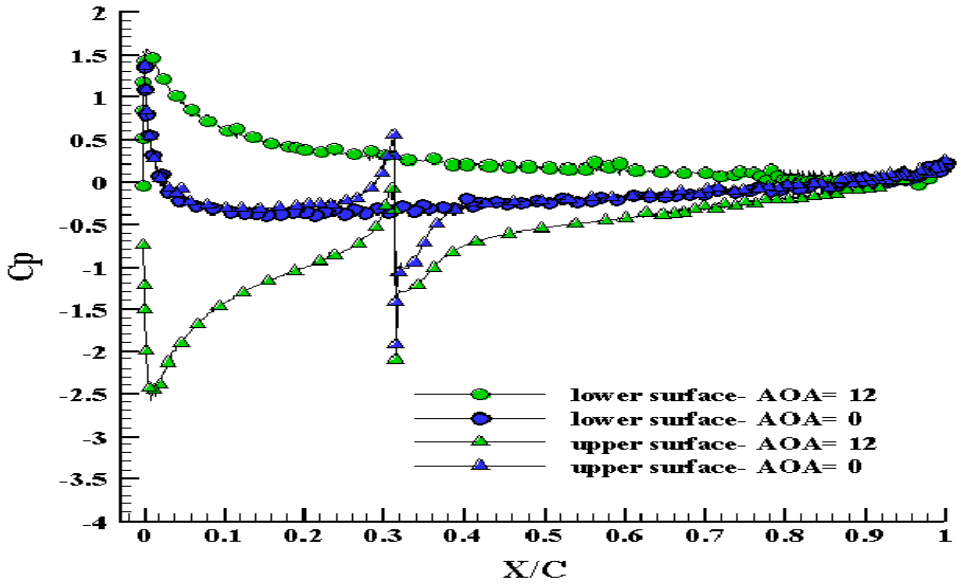

(a)

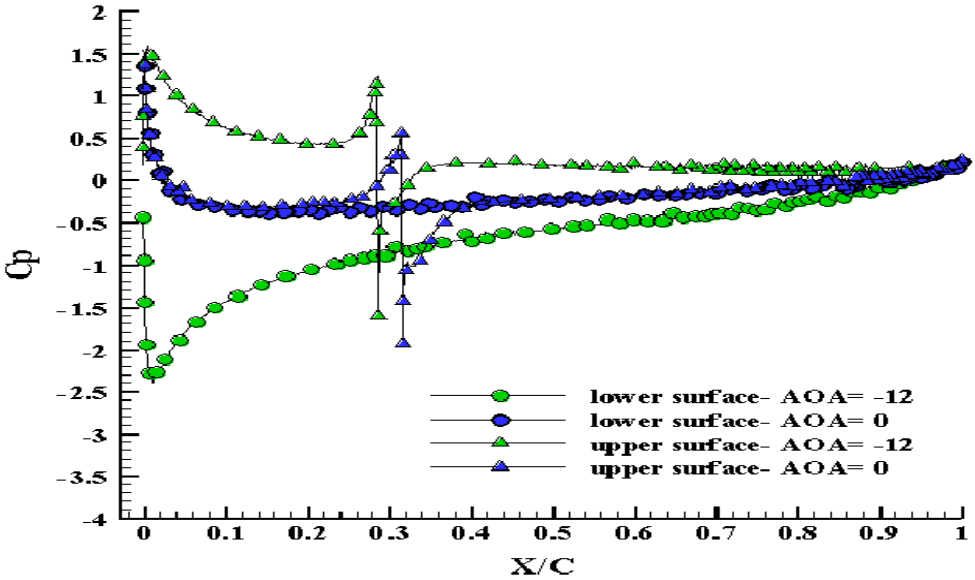

(b)

Figure 6. Pressure coefficient distribution of quarter round forward iced airfoil NACA 0012 at, (a) AOA (0°, 12°), (b) AOA (0°, -12°).

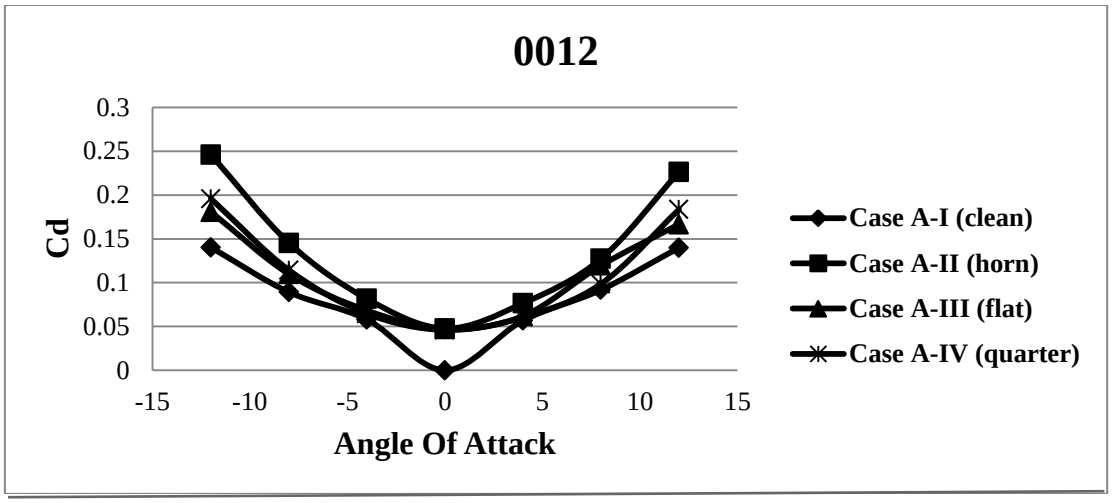

(a)

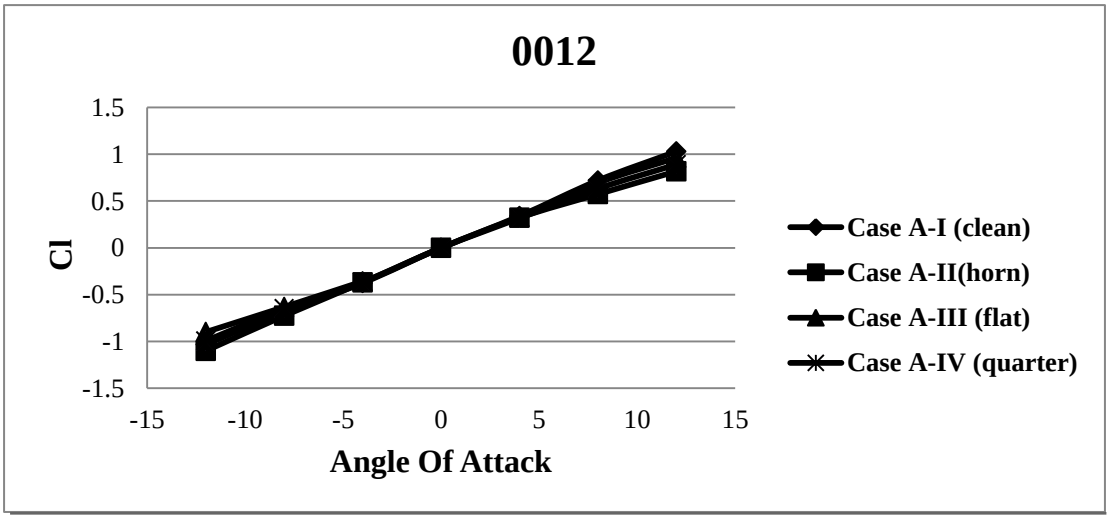

(b)

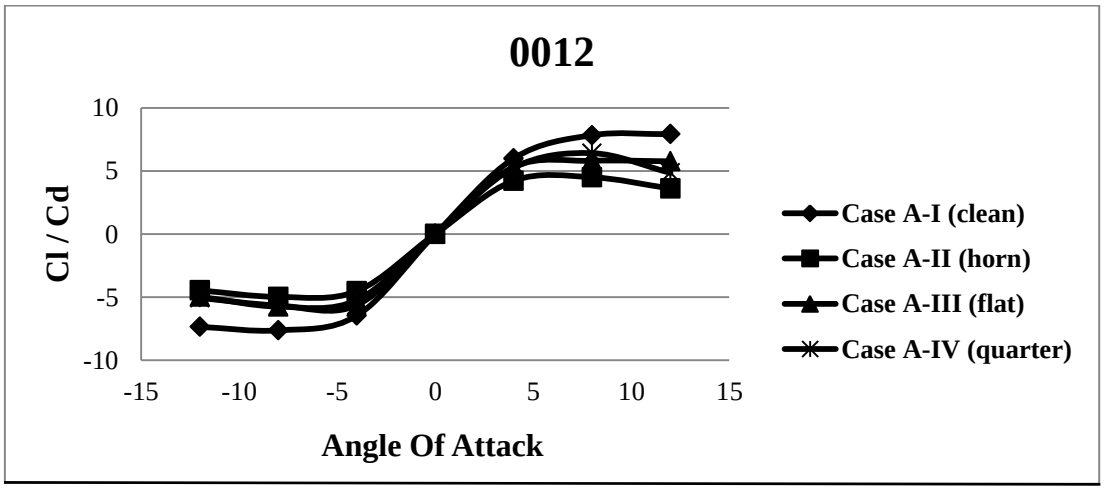

(c)

Figure 7. Numerical results for NACA 0012 at different AOA, (a) Cl, (b) Cd, (c) Cl/Cd.

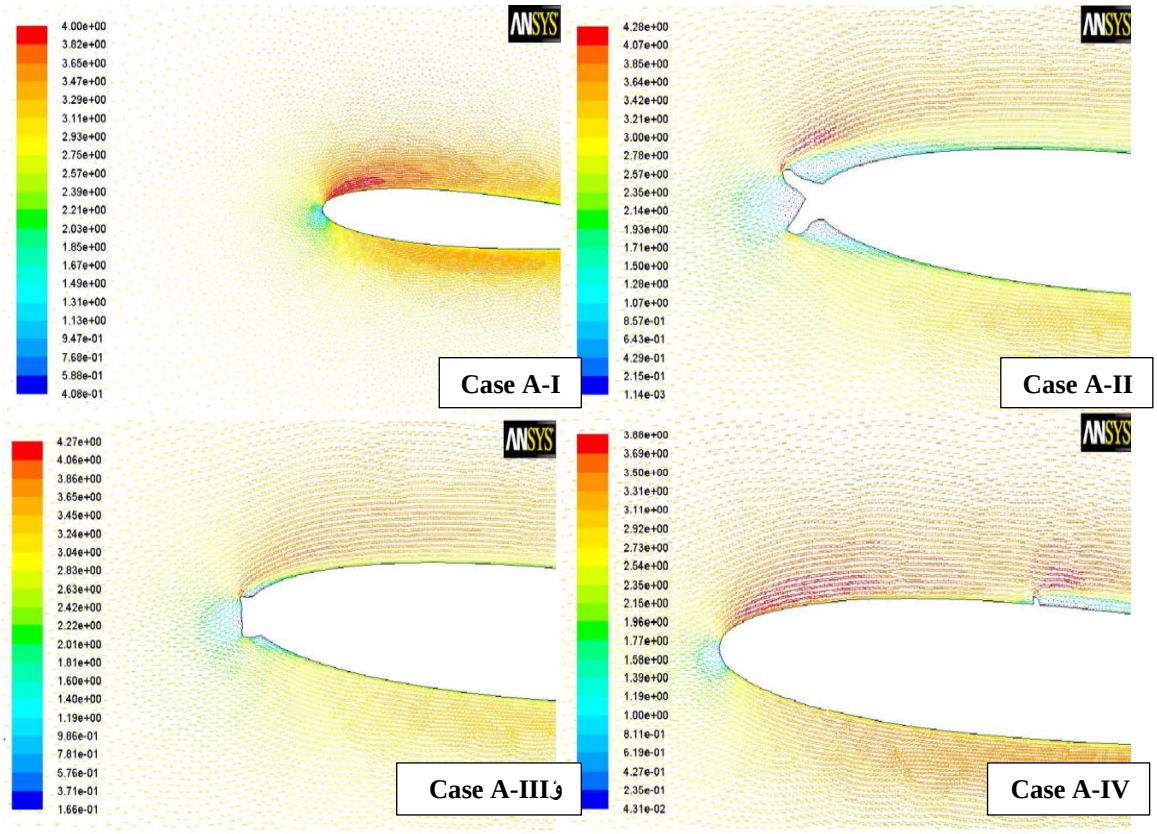

Figure 8. Velocity distribution for clean and iced airfoil at angle of attack (4°).

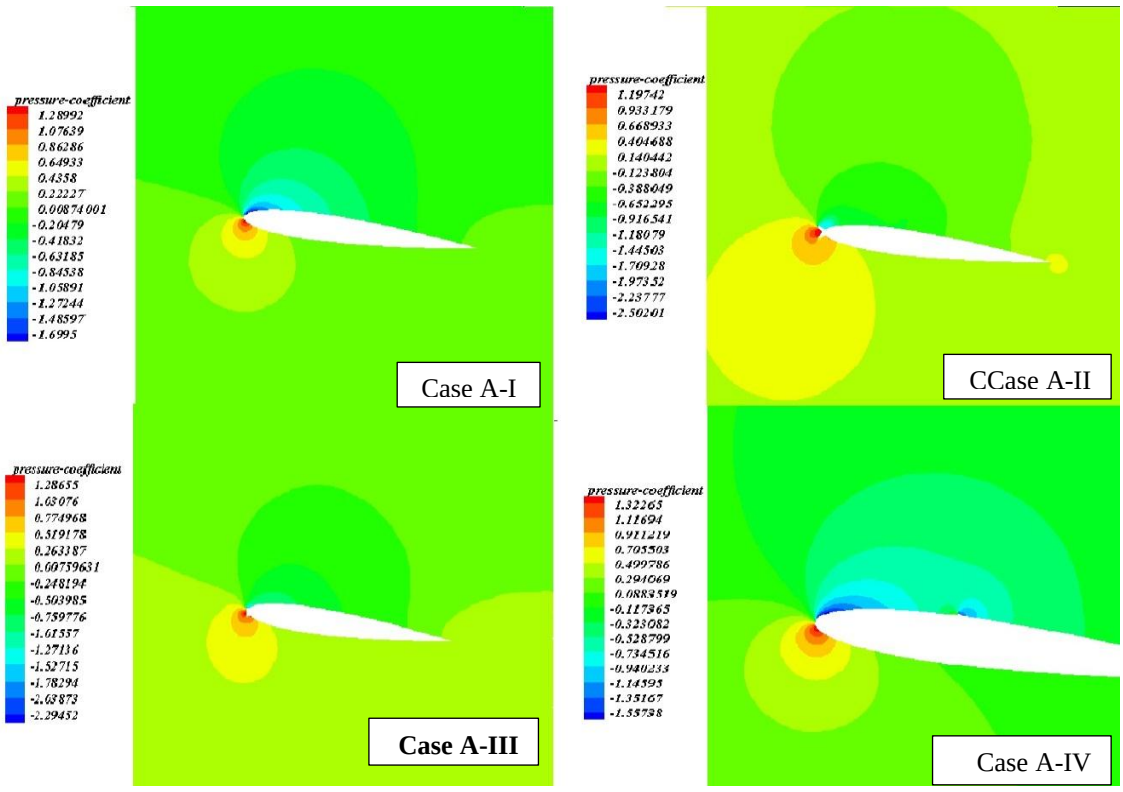

Figure 9. Pressure coefficient distribution over clean and iced airfoil NACA 0012 at angle of attack (8°).

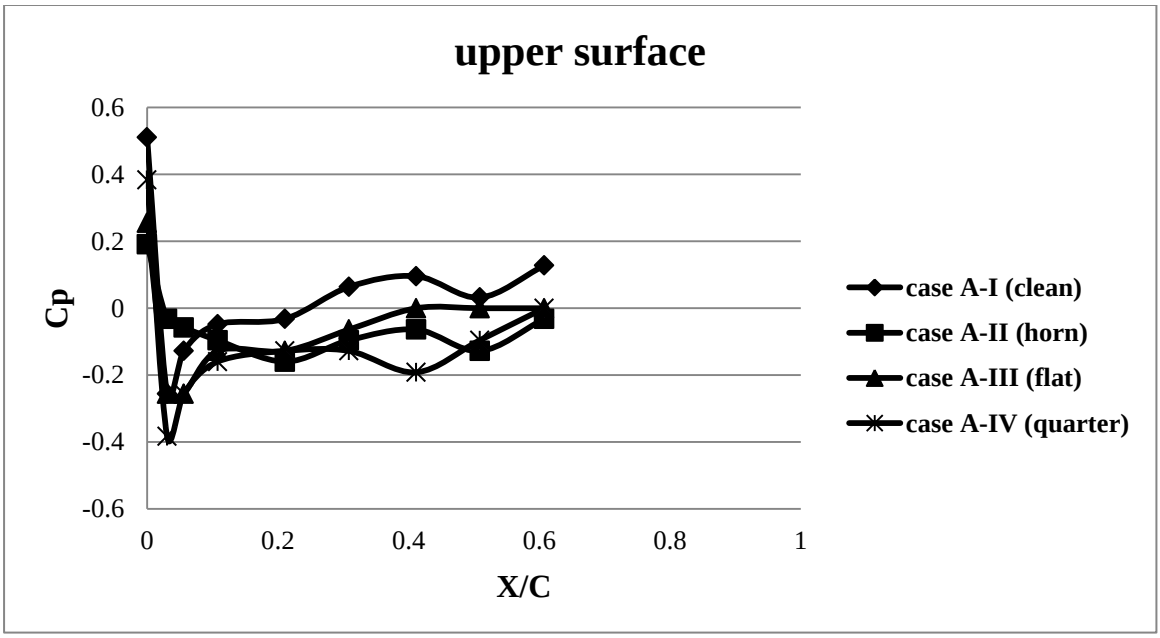

(a)

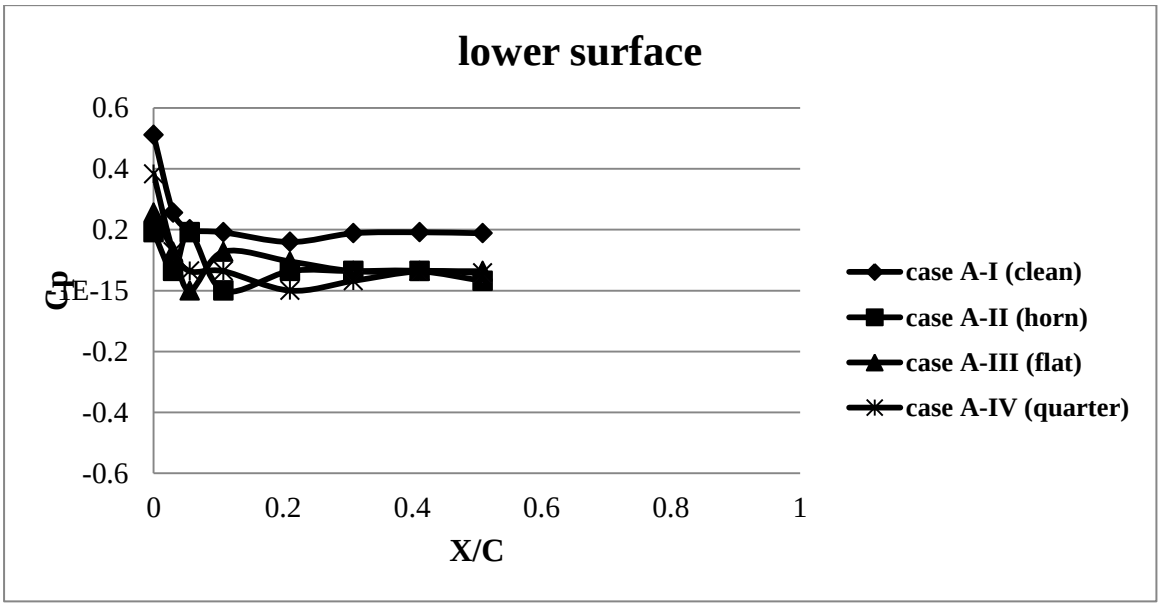

(b)

Figure 10. Pressure distribution of symmetrical airfoil NACA 0012 with chord equal to (340 mm) at AOA (12°) for different experimental cases, (a) upper surface, (b) lower surface.

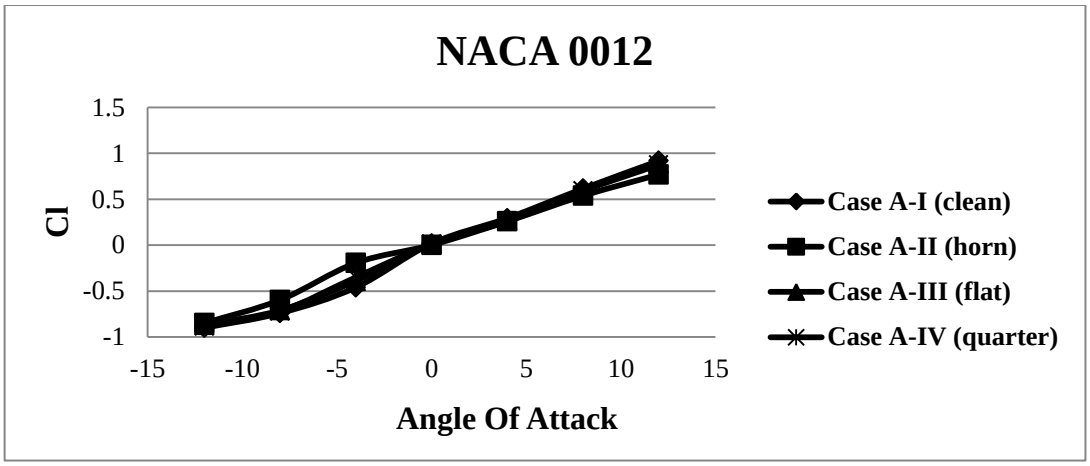

(a)

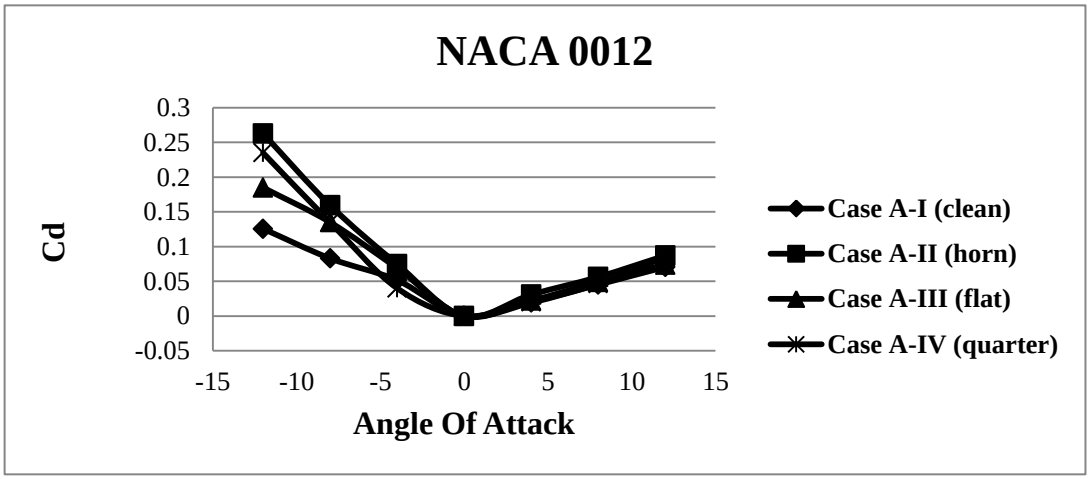

(b)

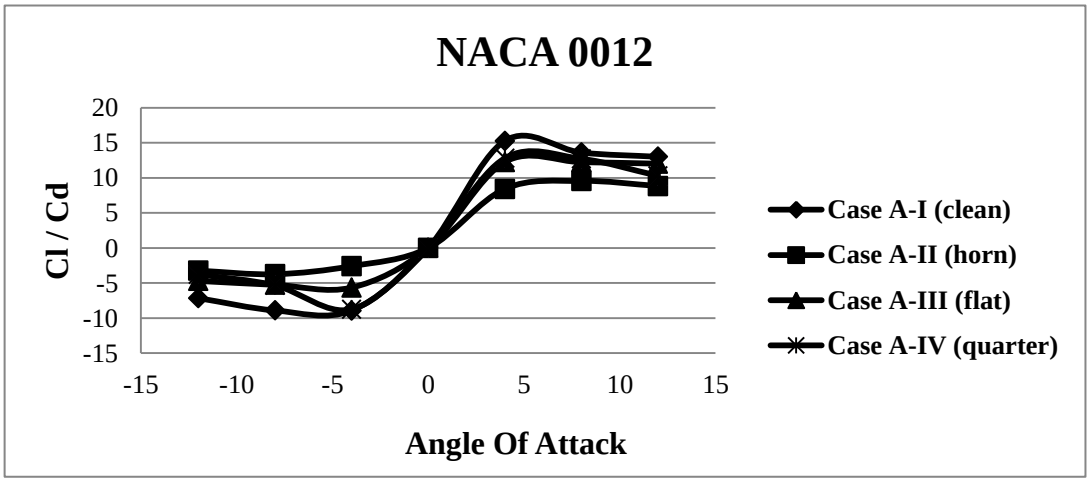

(c)

Figure 11. Experimental results for NACA 0012 at different AOA, (a) Cl, (b) Cd, (c) Cl/Cd.

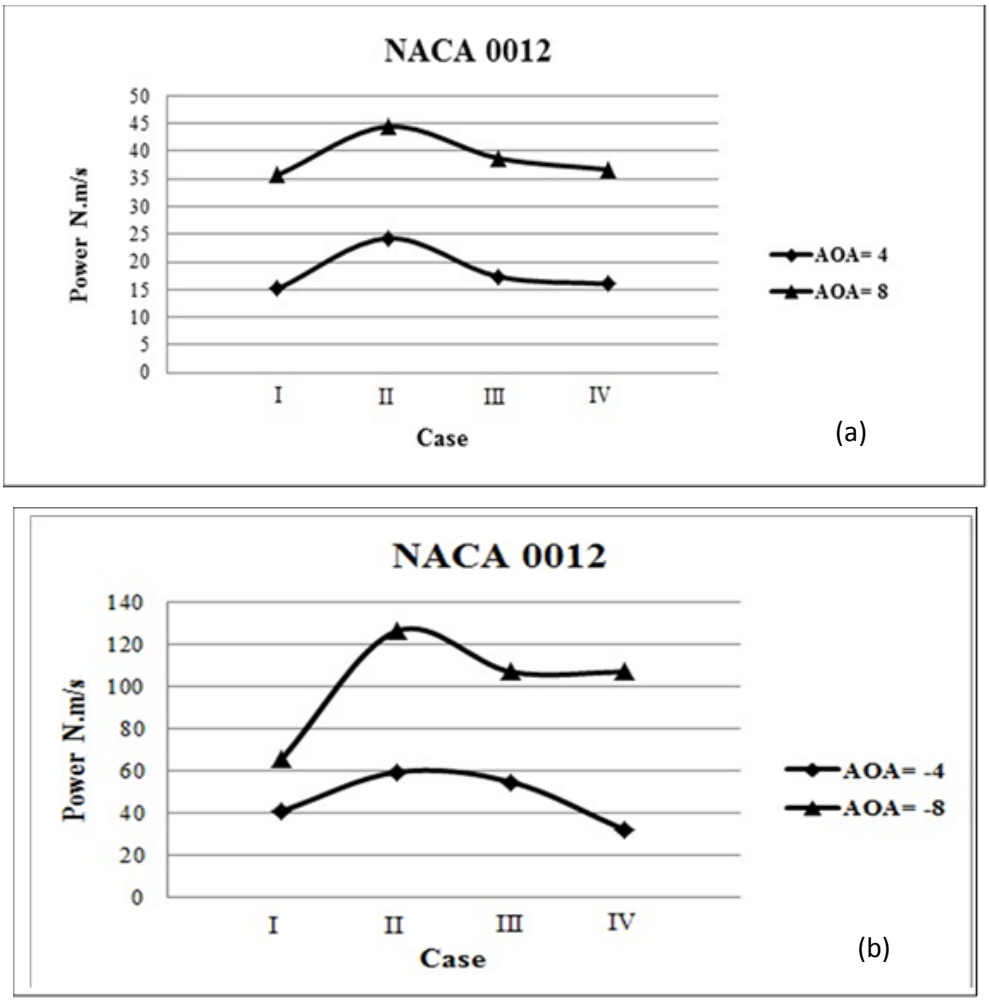

Figure 12. Power consumption due to drag force for clean and iced airfoil NACA 0012
At (a) AOA (4°, 8°), (b) AOA (-4°, 8°).

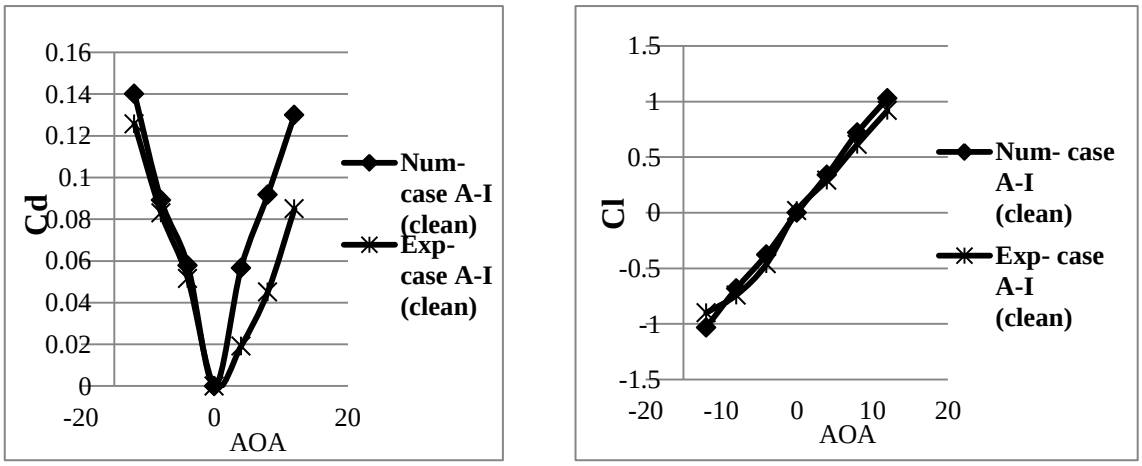

(a) (b)

Figure 13. Comparison between the numerical and experimental results for clean case NACA0012 at different angles of attack, (a) Drag coefficient, (b) Lift coefficient.

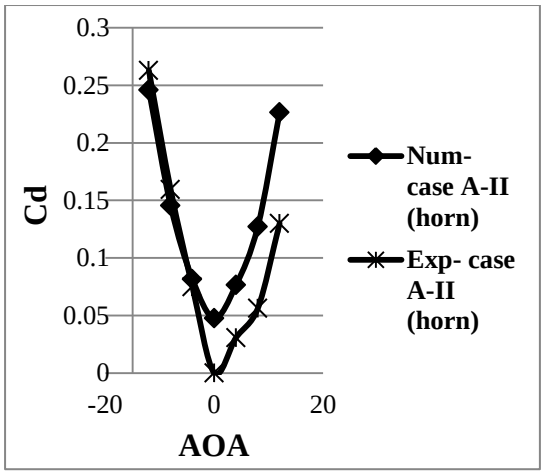

(a)

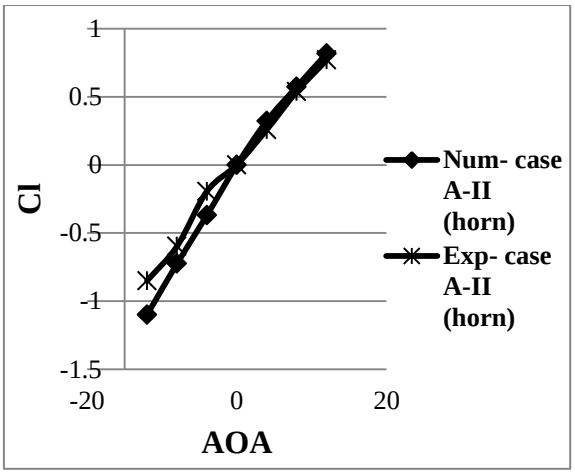

(b)

Figure 14. A comparison between the numerical and experimental results for horn iced airfoil case NACA0012 at different angles of attack, (a) Drag coefficient, (b) Lift coefficient.

Deep Desulfurization of Diesel Fuel by Guard Bed Adsorption of Activated Carbon and Locally Prepared Cu-Y Zeolite

Nada Mustafa Hadi
Lecturer
AL-Khwarizmi
College of Engineering
Baghdad University
Email:n_m2411@yahoo.com

Asst. Lect. Sarmad Abdul-Razzaq Rashid
Assistant Lecturer
College of Engineering
Baghdad University
Email:Sermedrashid@gmail.com

Asst. Lect. Suheila abdalreda
Assistant Lecturer
College of Engineering
Baghdad University
Email: Suheila_akkar@yahoo.com

ABSTRACT

Desulfurization of a simulated diesel fuel by different adsorbents was studied in a fixed-bed adsorption process operated at ambient temperature and pressure. Three different adsorption beds were used, commercial activated carbon, Cu-Y zeolite, and layered bed of 15wt% activated carbon followed by Cu-Y zeolite.Initially Y-zeolite was prepared from Iraqi rice husk and then impregnated with copper.

In general, the adsorbents tested for total sulfur adsorption capacity at break through followed the order Ac/Cu-Y zeolite>Cu-Y zeolite>Ac. The best adsorbent, Ac/Cu-Y zeolite is capable of producing more than 30 cm^3 of simulated diesel fuel per gram of adsorbent with a weighted average content of 5 ppm-S, while Cu-Y zeolite producing of about 20 cm^3 of diesel fuel per gram of adsorbent with a weighted average content of 2ppm-S. Activated carbon breaks through almost immediately.

Key words: Desulfurization of diesel fuel, desulfurization by adsorption, guard bed adsorption, Y- zeolite from rice husk

ازالة كبيرة للمركبات الكبريتيه من وقود الديزل باستخدام عمود امتزاز مكون من كاربون منشط و Cu-Y zeolite محضر محليا

ندى مصطفى هادي
مدرس
كلية هندسة الخوارزمي /جامعة بغداد

سرمد عبد الرزاق رشيد
مدرس مساعد
كلية الهندسة/جامعة بغداد

سهيلة عبد الرضا
مدرس مساعد
كلية الهندسة/جامعة بغداد

الخلاصة

تمت دراسة ازاله المركبات الكبريتية من وقود الديزل باستخدام العمود الثابت لعمليه الامتزاز تحت ظروف اعتياديه من درجه حراره وضغط. تمت العمليه باستخدام ثلاثه انواع من الاعمدة المحشوة بالمواد الممتزة وهي الكاربون المنشط (Ac) والنحاس المحمل على الزيولات Cu-Y zeolite وعمود مزدوج من 15% وزنا كاربون منشط والنحاس المحمل على الزيولايت تم تحضير الزيولايت Y من قشور الرز العراقي. اظهرت الدراسه ان سعة الامتزاز للمواد الممتزة كانت على الترتيب Ac/Cu-Y zeolite>Cu-Y zeolite>Ac حيث استطاع العمود الافضل Ac/Cu-Y zeolite , من انتاج اكثر من 30 سم مكعب من وقود الديزل الخالي من المركبات الكبريتيه لكل غرام من المادة الممتزة وبمعدل وزني للمركبات الكبريتية بحدود 5 ملغم/لتر. بينما كان انتاج المادة الممتزة Cu-Y zeolite من وقود الديزل الخالي من المركبات الكبريتية

بحدود 20 سم مكعب لكل غرام من المادة الممتزة وبمعدل وزني للمركبات الكبريتية بحدود 2 ملغم/لتر.بينما لم يتمكن العمود المحشو بالكاربون المنشط من انتاج وقود الديزل خالي من المركبات الكبريتية

INTRODUCTION

Ultra deep removal of sulfur from transportation fuels has become more and more important in research and development worldwide, not only because of the heightened interest for cleaner air and environmental protection but also due to the great need for making ultralow-sulfur fuels for use in fuel cells. Fuel cells are attractive for electric power generation because significantly higher efficiencies can be achieved in a more environmentally friendly way than in combustion engines for the automotive fuel cells and the portable fuel cells, liquid hydrocarbon fuels are candidate fuels due to their higher energy density and safety for transportation and storage **,Song, 2003, Babich, 2003**. This is why governments all over the world are implementing more stringent regulations and fuel specifications. The EU legislation set the upper limit of sulfur content in diesel fuel as well as gasoline fuels for 2009 to 10 mg/kg. The US Environmental Protection Agency (EPA) since 2006 reduced the limit for sulfur content of diesel to 15 mg/kg and gasoline fuel to 30 mg/kg **Jiang, et.al, 2006,**and **Ma. X., et.al, Sun2002**.

Industrially, the elimination of sulfur is carried out through the process called hydro desulfurization (HDS). This process uses Ni-MolAl_2O_3 and Co-Mo/Al_2O_3 catalysts. The disadvantages of this process are (i) the catalytic processes operated at elevated temperatures (320-380)^{o}C and elevated pressures 3-7 Mpa and (ii) HDS process is highly efficient for the removal of sulfur compounds such as thiols, sulfides and thiophenes, but less effective for removing refractory sulfur compounds: benzothiophene (BT), Dibenzothiophene (DBT), and their alkyl derivatives . These molecules are common in diesel fuels. The methyl groups in these species create a steric effect that hinders the capacity of HDS catalyst to chemisorb the sulfur atoms,**Baeza, et.al 2008**.

Adsorption is a viable option for motor fuel desulfurization and the idea behind this approach is to selectively separate less than 1wt% of fuel mass using selective adsorption for removing sulfur and leave the 99wt% of non-sulfur containing fuel mass untouched, besides to adsorption can be accomplished at low temperature and pressure (ambient conditions) **Ma, X., et.al, 2002,**and **Jiang, et.al, 2005.** Recently, many attempts have been made to develop adsorbents for desulfurization of liquid hydrocarbon fuels **C.S.Song, 2003,M.Breysse,et.al,2003, C.Song, et.al, 2003, and P.T.Vasudevan, et.al, 1996**.The reported adsorbents include the reduced metals**G.W.Bailey, et.al, 1987, L.J.Bonvillr, et.al,2000, R.R.Lesieur, et.al, 2002, X.Ma, et.al, 2002, T.Fukunaga, et.al, 2003, X.Ma, et.al,2005, and X.Ma,M. et.al, 2005**, metal oxides **B.S.Turk, et.al.2001,S.Watanabe,et.al. 2004]**, metal sulfides **[X.Ma.et.al., 2003]**, zeolite-based materials **[R.T.Yang , et.al., 2003, A.J.Hernandez-M, et.al., 2003, S.Velu, et.al., 2003, and A.J.Hernandez, 2004** and carbon materials, **S.Haji, et.al., 2003,Y.Sano, et.al.,2004 and ,A,Zhou, et.al. 2004]**.

Activated carbons and zeolites have been widely used as adsorbents in the separation and purification processes for gaseous or aqueous solution systems. Activated carbons have high adsorption capacity towards some organic and inorganic compounds due to large specific surface area, high adsorbate-adsorbent physical and chemical attraction and balanced macro-,

meso- and micro-porosity while at the same time the steric hindrance of particle diffusion is minimized with regard to the size of the molecules being adsorbed. Zeolite can be successfully used for the selective adsorption of polar or polarization molecules such as water and CO_2 and sulfur-containing molecules from some petroleum fractions. These adsorbents are hydrophilic and contain large void fraction. Synthetic zeolites have a well-defined crystalline lattice of metal alumina silicates which contains uniform pore size **Bagreev, et.al. 2004, and Johns, et.al. 1999]**.

There are several published reports investigating the use of activated carbons and zeolite for sulfur removal from hydrocarbon liquids **, Bakr, et.al. 1997, Lee, et.al. 2002, Sano, et.al, 2005, and Kim, et.al. 2006**.

In this study the ability of preparing Cu(I)-Y-zeolite by using Iraqi rice husk as agricultural residues to prepare Na-Y—zeolite adsorbents then activated it by copper using ion-exchange process and finally reduce Cu^{+2} species to Cu^{+} which is desired for π -complexation.

Also, adsorptive desulfurization of a model diesel fuel, which contained the same molar concentration of the species examined, including sulfur compounds, over three beds, commercial AC, Cu (I)-Y-zeolite prepared from rice husk and AC/Cu (I)-Y-zeolite as a guard bed were conducted in a fixed bed system to evaluate the performance of the prepared adsorbent.

1. MATERIALS AND METHODS

1.1 Preparation of Rice Husk Ash

Rice Husk (RH) is a forming waste, obtained from the rice mills, it needs some treatments to convert it to rice husk ash. It was treated with 10% sulfuric acid for 24 h for preliminary removing all impurities. Then washed, filtered, dried in air, and calcined at 750°C for 6 h. The calcined rice husk subjected for dissolution with 4M sodium hydroxide followed by refluxing at 90°C for 12 h. Concentrated hydrochloric acid was then added to the a forementioned base dissolved for complete precipitation, then filtered, washed and dried in an oven at 120°C for 6 h. The chemical composition of rice husk ash is showed in **Table 1**.

2.2 Synthesis of Y-zeolite

Type Y-zeolite was synthesized using Iraq rice husk as a silica source. A 500 ml Teflon beaker containing a magnetic stirrer was washed with deionized water. Sodium hydroxide of 1.6616 g was added slowly to deionized water and stir until clear and homogenous solution appeared for about 5 minutes. The aqueous solution of sodium hydroxide was ready for the preparation of seed. The gel was prepared according to the following molar chemical composition:

$$10.67Na_2O{:}1\ Al_2O_3{:}\ 10SiO_2{:}\ 180H_2O$$

2-milliliter aqueous solution of sodium hydroxide was added to 0.7515g sodium aluminate oxide until a homogenous mixture was formed; Iraq rice husk 1.5361g was added separately to 5.5ml sodium hydroxide aqueous until homogenously mixed. Both of preparations were heated under vigorous stirring to obtain a homogenous mixture. The sample was aged for 24 h at room temperature in the Teflon bottle. The aluminate and silicate solutions were mixed together in the polypropylene beaker, subsequently stirred for 2 h with the purpose of making it completely homogenized. This combined solution was used as the feed stock gel **M.M.Rahman, et.al.,**

2009, Mohammed.N, and Wadood, T.M. 2011.,The flow chart of the process is shown in **Fig. 1.**

2.3 Adsorbent Preparation

Cu(I)-Y zeolite (i.e. reduced Cu(II)-Y zeolite) was prepared by first ion exchanging Na-Y zeolite with a $Cu(NO_3)_2$ aqueous solution of 0.5 M for 48 hours followed by reduction of Cu^{+2} to Cu^{+}. The amount of copper (Cu) in the ion exchange solution was equivalent to a 10-fold cation exchange capacity. The adsorbent was recovered by filtration and washed with large amount of deionized water, followed by drying at 100°C for about 24 h. Activation of the adsorbent was performed at 450°C to promote auto reduction of Cu^{+2} to Cu^{+} , which is desired for π -complexation. A more detailed discussion on the Cu (I)-Y zeolite autoreduction process can be found elsewhere **,Johns, 1999, M., .Rahman, 2009, Iwamoto, et.al. 1991,Parrillo, et.al., 1993,Larsen, et.al., 1994,Takahashi, et.al., 2001, Takahashi, et.al., 2002, and Hernandez, et.al., 2003**.

2.4 Commercial Activated Carbon (AC)

Table 2 shows the physical properties of the commerical activated carbon .

2.5 Simulated Diesel Fuel

The detailed composition of the model fuel is listed in **Table 3**. The diesel was type “simulate Diesel - 40” according to British Petroleum BP`s specifactions. The average total sulfur concentration for the diesel was reported to be Benzothiophene (BT) and Dibenzothiophene (DBT) standards were purchased from sigma-Aldrich.

2.6 Fixed-Bed Adsorption/ Breakthrough

All adsorption/breakthrough experiments were perfermed in vertical column made quartz adsorbers equipped with a supporting glass fits. The setup consisted of a low-flow liquid pump, two pyrex feed tanks, and a heating element. Initially, the adsorbents were loaded inside the adsorber, and heated in situ at desired temperature. Both Cu-Yzeolite and activated carbon adsorbents were activated at about 300°C. After activation treatment, both the adsorbents under study were allowed to cool down to room temperture. Next, a sulfur-free hydrocarbone was allowed to flow through the sorbent. After wetting the adsorbent for about 10 min, the feed was switched to the simulated one to flow. Effluent samples were collected at regular intervals until saturation was achieved, which depended on the adsorption dynamics and the amount of adsorbent.

2.7 Total Sulfur Analysis

The total sulfur concentration in the simulated diesel fuel and desulfurized diesel fuel were detrmined using an Antek 9000s total sulfur analyzer. The instrument was calibrated to at least four different sulfur concentation rangs using standard samples, and linear calibration curves were obtained for each calibration range. The sulfur detection limit of the total sulfur analyzer in the normal working range is 0.5 ppmw sulfur.

3.RESULTS AND DISCUSSION

3.1 Adsorbent Characterization

The concentrations of Na and Al were determined based on comparison with two replicates of the standard reference material NIST1633A; the determination of Cu content was

determined relative to high-purity copper wire. As seen in the **Table 4** below, ion-exchanging Na-Y with Cu^{++} resulted in incomplete ion exchange. If it is assumed that one Cu^{++} cation compensates for two aluminium tetrahedra, then, for our experiment the ion exchange resulted in only 78% substitution of the original sodium ions, the others were compensating for aluminum tetrahedra. This is the simplest way to describe these zeolites.

3.2 Adsorption Equilibrium Analysis

Equilibrium adsorption data collected in this work is presented in **Fig. 2** , where it can be seen that saturation loading of the three tested adsorbents AC, Cu-Yzeolite, and AC-Cu Y zeolite were (0.28, 0.35, 0.39) mg/g respectively. These result are inline with generally accepted notions that adsorption process on activated carbon is in most cases of physical nature, when chemical bond is not formed. However adsorption on zeolite is supposed to be mainly chemisorption. Higher adsorption capacities that were obtained indicate the ability to form mild chemical bonds with organic sulfur compounds.

The idea of using a guard bed is to extend the capacity of Cu-Y zeolite for smaller S-compound because activated carbon adsorbs both aromatic and thiophenic compounds by vander waals and electrostatic interactions. Thus larger molecules were preferentially adsorbed by carbon, with no selectivity for thiophenic molecules **Takahashi, et.al., 2002,and Hernandez, et.al., 2003**.

3.3 Fixed-Bed Adsorption.

3.3.1 Adsorption on activated carbon bed

Fig.3 illustrated that total sulfur content during experiments with activated carbon breaks through almost immediately. This is expected with AC because activated carbon adsorbs both thiophenic and aromatic compounds by vander waals and electrostatic interaction with no selectivity for thiophenic molecules. Thus larger molecules with higher polarizabilities were preferentially adsorbed by activated carbon. These result are in agreement with the others **,Takahashi, et.al., 2002, and Hernandez, et.al., 2003b**.

3.3.2 Adsorption on Cu Y-zeolite bed

As seen in **Fig.4**, Cu-Y zeolite alone is capable of processing 20 Cm^3 of simulated diesel fuel per grams of adsorbent to be sulfur free. Among the many thiophenic compounds present in diesel fuel, only two were selected for the experiments:benzothiophene(BT) and dibenzothiophene (DBT). The last one molecules are the most difficult to remove in desulfrization treatment processes for transportation fuels. The order of breakthrough followed that of molecular weights **, Arturo, 2004**. For Cu-Y zeolite, the long delay of the breakyhrough of these thiophenic compounds was a direct result of π –complication and followed that of molecular weights. It also indicated some degree of diffusion limitation in zeolite.

3.3.3 Adsorption on guard Bed of Cu-Yzeolite and AC

The idea of using a guard bed of AC/Cu-Yzeolite is that to presorb not only aromatics, but also the largest sulfur-containing compounds, thus extending the capacity of Cu Yzeolite for smaller sulfur compounds.

Two guarded bed was used(i.e 5and 15 wt% of AC of the total bed weight). The results shown in **Fig. 5** indicated that the combination of activated carbon and Cu-Y zeolite as layers

had high selectivities for these large molecules, and, hence, prevented them from entering the Cu-Yzeolite bed. Without these layers of AC/Cu-Yzeolite, these largest molecules would have entered the mainbed of Cu-Yzeolite and subsequently occupied the adsorption site as well as partially blocking the pores of the zeolite. Thus ,the quard bed not only delayed the breakthrough of the sulfur compounds, but also sharpend their wavefronts by eliminating pore blockge.

As seen in **Fig. 5,** the combination of activate carbone (AC) and Cu-Yzeolite is by for the best adsorbent to produce sulfur free diesel fuel that content of equal or less than 1 ppm. The guard bed is capable of processing more than 30 cm^3 of simulated diesel fuel per gram of adsorbent.

Comparison between the two guard beds results (i.e 5 and 15 wt% of activated carbon) showed that there are a number of larger molecules than others. The best bed depends on the exited a significant number of larger aromatic, nonthiophenic compounds. In fact , the commerical diesel typically contains over 150 different compounds. For the present study, 15wt% of AC gives the best results for the simulated diesel fuel metioned previously.

4. CONCLUSION

Results have demonstrated that Y-zeolite prepared from Iraqi rice husk and impregnated with copper gives good results for the removal of sulfur compounds from simulated diesel fuel, based on dynamic fixed-bed adsorption experiment.

When Cu Y-zeolite adsorbent used with activated carbon as a quard bed, Cu-Y zeolite provides by for the best adsorption capacities both at breakthrough point and at saturation.

In general, the adsorbents tested followed the following order for sulfur removal:

AC/Cu-Y zeolite > Cu-Y zeolite > AC.

REFERENCES

Hernandez-Maldonado, A. J. and Yang, R.T., 2004, *New Sorbent for Desulfurization of Diesel Fuels via π a–Complication*, AIChE J., Vol. 50, pp. 791-801.

Hernandez-Maldonado, A. J., Stamaties, S. D., Yang, R. T., He, A. Z. and Cannel, W., 2004, *New Sorbent for Desulfurization of Diesel Fuels via pi-Complexation: Layer Bed and Regeneration*, Ind. Eng. Chem. Res. Vol.43, pp. 769-776.

Hernandez-Maldonado, A. J. and Yang, R.T., 2003, *Desulfurization of Commercial Liquid Fuels by Selective Adsorption via π - Complexation with Cu (I)-Y Zeolite*, Ind. Eng. Chem. Res., Vol. 42, pp. 3103-3110.

Hernandez-Maldonado, A. J. and Yang, R.T., 2004, *New Sorbent for Desulfurization of Diesel Fuels π –Complexation*, AIChE J., Vol. 50, N0. 4.

Zhou, A., Ma, X. and Song, C., 2004, *Deep Desulfurization of Diesel Fuels by Selective Adsorption with Activated Carbons*, Prep. Pap. Am. Chem.Soc. Div. pet .Chem., Vol. 49, pp. 329-332.

Babich, J. A. and Moulijn, J. A., 2003, *Science and Technology of Noval Processes for Deep Desulfurization of Oil Refinery Streams*: A review fuel, Vol. 82, pp. 607-631.

Baeza, P., Aguila, G., Gracia F. and Araya, P., 2008, *Desulfurization by Adsorption with Copper Supported on Zirconia*, Catal commun, Vol. 9, pp. 751-755.

Bagreev, A., Menendez, J. A., Dukhno, I., Tarasenko, Y. and Bandosz, T. J., 2004, *Bituminous Coal-based Activated Carbons Modified with Nitrogen as Adsorbents of Hydrogen Sulfied Carbon*, Vol.42, pp. 469-476.

Bakr, A., Salem, S. H. and Hamid, H. S., 1997, *Removal of Sulfur Compounds from Naphta Solution using Solid Adsorbents*, Chem. Eng. Tech., Vol. 20, pp.342-347.

Turk, B. S. and Gupta, R. P., 2001, *RTI`s TReND Process Deep Desulfurization of Naphtha*, prepr. Pap. Am .Chem. Soc., Div.pet. Chemm., Vol. 46, No. 2, pp. 392-393.

Song , C. S., 2003, *An Overview of New Approaches to Deep Desulfurization for Ultraclean Gasoline, Diesel Fuel and Jet Fuel*, Catal. Today, Vol. 86, pp. 211-263.

Song , C. S. and Ma, X., 2003, *New Design Approaches to Ultra-clean Diesel Fuels by Deep Desulfurization and Deep Dearomatization*, Appl.Catal. B. Environ., Vol. 41, pp. 207-238.

Bailey, G. W. and Swan, G. A., *US Pattent*, 4,634,514,1987.

Hernandez-Maldonado, A. J. and Yang, R.T., 2003a, *Desulfrization of Liquid Fuels by Adsorption via π–Complexation with Cu(I)-Y Zeolite and Ag-Y Zeolite*, Ind. Eng. Chem. Res., 42,123.

Hernandez-Maldonado, A. J. and Yang, R.T., 2003b, *Desulfrization of Commerical Liquid Fuels by Selective Adsorption via π–Complexation with Cu(I)-Y Zeolite*, Ind. Eng. Chem. Res., 42,3103.

Iwamoto, M., Yahio, H., Tanda, K., Mizuno, N., Mine, Y. and Kagawa, S., 1991, *Removal of Nitrogen Monoxide Through a Noval Catalytic Process: 1.Decomposition on Excessively Copper Ion Exchanged ZSM-5 Zeolites*", J. Phys. Chem., Vol. 95, 3727.

Johns, M. M., Marshall,W. E. and Toles, C. A, 1999, *The Effect of Activation Method on the Properties of Pecan Shell-Activated Carbons*, J. Chem. Tech. Biotech., Vol. 74, pp. 1037-1044.

Jiang, M. and Ng, F.T.T, 2006, *Adsorption of Benzothiophene on Y-Zeolites Investigated by Infrared Spectroscopy and Flow Calorimetry*, Catal Today, Vol. 116, pp. 530-536.

Jiang, M., Ng, F. T. T, Rahman, A. and Patel, V., 2005, *Flow Calorimetric and Thermal Gravimetric Study of Adsorption of Thiophenic Sulfur Compound on Na-Y Zeolite*, Thermochim Acta, Vol. 434, pp. 27-36.

Kim, J .H., Ma, X., Zhou, A. and Song, C., 2006, *Ultra-Deep Desulfurization and Denitrogenation of Diesel Fuel by Selective Adsorptive Selectivity and Mechanism*, Catal Today, Vol. 111, pp.74-83.

Larsen, S. C., Aylor, A., Bell, A. T. and Reimer, J. A., 1994, *Electron Paramagnetic Resonance Studies of Copper Ion-Exchanged ZSM-5*, J. Phys. Chem, Vol. 98, pp. 11533.

Lee, S. H. D, Kumar, R. and Krumplet, M, 2002, *Sulfur Removal from Diesel Fuel-Contaminated Method*, Sep purify Technol, Vol. 26, pp. 247-258.

Bovillr, L .J., Degerorge, C. L., Foley, P. F., Foley, J. X, Lesieur, R. R., Person, J. L.V., Szydlowski, D. F., 2000, *U.S.Patent* 6, 159, 256.

Ma, X., Sun, L. and Song,C., 2002, *A New approach to Deep Desulfurization of Gasoline, Diesel Fuel and Jet Fuel by Selective Adsorption for Ultra-Clean Fuels and Fuel Cell Applications*, Catal Today, Vol. 77, pp. 107-116.

Rahman, M .M., Hasnida, N., and WanNik, W. B., 2009, *Preparation of Zeolite Y Using Local Raw Material Rice Husk as a Silica Source*, J. Sci. Res. Vol. 1, No. 2, pp. 285-291.

Breysse, M., Mariadassou, G. D., Pessayre, S., Geantet, C., Vrinat, M., perot, G. and Lemaire, M., 2003, *Deep Desulfurization:Reaction, Catalysts and Technological Challenges*, Catal. Today, Vol. 84 (3-4), pp.129-138.

Mohammed N. Wadood T. M., 2011, Ph.D. Thesis College of Engineering University of Baghdad.

Sano, Y., Sugahara, K., Choi, K., Korai, Y. and Mochida, I., 2005, *Tow Step Adsorption Process for Deep Desulfurization of Diesel Oil Fuel*, Vol. 84, pp. 903-910.

Song, C.S., 2003, *An Overview of New Approaches to Deep Desulfurization for Ultra-Clean Gasoline, Diesel Fuel and Jet Fuel*, Catal. Today, Vol.86, pp. 211-263.

Song, C. S., Ma, X., 2003, *New Design Approaches to Ultra-Clean Diesel Fuels by Deep Desulfurization and Deep Dearomatization*, Appl. Catal. B, 41, pp. 207-238.

Song, C. S., 2002, *Fuel Processing for Low Temperature and High Temperature Fuel Cells-Challenges, and Opportunities for Sustainable Development in the 21st Century*, Catal. Today, 77, pp. 17-50.

Haji, S. and Erkey, C., 2003, *Removal of Dibenzothhiophene from Model Diesel by Adsorption on Carbon Aerogels for Fuel Cell Applications*, Ind. Eng. Chem. Res. Vol. 42, pp. 6933-6937.

Velu, S., Ma, X. and Song, C., 2003, Selective Adsorption for Removing Sulfur from Jet Fuel over Zeolite Based Adsorbents, Ind. Eng. Chem. Res. Vol. 42, pp. 5293-5304.

Watanabe, S., Ma, X. and Song, C., 2004, *Selective Sulfur Removal from Liquid Hydrocarbons over Regenrable CeO_2-TiO_2 Adsorbents for Fuel Cell Application*, Prepr. Pap, Am. Chem. Soc., Div.pet.Chem. 49 (2) 511.

Parrile, D. J., Dolenec, D., Gorte, R. J., and McCabe, R. W. 1993, *Adsorption Studies on CuZSM-5:Characterization of the Unique Properties of Ion Exchange Cu*, J. Catal., 142, 708.

Vasudevan, P. T. and Fierro, j.l.g., 1996, *A review of Deep Hydrodesulfurization Catalysis*, Catal. Rev. Sci. Eng. 38(2), pp. 161-188.

Takahashi, A. and Yang, R. T., 2001, *Cu (I)-Y-Zeolite as a Superior Asorbent for Diene/Olefin Separation*, Langmuir, 17, 8405.

Takahashi, A. and Yang, F. H., 2002, *New Sorbent for Desulfurization by π–Complexation: Thiophene/Benzene Adsorption*, Ind. Eng. Chem. Res, 41, 2487.

Fukunaga, T., Katsuno, H., Matsumoto, H, Takahashi, o. and Akai, Y., 2003, *Development of kerosene Fuel Processing System for PEFC*, Catal. Today 84, pp. 197-200.

Yang, R.T., Hernandez-Maldonado, A.J. and Yang, F.H., 2003, *Desulfurization of Transportation Fuels with Zeolite under Ambient Conditions*, Science, 301, pp. 79-81.

Lesieur, R. R., Teeling, C., Sangiovanni, J. J., Boedeker, L.R., Dardas, Z.A., Huang, H., Sun, J., Tang, X., , Spadaccini, L.J., 2002, *US Patent* 6, 454, 935.

Ma, X., Sprague, M., Sun, L. and Song, C., 2002, *Deep Desulfurization of Gasoline by SARS Processing using Adsorbent for Cells*, Prep. Am. Chem. Soc. Div. fuel. Chem. 47, pp. 452-453

Ma, X., Velu, S., kim, J. H. and Song, C., 2005, *Deep Desulfurization of Gasoline by Selective Adsorption over Solid Adsorbents and Impact of Analytical Methods on ppm-level Sulfur Quantification for Fuel Cell Applications*, Appl. Catal.B:Environ. Vol. 56, pp. 137-147.

Ma, X., Sprague, M., Sun, L, and Song, C., 2005, *Deep Desulfurization of Gasoline by Selective Adsorption over Nickel-Based Adsorbent for Fuel Cell Application*, Ind. Eng. Chem. Res. Vol. 44, pp. 5768-5775.

Ma, X., Velu, V., Sun, L. and Song, C., 2003, *Adsorptive Desulfurization of Diesel Fuel over a Metal Sulfide Based Adsorbent*, Prepr. Pap. Am. Chem. Soc., Div pet.Chem. Vol.48(2), pp. 522-523.

Sano, Y., Choi, K., Korai, Y., and Mochida I., 2004, *Energy Fuels*, Vol. 18, pp. 644-651.

NOMENCLATURE

C = sulfur conc. in effluent

Ce = sulfur conc. At equilbrium

C_o = initial conc. of sulfur in feed

q = a mount of ions per gram of adsorbtion

ABBRAVIATION

AC = Activated Carbon

BT = Benzothiophene

BP = British Petroleum

DBT = Dibenzothiophene

EU = European

HDS = Hydrodesulfurization

RH = Rice Husk

US: United State

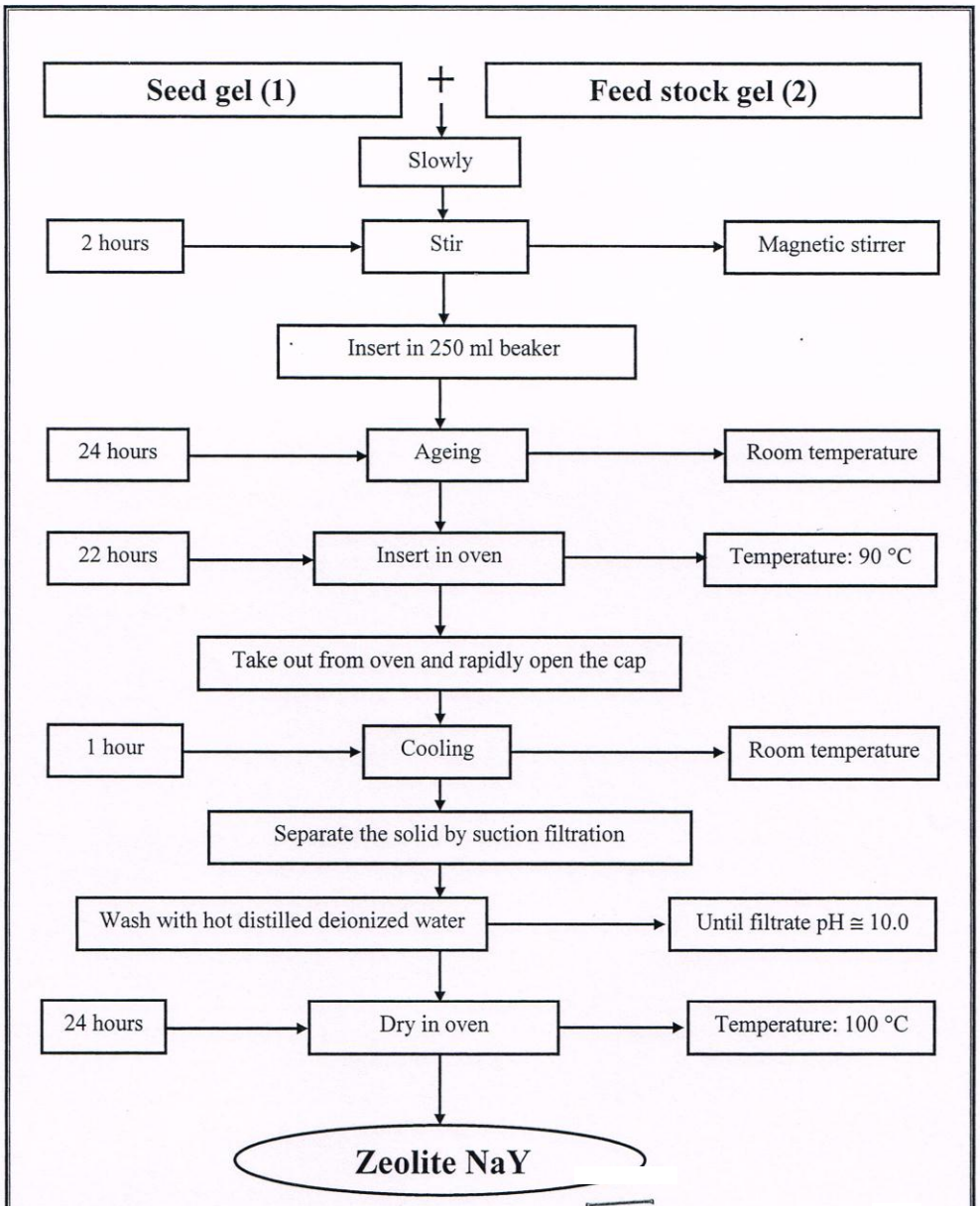

Figure 1. Flow chart of the synthesis of type Y-Zeolite catalyst using Iraqi

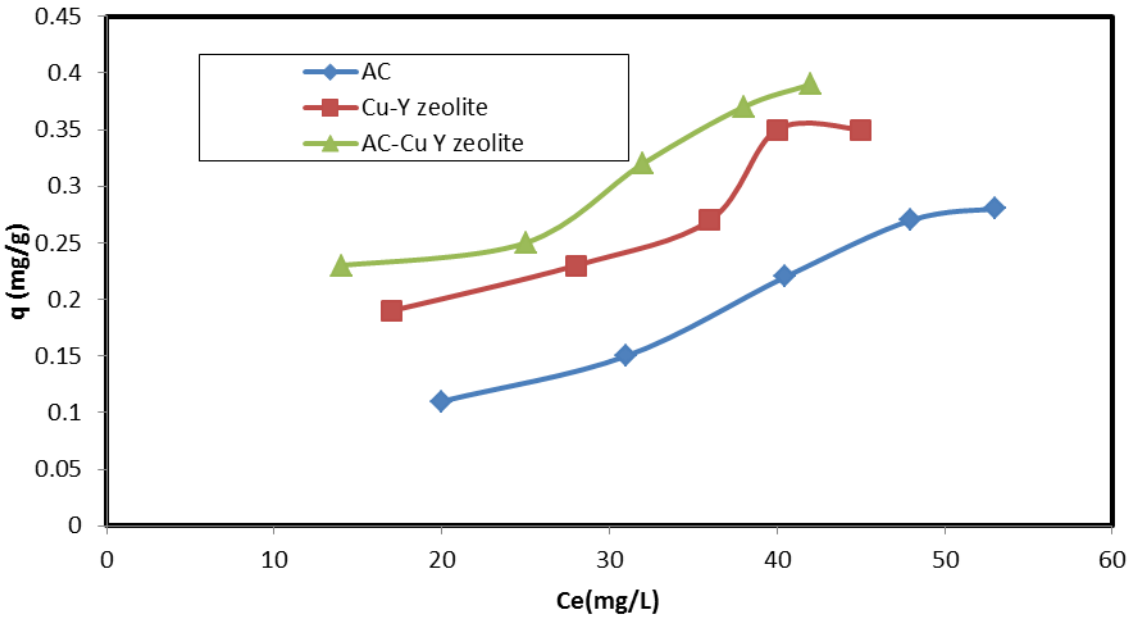

Figure 2. Adsorption Equilibrium Analysis.

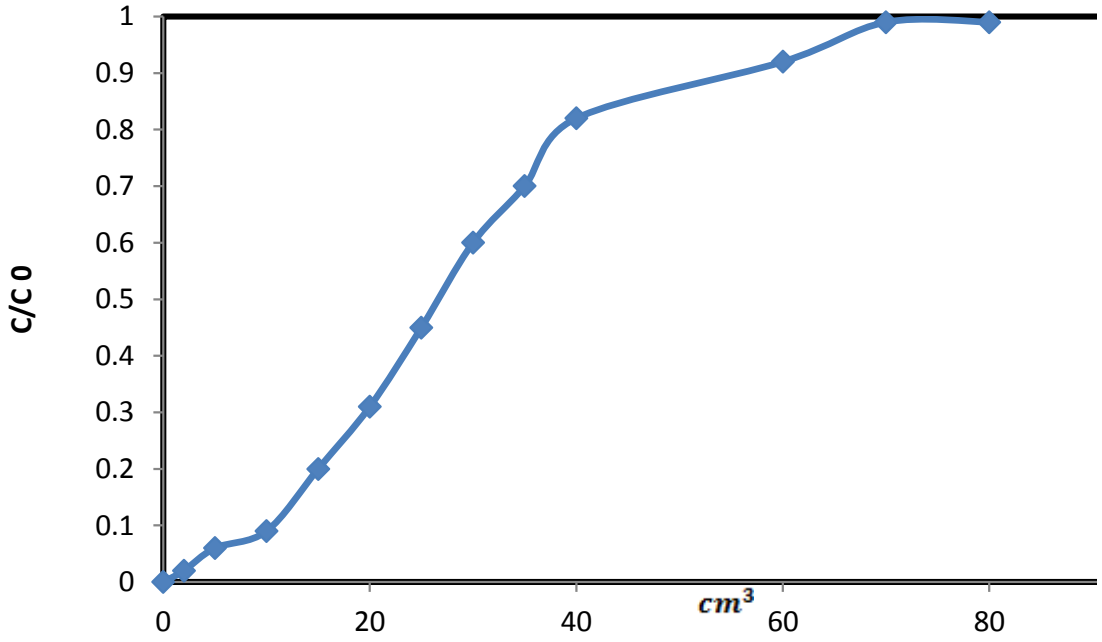

Figure 3. Breakthrough curve of sulfur compounds in a fixed bed adsorber of actived carbon adsorbent.

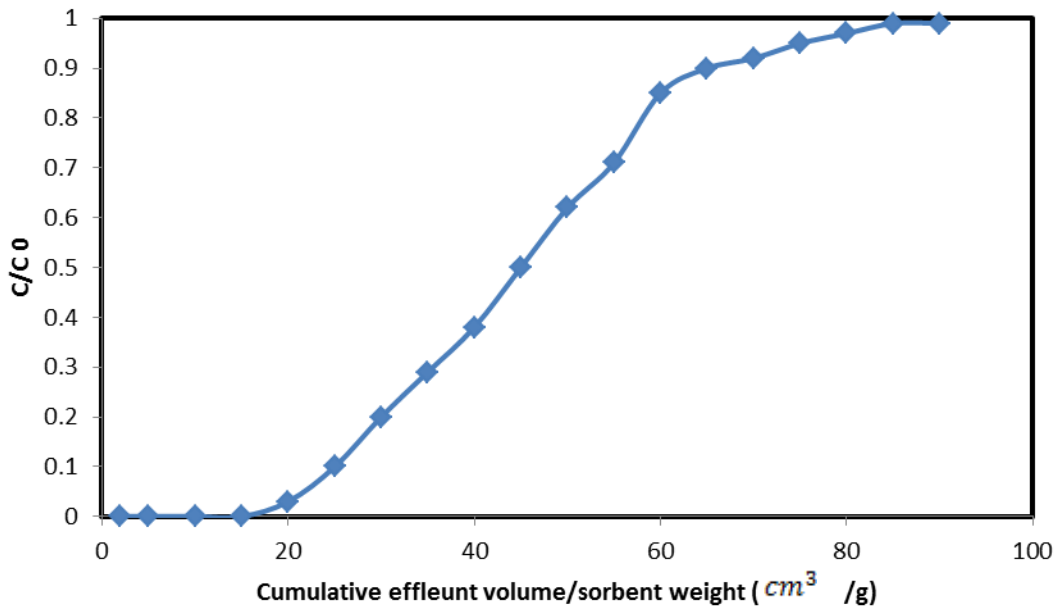

Figure 4. Breakthrough curve of sulfur compounds in a fixed bed adsorber of CuY-zeolit adsorbent.

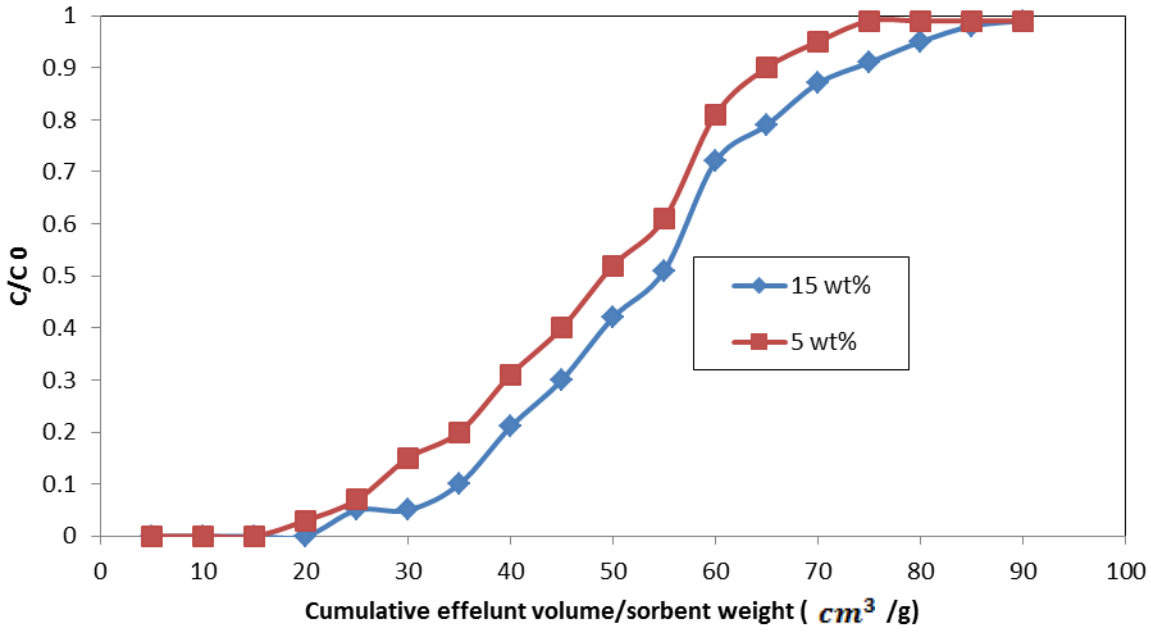

Figure 5. Breakthrough curve of sulfur compounds in a fixed bed adsorber of AC/CuY-zeolit adsorbent.

Table 1. The chemical composition of rice husk ash.

	Wt.%
SiO_2	94.5
Al_2O_3	2.23
Fe_2O_3	0.16
TiO_2	0.115
CaO	0.51
MgO	0.25
Na_2O	0.49
K_2O	0.63
P_2O_5	0.32
LOI	0.73

Table 2. physical properties of AC.

Particle size (mm)	0.006-0.080
Bulk density (g/cm^3)	0.35
Surface area (m^2/g)	1100

Table 3. Composition of the simulated diesel fuels (diesel 40).

compounds	composition
n-Dodecane	80wt%
Toluene	20wt%
Benzothiophene (BT)	150ppm
Dibenzothiophene (DBT)	148ppm

Table 4. Composition Data for Na-Y zeolite and Cu^{+2}-Y zeolite.

Adsorbent	Molar ratios		
	Si/Al	Na/Al	2Cu/Al
Na-Y	2.65	0.92	----
Cu^{+2}-Y	2.65	0.22	0.78

Gas Flow Formation in the Inertial Filtering (IF) Gas Separators Curvilinear Channels

Prof. Vsevolod Ivanovich Sklabinskyi
E-mail: sklabin@ukr.net

Asst. Prof. Aleksandr Aleksandrovich Liaposhchenko
E-mail: lyaposchenko@pohnp.sumdu.edu.ua

Asst.Lect. Andrey Vladimirovich Logvyn
E-mail: fench@ukr.net

Ph.D. Student. Mustafa Makki Al Rammahi
E-mail: *misto_8304@yahoo.com*

Department Processes and Equipment of Chemical and Petroleum-Refineries Department (PECPR Department) / College of Technical Systems and Energy Efficient Technologies /Sumy State University-Ukraine

ABSTRACT

This paper deals with an up to date problem for oil and gas industry- separation of the gas -fluid fogs. Here is described the worked out physical model of the gas movement process in the sections of the inertial filtering (IF) gas separators. One can find the mathematical model for research of the fields of velocities and pressures in the inertial curvilinear channel. The main simplifications and assumptions are explained. This mathematical model has been made using mathematical program Maple and it is received the 3-d graphic of the distribution componential speed parts in the channel and also 2-d graphics at the channel sectional view when the flow is flat. The new method for gas - fluid systems separation is suggested.

Keywords: separation; modeling; velocity; gas; liquid; curvilinear channel; filter.

انشاء نموذج لتدفق الغاز في قناة منحنية الاضلاع لعوازل غازية تعمل بالقصور الذاتي مع الفلاتر

بروف.فسيفولود ايفانوفيج سكلابينسكي., مساعد بروف.الكسندر الكساندريفيج لابوشينكو.,
محاضر.اندري فلاديمير لوغيفن.,طالب الدكتوراه.مصطفى مكي محمد علي .

قسم العمليات والمعدات للمصافي النفطية والبتروكيميائية
كلية النظم التقنية وتكنولوجيات كفاءة الطاقة
جامعة سومي الحكومية- اوكرانيا

الخلاصة

يتناول هذا البحث مشكلة ملحة لصناعة النفط والغاز وهي فصل رذاذ الغاز – السائل أو ما يسمى (بالضباب أو بخار الماء)حيث تم دراسة نموذج فيزيائي لحركة وتدفق الغاز داخل عوازل غازية تعمل بمبدأ القصور الذاتي مع المرشحات (الفلاتر).وبالتالي تم العمل على ايجاد ودراسة نموذج رياضي للبحث في مجالات السرعة والضغط داخل قناة منحنية الاضلاع تحت تاثير قوى القصور الذاتي .

ولتشخيص وتبسيط هذه المعطيات والافتراضات تم وضع هذا النموذج الرياضي ومعالجته باستخدام برنامج الMaple, من النتائج التي تم الحصول على مخطط بياني ثلاثي الابعاد يوضح توزيع قيم السرع على طول اجزاء القناة ,وكذلك تم الحصول على مخططات ثنائية الابعاد توضح مقاطع عرضية للقناة عندما يكون الجريان سطحي , بالاضافة الى مقترحات جديدة لانظمة فصل الغاز - السائل.

الكلمات الرئيسية: : فصل، نمذجة، السرعة، غاز، سائل، قناة منحنية الأضلاع، فلتر.

1. INTRODUCTION

Air dispersion systems which consist of solid and liquid particles weighted in the gas form play quite an important role in the nature and in humans life. But the problem of air dispersion systems separation is even more up to date in the science and techniques, **Poole, 2009**.

Many theoretical problems of air dispersion systems particles studying are of big mathematical hardships. It happens as a rule that their solution one finds using difficult mathematical formulas using which in practice needs immense calculating work. So in some of the cases it is reasonable to refuse from the exact solution and take the well known assumptions which make it much easier to get at least the rough idea about the examining phenomenon.

2. KEY ASSUMPTIONS AND PHYSICAL MODEL:

1. One finds out the hydrodynamic characteristics and separation elements constructive parameters making some simplifying assumptions which have the main features of the studying phenomenonin order to make practical calculations of the typical gas dynamical separation apparatus **Stepanov et al., 1986**.

2. First of all one neglects gas condensability and viscosity, flow turbulence and examine the settled (average as to time) ideal (no viscose) constant density fluid free-vortex movement. But it is possible only when there is a low viscous gas flow in the good profiled channels when the speeds are subsonic.

3. Then, the flow is considered to be 2-d which takes place in the layer which usually has variable thickness with the parameters depending only on two coordinates.,**Sinayskiy et al., 2002**.

4. But the real gas flow in the channels of louver inertial filtering gas separator generally is spatial and unsteady and that is why it is impossible to make its complete theoretical analysis **Barilovych, 2009; Lyaposchenko et al., 2005**; **Lyaposchenko, 2006**. Having such task considering limited demands to the gas parameters accuracy and approximate using model it is reasonable to apply quite simplified flow schemes and calculating formulas based on the further simplifying assumptions.,**Al Rammahi et al., 2011; and Lyaposchenko, 2006**. Solving such tasks it is enough to use equation indissolubility, vortex equation and impulse theory .,**Barilovych, 2009; and Lyaposchenko, 2006**. The stated above assumptions are of big help to make a qualitative modeling and to get rough results of calculating the gas flow in the IF gas separators louver boards.

In the **Fig.1**, it is shown the calculating zone geometrical configuration in the form of curvilinear channels which are formed by the louver board plates of the IF gas separator:

To analyze the physical model gas drop flow movement along the separation channel with filtering sections of the inertial filtering gas separator one should look through its separate pieces. **Fig.2.**

- gas drop flow movement along the inertial section of the curvilinear gas separation channel;
- penetration of the gas drop flow in the filtering section, dispersion particles ricochet or splashes carrying out in the separation channel depending on the angle which faces the “attack” by the layer filter flow;
- coalescence of the caught particles on the fibers in the filtering layer, the formation and withdrawal of the caught liquid pellicle to the drainage channels

Local gas flow speeds gradually rise after the rectilinear sections on the separation channel inlet on the transition from the curvilinear to linear (confusion) sections. After the rectilinear sections in the curvilinear section there is an inhibitory (diffusion) separation channel section with filtering sections which are situated on the inner surface of the crimping plates. In this section the dynamic force of the air decreases due to lower gas flow rate of fluid. This force pulls the dispersion particles in the gas stream, and it makes the particles inertial movement to the filter layer easier which makes separation effective. By the way pressure in the drainage channels of the double louver crimping plates rises and it makes the flowing and caught fluid withdrawal steady and filtering elements in the self-cleaning mode work effectively. When stationary regime is achieved stability, separation effectiveness, the liquid quantity in the filtering layer and liquid flowing from the layer remain constant in time when the filtering speed is permanent. In such a case the migrating liquid quantity is equal to the liquid quantity which gets into the filter layer. The boundary which divides separation channel inertial zones and filtering section is

a conditional wall (free stream boundary) where the gas flow speed is constant which corresponds to the permanent pressure in the filter layer and drainage channels. On the transition from curvilinear to the linear (confusion) sections beginning from the inhibitory points of the gas flow which comes upon the speeds gradually rise again. The special attention was necessary to pay to the separation channel curvilinear section profiling where the biggest pressure losses and resistance are connected with the flow separation. Separating flow limits the pressure speed gradient on the separation channel walls.

5. The special attention was necessary to pay to the separation channel curvilinear section profiling where the biggest pressure losses and resistance connected with the flow separation. Separating flow limits the pressure speed gradient on the separation channel walls. As to the theoretical and experimental data to get the continuous flow one should lower the gas speed no more that on the 25% on the wall length, which is equal to the separation channel width. Moreover as to the recommendations general speed reduction must not be more than three-times.

3. MATHEMATICAL MODEL:

The motion of viscous gas flow in a curvilinear channel is conveniently described by the Navier-Stokes equations in cylindrical coordinates. Turbulent gas flow can be accounted for by replacing the kinematic viscosity (ν) on the coefficient of turbulent viscosity (ε), that for the ax symmetric vortex flows can in some cases to obtain analytical solutions of the set of hydrodynamic problems. To close this system of Navier-Stokes equations complemented by the continuity equation of the fourth. The result is a system of four Eqs. (1)-(4) with four unknowns (the projection of the velocity of the gas flow on the three axes and the magnitude of the pressure):

$$V_r \frac{\partial V_r}{\partial r} + \frac{V_\phi}{r}\frac{\partial V_r}{\partial \phi} + V_z \frac{\partial V_z}{\partial z} - \frac{V_\phi^2}{r} = -\frac{1}{\rho}\frac{\partial P}{\partial r} + \\ +\varepsilon\left(\frac{\partial^2 V_r}{\partial r^2} + \frac{1}{r^2}\frac{\partial^2 V_r}{\partial \phi^2} + \frac{\partial^2 V_r}{\partial z^2} + \frac{1}{r}\frac{\partial V_r}{\partial r} - \frac{2}{r^2}\frac{\partial V_\phi}{\partial \phi} - \frac{V_r}{r^2}\right); \quad (1)$$

$$V_r \frac{\partial V_\phi}{\partial r} + \frac{V_\phi}{r}\frac{\partial V_\phi}{\partial \phi} + V_z \frac{\partial V_z}{\partial z} + \frac{V_r V_\phi}{r} = -\frac{1}{\rho r}\frac{\partial P}{\partial \phi} + \\ +\varepsilon\left(\frac{\partial^2 V_\phi}{\partial r^2} + \frac{1}{r^2}\frac{\partial^2 V_\phi}{\partial \phi^2} + \frac{\partial^2 V_\phi}{\partial z} + \frac{1}{r}\frac{\partial V_\phi}{\partial r} + \frac{2}{r^2}\frac{\partial V_r}{\partial \phi} - \frac{V_\phi}{r^2}\right) \quad (2)$$

$$V_r \frac{\partial V_z}{\partial r} + \frac{V_\phi}{r}\frac{\partial V_z}{\partial \phi} + V_z \frac{\partial V_z}{\partial z} = -\frac{1}{\rho}\frac{\partial P}{\partial r} + \\ +\varepsilon\left(\frac{\partial^2 V_z}{\partial r^2} + \frac{1}{r^2}\frac{\partial^2 V_z}{\partial \phi^2} + \frac{\partial^2 V_z}{\partial z^2} + \frac{1}{r}\frac{\partial V_z}{\partial r}\right); \quad (3)$$

$$\frac{\partial V_r}{\partial r} + \frac{1}{r}\frac{\partial V_\phi}{\partial \phi} + \frac{\partial V_z}{\partial z} + \frac{V_r}{r} = 0. \quad (4)$$

To transform the system of equations, in order to get the form in which it was possible to find an analytical solution, we introduce a number of simplifying assumptions.

Due to the fact that the basic movement of the gas flow occurs along a curved louver dripping, we assume that overflows the height of the louver channel in its magnitude is much less than the gas

velocities along the channel ($V_z \approx 0$). A change in other components of the velocity and pressure at an altitude of louver elements also occurs ($\partial/\partial z \approx 0$). This allows you to exclude from the above system of differential equations of the third equation and of the remaining equations of the system to exclude all terms that contain the axial component of the total gas flow rate. In addition, we assume that due to the small width of the curved channel the pressure across the width of the channel is changed slightly, but the main change occurs along the channel $\partial P/\partial r \approx 0$. That is to say. We obtain the following system of differential equations in partial derivatives. To simplify the recording is without the function of the radius and circumferential coordinates.

$$V_r \frac{\partial V_r}{\partial r} + \frac{V_\varphi}{r}\frac{\partial V_r}{\partial \varphi} - \frac{V_\varphi^2}{r} = \varepsilon \begin{pmatrix} \frac{\partial^2 V_r}{\partial r^2} + \frac{1}{r^2}\frac{\partial^2 V_r}{\partial \varphi^2} + \\ + \frac{1}{r}\frac{\partial V_r}{\partial r} - \frac{2}{r^2}\frac{\partial V_\varphi}{\partial \varphi} - \frac{V_r}{r^2} \end{pmatrix}; \tag{5}$$

$$V_r \frac{\partial V_\varphi}{\partial r} + \frac{V_\varphi}{r}\frac{\partial V_\varphi}{\partial \varphi} + \frac{V_r V_\varphi}{r} = -\frac{1}{\rho r}\frac{d\mathrm{P}}{d\varphi} + \varepsilon \begin{pmatrix} \frac{\partial^2 V_\varphi}{\partial r^2} + \frac{1}{r^2}\frac{\partial^2 V_\varphi}{\partial \varphi^2} + \frac{1}{r}\frac{\partial V_\varphi}{\partial r} + \\ + \frac{2}{r^2}\frac{\partial V_r}{\partial \varphi} - \frac{V_\varphi}{r^2} \end{pmatrix}; \tag{6}$$

$$\frac{\partial V_r}{\partial r} + \frac{1}{r}\frac{\partial V_\varphi}{\partial \varphi} + \frac{V_r}{r} = 0. \tag{7}$$

In the Eqs (5) and(7) consists of only two velocity components. These radial and circumferential velocity components of the gas stream. Set up a system of two Eqs (8) and (9) with two unknowns, which try to solve analytically.

$$V_r \frac{\partial V_r}{\partial r} + \frac{V_\varphi}{r}\frac{\partial V_r}{\partial \varphi} - \frac{V_\varphi^2}{r} = \varepsilon\left(\frac{\partial^2 V_r}{\partial r^2} + \frac{1}{r^2}\frac{\partial^2 V_r}{\partial \varphi^2} + \frac{1}{r}\frac{\partial V_r}{\partial r} - \frac{2}{r^2}\frac{\partial V_\varphi}{\partial \varphi} - \frac{V_r}{r^2}\right); \tag{8}$$

$$\frac{\partial V_r}{\partial r} + \frac{1}{r}\frac{\partial V_\varphi}{\partial \varphi} + \frac{V_r}{r} = 0. \tag{9}$$

Of the variety of possible solutions to choose the most appropriate solution. This solution, which is obtained in the field of real numbers

$$V_r(r,\phi) = \frac{r^2 C_1 \cdot \sin(2\phi) + r^2 C_2 \cdot \cos(2\phi) + C_3}{r} \tag{10}$$

$$V_f(r,\phi) = \frac{1}{r}(-r^2 C_2 \cdot \sin(2\phi) + r^2 C_1 \cdot \cos(2\phi) + +(r^4 C_1 \cos(2\phi)^2 \\ + r^4 C_1^{\,2} \cdot \sin(2\phi)^2 + r^4 C_2^2 - C_3^2)^{0.5}) \tag{11}$$

To determine the changes in the law, for example, the radial component of the velocity of the gas flow is necessary to determine the integration constants C1, C2, and C3. This can be done from the condition not overflow gas through the surface, which are limited to the radii R1 and R2. In addition, we

assume that at some angular coordinate is the known value of the radial component of velocity equal to V_{r1}.

$$0 = \frac{R_1^2 C_1 \cdot \sin(2\phi) + R_1^2 C_2 \cdot \cos(2\phi) + C_3}{R_1} \tag{12}$$

$$0 = \frac{R_2^2 C_1 \cdot \sin(2\phi) + R_2^2 C_2 \cdot \cos(2\phi) + C_3}{R_2} \tag{13}$$

$$V_{r1} = \frac{r^2 C_1 \cdot \sin(2\phi_0) + r^2 C_2 \cdot \cos(2\phi_0) + C_3}{r} \tag{14}$$

Graphically, the solution can be obtained in the form of a curved surface.

4. THE INFLUENCE OF LOCAL VELOCITIES IN THE CHANNEL IF GAS SEPARTORS ON ITS GEOMETRY

To reach the separation high effectiveness one needs to create high intensive hydro dynamical flows movement regimes in the gas separation apparatus. By experimental research of the created physical model of the separation channel with filtering sections inertial filtering gas separator (regimes2300≤Re≤100000) it is proved that in the transition regime the gas flow viscously continuously flows around the lugs and hollows and almost exactly copies geometrical curvilinear separation channel configuration. Maximal speed is a feature of the gas flow core. Laminar layers near the channels walls especially in the hollow places have minimal gas movement speeds. At some of them reverse currents and vortex flows can occur. When the turbulent flow stream is high (Re≥10000) one can see the local gas flow speeds increase in two times in the lugs of the curvilinear channel walls (at $\theta=70^0$). These are the zones of potential pellicle dispersion of the caught liquid pellicle and secondary spray carrying out **Fig.3**.

After observation and analysis of the gas flow local speeds distribution along the curvilinear separation channel one strictly determined the geometrical zones where it is reasonable to place the filtering elements in the separation channel hollows, closely to the louver walls, local speeds here are minimal, but on the other hand they are limited with the equal speeds lines, |v|=const with the speeds which are equal to the gas flow speed on the curvilinear channel inlet and the angle is $\theta=60^0$-110^0 **Fig.4**.

The fibrous filters (drop catchers) work peculiarity is in the coalescence of the caught high dispersion particles (fluid drops) when contacting with the fibers surface and creation the fluid pellicle on them which is removed as it is accumulated from the layer in the form of the squirts or big water drops which move in the layer under their own weight force or they are caught by the gas flow or capillary forces.

While creating the separation channel with filtering sections inertial filtering gas separator model one used as filtering element needle punched fabric made of polypropylene fibers. It is due to that polypropylene fibers apart from their universal chemical resistance also have good hygroscopic properties and so they are very effective for hydrogen particles from the condensation fog catching.

After gas fluid flow gets into the filtering sections fluid drop catching is accompanied with the difficult secondary processes in the filter layer as a result of which its structure changes greatly. Caught with the fiber drops spread about their surface creating a pellicle the thickness of which rises becomes unstable and ruins on the separate drops which flow down along the fibers in the places where they are bent and cross themselves under the gravitation forces and frontal friction in the gas flow. As a result of the capillary forces activity neighboring fibers can cling together and so separate small fibers disappear and make bigger pores. At the same time some little pores are filled with fluid which increases the real gas speed in the bigger pores. In such a way the first liquid accumulation leads to essential change of the fiber layer pattern and structure. Fluid accumulation continues till the filtering layer does not set off the self purification stationary regime. After that as it is stated above the caught liquid quantity in the

filtering layer and the quantity of the liquid flowing from it remains constant in time when the filtering speed and particles in the gas flow concentration parameters do not change.

Along with it the following sedimentation particles on the fibers mechanisms are possible. Touching effect (clutching) takes place when the gas flow current lines with which the particles move come over the surface of the barrier (fiber) on the distance equal to the particle radius or closer. Inertial contact takes place when particle mass or its movement speed are so considerable that it cannot move with gas flow completely along its current lines which roughly bend round the barriers. That is why the particles due to the inertial force continue their movement along the more linear trajectories and go off the current lines. High dispersion Brownian motion is a result of the gas molecules contact with the particles surface and is like mass changing based on molecular diffusion. Taking into consideration that inertial filtering separation apparatus are quite effective at catching fluid drops of the sizes $1 \geq 2R \geq 5\mu m$ from the gas fluid flows .,**Lyaposchenko, 2006.** one understands that it is not necessary to speak about the catching drops based on the Brown diffusion which becomes visible for the particles of the sizes $2R \leq 0.1$. In the result of the experimental research one found out that the most permeating (hard to catch) are the particles of the sizes $2R=0.3\text{-}1.0\mu m$, as the diffusion coefficient for them is small and inertial effect does not have the considerable influence yet.

Besides that the basic separation process can be actively accompanied with the following processes when non stationary filtering regimes take place. As the following processes one means the phenomena which cause change of the separation effectiveness and resistance in course of time. The non stationary filtering phase (which is characterized with the filtering environment structure changes) in the conditions of many industrial manufactures exploitation has the significant practical meaning because of short duration of the stationary filtering phase. Because the following processes are complicated and versatile the non stationery filtering phase has been much worse studied.

The caught fluid drops are distributed along the fibers uneven. As the drops accumulate the new ones sediment on the old sediment drops and form the chains which emerge on the sides and when develop they continually turn into the tree-like branching which fill the pores. The phenomenon of mudding makes the filter efficiency much higher. Sometimes thanks to insignificant resistance increasing. Filtering layer structure heterogeneities smooth out due to it and the particles aggregates fill the big pores. Capillary phenomena are very important for the fog filtering and are difficult processes which include: the sediment drops spreading out with the following connection them into big drops or with the liquid pellicle formation on the fibers; liquid accumulation in the places of the fibers crossings; capillary water steam condensation in the places where the caught particles contact with the fiber or with each other; neighboring fibers clinging because of capillary forces influence when soaking the fibers which leads to the small drops disappearing in the filters that are not enough hard and the formation of the bigger intervals to the increasing the heterogeneity of the layers structure.

It is worth noticing that flow speed increasing can lead to the following drops carrying away, which is connected with the taking them from the fibers surface. So fiber filtering element is characterized with two critical speeds: first speed limits the size of the drops caught with fiber and is defined with the Stokes criterion, the second one is the beginning of the secondary drops carrying away thanks to the fluid pellicle firmness loss that flow down the fibers.

5. RESULTS AND DISCUSSION

When modeling of the received mathematical systems for the curvilinear channel sizes with radiuses $R_1=50mm$, $R_2=25mm$ and the initial radial V_{r1} equal to 1 we got the 3-d graphic **Fig.5.**

This graphic dependence shows that when gas flow movement along the curvilinear channel near the walls radial speed component is zero, when rising the angle φ first the speed component value decreases to the minimal one and then after the redistribution and passing the maximal wide section it begin to increase. This phenomenon occurs because of the sufficient inertial force presence which let the drops be caught in the filtering element, which is situated in the louver hollows. The above stated ideas and research results of the fields speeds and pressure motivated us to invent a new mode of the high dispersion drop liquid separation from the gas fluid flow and to create a model of the high effective inertial filtering drop catcher with the low hydraulic resistance ., **Sklabinskiy et al., 2009**. Speed pressure in the windy zone of

the separation channel lug is enough to create the pressure drop (motive power) on the both sides of the double louver from the different channels sides for getting through the net louver but not in the thick filtering material layer between the channels. **Fig.6**. Besides in this section of the double louver from the other channel side there is a low pressure zone (pocketing zone) or the vortex zone, it depends on the intensiveness of the hydrodynamic regime entire rushing phase movement along the separation.

6. CONCLUSIONS

1. On the basis of the processes which take place in the IF gas separation channel the main assumptions are made which can be used for the mathematical model creation.
2. One selected and simplified the main mathematical dependences taking into consideration the taken assumptions and limit conditions Mathematical modeling is made in the program complex Maple and one received the 3-d graphic which shows the pole speed in the channel.
3. There are worked out the theoretical basis of the separation process in the IF separator and the main recommendations as to the fog separation using the new method.

REFERENCES

Al Rammahi Mustafa, Logvin A.V., 2011. *Lyaposchenko O.O./Physical Model Gas liquid Flows Movement in the Separation Channels and Filtering Sections of the Inertial Filtering Gas Separators* , Oil and Gas Energetic.. - №2(15), P.5-11.

Barilovych V.A., 2009. *The Main Principles of the Thermal Gas Dynamics in Two Phase Flows and Their Numeral Values: Study Guide* -SPb.: Polytechnical University Printing, 425 p.

Lyaposchenko O.O. 2005.*Increasing Effectiveness Separation Apparatus for the Gas and Oil Industry Compression Units*, Lyaposchenko O.O., Sklabinskiy V.I., Sumy State University Visnuk. Series “Technical Studies”, №1(73), P.58-68.

Lyaposchenko O.O. 2006. *Hydrodynamics of the Inertial Filtering Separation Apparatus for the Natural Gas Depuration:dissertation.* Associate of Technical Science : 05.17.08 : reported 18.05.06 : approved. 04.07.06 , Lyaposchenko Oleksandr Oleksandrovych, Sumy, 152 p. Bibliography.: p. 137–149.

Poole C.F., 2000 and *Cooke M., Wilson I.D. Encyclopaedia of Separation Science*. Academic Press, UK, 4927 p.

Sinayskiy E.G., 2002. *Lapiga E., Zayzev U.V, Multi Phase and Multi Components Systems Separation.* M.: Nedra-Business center, 621 p.: pic.

Sklabinskiy V.I., , 2009 L*yaposchenko O.O.,Logvin A.V., Mischenko O.S.,* Patent of Invention *№88558* C2 Ukraine, МПК B01D45/04. *The Method for High Dispersion Liquid Catching from the Gas Fluid Flow and The Apparatus For I*t. /№200802372; declared 25.02.2008; published 26.10.2009, bulletin №20. Stepanov G., Zitser I.M. 1986. *Inertial Air Cleaners*. – M.: Mashino stroyeniye,184 p .

Table.1. List of symbols

Symbol	Description	Unit
R_1, R_2	Raduius corrugations of the separation channel	m
ε	The coefficient of turbulent viscosity	m^2/sec
Vr, V_φ, V_z	The components of the gas velocity (the radial, tangential, axial)	m/sec
V_{r1}	The initial radial velocity of the gas	m/sec
C_1, C_2, C_3	The constants of integration	-
P	Pressure	Pa
θ	Angle of corrugation	rad
ρ	Density of gas	kg/m^3

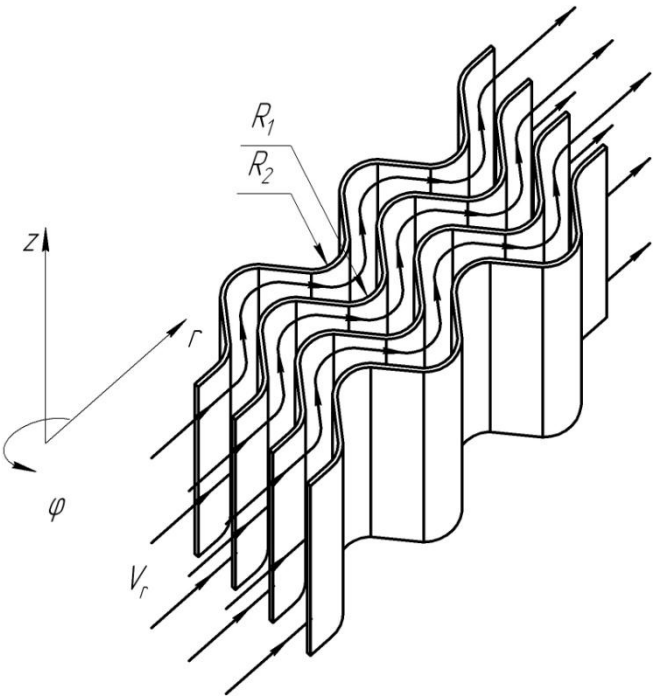

Figure. 1. The calculating scheme of the purifying gas movement through the IF separator louver board.

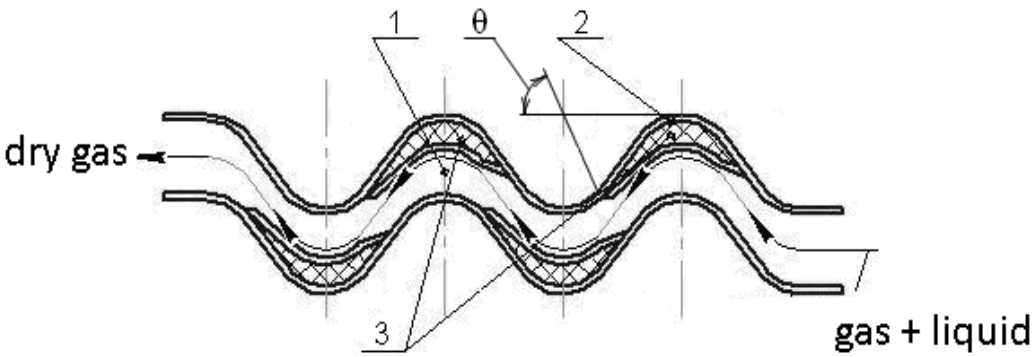

Figure.2. Calculating scheme of the gas liquid drop flow movement along the separation channel with filtering sections IF separation apparatus: 1. - separation channel; 2- double louver crimping plates; 3- filtering sections.

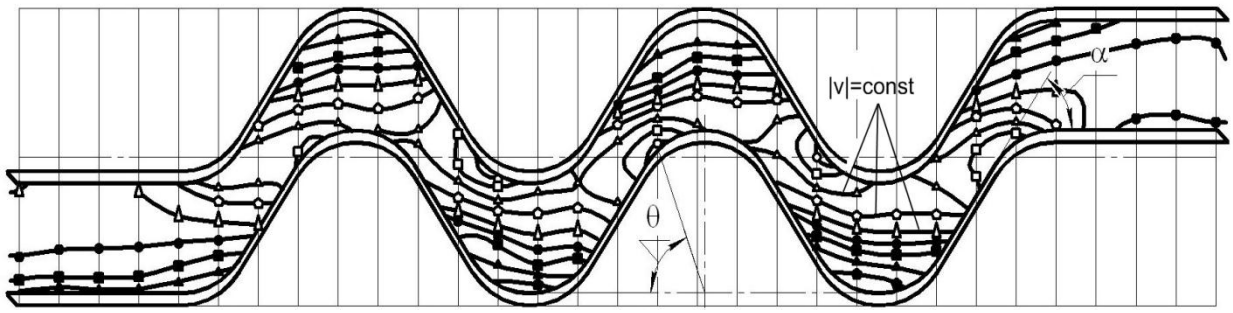

Figure.3. Local speeds distribution.
v, m/s, gas flow movement along the inertial separation channel section of the inertial filtering gas separator physical model
(Re=50000): ○ – v=7,0 m/s м/с; □ – v=6,00 m/s; Δ – v=4,0m/s; ■– v=2,0 m/s; ▲– v=1,5 m/s; ● – v=1,0 m/s.

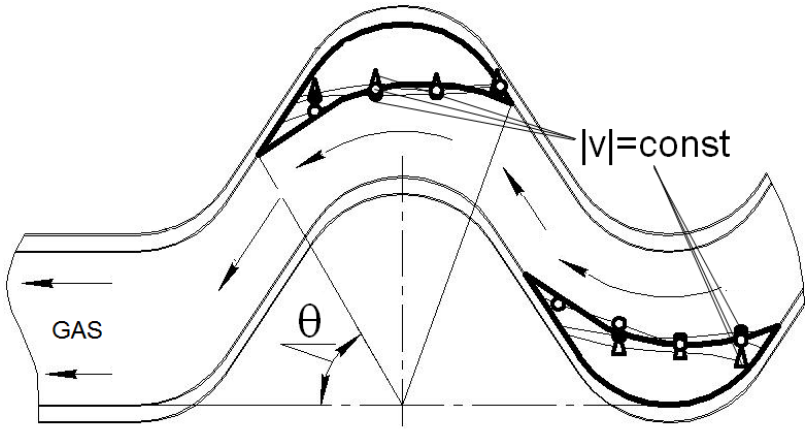

Figure.4. Geometrical zones of the filtering sections in the separation channel of the louver inertial filtering gas separator disposition. (Re≥10000).

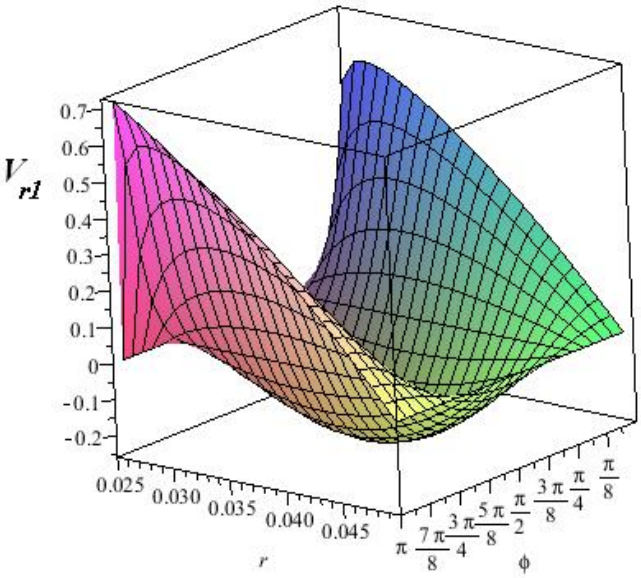

Figure.5. The example of the graphic results for calculation the changes of the radial component for the gas flow speed along curvilinear channel with sizes R_1=50mm, R_2 =25mm and the radial component of the gas flow speed atφ_0=0 equal toV_{r1}=1 m/sec.

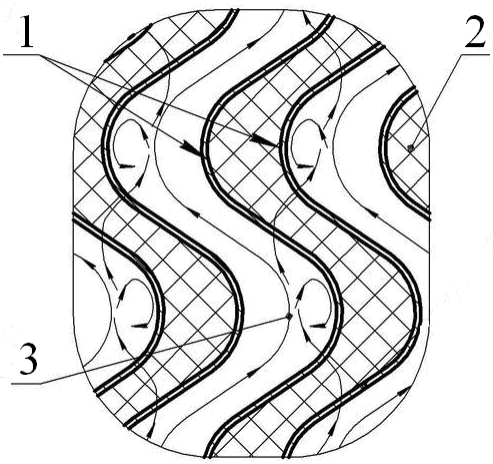

Figure 6. the gas fluid movement along the separation board of the IF drop catcher scheme:
1 – double louver crimped plate made of net, 2 – filtering element, 3 – gas fluid flow.

List of Contents

English Section: Page

Fabricating a New Rheometer for Concrete 1 - 24
Prof. Dr. Rafa Hashem Shaker
Prof. Dr. Nada Mahdi Fawzi
Lect. Dr. Laith Al-Jabri

Studying the Behavior of Asphalt Stabilized Gepseous Soil for Earth Embankment Model 25 - 43
Hussein Q. Kasim Abdulameer
Saad I. Sarsam
Mahmood D. Ahmed

A Comparative Study of Various Intelligent Algorithms Based Nonlinear PID Neural Trajectory Tracking Controller for the Differential Wheeled Mobile Robot Model 44 - 60
Ahmed Sabah Al-Araji

Analysis of Mosul and Haditha Dam Flow Data 61 - 75
Ahmaed Mohammed Ali
Maryam Naeem Odaa

Dynamic Behavior of Pb(II) and Cr(III) Biosorption onto Dead Anaerobic Biomass in Fixed-Bed Column, Single and Binary Systems 76 - 94
Abbas Hameed Sulaymon
Shahlaa Esmail Ebrahim
Mohanad Jasim Mohammed Ridha

Biogas Recovery from Anaerobic Co-Digestion of Poultry House Wastes for Clean Energy Production 95 - 108
Dr. Zainab Ziad Ismai
Ali Raad Talib

A study of the Effect of Air Inlet and Exit on Indoor Air Movement 109 - 125
Abdual Hadi Nema Khalifa
Ahmed Jasim Hamad
Johain Joudet Faraj
Ahmed Qasim Ahmed

Experimental and Numerical Analysis of Incompressible Flow over an Iced Airfoil 126 - 145
Karima E. Amori
Ethar Saad Ahmed

Deep Desulfurization of Diesel Fuel by Guard Bed Adsorption of Activated Carbon and Locally Prepared Cu-Y Zeolite 146 - 159
Nada Mustafa Hadi
Asst. Lect. Sarmad Abdul-Razzaq Rashid
Asst. Lect. Suheila abdalreda akkar

Gas Flow Formation In The Inertial Filtering (IF) Gas Separators Curvilinear Channels **160 - 169**
Prof. Vsevolod Ivanovich Sklabinskyi
Asst. Prof. Aleksandr Aleksandrovich
Asst.Lect. Andrey Vladimirovich Logvyn
Ph.D. Student. Mustafa Makki Al Rammahi

اثر تكنولوجيا النظم ألمنشئية في النتاج المعماري المعاصر

م.د.صفاء الدين حسين علي
الجامعة التكنولوجية/ قسم الهندسة المعمارية
Inana_ar@yahoo.com

الملخص

يتناول هذا البحث دراسة اثر تكنولوجيا النظم المنشئية في النتاج المعماري المعاصر من خلال دراسة التطور الحاصل في تكنولوجيا النظم المنشئية من مواد وطرق تشييد فضلاً عن الثورة الرقمية وما وفرته من امكانيات التصميم المعماري والانشائي في خلق نتاج معماري متميز، اذ أعدت تكنولوجيا النظم المنشئية هي مصدر الابداع في النتاج المعماري.

يفترض البحث ان تكنولوجيا النظام الانشائي قد حققت الابداع في النتاج من خلال المواد وطرق التشييد والتصميم الرقمي، طالما ارتبطت التكنولوجيا بالتوجه العالمي والعولمة ولكن التوجهات المعاصرة تؤكد امكانية التكنولوجيا كفكر من تحقيق سمات المكان وتاكيد المحلية من خلال تكنولوجيا النظم المنشئية، وعليه اصبح هدف البحث توضيح مفهوم تكنولوجيا النظم المنشئية من خلال تعريف مفاهيم النظام بصورة عامة والنظام الانشائي بصورة خاصة لتحديد الجوانب التي يدعم فيها التطور التكنولوجي للنظم المنشئية والتي تم تلخيصها في البحث اولا، ثم تحليل العلاقة بين تكنولوجيا النظم المنشئية والنتاج المعماري. توصل البحث الى بناء اطار نظري للمفردات الرئيسة والثانوية وصيغها الممكنة لتكنولوجيا النظم المنشئية وتطبيقها في عدد من المشاريع المعمارية التي عرفتها الادبيات بالتميز المعماري في تكنولوجيا النظم المنشئية.

وقد اشر البحث دور التكنولوجيا وتقدمها وتطورها في كافة المجالات وخاصة في استعمال وتطور المواد الانشائية وطرق الانشاء وكذلك التقدم الحاصل في استعمالات وتطبيقات البرامج الرقمية في خلق نتاج معماري مميز ضمن سياقه المكاني–الزماني.

الكلمات المفتاحية: التكنولوجيا، ألنظم المنشئية، النتاج المعماري المعاصر، البرامج الرقمية.

The Impact of Construction Systems Technology in Contemporary Architectural Product

Dr. Safaa AlDeen Hussain Ali
Lecturer
University of Technology/ Architectural Department
Inana_ar@yahoo.com

ABSTRACT

This research examines the impact of construction technology systems in contemporary architectural production through the study of the evolution in it systems, construction materials and methods of construction in addition to the digital revolution which provided possibilities of structural and architectural design in creating a distinct architectural product, as considered construction systems technology is the source of creativity in the architectural product, the

research is assumed that the construction systems technology have achieved a structural innovation in production through the materials and methods of construction and digital design.
For Long time technology was connected to the global trend, but the contemporary trends of technology pointed out the possibility of achieving the character of place and confirm locality through construction systems technology, And it became this research to clarify the concept of construction systems technology through the definition of the concepts of the system in general and structural system in particular to identify aspects that supports the technological development of construction systems Which are summarized first, then analyze the relationship between construction systems technology and architectural product.
The research reached to build a theoretical framework for the main and secondary vocabularies of construction systems technology and their possible formulations and their applications in a number of architectural projects that have defined by the literatures as excellence in construction technology systems .
The research pointed out the role of technology and its progress and development in all fields, especially in the use and development of construction materials and methods of construction as well as advances in the computer applications in creating distinctive architecture within its spatial - temporal context.
Keywords: Technology, Construction Systems, Contemporary Architectural Product, Construction materials, Computer Applications.

المقدمة

يشمل تطور تكنولوجيا البناء اكثر من حقل من مجالات العمارة ولكن أصبح هذا التطور فى كل جوانب العمارة المعاصرة، حيث بدأ المصممون المعماريون والإنشائيون استخدام كل ما هو جديد من تطورات المواد البنائية وتقنيات الإنشاء الحديثة والنظم المنشئية التي أصبحت تلبى كل متطلبات العمارة الحالية.

يتناول البحث موضوع تكنولوجيا النظم المنشئية واثرها في النتاج المعماري المعاصر من خلال تعريف مفهوم النظام بصورة عامة وتاثير التكنولوجيا كنظام متعدد الابعاد في النظم المنشئية وعليه حددت:

مشكلة البحث: عدم وجود تصور واضح حول اثر تكنولوجيا النظم المنشئية كنظام (فكري انشائي) في النتاج المعماري المعاصر.

فرضية البحث: يتباين تحقيق ابعاد التكنولوجيا في النظم المنشئية باختلاف طبيعة المشاريع واهداف المصمم.

أهداف البحث:-

بناء اطار نظري شامل لابعاد تكنولوجيا النظام الانشائي.

توضيح اثر تكنولوجيا النظم المنشئية في النتاج المعماري المعاصر.

ولتحقيق اهداف البحث تم اعتماد الهيكل الاتي:

1. تعريف مفهوم النظام الانشائي من خلال تعريف مفهوم النظام بصورة عامة والنظام الانشائي بصورة خاصة واهم خصائصها.
2. وضع اطار نظري للتكنولوجيا كنظام متعدد الابعاد واثرها في النظم المنشئية للنتاج المعماري المعاصر.
3. اختبار فرضية البحث من خلال تطبيق مفردات الاطار النظري في عدد من المشاريع المنتخبة.

1- النظم المنشئية

1-1 مفهوم النظام

يشير (بريجز)، الى ان مفهوم النظام يسشمل معظم جوانب الحياة المختلفة ، فهناك نظم الارقام، والزمان ، والمكان ....الخ لذا فمن الصعب ايجاد تعريف محدد لنظام ولكن المهم اسلوب التفكير في هذا النظام [ابريجز 1986 ،ص 32] ، ولهذا نجد مجموعة من التعاريف للنظام تشترك معظمها بجوانب معينة , منها:

اولا: لغويا[1]

في العربية : مشتق من الفعل نظم ، ينظم، اي الجمع. ونظمت الشعر اي التاليف، وفي الانكليزية.

system : A group of interacting, interrelated, or interdependent elements forming a complex whole. A functionally related group of elements.

ثانيا: اصطلاحيا

اصطلاحيا نجد مجموعة من التعاريف للنظام تشترك معظمها بجوانب معينة , منها:

1- هو الكيان المتكامل الذي يتكون من اجزاء وعناصر متداخلة تربطها علاقة تبادلية من اجل اداء وظائف وانشطة تكون محصلتها النهائية الناتج الذي يحققه النظام كله . [السلمي، 1978، ص73]

2-مجموعة من عدة عناصر او الأجزاء التي تتفاعل وتتكامل مع بعضها البعض ومع بيئتها، وفق قواعد محددة، لتحقيق أهداف معينة.(العمري، 2009، ص10)

3-يتكون النظام من مجموعة من الانظمة الثانوية بوصفها مكونات او عناصر او اجزاء، ويشترك مع انظمة اخرى ليشكل نظاما اكبر، وان ما نسميه بنظام رئيس يمثل حالة نسبية لا حالة مطلقة. (العلي،2001، ص 121-134)

وتعرفه الاكاديمية العربية للتعليم العالي[2] بانه:

4-مجموعة عناصر متفاعلة فيما بينها، لأجل تحقيق هدف محدد .أو هو ببساطة مجموعة من النظم المتفاعلة، فالكون نظام، والذرة نظام، ووزارة التجارة نظام، وإدارة الموارد البشرية نظام.... الخ.

5-مجموعة من النظم الفرعية Subsystems ترتبط مع البيئة Environment بواسطة علاقات Relationships لتحقيق هدف Goal. والنظم الفرعية هي المكونات الأساسية للنظام، أما البيئة فهي ما يحيط بالنظام وتؤثر وتتأثر بذلك النظام، من خلال العلاقات التي تربط النظم الفرعية مع النظام، وكذلك العلاقات بين النظام البيئة.

6- هو مجموعة من الاجزاء المصممة والمتوافقة بهدفها ومحتوياتها ومكوناتها الثانوية,مرتبطة وفق سياسية تنفيذية متسلسلة وفق نسق يؤدي الى تركيب او تشكيل مقصود لتحقيق مقاصد معينة لاداء فعاليات متغيرة.

7- هو تكوين متكامل لمجموعة من الاشياء او الاجزاء المادية والروحية المترابطة مع بعضها وفق قواعد معينة وبتسلسل ثابت لتشكل مجتمعة مفهوما.

8- مجموعة من الانظمة المتسلسلة بالاهميات تشكل مجتمعة و وفق اسس محددة نظما اكبر واكثر اهمية.

من التعاريف اعلاه نلاحظ تكرار كلمات مفتاحية كالمكونات والعلاقات, أن تكرار بعض المفردات في هذه التعاريف يؤكد أهميتها, ومن جهة اخرى بعض هذه التعاريف رغم توافقها مع التعاريف الاخرى الا انها تمتلك خصوصية للتوجه المقصود فالتعريف الثاني الذي يخص البحث قادر على ان يلي مقاصد تكنولوجية او تصنيعية او تنفيذية في مؤسسات التشييد مثلا.

---

[1] http://www.thefreedictionary.com

[2] **Arab British Academy for Higher Education p. 1, www.abahe.co.uk,**

الملاحظة المهمة الاخرى هو انه النظام الذي نعرفه يتكون من مجموعة من انظمة ثانوية كالمكونات او عناصر وهو بحد ذاته يشترك مع انظمة اخرى ليشكل نظام اكبر وان ما نسميه بنظام رئيسي يمثل حالة نسبية لاحالة مطلقة كما ان هذا يعني ان كل مافي الكون يتشكل من مجموعة انظمة اصغرها(ربما نظام نواة الذرة) واكبرها ما يشكل النظام الكوني المتكامل الذي هو دون خالق الانظمة وفاطر السموات والارض.

لذا فالنظام يختلف عن المكونات والعلاقات والقواعد ولا يمثل مجموعة الاجزاء بل تتحقق بهدف ويطبق بهدف ويتغير بهدف ويحدث كل هذا بمنهجية دقيقة وهكذا تصبح المنهجية والنظام متطابقان بالاهداف..

بالاعتماد على التعاريف نستطيع القول بان كل نظام يتكون من عناصر (او نظم ثانوية) لا تقل عن ثلاثة ترتبط بعلاقات تحكمها قواعد ويتحقق النظام بهدف ويتفاعل ضمن حدود "

أن هدف التعريف يمثل ما تطرحه نظرية النظام العامة ويشكل الاساس النظري لمفهوم يتحقق على الصعيدين الفكري والتطبيقي (الممارساتي).. (نظام من عناصر + علاقات + قواعد + اهداف + حدود) يقودنا الى التفكير بالنظام (system Thinking) وان اهم ما يميز النظم قدرتها على التطور والحركة فهي ليست كيانات ثابتة والا تعرضت الى الاندثار سائر الانظمة الحية الاخرى التي لم تستجيب للتطور ولم تمتلك القدرة على التكيف لمتطلبات الزمان والمكان.

2-1 تصنيفات النظم

يمكن تصنيف النظم إلى عدة تصنيفات حسب طبيعة النشاطات والإجراءات الخاصة بالنظام أو حسب طبيعة البيئة المحيطة بهذا النظام، وقد قسم النجار النظم إلى عدة تصنيفات وهي كالتالي: (العمري،2009، ص11-12)

اولاً: النظم الطبيعية والصناعية

تمثل النظم الطبيعية النظم الموجودة بالطبيعة مثل : نظام دوران الأرض ، الفصول الأربعة ، وتسمى هذه النظم بالنظم الكونية ، أما النظم الصناعية فهمي نظم من ابتكار الإنسان مثل: أنظمة الحاسوب ، ألانظمة الانشائية، الانظمة الادارية...الخ.

ثانيا: النظم المغلقة والمفتوحة

النظام المغلق هو النظام المفصول عن البيئة المحيطة لا يتأثر ولا يؤثر بها ولا توجد بينهما أي حدود مشتركة مثل: النظام الذري، التفاعل الكيماوي المعزول . أما النظام المفتوح فهو النظام الذي يتفاعل مع البيئة المحيطة يتأثر ويؤثر بها، ويكون له علاقة مستمرة معها مثل نظم المنظمة المختلفة.

ثالثاً: النظم المحسوسة والمجرد:

تتكون النظم المحسوسة من مجموعة من العناصر الطبيعية أو الصناعية المحسوسة مثل: نظم الحاسوب وتسمى أيضا بالنظم المادية أما النظم المجردة فهي النظم التي لا يمكن لمسها ، إنما يكون تصورها عقليا مثل نظام العد والنظرية النسبية.

رابعاً: النظم الثابتة والنظم المتغيرة:

النظام الثابت هو النظام الذي عمل ضمن آليات محددة سلفا وبشكل شبه مطلق، ويمكن التنبؤ بدقة سلوكه مستقبلا مثل: النظام الكوني، نظام البرنامج الحاسوبي . أما النظام المتغير فهو النظام الذي يعمل وفق آلية معينة ثابتة وبشكل مستمر، ولا يمكن التنبؤ بسلوكه مستقبلا بشكل حتمي مثل: النظم الإدارية والمالية والاجتماعية.

وبالنظر إلى تصنيفات النظم اعلاه نلاحظ ان النظم الصناعية هي نظم من ابتكار الانسان وانها نظم مفتوحة تتعامل مع البيئة المحيطة وسياقها المحيط ولها علاقة مستمرة معها وهذا ما يعرف النظم المنشئية.

3-1 النظم المنشئية

يتكون النظام الانشائي من عناصر ومكونات انشائية مترابطة ومتفاعلة مع بعضها البعض لاتمام الوظيفة الانشائية المحددة للمنشأ مع توفير عناصر الثبات والاستقرار. (Macdonald, 2001, p.xi)

هنالك تمييز بين مفهومي العلاقة (Relationship) والمكونات التي تشكل لوحدها نظام فهنالك عدة فوارق بين العلاقة (Relationship) والنظام (System) ونخص بالذكر المقاصد التنفيذية والانشائية وللاسباب التالية : Broadbent, (1973,375)

أ- تتكون العلاقة بين عنصرين او عضوين ويمكن تحليل العلاقات المركبة بصورة ثنائية. أما النظام فيشمل عددا غير محدد من العناصر والمكونات غير قابلة للتحليل في بعض الاحيان بصورة ثنائية.

ب- تكون العلاقة بين عنصرين فقط ترابطا ولايشكل هذان العنصران المترابطان نظاما بل ترابطية كما ان الترابطية تدخل بعلاقة العنصرين بموجب مواصفات وخصائص بارزة وثابتة.

ت- لكي يوجد النظام يجب وجود ارضية بعدية (Dimensional Domain) وان النظام تشكيل محدد تتوزع المكونات وتربط بعلاقات وفق قواعد محددة ضمن ارضية محددة اي هنالك حدود لوجود النظام كما في الشكل (1).

تختلف النظم المنشئية في اشكالها وعناصرها وفي الياتها في نقل القوى المؤثرة والاحمال المسلطة عليها، كما تختلف في كيفية التعامل مع مواد البناء الحديثة. ويعتمد اختبار النظام الانشائي على طبيعة الفعالية الوظيفية، والعامل الاقتصادي، ومواد البناء المستخدمة. **(Ali & Kyoung Sun (2007)**

مما تقدم ان النظم المنشئية تعتمد على نوع وترتيب العناصر الانشائية الرئيسية وطريقة التكوين وانتقال الاحمال المسلطة عليها.

2- تكنولوجيا النظم المنشئية

2-1 تعريف التكنولوجيا

تتزايد اهمية التكنولوجيا في عالمنا المعاصر لانها تؤدي دورا واضحا يؤثر في النتاجات المعمارية في عصرنا الراهن الذي يمثل ذروة التطور التكنولوجي وزيادة القدرات التكنولوجية، وتمثل التكنولوجيا في بعض جوانبها آلية تحقيق حاجة الانسان المادية والروحية بتوفير وسيلة.وما الاختراعات الا اضافات الى الخزين التأريخي كجزء من التطور التأريخي فاختراع العجلة يمثل قفزة تاريخية حققتها التكنولوجيا لخدمة الانسان.

تشير الدراسات الى عدم وجود تعاريف متفق عليها للتكنولوجيا فالتعريف يختلف باختلاف التوجه المعرفي، ويمكن تعريفها بانها تقنية الاستخدام التطبيقي للعلاقات والقوانين والخصائص الجوهرية للمواد وتركيباتها للوصول الى شكلية مادية جديدة قادرة على اداء مهمة معروفة الابعاد والخصائص.

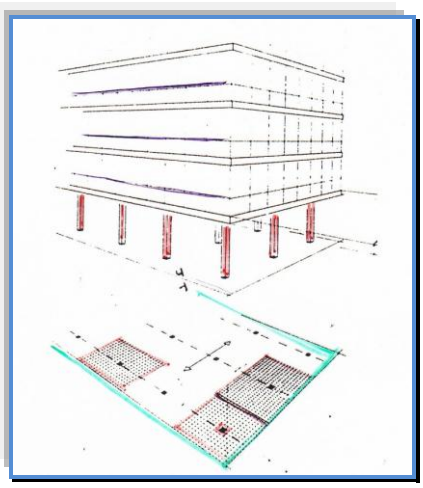

شكل 1: علاقة العناصر المنشئية ضمن قاعدة بعدية / اعداد الباحث

2-2 التكنولوجيا والعمارة

يرى الجادرجي العمارة من المنظور التكنولوجي بوصفها عملية يتفاعل فيها الحاجة والفكر والتكنولوجيا من جهة والمواد الاولية من جهة اخرى. فالتكنولوجيا منظومة فعل انساني تتداخل مع منظومات معرفية او اخلاقية لتكون نظاما (كلا ثقافيا) يميز مجتمع عن اخر ويتحكم في النتاج المادي والفكري للمجتمع.

كان مصطلح تكنولوجيا العمارة Architectural Technology يعني في خمسينات القرن الماضي بانه التفاصيل الانشائية للمبنى Building Details وتفاصيل مواد البناء وطرق التشييد دون الاشارة الى القيم المعمارية والفكرية، بداية السبعينات بدأ التوجه اكاديميا ومهنيا نحو التعامل مع التكنولوجيا بشمولية وكنظام متكامل فكري ومادي يتم فيه التعامل مع جميع المعطيات الفكرية والتي تشمل المحلية والطراز المعماري والمادية والتي تشمل دراسة المواد والتفاصيل الانشائية والتصنيع ...الخ. (Matteol and Peretti 2013)

هناك علاقة بين العمارة وتكنولوجيا الانشاء، تاخذ هذه العلاقة عدة اشكال والدور الذي تلعبه التكنولوجيا في النظم المنشئية يؤثر بصورة كبيرة في العمارة كنتاج، ترتبط العمارة وتكنولوجيا الانشاء بطرق عدة ابتداءا من السيطرة التامة للهيكل الانشائي في الشكل المعماري الى الاهمال الكلي للمتطلبات الانشائية مقابل المعالجات المعمارية. (Macdonald, 2001,p73)

أصبحت عملية التطور التكنولوجى للعمارة واثرها في النتاج المعمارى هامة جداً فى ظل طفرات معمارية هائلة انتقلت من مرحلة إلى أخرى فى مراحل التطور التكنولوجى الهائل حيث اكتشاف المواد الإنشائية الجديدة والنظم الإنشائية المتعدة وآلية التنفيذ المتقدمة وفائقة السرعة والتقدم لتوفير الوقت والجهد، واكتشاف بعض مواد البناء الجديدة كالالياف الزجاجية واللدائن ورقائق الالمنيوم والمواد النانوية وقد تأثر التصميم المعمارى على وجه الخصوص والمنشآت المعمارية على وجه العموم بهذا التطور التكنولوجى الهائل.

إن تطورات تكنولوجيا العمارة فى تحديث دائم حيث أنه من الممكن أن مواد البناء ووسائل التنفيذ ونظم الإنشاء المستخدمة اليوم لا تستخدم بعد مرحلة زمنية قادمة ويتم تحديث هذه المواد وغيرها.

التكنولوجيا ← فكري (نظم فكرية)

التكنولوجيا ← مادي (نظم منشئية)

ولهذا سياخذ البحث في المحور الاتي دراسة تكنولجيا النظم اللمنشئية واثرها في النتاج المعماري المعاصر.

3- استعراض الدراسات السابقة

ولغرض دراسة العلاقة بين تكنولوجيا النظم المنشئية والنتاج المعماري (العمارة) تم استعراض اهم الادبيات التي تناولت الموضوع باختلاف توجهاتها البحثية.

3-1 الدراسات العالمية

وشملت مجموعة الدراسات الاتية:

اولا: دراسة كريس ايبل (Abel,Chris 2004) في كتاب تكنولوجيا ومراحل العمارة،

Architecture Technology and Process

طرح الكتاب من خلال استعراض تكنولوجيا العمارة وعمارة التكنولجيا اسلوب الدمج بين التقنية العالية والعوامل المكانية وامكانية استخدام التقنيات الحديثة مع الاخذ بالاعتبار امكانيات الموقع والمواصفات المحلية (خصائص المكان).

طرح الكتاب في الفصل الرابع المقارنة بين اسلوب المعماريين نورمان فوستر وفرانك كيري والمنهج المعتمد من قبل كا منهما في التصميم والذي يركز على جوانب التشابه في اعمالهم في التعامل مع سياقية المكان والاختلاف في التكنولوجيا الرقمية المعتمدة في تطوير افكارهم التصميمية.

بهذا نجد ان الكتاب طرح اهمية العوامل المكانية كاحد الجوانب التي يجب ان تتباناه تكنولوجيا العمارة والانشاء ودور التكنولوجيا الرقمية في التصميم في اختلاف النتاج المعماري، نظرا لامكانياتها التعبيرية الكبيرة في خلق الفضاءات والاشكال الافتراضية من جهة وفي معالجة الجوانب الانشائية من جهة اخرى.

ثانيا: دراسه جيولا سيبستين (Gyula Sebestyen2003) في كتاب العمارة الجديدة والتكنولوجيا

New Architecture and Technology

يتناول الكتاب العمارة الجديدة والتكنولوجيا والإمكانات القوية الممكن في تقاطع الممارسة المعمارية والهندسية المتقدمة. ويقترح توجيه المهندسين المعماريين والمهندسين على إمكانات التكنولوجيات الجديدة في مشاريعهم و على القضايا التي يجب معالجتها لدمج هذه التقنيات بنجاح.

وضح الكتاب التداخل بين العماره وتكنلوجيا المواد البنائيه وكيفيه مواكبة التطور الاجتماعي والاقتصادي موضحا انواع الهياكل الانشائيه تبعا لتطور التصميم الانشائي. واشر امكانية فهم تأثير التكنولوجيا من خلال الأمثلة من المباني المعاصرة، والتعلم من التقييم العملي من النجاحات والإخفاقات في مجال العمارة الحديثة، فضلاً عن الإلهام من تفسير اتجاهات التصميم الحالي.

يوضح الكتاب كيف تطورت المباني والمدن لتلبية احتياجات الناس الذين يستخدمون أحدث التقنيات، ليس فقط المهندسين المعماريين في التخطيط والتصميم باستخدام برامج الكمبيوتر المطورة حديثا ، ولكن يتم بناؤها هياكلها مع تقنيات البناء الحديثة وتحسين مواد البناء باستمرار.

تناول الكتاب في الفصلين الاول والثاني تاثير التكنلوجيا على مواد البناء من خلال استعراض مواد البناء الحديثة وتاثير التكنلوجيا في الهياكل ألمنشئية للمباني من خلال التعرف على تفاصيل التصاميم الانشائيه فيما بين الفصل الثالث دور التكنلوجيا في تغيير نمط الخدمات كما وضح الفصل الرابع تاثير التكنلوجيا في التصميم المعماري من حيث الشكل المعماري.

ثالثا: دراسة ستيفان ايمت[3] (Stephen Emmitt,2011)، التصميم التكنولوجي في السياق المتعدد التخصصات الحسية، Technological design in A Multidisciplinary Sensory Context,

تناول البحث العلاقة بين تكنولوجيا العمارة من خلال تكنولوجيا الرقمية في التصميم وتكنولوجيا الانشاء والتصاميم التفصيلية، موكداً التحدي الذي يوجه المصمم في اختيار الحلول الانشائية والمواد الي تناسب الطراز المعماري، كما طرح البحث اعتماد المواد البنائية الجديدة او اعادة استخدم المواد التقليدية بطرق انشائية جديدة.

ان تكنلوجيا العماره قد جلبت المعرفة بين التصميم المعماري ونظم الانشاء ومكنت المعماريين من اظهار المهارات الفنيه لخلق الاشكال المبدعة. كما اكد البحث اهمية الاستدامة المحلية ليس من خلال التكرار الحرفي ولكن من خلال توظيف الانماط التي ممكن ان تضيف قيم جديدة للمجتمع، من خلال تقنيات البناء والتفاصيل المعمارية الجديدة.

رابعا: دراسة ماريو لوساسو (Mario Losasso 2011) المشروع كنتاج للبحث العلمي
The Project as Product of Scientific Research

يطرح البحث دور البحث العلمي التقليدي في المشروع المعماري من خلال دراسة التاثير الاجتماعي والاقتصادي والبيئي، ومع ازدياد الحقول المعرفية المرتبطة بتصميم المشروع وازدياد اهمية التصميم التكنولوجي في تقديم الحلول لكثير من المشكلات او المعوقات الانشائية التي تضمن نجاح المشروع، مشيرا بذلك الى المعرفة (know–how)، مع المناهج النظرية والتطبيقية للمعرفة.

اشار الباحث الى ان التصميم المعماري المعاصر هو تصميم تكنولوجي قائم على المناهج والادوات لربط الجوانب الوظيفية والانشائية للمبنى مع السياق المحيط، اذ تزداد اهمية تطور العناصر التكنولوجية في المشروع مع ازدياد حجم وتعقيد المشروع، وطرح اهمية تكنولوجيا الانشاء في الاخذ بنظر الاعتبار التوجهات المعاصرة في الاستدامة في المعالجات البيئة والمكانية وبما يتوافق مع متطلبات السياق المحيط بيئيا واجتماعيا ومكانيا.

2-3 الدراسات المحلية وتشمل:

اولا: دراسة هوشيار قادر 2003، العمارة والتكنولوجيا، اطروحة دكتوراة ، جامعة بغداد، كلية الهندسة، قسم الهندسة المعمارية.

عرفت الدراسة العمارة كفعالية تكنولوجيا لانها تتعامل مع ظاهرتي العمارة والتكنولوجيا، على انهما ظاهرة واحدة تشكلان في النهاية ظاهرة واحدة.

ناقشت الدراسة خصوصية حركة التكنولوجيا في العمارة واعتماد الافعال التكنولوجيا في نظم العمارة الرئيسية، كما تطرقت الى العلاقة بين العمارة والنظام وتحديد النظم الرئيسية المتمثلة بالفكر والمادة والشكل. وان العمارة خاضعة لمفهوم النظام وقواعده ، ذلك النظام الذي يتالف من مجموعة من الاجزاء لها وظائفها وتربطها علاقات منظمة وهذه الترابطات هي التي تقرر نوع النظام، واوضحت الدراسة مصادر الشكل المعماري التي قد تكون ناتجة عن امكانيات المواد البنائية او عناصر المنشأ، او الخواص الهندسية التي تقرر الشكل النهائي للعمل المعماري.

[3] طرح دراسة ستيفان ايمت (Stephen Emmitt) في هذه الدراسة ملخصا لكتابه تكنولوجيا العمارة Architecture 2002 technology ، والذي اعيد نشره عام 2012.

ثانيا: دراسة منورة صباح الشابندر 2004، اثر التكنولوجيا على العمارة العراقية المعاصرة، رسالة ماجستير، الجامعة التكنولوجية، قسم الهندسة المعمارية.

عرفت الدراسة التكنولوجيا بالتعامل مع المادة البنائية والمفاصل الانشائية واسلوب الربط في النظم الانشائية الهيكلية من خلال المستويات الخمسة المتمثلة بخصائص المكان والخصائص الوظيفية والخصائص الشكلية وخصائص الجمال وخصائص المعنى.

اشرت الدراسة ان التكنولوجيا المعاصرة للمواد البنائية الحديثة تتعامل تصميمياً مع المادة والمفاصل الانشائية واسلوب التركيب والربط سواء كان لمادة واحدة او لعدد من المواد البنائية المنظمة هيكلياً لاعطاء هيئة او شكل يحقق المعنى او المنفعة. كما طرحت الباحثة امكانية تطويع المادة البنائية المحلية في تعزيز الفكر المحلي العراقي من خلال عدد من المفردات الرئيسة والثانوية اهمها على مستوى المواد البنائية كخصائص فنية: الصلادة الخارجية، المرونة، الشفافية، العزل الحراري، وخصائص منشأية للمواد(استعمال مواد تخفي الخصائص الانشائية او اظهارها). اما على مستوى خصائص المكان فقد طرحت الباحثة مفردتين رئيسة هي المعالجات المناخية (الانفتاح نحو الخارج –الانفتاح نحو الداخل).

ثالثا: دراسة رشا نوفل العزاوي 2005، اثر برامج التحليل الانشائي على الشكل المعماري للابنية الضخمة، رسالة ماجستير، جامعة النهرين، كلية الهندسة، قسم الهندسة المعمارية.

طرحت الباحثة الربط بين العمارة والنظم المنشئية في الابنية الضخمة (Mega Structure)، والعلاقة بين تطور وسائل تصميم الهيكل الانشائي والابداع المعماري. طرحت الدراسة العلاقة بين الشكل المعماري والشكل الانشائي من خلال الخصائص المنشئية للمواد البنائية في اخفاء او اظهار النظام الانشائي.

طرحت الباحثة النظم المنشئية في الابنية المعاصرة واهمها القشرية ،والغشائية، والمضلعة، والمقوسة والمؤطرة.

أعدت الدراسة ان برامج التحليل الانشائي ساهمت في سد الثغرات او الفجوات في عمل النظام الانشائي واجزائه داخل الابنية الضخمة (Mega Structure) ودور هذه الاجزاء واعطاء الامكانات لتغيير شكله وانحناءه او مكوناته الانشائية او المادية للوصول الى التوازن والاستقرار.

استنتجت الدراسة اهمية العلاقة بين الشكل المعماري والنظام الانشائي واهمية التطور في برامج التحليل الانشائي في الاشكال المعمارية، موضحا دور تكنولوجيا الانشاء المستخدمة في ايجاد الاشكال الحرة الجديدة، ودور التكنولوجيا في تخطي العقبات الانشائية من خلال البرامج الرقمية المتعددة التي تعالج ذلك.

رابعا: هاشم عبود الموسوي (2006)، الواقع الافتراضي للعمارة والعمران، بحث منشور.

عرض الموسوي الملامح النظرية لتأثر التشكيل المعماري بالثورة الرقمية دون التأثر بالمحددات المكانية، من خلال مناقشة العلاقة بين العمارة والثورة الرقمية، وتحليل المؤثرات الجديدة التي تؤثر حالياً وستؤثر أكثر في المستقبل على اتجاهات التشكيل المعماري: ومنها برامج الحاسوب وأدوات التصميم المستجدة، والتأثر المتزايد بالإمكانيات التكنولوجية.

تعرض الدراسة الملامح النظرية لمستقبل التشكيل المعماري موضوعةً في صورة مجموعة من الفرضيات توكد بمجملها تغير الشكل والتشكيل المعماري بسبب التدخل التكنولوجي الرقمي المباشر في أسلوب التفكير والتصميم ومكونات ومواد وعناصر الإنشاء وتنفيذ المنشآت، اذ تلاشى الحدود بين الخارج والداخل في عصر الثورة الرقمية لتتميز الحوائط الخارجية للمنشآت بإزالة تلك الحدود عند الضرورة.

حاول الباحث وضع خطوط عريضة للتحولات التشكيلية المعاصرة المأخوذة من مشاريع ظهرت اليوم وتم تنفيذها، أو من تصميمات تجريبية بدأت تظهر في المحافل المعمارية، والتي يعتقد أنها تأثرت بطريقة مباشرة أو غير مباشرة بالثورة الرقمية وما أنتجته تلك الثورة من أدوات وإمكانيات مستحدثة تخوض بها اليوم حقولا فكرية مختلفة، في عصر الثورة الرقمية يخضع التشكيل المعماري لقواعد إضافية غير التي ظهرت في عصر الثورة الصناعية مثل النسب والنمطية والوظيفية. اذ تتلاشى الحدود بين الداخل والخارج وتزداد المواد لبنائية رشاقة وخفة. وفي الحديث عن الثورة الرقمية وعلاقتها بالعمارة قسم الباحث مجالات تأثر التشكيل المعماري بالثورة الرقمية إلى خمس نقاط :

1. أدوات التصميم المعماري.
2. المستعمل.
3. المكونات الرقمية الجديدة للمنشآت.
4. الفضاءات غير المادية
5. المتطلبات والتحولات الوظيفية .

وقد اعطى الباحث مثالاً للفضاءات غير مادية التي توضح المكونات الرقمية للمنشات لتحقق المتطلبات والتحولات الوظيفية في مشروع تصميم متحف غوغن هايم الافتراضي ، فالمعماري الذي اعتاد أن يصمم فضاءات مادية ملموسة " **PHYSISCAL SPACES** " بدأ يتعلم تصميم الفضاءات الممثلة بصرياً " **CYBERSPACES** "، وتعلم أن يعي بأن هذه الفضاءات محكومة بقواعد وقوانين مستجدة أكثر تحرراً من تصميم الفضاءات الفيزيائية. شكل (2)

مما تقدم يتضح ان اهمية تكنولوجيا العمارة في النظام الانشائية من حيث المواد والتفاصيل الانشائية وطرق الانشاء والواقع الافتراضي الذي سمح للمصمم لتخطي كثير من العقبات التصميمية والتعبيرية.

4- استخلاص الاطار النظري والدراسة التطبيقية

تم استخلاص الاطار النظري للمفردات الرئيسة لتكنولوجيا النظم المنشئية والذي يشمل مفردات التكنولوجيا (الفكرية والمادية)، ومفرداتها الثانوية وكما موضح في الجدول (1).

شكل 2: التصميم الفتراضي لمعرض غوغن هايم / الموسوي ص4

جدول 1: خلاصة الاطار النظري لتكنولوجيا التظم المنشئية / المصدر : الباحث

	فكري	عالمي		
		محلي- مكاني - بيئي		
ابعاد تكنولوجيا النظم المنشئية	مادي (النظم المنشئية)	مواد البناء	خصائص فنية	الصلادة
				المرونة
				الشفافية
				العزل
			خصائص منشئية	اخفاء
				اظهار
		النظام الانشائي	قشري Shell	
			منفاخي Pneumatic	
			غشائي Membrane	
			هيكلي Skelton	
			مضلع Ribbed	
			الاطارات الفراغية Space	
		اليات التنفيذ	وحدات انشائية قياسية	
			عناصر انشائية مسبقة	
			الية تجميع الاجزاء	
			تعقيد النظام	
		التكنولوجيا الرقمية	ازلة الحدود بين الداخل	
			خفة المواد البنائية	
			تجاوز العقبات التعبيرية	
			تجاوز العقبات الانشائية	
			تجاوز العقبات الانشائية	

4-1 طرق القياس والتحليل

اعتمد البحث المنهج الوصفي التحليلي للشروحات والنصوص التفصيلية لكل مشروع مع تحليل الرسوم التي توضح الفكرة التصميمية والنظام الانشائي، ولغرض توضيحها بشكل مفصل تم تحليلها في استمارة خاصة وحسب مفردات الاطار النظري. ثم تم جمع القيم لمتحققة في جدول (2) وصولا الى الاستنتاجات.

4-2 العينة المنتخبة

تم انتخاب عينة قصدية شملت عدد من المشاريع المعمارية التي وصفتها الادبيات بالتميز والتنوع في تكنولوجيا النظم المنشئية، على مستوى تطور تكنولوجيا الانشاء وتطور تقنيات التنفيذ للنظم المنشئية، وصولا الى الشكل المعماري المتميز بالنظام الانشائي، شملت المشاريع:

اولا: مشروع مقهى وكافتريا رياح ومياه في فيتنام[4] Wind and Water 2008

تصميم: المعماري الفيتنامي "Vo Trong Nghia" – (A)

فاز المعماري الفيتنامي "فو ترونج نجيا" بجائزة العمارة العالمية (IAA) المخصصة لاستخدام مواد صديقة للبيئة في المباني الحديثة, وذلك بعد ان ابدع في مشروع مقهى "ويند اند ووتر" أو "رياح ومياه" والذي صممه ليتم تنفيذه بالكامل من "البامبو". يقول "نجيا" بعد ان استلم تلك الجائزة المرموقة, انه بدأ المشروع ليعارض به المفاهيم المستقرة عن العمارة, حيث استخدم مواد بناء تقليدية من بلده فيتنام.

وعن الجائزة يقول ان اهميتها تمثل في انها تعطي للاعمال التي نفذت على الارض وليس لمجرد مشروعات, وهذا يثبت ان الناس يبدأون في تقدير قيمة العمل بعد ان يصبح واقعاً وليس فقط نظريات. فالمبنى لايزال جميلا بعد مرور اربع سنوات من التشغيل, كما استطاع جذب الكثير من الزوار من خارج البلاد, وظهرت الكثير من المقاهي التي بنيت بنفس التصميم في اماكن اخرى تقليدا لما بدأته, والان فقد تم تأصيل هذا التيار الجديد من العمارة. شكل (3)

لقد اراد "نجيا" ان يظهر للعالم انه من الخطأ الاعتقاد بان المواد الفاخرة او عالية التصنيف مثل الزجاج والالمنيوم هي الوحيدة التي يمكن استخدامها في انشاء منازل جميلة, بل وان المواد الطبيعية وايضا عناصر الطبيعة مثل الرياح والضوء يمكن الاستعانة بها. ويضيف ان المغزى من هذه الجائزة بالنسبة له شخصيا انها دليل على ان العالم يسير في الاتجاه الذي يتبناه هو من حيث استخدام الاماكن المفتوحة والعناصر الطبيعية الخام والصديقة للبيئة مثل البامبو، فمسؤولية المعماري هي خلق عمارة قريبة من الطبيعة حتى يمكن للفقراء التمتع بها والاستفادة منها.

صنع الهيكل الانشائي بالكامل من الواح الخوص المجهزة بطرق محلية وهي رخيصة جدا، وباعتماد نظام انشائي وطرق تنفيذ محلية، معتمداً اليات النظام الانشائي القشري والتمازج مع نظام المضلعات اعتماداً على الوحدات الانشائية القياسية وآلية تجميعها وتنفيذها باشكال تتابعية تعكس خصائص المواد المرنة، بمساعدة البرامج الرقمية في تخطي وضع الرسوم والتصورات الاولية والانشائية للمشروع[5]، لاحظ استمارة القياس (1) لتفاصيل تكنولوجيا النظام الانشائي.

استمارة (1): وصف تكنولوجيا النظام الانشائي لمشروع Wind and Water /الباحث عن http //votrongnghia.com

رمز	الفكرة التصميمية	مواد البناء	النظام الانشائي واليات التنفيذ	التكنولوجيا الرقمية
A	**محلية** - خلق عمارة قريبة من الطبيعة باستخدام مواد بناء تقليدية من بلدة فيتنام. - معايشة بين المقهى والطبيعة. - الطبيعة هو مصدر معرفي.	استعمال الخوص والرباطات الخشبية في العلاقات الترابطية في نقل الاحمال والقوى ضمن الاشكال المقوسة وباشكال تتابعية منسقة تعكس طبيعة الموادالمرنة في التشكيل لاظهار الهيكل الانشائي للمبنى	يتكون الهيكل من 48 قطعة مسبقة الصنع يتكون كل منها من عدد من قطع نبات البامبو المبروطة معا ، لاحظ تفصيل (1) الشكل 3-ج استعمال الموديول التكراري في التصاميم الخارجية والداخلية.	- استخدام التكنولوجيا من خلال النظام الانشائي في العلاقات بين العناصر الخشبية ضمن برنامج حاسوبي دقيق. - اعتماد التكنولوجيا الرقمية في دراسة العوامل البيئة مثل الرياح ، لاحظ الشكل 3-ج

[5] http://votrongnghia.com/projects/wnw-bar

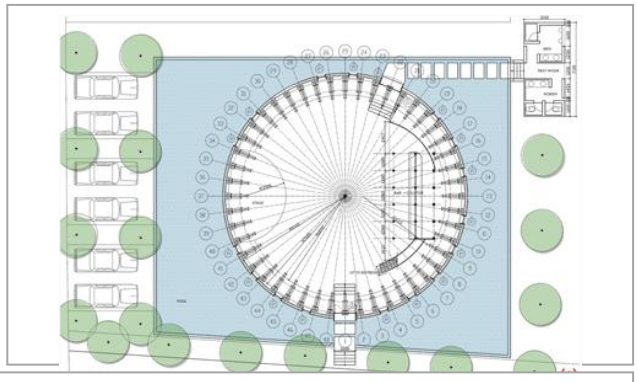

ب : مخطط افقي يوضح قطر المبنى (15 m)، وشبكة الهيكل الانشائي المعتمد

أ: المبنى ضمن الطبيعة المحيطة وتكامله معها

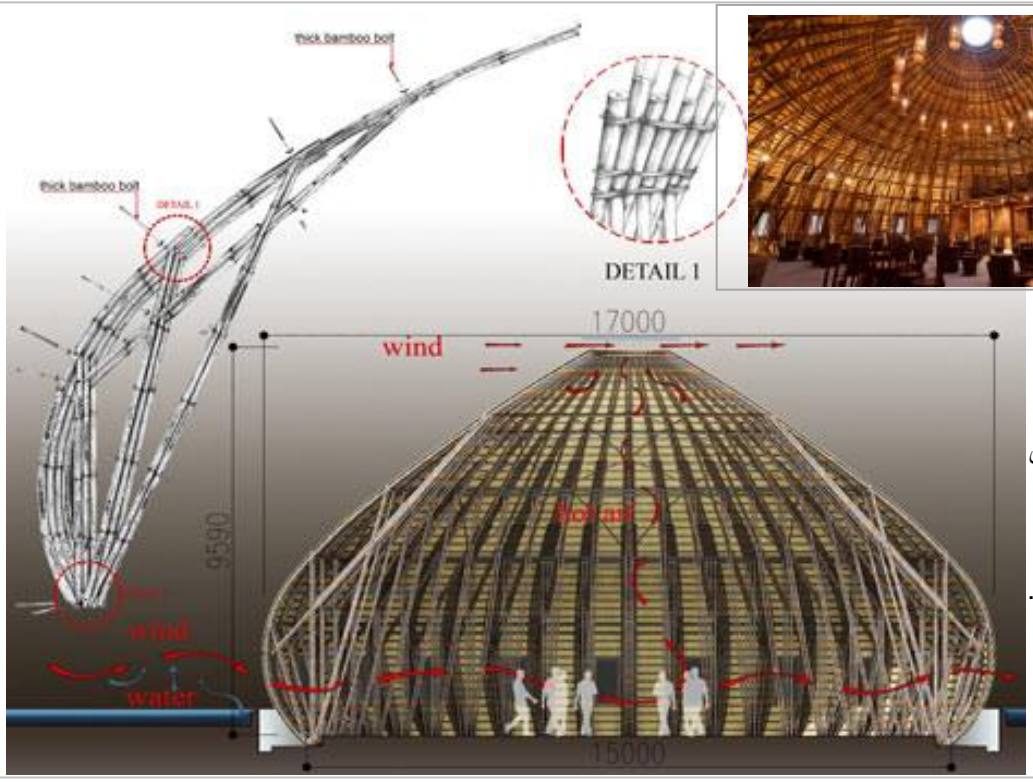

ج: تفاصيل انشائية ورسوم توضيحية في البرنامج الرقمي المعتمد لتصميم الهيكل الانشائي، يوضح النظام الحديدي الساند للهيكل النباتي، والدراسة البيئة للرياح. والانارة السقفية والتهوية

شكل 3: صور توضيحية لمشروع Wind and Water / https://www.google.com

ثانيا: مشروع Exibition in Zaragoza 2008

تصميم:Benedetta Tagliabue, Miralles Tagliabue EMBT – (B)

نفذ هذا المشروع في مدينة سرقسطة في اسبانيا وقدم في مسابقة تصميم الجناح الاسباني في معرض (Expo 2010)، في شانغهاي في الصين وفاز بالجائزة الاولى.

ترتكز فكرة التصميم الى تحقيق عمارة اكثر ارتباطا بالبيئة واكثر تكنولوجيا. يستكشف المشروع إمكانيات لا تعد ولا تحصى لتقنيات نسج الخوص من البعد الحجمي والمادي والهيكلي من سلة الخوص.

يتكون الهيكل الانشائي من الإطار الأنبوبي الفراغي المزدوج لتشكيل الواجهات التي يمكن أن تلبي بفعالية لمتطلبات الأحمال المختلفة، وقد استخدمت نوعية شبه شفافة من منسوجات الألياف النباتية لتغليف الواجهات وتعريف الفضاءات الداخلية، مثل سلال الخوص، وخلق جو رائع من الضوء أقرب إلى الورق الشفاف والذي يمثل استعارة من بعض العناصر المعمارية الاسبانية الإسلامية – المتغيرة باستمرار عبر الضوء والظل. تطلب المشروع تعاونا كبيرا بين الفريق التصميمي والانشائي، فان اختيار الهيكل الملائم لخلق هذا الشكل العالي التعقيد في الاشكال المنحنية الحرة. **شكل (4)**

اعتمد الحل الانشائي برامج رقمية متخصصة استخدمت فيها نماذج ثلاثية الأبعاد معقدة وفرت نظاما للاتصال بين الفريق المعماري، والمهندسين والشركات المصنعة في ورشات العمل. Jodidio,2011, , pp270–275

انظر استمارة (2) لتفاصيل تكنولوجيا النظام الانشائي.

استمارة (2): وصف تكنولوجيا النظام الانشائي لمشروع Exibition in Zaragoza /الباحث عن Jodidio,2011, , pp270–

رمز	الفكرة التصميمية	مواد البناء	النظام الانشائي واليات التنفيذ	التكنولوجيا الرقمية
B	**محلية-عالمية** -من المشاريع الأكثر استدامة من الناحية البيئية ، ولكن في الوقت نفسه الأكثر التكنولوجية -يتكون على تطوير تقنية الحرف الفنية اليدوية من الخوص في ممارسة البناء. مع مجموعة الالهامات الحجمية والمادية والهيكلية التي استلهمت من سلة الخوص وتقنية صنع السلة،، وهو تقليد محلي.	-استعمال نسيج من الالياف النباتية شبه الشفافة لتغطية الفضاءات الخارجية لربط الداخل والخارج.	-يتكون الهيكل الانشائي من هيكل معدني انبوبي (اطارات فراغية) مغطي بالواح نسيج الخوص التي تغطي واجهة المبنى على وفق تقنية الطي. والتلاعب بالظل والضوء.	-استخدام التكنولوجيا من خلال النظام الانشائي في العلاقات بين العناصر الخشبية ضمن برنامج حاسوبي دقيق. -امتاز التصميم بالتكنولوجيا الرقمية في تجاوز العقبات التعبيرية في تكوين الشكل.

أ: الهيكل الانشائي لسلة الخوص وتمثيله الرقمي

ج: التكوين الشكلي للمعرض يوضح الواح الخوص في تغليف الواجهة

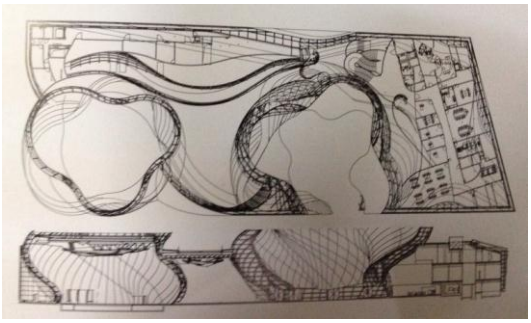

ب: مخطط افقي ومقطع عمودي يوضح الهيكل الانشائي

د: شفافية المواد البنائية ودورها في تحقيق الانارة الطبيعية والحيوية في الفضاءات الداخلية

شكل 4: صور توضيحية لمشروع Jodidio,2011 ,pp270-275/ Exibition in Zaragoza 2008

ثالثاً: مشروع المكتبة الوطنية في مدينة استانا – كازاخستان[6] 2009(Kazakhstan's new National Library in Astana تصميم: المعماريون BIG–(C)

فاز المعماريون"بيج""BIG" على منافسيهم "نورمان فوستر" و"زهاء حديد" في المسابقة المفتوحة لتصميم المكتبة القومية الجديدة لكازاخستان.والتي تضمنت تسعة عشر مشترك.

يمكن تصور المكتبة على انها حالة من المعايشة بين المدينة والطبيعة. وهو ما ينطبق على مدينة استانا ايضا, فهي تتوسط الفضاءات الخارجية الطبيعية لقلب كازاخستان. تعدى تصميم المكتبة عن كونه مجرد تحدي معماري, اذ ان المكتبة تمثل احدى الركائز المستقبلية لبناء امة كازاخستان, ومؤسسة رائدة تمثل الهوية القومية للبلاد, وسوف تمثل مركزا فكريا متعدد الوظائف ومركزا ثقافيا يهدف اساسا لاعادة تاسيس وتطور كازاخستان. شكل (5)

تم تصميم المكتبة بمساحة 33000 متر مربع, وهي مكونة من شكل متوازي مستطيلات ينحني حول نفسه وحول مسار دائري في نفس الوقت, ويتجاوز تصميم المكتبة القومية الانماط الهندسية التقليدية للتصميم المعماري مثل الجدار والسقف, فيصبح الجدار سقفاً الذي بدوره يصبح ارضية, والارضية بدورها تصبح جداراً مرة اخرى. يدمج تصميم المكتبة القومية اربعة

[6] http://www.archdaily.com/33238/national-library-in-astana

نماذج اصلية عالمية عبر الزمن والمكان لتكون رمزا قوميا جديدا وهي الدائرة والعجلة والعقد والخيمة حيث يتم دمجهم في صياغة واحدة: الدائرة في بساطة التكوين, والعجلة تخلق الفناء, واحتواء العقد, وحماية الخيمة. لذلك يبدو تصميم المكتبة محليا وعالميا معاصرا, غير محدود بالزمن, واصيل في نفس الوقت. لتفاصيل تكنولوجيا النظام الانشائي لاحظ استمارة (3).

استمارة (3): وصف تكنولوجيا النظام الانشائي لمشروع Kazakhstan's National Library/الباحث عن www.archdaily.com

رمز	الفكرة التصميمية	مواد البناء	الهيكل الانشائي واليات التنفيذ	التكنولوجيا الرقمية
C	**محلية-عالمية** -خلق مركز فكري متعدد الوظائف يمثل الهوية القومية للبلاد. -دمج اربع نماذج اصلية عالمية عبر الزمان والمكان (دائرة,عجلة,خيمة,عقد) لتكون احد الركائز المستقبلية لبناء امة كازاخستان (مركز فكري). -المعايشة بين المدينة والطبيعة.	-اعتماد المواد الخرسانية المتطورة التي تمثل الصلابة في الهيكل الانشائي الداخلي. -الانابيب الحديدية المجوفة كاطارات فراغية مغطاة بالوح زجاجية شفافة في القشرة الخارجية.	-تقنية عالية في ربط هياكل انشائية صلدة واطارات فراغية. - وابتكار مواد بناء جديدة مرنة تعمل في بعض اجزاء المشروع في اخفاء الهيكل الانشائي الداخلي واظهاره في الاجزاء الخارجية.	-استعمال التكنولوجيا الرقمية في التصميم الافتراضي متجاوزل بذلك العقبات التعبيرية والانشائية. -تحرر الشكل من الثوابت التصميمية.

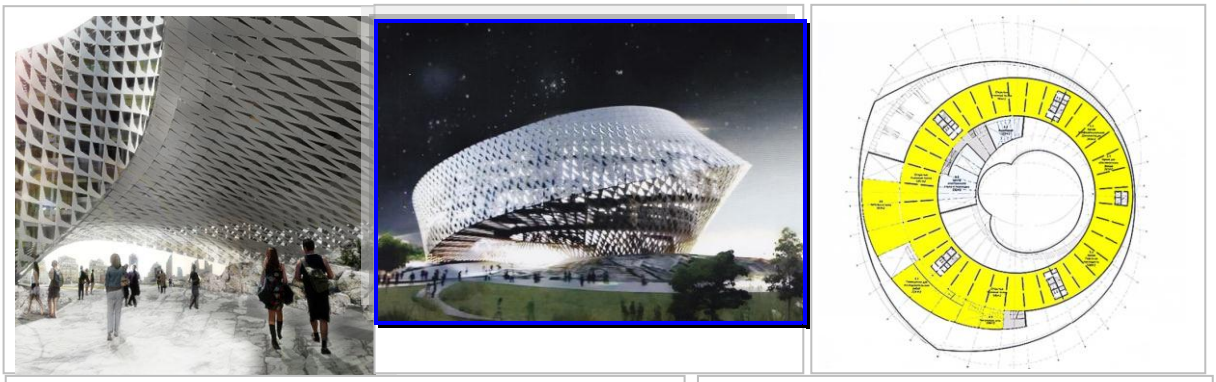

ب: مخطط افقي يوضح نقاط استناد الهيكل الانشائي

ج،د:مرونة الهيكل الانشائي وشفافية الغلاف الخارجي

شكل 5: صور توضيحية لمشروع :- المكتبة القومية الجديدة-كازخستان / http://www.archdaily.com/33238/national-library-in-astana

رابعاً: مشروع السحب للالعاب والمعارض الاولمبية في لندن 2012[7]: London Olympics & Expo Cloud Project –structures تصميم: Massachusetts Institute of Architecture – (D)

في مشروع يشابه افلام الخيال العلمي وفي نفس المكان الذي ارتفع فيه دخان المصانع عندما كانت لندن ورشة العالم ومهد الثورة الصناعية تحلق السحب لتكون معلما جديدا في مدينة لندن.

يتكون المشروع من ابراج شبكية ترتفع 130 متر على قمتها فقاعات بلاستيكية تعمل بالطاقة الشمسية وتظهر عليها صور وبيانات المتسابقين اثناء الالعاب الاولمبية لتبدو وكانها منصة مشاهدة ومتنزه عام. السحب لن تمثل اي اعباء على شبكة الطاقة الوطنية حيث تعتمد على طاقة الشمس والرياح وحركة البشر داخلها.

مشروع السحب بغرض لفت الانتباه الى الرحلة الطويلة التي اجتازها الانسان ...والمشروع عبارة عن منصة مشاهدة معلقة في السماء على شكل سحابة فوق الساحة الاولمبية التي استضافت اولمبياد لندن 2012.

تعتمد السحب في تكوينها على النظم الرقمية في العرض والاتصال وهي في النهاية مقصد سياحي لكل محبي الترجل وركوب الدراجات والاستكشاف كما انه يوفر منظومة بيئية مائية تتوافق مع معالم الموقع في ستراتفورد.

تنبع القيم الجمالية والتصميمية في المشروع وتكتسب اثرها من السياق المحيط بها. فهو عبارة عن مجموعة من احدث التكنولوجيات التي تستخدم في البناء ويمثل عقدة للتنوع السكاني في لندن ويسبح في جو الفضاء الذي يحتضن جميع البشر. يتكون المشروع من شبكة مركزية من الاعمدة تعمل كمحاور حركة وتتدلى من السماء كافرع شجرة البنغال و ترتفع هذه الاعمدة الى الاعلى وتقسم الى منصات مشبكية خفيفة الوزن داخل بالونات منتفخة ومكثفة وشفافة. شكل (6)

تؤدي سحب البالونات هذه الى حلقات من المنصات الاخرى يخرج الزوار للسير فوق المشروع وعند الحواف حيث تجمعات متفرقة من البالونات تتنوع اوضاعها ومساراتها على حسب درجة الحرارة الداخلية ممايسمح باعادة تجميع البالونات وتكوينها. تكسر السحابة الحاجز التقليدي بين البشر والمشروع فالبشر هم اساس المشروع وهم هدفه في نفس الوقت.

تم تثبيت البالونات المنتفخة بنظم LED[8] التي تكثف صور العرض في الداخل لتتحول البالونات الى شاشات ومعلومات يتصفحها الزوار اثناء تواجدهم في اي مكان في لندن. بذلك يتضمن المشروع منهجا مختلفا تماما عن المبادئ الديكارتية في الرياضيات حيث يتم العرض بنظام (العرض المكاني) من خلال مجال معلق يتكون من اشارات مكثفة من LED وبذلك يمكن رؤيتها من كل المجالات... يتم التحكم بكل عوامل الحركة ودرجة الحرارة والمعلومات من خلال شبكة متكاملة داخل المشروع. لاحظ استمارة (4).

[7] www.insidethegames.biz/**olympics**/...**olympics/2012**/

[8] الديودات الباعثة للضوء

استمارة (4): وصف تكنلوجيا النظام الانشائي لمشروع London Olympics & Expo Cloud Project -structures
/الباحث عن http://www.raisethecloud.org/

رمز	الفكرة التصميمية	مواد البناء	الهيكل الانشائي واليات التنفيذ	التكنولوجيا الرقمية
D	**محلية- عالمية** منصة مشاهدة معلقة في السماء على شكل سحابة موقعه في الساحة الاولمبية لاولمبياد 2010.ضمن مشروع متنزه عام.	- مقصد سياحي لكل محبي الترجل وركوب الدراجات. - البشر اساس المشروع وهدفه في نفس الوقت.	استعمال الهياكل الحديدية في الابراج الشبكية مع الفقاعات البلاستيكية الشفافة ليعكس القيم الجمالية التصميمية وتكتسب اثرها من السياق المحيط بها ضمن الترابطات بين النظم الانشائية (المنفاخية,الغشائية, الاطارات الهيكلية).	1-تعتمد على طاقة الشمس والرياح وحركة البشر داخلها. 2-يعتمد على النظم الرقمية في الاتصال.

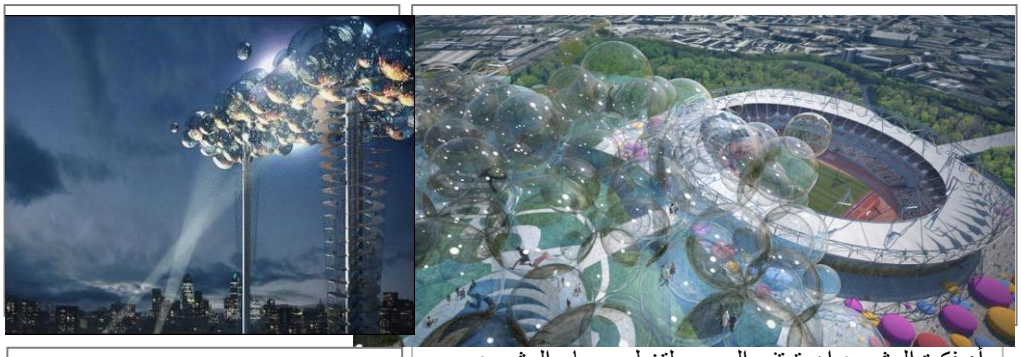

أ: فكرة المشروع ان ترتفع السحب لتغطي سماء المشروع

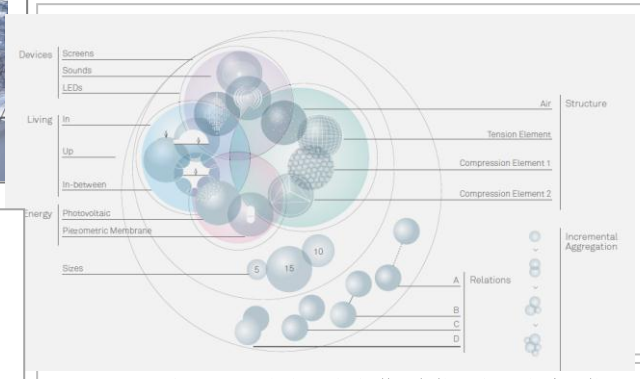

ج: الهيكل الانشائي الكلي للفقاعات وانواع تجميعها

ب: تعمل الهياكل المنشئية التي ترفع السحب كفضاءات للفعاليات الترفيهية ، وتسمح للزائرين، وتتحول ليلا الى سطوح لعرض فعاليات الالعاب الاولمبية.

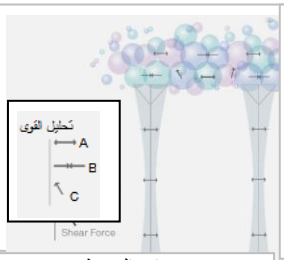

A: قوة الضغط
B: قوة الضغط
C: قوة القص

مكونات الهيكل الانشائي: هيكل منفاخيمن الخلايا الشفافة، الكيبلات والهواء المضغوط .

د.تحليل الهيكل الانشائي للفقاعات

شكل 6: صور توضح الفكرة التصميمية لمشروع London Olympics Cloud Project/
www.insidethegames.biz/olympics/...Olympics/2012/

خامساً : مجمع سينمائي في مدينة بوسان[9] Busan Cinema Complex – 2012

تصميم Wolf D. Prix & Partne من شركة Coop Himmelb – (E)

صمم هذا المشروع في مسابقة معمارية عام 2005، وتم الانتهاء من تنفيذ المشروع عام 2012، كان المفهوم الأساسي لهذا المشروع الخطاب حول تداخل المساحات المفتوحة والمغلقة والأماكن العامة والخاصة. شكل (7)

اقترحت الشركة المصممة مبنى بوسان للسينما و لاقامة مهرجان بوسان السينمائي الدولي حيث يشيرالمبنى إلى وجود تقاطعات جديدة بين الفضاء العام والبرامج الثقافية، والتكنولوجيا، والهندسة المعمارية ضمن المشهد الحضري بوصفها رموز الثقافة المعاصرة. تنص الفكرة على انشاء بلازا في أربع مناطق متداخلة ضمن مشروع تندمج فيه التقنيات التكنولوجية والمعمارية لخلق بلازا حضرية حيوية ضمن الفضاء الخارجي.

يعكس الهيكل الانشائي للمشروع التكنولوجيا الحديثة لنظم الاطارات الفراغية (SPACE FRAME) كعناصر سقفية تستند على قاعدة مخروطية مزدوجة من جهة واحدة ، ويظهر السقف كبروز يمتد 85 متر مقاربا في تصميمه مرتين لطول جناح طائرة ".Airbus 380، يثبت الهيكل المخروطي السطح من جهة واحدة ، ويغلف كعمود من شبكة معدنية شعرية وهنا يشير المصمم الى ان التصميم على وفق مبدأ جناح الطائرة سوف يلغي الحاجة الى الاعمدة.

تم اعتماد التصميم الافتراضي لخلق سماء افتراضية (VIRTUAL SKY) من خلال الواح الطاقة LED، تغطي المدخل والمسرح المدرج المفتوح ليعكس الفضاء الحضري العام المستمر والمتعدد الوظائف لتعكس الثقافة المعاصرة، ولخلق حياة حضرية تتسم بالحيوية ليلا، وتبقى مرئية خلال النهار.لاحظ استمارة (5) لتفاصيل تكنولوجيا النظام الانشائي.

استمارة (5): وصف تكنولوجيا النظام الانشائي لمشروع Busan Cinema Complex /الباحث عن http://www.archdaily.com

رمز	الفكرة التصميمية	مواد البناء	الهيكل الانشائي واليات التنفيذ	التكنولوجيا الرقمية
E	**عالمية** -تنص الفكرة على انشاء بلازا في أربع مناطق متداخلة ضمن مشروع تندمج فيه التقنيات التكنولوجية والمعمارية لخلق بلازا حضرية حيوية ضمن الفضاء الخارجي. -تداخل المساحات المفتوحة والمغلقة والأماكن العامة والخاصة في البيئة الحضرية.	- اعتماد الهيكل الكونكريتي في الابنية الداخلية(الجدران والسقوف). - استعمال الهيكل الحديدي في تسقيف الفضاءات المفتوحة. - استعمال الكيبلات الحديدية في الشد والتعليق	-اعتماد نظم الاطارات الفراغية (SPACE FRAME) في تسقيف الفضاءات الواسعة المفتوحة , كعناصر سقفية تستند على قاعدة مخروطية مزدوجة ويغلف كعمود من شبكة معدنية شعرية تغطى بالواح شفافة تظهر الهيكل الانشائي اضافة الى الواح غير شفافة في السطوح الخارجية تخفي الهيكل الانشائي.	-اعتماد تقنية خفة المواد الانشائية في السقوف. -اعتماد التصميم الافتراضي لخلق سماء افتراضية. (VIRTUAL SKY) من خلال الواح الطاقة. -اعتماد تكنولوجياالبرامجيات في تشكيل القطع المتكررة في الاشكال المخروطية.

[9] http://www.archdaily.com/

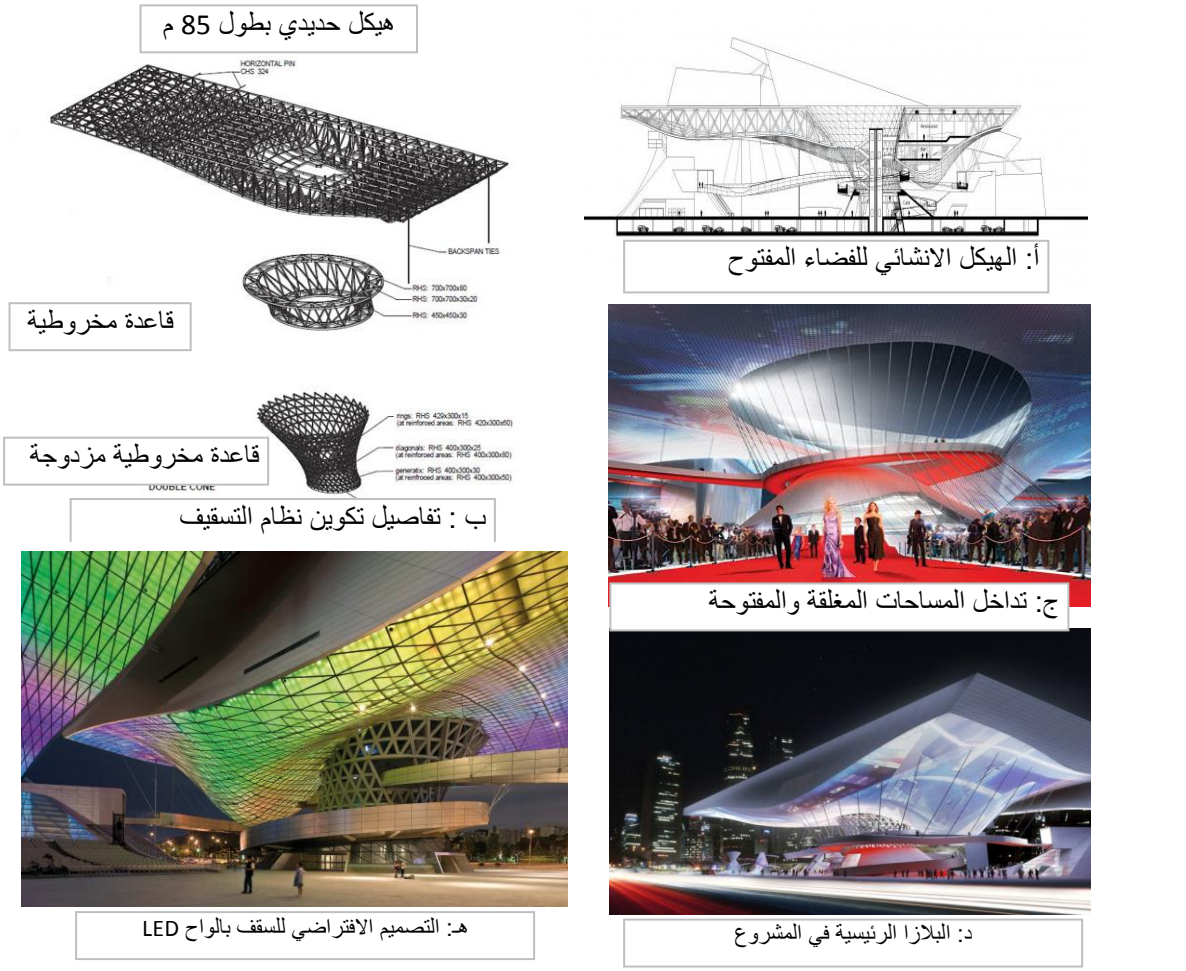

شكل 7: صور توضح الفكرة التصميمية لمشروع: http://english.visitkorea.or./Busan Cinema Complex

سادساً: مشروع مبنى جزيرة الكرستال في موسكو (2005-2013 Crystal Island building project in Moscow)[10]، تصميم: Norman Foster - (F)

جزيرة الكريستال هو احد اكبر المشاريع البنائية في العالم والأكثر طموحاً، يمثل علامة فارقة في تاريخ 40 سنة من الممارسة الانشائية. يخلق المشروع وجهة دينامية جديدة في المناطق الحضرية على مدار السنة لموسكو ويجسد التوجهات المستدامة في التصميم. يمثل المشروع نموذجاً للتعاقد متعدد الاستخدامات، التخطيط المستدام للمدينة مع استراتيجية الطاقة المبتكرة والذكية.

يوفر التصميم امكانية دمج الفضاءات الداخلية للمبنى مع فضاءات الحديقة المحيطة، التي من شأنها أن توفر مجموعة من الأنشطة على مدار السنة، مع التزلج والتزحلق على الجليد في الشتاء. شكل (8)

من المقرر أن تكون المساحة البنائية (2500000 متر مربع) ، وعلى ارتفاع (450 مترا). يحتوي المبنى على عدد وافر من المعارض الثقافية،، والأدائية، والفنادق والشقق والمساحات المكتبية، فضلا عن المدرسة الدولية لـ500 طالب.

[10] http://www.dezeen.com/2008/01/02

يتكون الهيكل الانشائي من هياكل حديدية عملاقة الأبعاد ، ترتفع البنية الفوقية بشكل الخيمة إلى 450 متر، لتشكيل "الغلاف الثاني" والطبقة العازلة الحرارية مع تدرج المساحات الداخلية لحماية المبنى الرئيسي من الجو الخارجي، اذ يتم اغلاق الغلاف الثاني في فصل الشتاء لتقليل فقدان الحرارة، ويفتح في الصيف.لاحظ استمارة (6)

استمارة (6): وصف تكنلوجيا النظام الانشائي لمشروع Crystal Island building project/ الباحث عن http:// www.dezeen.com

رمز	الفكرة التصميمية	مواد البناء	الهيكل الانشائي واليات التنفيذ	التكنولوجيا الرقمية
F	**محلية- عالمية** -جزيرة الكريستال هو احد المشاريع البنائية في العالم الأكثر طموحا ودينامية جديدة في المناطق الحضرية. بل هو نموذج للتعاقد متعدد الاستخدامات، التخطيط المستدام للمدينة، مع استراتيجية الطاقة المبتكرة والذكية.	-اعتماد الكونكريت مادة بنائية اساسية في الهيكل الداخلي. -الحديد مادة اساسية في القشرة الخارجية. -المواد الشفافة في تغليف الهيكل الحديدي واظهار الشكل.	-يتكون الهيكل الانشائي من هياكل حديدية عملاقة الأبعاد ، ترتفع البنية الفوقية بشكل الخيمة، لتشكيل "الغلاف الثاني" والطبقة العازلة الحرارية لحماية المبنى الرئيسي.	- امتاز التصميم بالتكنولوجيا الرقمية في تجاوز العقبات التعبيرية وتجاوز العقبات الانشائية لاخراج الشكل المعماري المتميز.

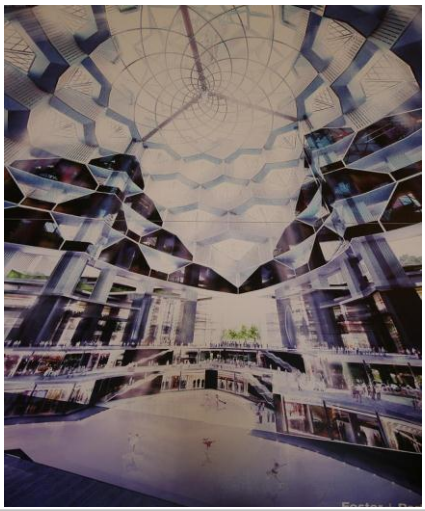

أ: الخلايا الشمسية المتحركة في الغلاف الخارجي

ب: اعتماد شكل الخيمة في النظام الانشائي

ج: تكامل المشروع مع البيئة الطبيعية المحيطة

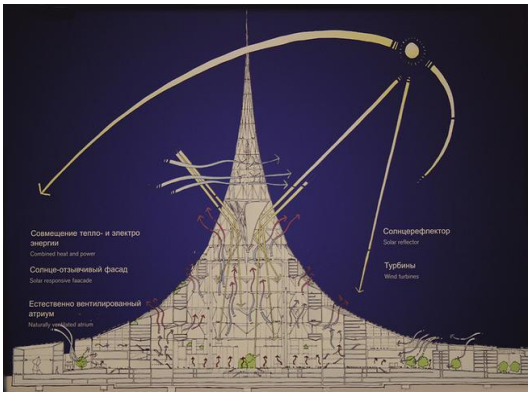

د: الدراسة الرقمية للمعالجات البيئية

شكل 8: صور توضيحية لمشروع Crystal Islan building project/ http://www.dezeen.com

5- النتائج والاستنتاجات

بعد تحليل المشاريع على وفق مفردات الاطار النظري وتنظيم الشروحات في استمارة خاصة لكل مشروع، وتوضيح مفردات تكنولوجيا النظم ألمنشئية، تم تحديد المفردات المتحققة في جدول مفردات الاطار النظري جدول (2)، ليتم استخلاص اهم الاستنتاجات.

جدول (2): تطبيق الاطار النظري في المشاريع المنتخبة / المصدر : الباحث

رمز المشروع	أبعاد تكنولوجيا النظم المنشئية																							
	فكري		مادي (النظم المنشئية)																					
			مواد البناء						النظام المنشئي						اليات التنفيذ				التكنولوجيا الرقمية					
			خصائص فنية				خائص منشئية																	
	عالمي	محلي - مكاني - بيئي	الصلابة	المرونة	الشفافية	العزل الحراري	اخفاء	اظهار	قشري Shell	منفاخي Pneumatic	غشائي Membrane	هيكلي Skelton	المضلع Ribbed	الاطارات الفراغية Space Frame	وحدات انشائية قياسية	عناصر انشائية مسبقة الصنع	الية تجميع الاجزاء	تعقيد النظام	ازالة الحدود بين الداخل والخارج	خفة المواد البنائية	تجاوز العقبات التعبيرية	تجاوز العقبات الانشائية	حرية الشكل
A	*	*			*			*	*				*							*		*	
B	*	*		*	*		*		*						*		*		*	*	*		*
C	*	*					*		*				*		*		*	*			*	*	*
D					*			*						*		*	*			*		*	
E	*	*		*	*			*						*	*	*			*	*		*	
F		*			*	*	*				*			*	*			*	*		*	*	*

6- الاستنتاجات النهائية

1. وفرت التقنيات الحديثة في النظم المنشئية مجالاً لظهور مواد بنائية جديدة بتجليات تعبيرية تعكس الامكانات التكنولوجية.
2. حررت تكنولجيا النظم ألمنشئية من خلال تكنولوجيا صناعة المواد المنشئية المرنة النتاج المعماري من سيادة الأشكال البسيطة.
3. أخرجت التكنولوجيات الرقمية للنظم المنشئية اشكال وفضاءات معمارية شكلية وانشائية غير محدودة، يمكن تمثيلها بصرياً بعناصر انشائية وعلاقات ترابطية وقوانين ضمن مفهوم النظام، مستجدة أكثر تحرراً من تصميم الاشكال التقليدية.
4. مع ازدياد امكانية تكنولوجيا النظم المنشئية والتكنولوجيات الرقمية تزداد العناصر الإنشائية والمعمارية خفة وشفافية، كما أن بعض العناصر تصبح قادرة على تغيير صفاتها وتتغير تلك الصفات لتحقق أهدافاً تشكيلية وتكنولوجية.
5. وفرت التكنولوجيا الرقمية تجاوز العقبات التعبيرية والانشائية من خلال البرامج المتخصصة في التمثيل الشكلي.
6. يمكن تحقيق الخصائص المكانية من خلال اعتماد تكنولوجيا النظم المنشئية باستثمار المواد الانشائية المحلية التي تعكس خصوصية المكان، وبهذا تتحرر التكنولوجيا من الاتجاه العالمي والعولمة لتاكد الخصوصية المحلية.
7. ساهم تطور تكنولوجيا المواد في دعم الخصائص الفنية لمواد البناء كالشفافية، التي ساهمت في تجاوز الحدود بين الداخل والخارج، واظهار النظام الانشائي كنتاج معماري.
8. ساعدت تكنولوجيا النظم المنشئية في تطوير الالواح الشمسية والواح LED ، لاستغلال القشرة الخارجية للمبنى في توليد الطاقة او كسطوح افتراضية، وفي تحقيق معالجات بيئية متميزة .

7- المصادر

1- بريجز، جون، 1986: **الكون المرآة**، ترجمة نهاد العبيدي،الدار العربية، بغداد.

2- السلمي، علي،1978: **اتجاهات جديدة في الفكر التنظيمي** ، مجلة عالم الفكر، المجلد الثامن، العدد الرابع، وزارة الاعلام ، الكويت

3- الشابندر، منورة صباح، 2004: **اثر التكنولوجيا على العمارة العراقية المعاصرة**، رسالة ماجستير غبر منشورة، الجامعة التكنولوجية، قسم الهندسة المعمارية،بغداد،.

4- العلي، خليل ابراهيم والامام، محمد، 2001 :**التكنولوجيا والنظام التواصلي** ، المجلة العراقية للهندسة المعمارية / السنة الاولى/، العدد الاول، الجامعة التكنولوجية ،.

5- العمري، أيمن أحمد إبراهيم، 2009 :**أثر نظم المعلومات الإدارية المحوسبة على أداء العاملين في شركة الاتصالات الفلسطينية**، رسالة ماجستير ، الجامعة الإسلامية، كلية التجارة،غزة، **منشورة على الموقع الالكتروني ، www.iugaza.edu.ps، اخر زيارة للموقع في 2013/12/20**

6- العزاوي، رشا نوفل فاضل 2008: **أثر برامج التحليل الانشائي على الشكل المعماري للابنية الضخمة**, رسالة ماجستير غير منشورة، كلية الهندسة، جامعة النهرين، بغداد

7- **هاشم عبود الموسوي 2009: الواقع الافتراضي للعمارة والعمران**، كلية الهندسة، جامعة المرقب، ليبيا، منشورة على الموقع الالكتروني http://www.alnoor.se/ ، **اخر زيارة للموقع في 2013/12/20**

8- **هوشيار قادر، 2003: العمارة والتكنولوجيا** , اطروحة دكتوراه غير منشورة، جامعة بغداد ، كلية الهندسة، قسم الهندسة المعمارية.

9- Arab British Academy for Higher Education, www.abahe.co.uk,1l10l2012

10- Abel, Chris (2004) ,**Architecture, Technology and Process**, Oxford: Architectural Press.

11- Ali, Mir M.; Moon, Kyoung Sun (2007). "**Structural Developments in Tall Buildings: Current Trends and Future Prospects**". Architectural Science Review Volume 50.3, pp 205-223, University of Sydney. reserved.www.arch.usyd.edu.au/asr **last visit 2012-04-30**.

12- Broadbent, Geoffrey , 1973,**Design in architecture: architecture and the human sciences**, John Wiley & Sons. London.

13- Gyula,sebestyen 2003, **New Architecture and technology** , Architectural Press UK.

14- Jodidio, Philip,2011 **Contemporary Architecture Now**, Taschen, Italy.

15- Matteoli,Lorenzo and Gabriella Peretti,2013, **Forty years of environmentally conscious building technology design**, Firenze University Press, **IVSL** : http://www.fupress.com/techne

16- Losasso, Mario ,2011, The **project as product of scientific research**, Firenze University Press, **IVSL**: http://www.fupress.com/techne

17- Emmitt, Stephen ,2011, **Technological Design in a Multidisciplinary, Sensory, Context**, Firenze University Press, **, IVSL**: http://www.fupress.com/techne, last visit 5-11-2013

18- Emmitt, Stephen, 2012 ،**Architecture technology**, Second edition, University Press. http://www.fupress.com/techne

19- Macdonald, Angus J.,2001, **Structure and Architecture,** first edition1994,1998,2001, Architectural Press.

مواقع الانترنيت:

http://www.archdaily.com/

http://www.dezeen.com/

www.inside the games.

http://www.the free dictionary.com